SPATIAL MODELING OF AIRBORNE PARTICULATE MATTER DISTRIBUTION BASED ON MODIS DATA IN THE UPPER NORTHERN THAILAND

Chat Phayungwiwatthanakoon

A Thesis Submitted in Partial Fulfillment of the Requirements for the Degree of Doctor of Philosophy in Geoinformatics

Suranaree University of Technology

Academic Year 2013

การจำลองเชิงพื้นที่ของการกระจายฝุ่นละอองในอากาศโดยใช้ข้อมูล MODIS ในภาคเหนือตอนบนของประเทศไทย

นายฉัตร พยุงวิวัฒนกูล

มหาวิทยาลัยเทคโนโลยีสุรนารี

วิทยานิพนธ์นี้เป็นส่วนหนึ่งของการศึกษาตามหลักสูตรปริญญาวิทยาศาสตรดุษฎีบัณฑิต
สาขาวิชาภูมิสารสนเทศ
มหาวิทยาลัยเทคโนโลยีสุรนารี
ปีการศึกษา 2556

SPATIAL MODELING OF AIRBORNE PARTICULATE MATTER DISTRIBUTION BASED ON MODIS DATA IN THE UPPER NORTHERN THAILAND

Suranaree University of Technology has approved this thesis submitted in partial fulfillment of the requirements for the Degree of Doctor of Philosophy.

Thesis Examining Committee

(Asst. Prof. Dr. Sunya Sarapirome)
Chairperson

(Asst. Prof. Dr. Songkot Dasananda)
Member (Thesis Advisor)

(Assoc. Prof. Dr. Sura Pattanakiat)
Member

(Assoc. Prof. Dr. Suwit Ongsomwang)
Member

(Asst. Prof. Dr. Nares Chuersuwan)
Member

(Dr. Dusdi Chanlikit)
Member

(Prof. Dr. Sukit Limpijumnong)
Vice Rector for Academic Affairs and Innovation

(Assoc. Prof. Dr. Prapun Manyum)
Dean of Institute of Science

ฉัตร พยุงวิวัฒนกูล : การจำลองเชิงพื้นที่ของการกระจายฝุ่นละอองในอากาศโดยใช้ข้อมูล MODIS ในภาคเหนือตอนบนของประเทศไทย (SPATIAL MODELING OF AIRBORNE PARTICULATE MATTER DISTRIBUTION BASED ON MODIS DATA IN THE UPPER NORTHERN THAILAND) อาจารย์ที่ปรึกษา : ผู้ช่วยศาสตราจารย์ ดร.ทรงกต ทศานนท์, 279 หน้า.

การจัดทำแผนที่ของสารแขวนลอยในอากาศใกล้ผิวดินจากข้อมูลดาวเทียม ได้รับความสนใจอย่างกว้างขวางเพื่อการวิเคราะห์มลภาวะทางอากาศในปัจจุบัน อย่างไรก็ตาม การทำแผนซึ่งมีระดับความละเอียดสูงยังคงไม่ประสบความสำเร็จมากนัก ซึ่งข้อบกพร่องนี้ได้รับการแก้ไขอย่างสำคัญในงานวิจัยนี้ ซึ่งประกอบด้วยวัตถุประสงค์หลักสามประการคือ (1) เพื่อระบุความสัมพันธ์ของพารามิเตอร์ที่พัฒนาจากข้อมูล MODIS (และค่า AERONET-AOD) และค่า PM10 อ้างอิง(2) เพื่อพัฒนาและประยุกต์แผนที่ข้อมูลรายวันของ NDAI, AOD, PM10 และ AQI จากข้อมูล MODIS ที่เกี่ยวข้องและวิธีการที่เลือกมา สำหรับการตรวจสอบและประมาณค่าความรุนแรงของมลภาวะของสารแขวนลอยเหนือพื้นที่ศึกษาทั้งหมด (ภาคเหนือตอนบนของประเทศไทย) และ (3) เพื่อประยุกต์แบบจำลอง HYSPLIT สำหรับวิเคราะห์เส้นทางการเคลื่อนที่และรูปแบบการกระจายตัวของกลุ่มเขม่าควันที่เกิดจากไฟของฤดูไฟป่า พ.ศ. 2553

สำหรับวัตถุประสงค์แรก พบว่าค่าการสะท้อนแสงของ MODIS ในช่วงคลื่นสีน้ำเงิน มีความสัมพันธ์ที่ค่อนข้างสูงกับค่า PM10 อ้างอิง (R^2 = 0.71) ส่วนข้อมูลการสะท้อนแสงที่ค่าความยาวคลื่นมากขึ้นคือแบนด์สีเขียวและสีแดง พบว่ามีระดับความสัมพันธ์ต่ำกว่า (R^2 = 0.616 และ 0.563 ตามลำดับ) ขณะที่แบนด์ Mid-IR แสดงผลของความสัมพันธ์ต่ำสุด (R^2 = 0.029) สำหรับพารามิเตอร์อื่นที่ได้พิจารณาต่างมีค่าระดับความสัมพันธ์ที่น่าพอใจกับค่า PM10 อ้างอิง ได้แก่ ΔR (Blue) (R^2 = 0.667) NDAI (R^2 = 0.661) MODIS-AOD (R^2 = 0.72) BAER-AOD (R^2 = 0.784) และ AERONET-AOD (R^2 = 0.86) ทั้งนี้พบว่า BAER-AOD เป็นพารามิเตอร์ที่เหมาะสมที่สุดอิงจากระดับความสัมพันธ์ที่สูงของมันกับค่า PM10 อ้างอิง และการมีศักยภาพสูงสำหรับพัฒนาแผนที่ AOD และ PM10 ใกล้ผิวดินที่ระดับความละเอียดเชิงพื้นที่ 500 เมตร นอกจากนี้ BAER-AOD ยังแสดงระดับความสัมพันธ์ที่สูงกับค่า AERONET-AOD โดยมีค่า R^2 ที่ 0.828 ซึ่งใกล้เคียงกับค่าที่พบจากงานวิจัยอื่น

สำหรับวัตถุประสงค์ที่สอง พบว่า NDAI ซึ่งเป็นดัชนีคุณภาพอากาศที่เสนอขึ้นใหม่สามารถทำงานได้ดีสำหรับการเป็นตัวชี้วัดเบื้องต้น ของระดับความรุนแรงของมลภาวะที่เกิดจาก PM10 นอกจากนี้ยังพบว่าแผนที่ PM10 ที่พัฒนามาจากแบบจำลอง BAER มีระดับของความ

สอดคล้องที่น่าประทับใจกับข้อมูลที่ตรวจวัดได้จริงโดยมีค่า R^2 ที่ 0.744 และมีค่าเฉลี่ยความผิดพลาดแบบสัมบูรณ์ (MAE) อยู่ที่ร้อยละ 6.62 โดยแผนที่ดังกล่าวได้ถูกนำไปใช้เพื่ออธิบายสถานการณ์ของมลภาวะที่เกิดจากสารแขวนลอยประจำวัน ที่พบในพื้นที่ศึกษาได้เป็นอย่างดี ส่วนวิธีการสร้างแผนที่คุณภาพอากาศ (AQI map) ที่เสนอขึ้นมาใหม่ในการศึกษาครั้งนี้ พบว่าสามารถทำงานได้ดีกว่าวิธีการมาตรฐานที่ใช้ในประเทศไทย อังกฤษ และสหรัฐอเมริกา ในการจำแนกระดับของมลภาวะที่เกิดจากสารแขวนลอยสำหรับค่า PM10 ที่ 100-300 $\mu g/m^3$

สำหรับวัตถุประสงค์ที่ 3 ผลการจำลองการกระจายตัวและเส้นทางการเคลื่อนที่ของกลุ่มเขม่าควันโดยแบบจำลอง HYSPLIT บ่งชี้ว่าการกระจายตัวเป็นระยะไกลของกลุ่มเขม่าควันที่เกิดขึ้นในประเทศพม่ามีผลกระทบเป็นอย่างสูง กับสถานการณ์มลภาวะทางอากาศที่เกิดจากสารแขวนลอยที่ตรวจพบในเกือบทุกจังหวัดในพื้นที่ศึกษา ทั้งนี้เนื่องมาจากการมีปริมาณของเขม่าควันเป็นจำนวนมากที่เกิดมาจากปรากฏการณ์ไฟป่าซึ่งพบมากในประเทศพม่า ซึ่งมันสามารถถูกพาเข้ามาในพื้นที่ศึกษาโดยลมสำคัญประจำถิ่นคือลมมรสุมตะวันตกเฉียงใต้ในช่วงฤดูไฟป่าโดยเฉพาะในเดือนมีนาคมและเมษายน ทางทิศตะวันตกหรือตะวันตกเฉียงใต้เป็นประจำทุกปี

มหาวิทยาลัยเทคโนโลยีสุรนารี

สาขาวิชาการรับรู้จากระยะไกล ลายมือชื่อนักศึกษา_____

ปีการศึกษา 2555 ลายมือชื่ออาจารย์ที่ปรึกษา_____

CHAT PHAYUNGWIWATTHANAKOON : SPATIAL MODELING OF AIRBORNE PARTICULATE MATTER DISTRIBUTION BASED ON MODIS DATA IN THE UPPER NORTHERN THAILAND.
THESIS ADVISOR : ASST. PROF. SONGKOT DASANANDA, Ph.D.
279 PP.

AEROSOL POLLUTION/MODIS AOD/BAER AOD/AIR QUALITY INDEX NDAI/HYSPLIT MODEL

Satellite-based mapping of the near-ground atmospheric aerosol has found wide attention for air pollution analysis nowadays, however, the mapping at fine scale is still not commonly achieved. This shortcoming is essentially fulfilled in this work, which contains three main objectives: (1) to identify relationships of MODIS-based parameters (and AERONET-AOD) and reference PM10 data, (2) to develop and implement daily NDAI, AOD, PM10 and AQI maps from the relevant MODIS data and selected methods for the monitoring and quantifying aerosol pollution severity over the entire study area (upper northern Thailand) and (3) to apply the HYSPLIT model for the analysis of the fire-induced smoke plume trajectory and dispersion pattern for the 2010 fire season.

For the first objective, relatively strong correlations were found between MODIS reflectance radiance in the blue band and reference PM10 data (R^2 = 0.71). Longer wavelength data, i.e. green and red bands, demonstrated lesser correlation levels (with R^2 = 0.616 and 0.563, respectively), while the Mid-IR band exhibited the least correlation (with R^2 = 0.029). Other considered parameters also yielded satisfactory correlation levels to the reference PM10 data; i.e. ΔR (Blue) (R^2 = 0.667),

NDAI (R^2 = 0.661), MODIS-AOD (R^2 = 0.72), BAER-AOD (R^2 = 0.784) and AERONET-AOD (R^2 = 0.86). Among these, BAER-AOD was considered to be the optimal parameter, due mainly to its high correlation to the reference PM10 data and its high potential to develop AOD and associated near-ground PM10 maps at 500-m resolution. BAER-AOD also showed a strong link to AERONET-AOD with R^2 of 0.828, which is comparable to those attained in other reports.

For the second objective, NDAI, a newly-proposed air quality index, was found to perform well as a primary indicator of the PM10 pollution severity level. Daily PM10 maps derived from the BAER method also had impressive agreement to the observed data with R^2 of 0.744 and mean absolute error (MAE) of 6.62%. As such, they were fruitfully applied to explain the daily situation of the aerosol pollution seen over the area. The newly-proposed method to develop AQI maps in this study was also found to perform better than standard methods adopted in Thailand, UK and USA in differentiating levels of aerosol pollution for PM10 data 100-300 $\mu g/m^3$.

For the third objective, HYSPLIT's simulation of smoke plume dispersion and trajectory pattern indicated that the long-range dispersion of the smoke plumes originating in Myanmar may have significant impact on the observed air pollution over most provinces in the study area. This is due to the substantial amount of smoke plume that originated from the abundant fire activities in Myanmar, which can be carried into the area by the prevailing southwest monsoon wind during the fire season along western or southwestern directions every year, especially in March and April.

School of Remote Sensing Student's Signature _____

Academic Year 2012 Advisor's Signature _____

ACKNOWLEDGEMENTS

First of all, I wish to express my sincere gratitude to my advisor, Asst. Prof. Dr. Songkot Dasananda for his support, guidance, encouragement and valuable suggestions throughout this study. I would also like to thank Asst. Prof. Dr. Sunya Sarapirome, the committee chairperson, for his several useful comments on my work. And I wish to extend my special thanks to the other committee members, Assoc. Prof. Dr. Suwit Ongsomwang, Asst. Prof. Dr. Nares Chuersuwan, Dr. Dusde Chanlikit and Assoc. Prof. Dr. Sura Pattanakiat for their contributions to my study.

I would also like to thank the following organizations for providing essential data required in the research: the Air Quality and Noise Management Bureau, Pollution Control Department, and Land Development Department (LDD).

I gratefully express my full appreciations to Lt. Col. Watcharaporn Pimpa, Mrs. Sirilak Tanang, Ms. Ratchaneekorn ChatUthai and all my friends at the School of Remote Sensing, for their help and being good friends for a long time.

Thanks are also due to the School of Remote Sensing, Institute of Science, Suranaree University of Technology, for giving me the opportunity to pursue a Ph.D. program in geoinformatics and to learn more about geoinformatics techniques, which are useful for my work in the future. Also, I would like to thank the Rajamangala University of Technology Isan for the scholarship granted for my study.

Finally, I would like to express my deepest gratitude to my family including my mother, my father, my brothers, my wife, my daughter and my son, for giving me the inspiration and continuous love, care and support.

Chat Phayungwiwatthanakoon

CONTENTS

Page

ABSTRACT IN THAI I

ABSTRACT IN ENGLISH III

ACKNOWLEDGEMENTS V

CONTENTS VII

LIST OF TABLES XI

LIST OF FIGURES XV

LIST OF ABBREVIATIONS XXV

CHAPTER

I INTRODUCTION 1

1.1 Background and significance of the study 1

1.2 Research objectives 4

1.3 Scope and limitations 5

1.4 Benefits of the study 6

1.5 Study area 6

1.6 Outline of the thesis 11

II LITERATURE REVIEW 12

2.1 Aerosol pollution 12

2.1.1 Aerosol impacts on human health 15

2.1.2 Aerosol impacts on climate 17

CONTENTS (Continued)

Page

2.2 AQI development and implementation 20
2.2.1 Derivation of AQI 21
2.2.2 WHO guidelines on aerosol regulation 25
2.3 Determination of AOD and PM concentration 27
2.3.1 Definition and derivation of aerosol optical depth (AOD) 27
2.3.2 Satellite-based measurement of AOD data 30
2.3.3 AERONET Network 33
2.3.4 Relationship between AOD and observed PM data 37
2.4 MODIS and BAER retrieval methods for AOD assessment 40
2.4.1 MODIS sensors and their standard products 40
2.4.2 MODIS-AOD retrieval algorithm 42
2.4.3 BAER-AOD retrieval algorithm 46
2.5 Atmospheric Dispersion Models 52
2.5.1 Types of air dispersion models 53
2.5.2 Prominent air dispersion models 58
2.5.3 The HYSPLIT dispersion model 61
III METHODOLOGY AND PRELIMINARY ANALYSIS 68
3.1 Conceptual framework 68
3.2 Data preparation 72
3.3 Research procedure 75

CONTENTS (Continued)

Page

3.3.1 Relationship analysis of MODIS-based parameters and PM10 data 75
3.3.2 Development of the fine-scale maps of NDAI, PM10 and AQI data 79
3.3.3 Newly-proposed method for AQI map 82
3.3.4 Applications of the HYSPLIT model 85
3.4 Preliminary analysis 86
3.4.1 General situation of PM10-based air pollution 86
3.4.2 General PM10 information of the preferred dates 100
3.4.3 MODIS radiance response to PM10 pollution severity 101
3.4.4 Applied details of the BAER retrieval method 103
IV RESULTS AND DISCUSSION 109
4.1 Relationships of MODIS-based parameters and PM10 data 109
4.1.1 Relationships of MODIS radiances with the reference PM10 data 109
4.1.2 Relationships of the MODIS-based parameters and AERONET-AOD with reference PM10 data 113
4.1.3 Mutual relations of MODIS-based parameters and AERONET-AOD 119
4.2 Applications of the derived NDAI, PM10 and AQI maps 122

CONTENTS (Continued)

Page

4.2.1 Derivation and application of the NDAI maps 122

4.2.2 Derivation and application of the BAER-AOD maps 132

4.2.3 Derivation and application of the AQI maps 154

V APPLICATIONS OF HYSPLIT MODEL 179

5.1 Forward trajectory and dispersion analysis 179

5.2 Backward trajectory assessment 196

5.2.1 Backward trajectory analysis for March 2010 196

5.2.2 Backward trajectory analysis for 2010 fire season 215

VI CONCLUSIONS AND RECCOMENDATION 224

6.1 Relationships of MODIS-based parameters and PM10 data 224

6.2 Derivation and application of NDAI, AOD, PM10 and AQI maps 225

6.3 Applications of HYSPLIT model 229

6.4 Recommendations 231

REFERENCES 233

APPENDICES 259

APPENDIX A VALIDATION OF DERIVED PM10 MAPS 260

APPENDIX B ADDITIONAL MODIS-BASED DAILY DATA 264

APPENDIX C AEROSOL SIZE DISTRIBUTION AND RELATED OPTICAL PARAMETERS 275

CURRICULUM VITAE 279

LIST OF TABLES

Table		Page
1.1	List of the known PM10 and AERONET measuring stations in the area	10
2.1a	Breakpoint data for AQI calculation by the US-EPA	22
2.1b	Breakpoint data for AQI calculation by the Thailand-PCD	22
2.1c	AQI categories and meaning adopted by the US-EPA and Thailand PCD	22
2.2a	Breakpoint data for AQI calculation in the UK	23
2.2b	AQI categories and meaning adopted by the UK-DEFRA (2012)	23
2.3	Breakpoint data for AQI calculation in the EU countries	25
2.4a	WHO air quality guideline and the interim targets for particulate matter (PM) based on the observed 24-hour concentrations	26
2.4b	WHO air quality guideline and the interim targets for particulate matter (PM) based on the annual mean concentrations	26
2.5	Notable satellite-based sensors for global aerosol observations	30
2.6	Reports of correlation between satellite-based AOD and AERONET-AOD.	35
2.7	Reports of linear relationship between AOD and near-ground PM	39
2.8	Major properties of the MODIS sensors.	41
2.9	List of MODIS spectral bands and their proposed primary uses.	41
3.1	Information of required input data and their contributing sources..	70

LIST OF TABLES (Continued)

Table		Page
3.2	Proportion of the LULC distribution presented in Figure 3.2	74
3.3	Classifying criteria of the PM10 (24-hour running mean concentration) and associated AQI data used in the three applied methods (PM10 unit: µg/m^3)...	81
3.4	Classifying criteria of the PM10 (24-hour running mean concentration) and associated AQI data used in the Newly-propose method (PM10 unit: µg/m^3)...	83
3.5	Monthly-mean PM10 data during 1996-2012 (unit: µg/m^3).....	87
3.6	Mean and 24hr-maximum measured PM10 data for annual fire seasons during 1996-2012 (unit: µg/m^3)...	88
3.7	Daily PM10 data during 2010 fire season recorded at the CM1 station in Chiang Mai Province (unit: µg/m^3).....	90
3.8	Daily observed PM10 data during 4th-9th April 2010 (unit: µg/m^3).....	98
3.9	Hourly variations of the observed PM10 data during 4th-8th April 2010 at Chiang Mai Province (average from stations CM1 and CM2) (µg/m^3).....	98
4.1a	Found linear relationships between the reference PM10 data and different MODIS-radiance.....	111
4.1b	Found linear relationships between the reference PM10 data and different MODIS-based parameters and AERONET-AOD data.....	114

LIST OF TABLES (Continued)

Table		Page
4.1c	Found linear relationships between MODIS-NADI and AERONET-AOD data	120
4.2	Distribution of NDAI and PM10 concentration over the area on 4^{th}-9^{th} April. 2010 (PM10 has unit of $\mu g/m^3$)	130
4.3	Distribution of BAER-AOD and PM10 over the area on 4^{th}-9^{th} April...	149
4.4	Proportion of PM10 data distribution at 0-400 $\mu g/m^3$...	150
4.5a	Averaged PM10 concentration ($\mu g/m^3$) over different LULC types (from Figure 4.8)	153
4.5b	Averaged PM10 concentration ($\mu g/m^3$) over different altitudes (from Figure 4.8)	153
4.6	Instructions for reducing risk from aerosol pollution.	157
4.7a	Distribution of the PM10 density over entire area on 4^{th} April 2010 based on the derived AQI maps by the four chosen methods (in Figure 4.11)...	173
4.7b	Distribution of the PM10 density over entire area on 5^{th} April 2010 based on the derived AQI maps by the four chosen methods (in Figure 4.12)...	174
4.7c	Distribution of the PM10 density over entire area on 6^{th} April 2010 based on the derived AQI maps by the four chosen methods (in Figure 4.13)..	175

LIST OF TABLES (Continued)

Table		Page
4.7d	Distribution of the PM10 density over entire area on 7th April 2010 based on the derived AQI maps by the four chosen methods (in Figure 4.14)..	176
4.7e	Distribution of the PM10 density over entire area on 8th April 2010 based on the derived AQI maps by the four chosen methods (in Figure 4.15)..	177
4.7f	Distribution of the PM10 density over entire area on 9th April 2010 based on the derived AQI maps by the four chosen methods (in Figure 4.16)..	178
5.1a	Location distribution of active fire spots during 4nd-8th April 2010....	181
5.1b	Location distribution of fire clusters during 4nd-8th April 2010.....	181
5.2	Percentage of total data associated to each mean back trajectory (or cluster) for each month (from Figure 5.15). Note: DIR ≡ Direction.....	219
5.3	Predominant directions for each province during 2010 fire season.....	221
5.4	Percentage of total data associated to each mean back trajectory (or cluster) for the 2010 fire season (from Figure 5.16).....	221

LIST OF FIGURES

Figure **Page**

1.1 Map of the study area showing provincial boundary, elevation (DEM) and locations of the ground-based PM10 and AERONET measuring stations 7

1.2 Classified LULC map of the study area 8

2.1 Diagram showing size distribution in micrometers (μm) of various types of atmospheric particulate matter (PM) 14

2.2 Penetration of airborne particulates into the respiratory system 17

2.3 Main radiative forcing components of the earth's radiative balance system as described in the IPCC reports in 2007 19

2.4 Global maps of the satellite-based AOD for the aerosols both in fine and coarse modes derived from the MODIS data. 32

2.5 Locations of the AERONET instruments in Thailand 36

2.6 AERONET instruments at Chulalongkorn University in Bangkok..... 37

2.7 The linear relationship between MODIS-AOT and observed PM 2.5 data at several cities around the world..... 38

2.8 Flowchart of MODIS's aerosol retrieval algorithm..... 44

2.9 Original AOD retrieval procedure of the BARE method..... 51

LIST OF FIGURES (Continued)

Figure **Page**

2.10 Example of the LUT for the relationship between the aerosol reflectance and AOT (for 0.412 μm) at different values of surface reflectance (0.02±0.02) 52

2.11 Conceptual presentation of the box dispersion model 54

2.12 Dispersing pattern of air pollutant plume in the Gaussian models 56

2.13 The Eulerian and Lagrangian approach used in the HYSPLIT model 62

2.14 Examples of (a) particle-based and (b) puff-based concentration maps produced by the HYSPLIT model 64

3.1a Conceptual framework of the study for Objectives 1 and 2 69

3.1b Conceptual framework of the study for Objectives 3 70

3.2 Classified LULC map of the study area 74

3.3 Example of derived MODIS-based data maps on 6th April 2010 77

3.4 Variation of the monthly-mean PM10 data in the area. The maximum and minimum values occur in March and August, respectively 87

3.5a Mean observed PM10 data in the area for annual fire seasons during 1996-2012 (from Table 3.5) 89

3.5b Variation of the 24hr-maximum PM10 data for annual fire seasons during 1996-2012 (from Table 3.5) 89

3.6 Daily PM10 data in 2010 fire season recorded at the CM1 station 91

LIST OF FIGURES (Continued)

Figure **Page**

3.7 Composite MODIS images taken during 4^{th}-9^{th} April 2010 including the visible image [RGB: 1(red)/4(green)/3(blue)] and Mid-IR image..... 92

3.8 Time sequences of the PM10 concentrations during 4^{th}-9^{th} April 2010 at Chiang Mai Province (average from stations CM1 and CM2)..... 99

3.9 Averaged reflectance values of MODIS Bands 1-7 at different levels of PM10 pollution severity from very low to high (based on MODIS-AOD data)…… 102

3.10 Linear relationship of reflectance data in MODIS-Band 3 (blue) and Band 7 (MIR) over the study area with $R^2 = 0.82$……..... 102

3.11 Modified BAER-AOD retrieval algorithm used in Song et al. (2008) and was adopted for the study in this thesis (with some modifications) …... 104

3.12 Derived monthly surface reflectance maps (A_{SF}) of January-April 2010 106

3.13 Established relationship between the AERONET-AOD (at 440 nm) and defined aerosol reflectance (ρ_{AS}) (at 470 nm) found in this study…....…108

4.1a Linear relationship of the reflectance data for blue band (Band 3) and reference PM10 data ($R^2 = 0.710$)..... 111

4.1b Linear relationship of the reflectance data in green band (Band 4) and measured PM10 data ($R^2 = 0.616$)..... 112

4.1c Linear relationship of the reflectance data for red band (Band 1) and reference PM10 data ($R^2 = 0.563$)..... 112

LIST OF FIGURES (Continued)

Figure		Page
4.1d	Linear relationship of the reflectance data in MIR band (Band 7) and measured PM10 data ($R^2 = 0.029$)	113
4.2a	Linear relationship of ΔR and reference PM10 data ($R^2 = 0.667$)	115
4.2b	Linear relationship of NADI and reference PM10 data ($R^2 = 0.661$)	115
4.2c	Linear relationship of MODIS-AOD (at 550 nm) and the reference PM10 data (with $R^2 = 0.720$)	117
4.2d	Linear relationship of the BAER-AOD (at 440 nm) and the reference PM10 data (with $R^2 = 0.784$)	117
4.2e	Linear relationship of AERONET-AOD (at 440 nm) and reference PM10 data (with $R^2 = 0.86$)	119
4.3a	Linear relationship of NADI and ΔR (blue) data (with $R^2 = 0.803$)	120
4.3b	Linear relationship of the AERONET-AOD (440 nm) and MODIS-AOD (550 nm) (with $R^2 = 0.832$)	121
4.3c	Linear relationship of the BAER-AOD (440 nm) and AERONET-AOD (440 nm) (with $R^2 = 0.828$)	121
4.4a	(a) NDAI and (b) the associated PM10 maps on 4th April 2010	124
4.4b	(a) NDAI and (b) the associated PM10 maps on 5th April 2010	125
4.4c	(a) NDAI and (b) the associated PM10 maps on 6th April 2010	126
4.4d	(a) NDAI and (b) the associated PM10 maps on 7th April 2010	127
4.4e	(a) NDAI and (b) the associated PM10 maps on 8th April 2010	128

LIST OF FIGURES (Continued)

Figure		Page
4.4f	(a) NDAI and (b) the associated PM10 maps on 9th April 2010	129
4.5a	Comparison of the derived PM10 data (PM_{NDAI}) and reference PM10 data (PM_{REF}) (with MAE = 10.78 %)	131
4.5b	Relation of the derived PM10 data (PM_{NDAI}) and reference PM10 data (PM_{REF}) (with $R^2 = 0.628$)	132
4.6a	Maps of (a) MODIS-AOD and (b) BAER-AOD data on 4th April 2010	136
4.6b	Maps of (a) MODIS-AOD and (b) BAER-AOD data on 5th April 2010	137
4.6c	Maps of (a) MODIS-AOD and (b) BAER-AOD data on 6th April 2010	138
4.6d	Maps of (a) MODIS-AOD and (b) BAER-AOD data on 7th April 2010	139
4.6e	Maps of (a) MODIS-AOD and (b) BAER-AOD data on 8th April 2010	140
4.6f	Maps of (a) MODIS-AOD and (b) BAER-AOD data on 9th April 2010	141
4.7a	Maps of PM10 derived from (a) MODIS-AOD and (b) BAER-AOD data on 4th April 2010 (using relationships expressed in Table 4.1)	142
4.7b	Maps of PM10 derived from (a) MODIS-AOD and (b) BAER-AOD data on 5th April 2010 (using relationships expressed in Table 4.1)	143
4.7c	Maps of PM10 derived from (a) MODIS-AOD and (b) BAER-AOD data on 6th April 2010 (using relationships expressed in Table 4.1)	144
4.7d	Maps of PM10 derived from (a) MODIS-AOD and (b) BAER-AOD data on 7th April 2010 (using relationships expressed in Table 4.1)	145

LIST OF FIGURES (Continued)

Figure **Page**

4.7e Maps of PM10 derived from (a) MODIS-AOD and (b) BAER-AOD data on 8th April 2010 (using relationships expressed in Table 4.1) 146

4.7f Maps of PM10 derived from (a) MODIS-AOD and (b) BAER-AOD data on 9th April 2010 (using relationships expressed in Table 4.1) 147

4.8 Maps of (a) the averaged AOD and (b) PM10 on period of 4th-9th April 2010 (based on AOD and PM10 maps expressed in Figures 4.6 and 4.7).. 148

4.9 Histogram of the PM10 data occurred in the area during 4th-9th 2010 151

4.10a Comparison of the derived PM10 data (PM_{BAER}) and the reference PM10 data (PM_{REF}) (with MAE = 2.2 %)..... 152

4.10b Correlation of the derived PM10 data (PM_{BAER}) and reference PM10 data (PM_{REF}) (with $R^2 = 0.744$)..... 152

4.11 Derived AQI maps on 4th April 2010 based on (a) standards of the PCD, (b) US-EPA, (c) UK-DEFRA and (d) by the newly-proposed method 161

4.12 Derived AQI maps on 5th April 2010 based on (a) standards of the PCD, (b) US-EPA, (c) UK-DEFRA and (d) by the newly-proposed method 163

4.13 Derived AQI maps on 6th April 2010 based on (a) standards of the PCD, (b) US-EPA, (c) UK-DEFRA and (d) by the newly-proposed method 165

4.14 Derived AQI maps on 7th April 2010 based on (a) standards of the PCD, (b) US-EPA, (c) UK-DEFRA and (d) by the newly-proposed method 167

LIST OF FIGURES (Continued)

Figure **Page**

4.15 Derived AQI maps on 8th April 2010 based on (a) standards of the PCD, (b) US-EPA, (c) UK-DEFRA and (d) by the newly-proposed method 169

4.16 Derived AQI maps on 9th April 2010 based on (a) standards of the PCD, (b) US-EPA, (c) UK-DEFRA and (d) by the newly-proposed method 171

5.1 Example of the forward trajectories of smoke plumes (starting from 03.00 UTC of 2nd April 2010 onward) originated at three different locations 180

5.2 MODIS-based fire map over period of 4th-9th April 2010 and the assumed locations of fire spots for each grid cell.. 180

5.3a Forward trajectories of smoke plumes originated on 4th April 2010 from the pre-assigned fire clusters (starting at 03.00 UTC or 10.00 LST)..... 183

5.3b Distributing pattern of smoke plumes originated on 4th April 2010 from the pre-assigned fire clusters (12-hour forward starting at 10 AM) 183

5.3c Distributing pattern of smoke plumes originated on 4th April 2010 from the pre-assigned fire clusters (24-hour forward starting at 10 AM) 184

5.3d Distributing pattern of smoke plumes originated on 4th April 2010 from the pre-assigned fire clusters (48-hour forward starting at 10 AM) 184

5.4a Forward trajectories of smoke plumes originated on 5th April 2010 from the pre-assigned fire clusters (starting at 03.00 UTC or 10.00 LST)..... 185

LIST OF FIGURES (Continued)

Figure **Page**

5.4b Distributing pattern of smoke plumes originated on 5th April 2010 from the pre-assigned fire clusters (12-hour forward starting at 10 AM) 185

5.4c Distributing pattern of smoke plumes originated on 5th April 2010 from the pre-assigned fire clusters (24-hour forward starting at 10 AM) 186

5.4d Distributing pattern of smoke plumes originated on 5th April 2010 from the pre-assigned fire clusters (48-hour forward starting at 10 AM)….. 186

5.5a Forward trajectories of smoke plumes originated on 6th April 2010 from the pre-assigned fire clusters (starting at 03.00 UTC or 10.00 LST)..... 187

5.5b Distributing pattern of smoke plumes originated on 6th April 2010 from the pre-assigned fire clusters (12-hour forward starting at 10 AM) 187

5.5c Distributing pattern of smoke plumes originated on 6th April 2010 from the pre-assigned fire clusters (24-hour forward starting at 10 AM) 188

5.5d Distributing pattern of smoke plumes originated on 6th April 2010 from the pre-assigned fire clusters (48-hour forward starting at 10 AM) 188

5.6a Forward trajectories of smoke plumes originated on 7th April 2010 from the pre-assigned fire clusters (starting at 03.00 UTC or 10.00 LST)..... 189

5.6b Distributing pattern of smoke plumes originated on 7th April 2010 from the pre-assigned fire clusters (12-hour forward starting at 10 AM) 189

5.6c Distributing pattern of smoke plumes originated on 7th April 2010 from the pre-assigned fire clusters (24-hour forward starting at 10 AM) 190

LIST OF FIGURES (Continued)

Figure **Page**

5.6d Distributing pattern of smoke plumes originated on 7th April 2010 from the pre-assigned fire clusters (48-hour forward starting at 10 AM) 190

5.7a Forward trajectories of smoke plumes originated on 8th April 2010 from the pre-assigned fire clusters (starting at 03.00 UTC or 10.00 LST)..... 191

5.7b Distributing pattern of smoke plumes originated on 8th April 2010 from the pre-assigned fire clusters (12-hour forward starting at 10 AM) 191

5.7c Distributing pattern of smoke plumes originated on 8th April 2010 from the pre-assigned fire clusters (24-hour forward starting at 10 AM) 192

5.7d Distributing pattern of smoke plumes originated on 8th April 2010 from the pre-assigned fire clusters (48-hour forward starting at 10 AM) 192

5.8 Back trajectory maps for the CM1 station in Chiang Mai Province (during March 2010) over the (a) 3, (b) 12, (c) 24, and (d) 48-hour periods . 197

5.9 Back trajectory maps for the CR1 station in Chiang Mai Province (during March 2010) over the (a) 3, (b) 12, (c) 24, and (d) 48-hour periods . 199

5.10 Back trajectory maps for the LPA1 station in Chiang Mai Province (during March 2010) over the (a) 3, (b) 12, (c) 24, and (d) 48-hour periods . 201

5.11 Back trajectory maps for the LPH1 station in Chiang Mai Province (during March 2010) over the (a) 3, (b) 12, (c) 24, and (d) 48-hour periods . 203

5.12 Back trajectory maps for the MHS1 station in Chiang Mai Province (during March 2010) over the (a) 3, (b) 12, (c) 24, and (d) 48-hour periods . 205

LIST OF FIGURES (Continued)

Figure **Page**

5.13 Back trajectory maps for the NAN1 station in Chiang Mai Province (during March 2010) over the (a) 3, (b) 12, (c) 24, and (d) 48-hour periods . 207

5.14 Back trajectory maps for the PH1 station in Chiang Mai Province (during March 2010) over the (a) 3, (b) 12, (c) 24, and (d) 48-hour periods . 209

5.15 Back trajectory maps for the PY1 station in Chiang Mai Province (during March 2010) over the (a) 3, (b) 12, (c) 24, and (d) 48-hour periods . 211

5.16 Mean back trajectory maps (48-hour period) for January-April 2010. The presented numbers (in percent) are propotion of data along each direction... 216

5.17 Back Mean back trajectory map (48-hour period) for the 2010 fire season. The presented numbers (in percent) are propotion of data along each direction 218

5.18 Mean back trajectory diagram (48-hour period) for 2010 fire season for all provinces in the study area 222

LIST OF ABBREVIATIONS

AERONET	=	Aerosols Robotic Network
AOD	=	Aerosol Optical Depth
AOT	=	Aerosol Optical Thickness
AQI	=	Air Quality Index
ARL	=	Air Resources Laboratory
BAER	=	Bremen Aerosol Retrieval
DEFRA	=	Department for Environment Food and Rural Affairs
DEM	=	Digital Elevation Model
GDAS	=	Global Data Assimilation System
HYSPLIP	=	Hybrid Single-Particle Lagrangian Integrated Trajectory
LDD	=	Land Development Department
LULC	=	Land Use and Land Cover
LUT	=	Look-up table
m. MSL.	=	meter above Mean Sea Level
MODIS	=	Moderate Resolution Imaging Spectroradiomer
PCD	=	Pollution Control Department
PD	=	Polluted dates
PFD	=	Pollution-free date
PM10	=	Particulate Matter with size of less than 10 μm
PM2.5	=	Particulate Matter with size of less than 2.5 μm

LIST OF ABBREVIATIONS (Continued)

TMD	=	Thai Meteorological Department
TOA	=	Top of Atmosphere
US-EPA	=	US-Environmental Protection Agency
WHO	=	World Health Organization

CHAPTER I

INTRODUCTION

1.1 Background and significance of the study

Airborne particulate matter (PM) is typically referred to a mixture of the fine solid particles and liquid droplets that are suspended in the atmosphere with size ranging from approximately 0.001 to 100 micrometers (μm) in aerodynamic diameter. Elementary compounds of most PM particles are sulfate, nitrate, chloride, elemental and organic carbons, crustal material, and biological material. In general, only a portion of the PM with size of < 10 μm (called PM10) is having most attention in field of air pollution research due to their ability to get pass body's natural defenses in the nose and throat before travelling deeper into the lung that might cause adverse health effects afterwards. At present, three broad categories of the PM particles are traditionally measured: coarse (2.5-10 μm), fine (< 2.5 μm) or PM2.5, and ultrafine (< 0.1 μm) or PM0.1 (Harrison and Yin, 2000; WHO, 2006a; U.S. EPA, 2013).

PM is regarded as being one of the fundamental pollutants that lead to the formation of critical air pollution around the world. If inhaled beyond certain limits for a considerable amount of time, it can introduce several severe health problems, e.g. asthma and respiratory, lung or cardiovascular diseases (Brunekreef and Holgate, 2002; Curtis, Rea, Smith-Willis, Fenyves, and Pan, 2006; Kampa and Castanas, 2008; Rückerl, Schneider, Breitner, Cyrys, and Peters (2011).

Recently, as reported in Lim et al. (2012), current air pollution (especially that caused by fine particles) has contributed to an estimate of over 3 million premature deaths each year and become a great threat for health and life of people worldwide. In addition, aerosol is also believed to have an important role in the controlling of some fundamental climatic mechanisms, like rainfall formation or earth radiation balancing system (Charlson et al., 1992; IAPSAG, 2007; Andreae and Rosenfeld, 2008; Tao, Chen, Li, Wang, and Zhang, 2012). As a consequence, great attention was paid to get insightful understanding on the spatial and temporal characteristics of PM pollution characteristics and their associated effects in recent decades (WHO, 2006b; Daly and Zannetti, 2007; Fenger, 2009).

In the past, knowledge of PM concentration (in both temporal and spatial aspects) was mostly contributed from data series obtained from air quality monitoring networks or from occasional measuring campaigns. These practices often require high implementation and maintenance costs and are rather limited in terms of the spatial coverage. However, at present, these usual drawbacks can be minimized through the continuous observation of the near-ground aerosol data by a wide range of satellite-based sensors, e.g. MODIS, MISR or CALIOP, that can be used as complementary information to the conventional ground-based database. Satellite-based observations are now acknowledged as a useful resource for the analysis of the spatial structure and concentration distribution of aerosol pollution and its impacts at global, regional, or local scales, especially with support of advanced GIS data analyzing and management tools (Kaufman, Tanŕe and Boucher, 2002; Engel-Cox, Hoff, and Haymet, 2004; Hoff and Christopher, 2009; Kokhanovsky and Leeuw, 2009).

In Thailand, two main sources of the persistent observed aerosol pollution are the crowded transportation and expansive biomass burning (e.g. forest fires). The first one can lead to aerosol pollution observed in big cities like Bangkok and Chiang Mai while the second can introduce severe air pollution usually found during dry period in the northern and western parts of Thailand (Pollution Control Department, 2012). For example, during March 2007, expansive forest and agricultural fires had introduced intensified air pollution in four provinces of the upper northern Thailand: Nan, Chiang Mai, Chiang Rai and Mae Hong Son. As a consequence, some areas were subsequently declared disaster zones due to the almost zero visibility and notably high numbers of people seeking medical assistance for respiratory illness (Ministry of Natural Resources and Environment, 2007). Serious aerosol pollution conditions over upper northern Thailand were also reported in 2010 and 2012.

Though, merit of the satellite-based PM observations has been recognized worldwide at present, the study of this kind is still rather infrequent in Thailand (e.g. Kim, Upadhyay, Zhuang, Hao and Murthy, 2006; Chew, Chang, Salinas and Liew, 2007; Kishi, Takeuchi and Sawada, 2008). Moreover, measurement of PM concentration at a relatively fine scale (e.g. < 1 km resolution) has never been reported here before. As a result, most knowledge on severity and distributing pattern of concerned aerosol pollution experienced in the country is still drawn principally from network of sparse ground-base measurements under supervision of the Pollution Control Department (PCD) or from the limited measuring campaigns conducted over some hot spot areas. These methods are theoretically still inadequate for the monitoring and modeling of air pollution evolution over large area, e.g. at provincial or regional scales, which is necessary for the better understanding and more effective

management of the referred incidence by the responsible agencies.

To fulfill the still lack of satellite-based aerosol observation and mapping in Thailand, this thesis has explored potential capability of the satellite-based data from MODIS instrument onboard NASA's Terra satellite, in the monitoring and mapping of the near-ground PM10 concentration (due to biomass burning) over eight provinces of the upper northern Thailand (at a resolution of 500 m). In addition, applications of the HYSPLIT model to simulate trajectory and distributing pattern of the fire-induced smoke plume were also performed with principal aim to acquire better understanding about impact of fire locations on air pollution situation observed over the area during 2010 fire season. It is hoped that the results achieved from all works carried out in this thesis shall yield efficient PM10 and AQI determination and mapping methods from the MODIS imagery that could be applied fruitfully both in Thailand and elsewhere, and to gain better understanding on influence of the fire locations on aerosol pollution situation encountered over the entire study area.

1.2 Research objectives

This research has three specific objectives as follows:

1.2.1 To establish a spatial model of MODIS data and its significance and PM10 concentration data.

1.2.2 To produce, implement and identify fine-scale NDAI, PM10 and AQI maps using the developed algorithms for the analysis of the daily aerosol pollution situation.

1.2.3 To apply the chosen air dispersion and trajectory model (HYSPLIT) to predict the smoke plume trajectory and distributing pattern during the 2010 fire season (both forward and backward analysis) in the upper northern Thailand.

1.3 Scope and limitations

1.3.1 The study area covers 8 provinces situated in the upper part of northern Thailand, which are, Chiang Mai, Chiang Rai, Lampang, Lamphun, Mae Hong Son, Nan, Phayao, and Phrae, with a total area of about 88,370 km^2 (Figure 1.1).

1.3.2 Only dates with relatively high levels of PM10 (as reported by PCD) and with high quality of MODIS data (in terms of cloud cover in particular) were chosen for the detailed analysis.

1.3.3 Only those PM particles with size of less than 10 μm (PM10), not including particles with size of less than 2.5 μm were studied during the fire season.

1.3.4 All relationships of the data obtained from studies with PM10 were assumed to be linear equation.

1.3.5 The HYSPLIT model was chosen for performing smoke plume dispersion analysis in forward and backward analysis of air trajectory.

1.3.6 The dispersion of PM10 in the HYSPLIT model is calculated by assumption in puff-based dispersion with GDAS-meteorological data.

1.3.7 All obtained secondary data were assumed to be valid and proper for use in the relevant analysis.

1.4. Benefits of the study

1.4.1 Knowledge on the relationships of MODIS radiances (in blue, green, red, and Mid-IR bands), MODIS-AOD, BAER-AOD, AERONET AOD, and NDAI with the reference PM10 data was obtained.

1.4.2 Effective AOD, PM10 and AQI mapping methods from the MODIS imagery to support air pollution monitoring and quantification over large area were developed.

1.4.3 MODIS-based NDAI, PM10 and AQI maps (at 500-m resolution) which are appropriate for the assessment of aerosol pollution over the entire study area during the 2010 fire season of interest were produced.

1.4.4 Understanding of the impact of the fire locations on the PM-led air pollution situation that occurred over the study area during the 2010 fire season based on the applications of the HYSPLIT model was gained.

1.4.5 Understanding of the trajectory of smoke plume and its probable effects on the health of the community was obtained.

มหาวิทยาลัยเทคโนโลยีสุรนารี

1.5 Study area

The chosen study area covers eight provinces in the upper northern part of Thailand: Chiang Mai, Chiang Rai, Lampang, Lamphun, Mae Hong Son, Nan, Phayao, and Phrae, with a total area of 88,370 km^2 (Figure 1.1). Among these, Chiang Mai is acknowledged as being the key economic, administrative and tourism center of the region, with size of about 20,107 km^2 and population of about 1.65 million in 2011 (out of the overall 5.67 million in the area). The location is bordered by two neighboring countries, Myanmar (Burma) on the west and Laos on east. Dominant topography is a network of high mountain ranges in, which forest has occupied about

70% and agricultural land contributes about 25% of the entire region (LDD, 2007). Its elevation ranges from 100 to 2,600 m above mean sea level. In addition, only a small portion of the total area (about 3%) is classified as urban and built-up land (Figure 1.2).

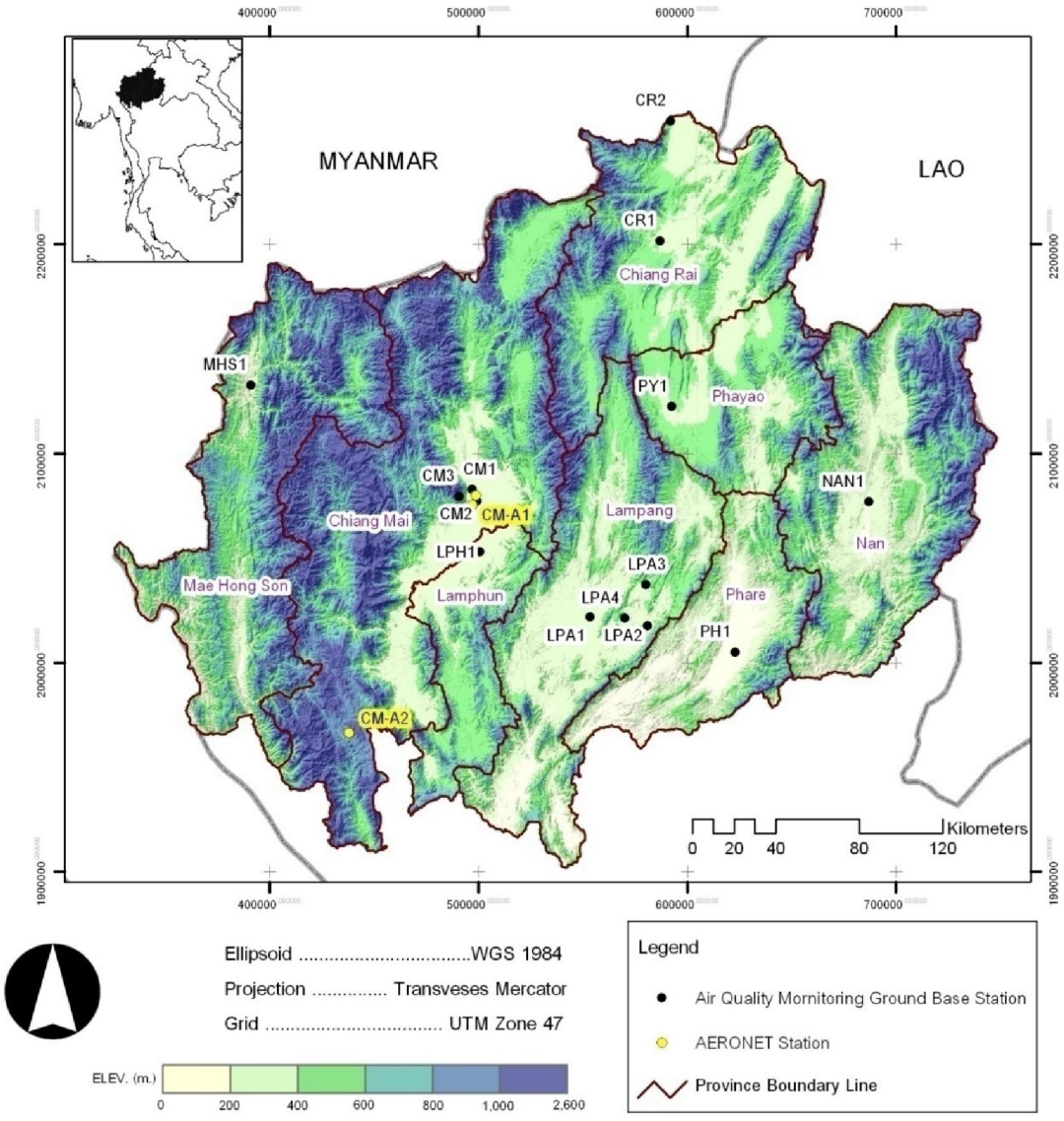

Figure 1.1 Map of the study area showing provincial boundary, elevation (DEM) and locations of the ground-based PM10 and AERONET measuring stations.

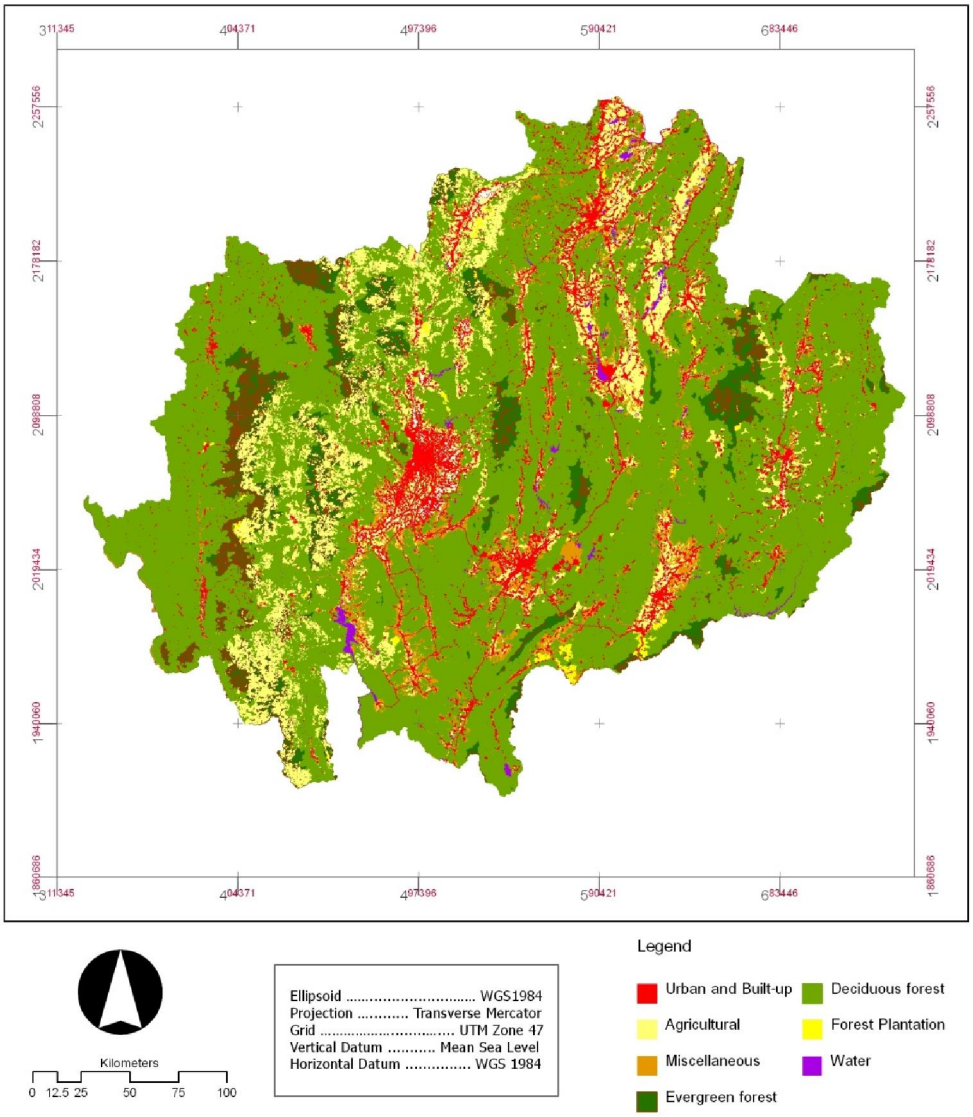

Figure 1.2 Classified LULC map of the study area (LDD, 2007).

Among the forest lands, deciduous forest is found most abundant followed by evergreen forest while paddy fields and field crop plantations are distributed mostly within the lowland flood plain close to several main water resources, e.g., Ping River. The weather is normally hot and humid where most rainfall occurs during monsoon season (from May to mid-October) while for the rest of the year is rather dry. During

rainy period, climate is mainly controlled by the southwest monsoon (originated in the Indian Ocean), the tropical monsoon trough, and the Pacific-born tropical cyclones (e.g. typhoon), respectively. In dry season (from mid-October to April), the weather is relatively cold during November to February (winter period) due to strong influences of the dry and cold northeast monsoon (originated in Siberia) and huge cold air mass occasionally moving down to the area from China. Summertime is most pronounced in March and April due mainly to the high insolation during this time (Thai Meteorological Department, 2007).

One of the persistent environmental problems found in the area is critical air pollution due to sharp increase of the PM concentration during February-April each year. Origin of this incidence is often contributed to the dramatic rise in total number of the vegetation fires observed both within and outside the area (mainly by the local people for the gathering of forest product and for agricultural purposes). In general, the aerosol pollution is getting worst during fire season (January-April) for all studied provinces with peak values often recorded in March and April and the lowest values are mostly exhibited during monsoon season, especially August and September (Pollution Control Department, 2013). Most knowledge about air pollution situation in the area at present is derived from daily data of some key pollutants like PM, O_3, and CO recorded at ten air quality measuring stations of the Pollution Control Department (PCD) located within the area (Table 1.1 and Figure 1.1).

Table 1.1 List of the known PM10 and AERONET measuring stations in the area.

Province	Station/Location	Operating since		Code
		A.D.	B.E.	
Chiang Mai	1. Chiang Mai Provincial Hall	1996	2539	CM1
	2. Yupparaj Wittayalai School	1996	2539	CM2
	3. The Bhubing Palace	2008	2551	CM3
	4. TMD Provincial Office (AERONET)	2006	2548	CM-A1
	5. Omkoi District (AERONET)	2003	2545	CM-A2
Chiang Rai	1. MNRE Provincial Office	2008	2551	CR1
	2. Mae Sai Health Office	2011	2554	CR2
Lampang	1. The City Pillar Shrine	1996	2539	LPA1
	2. Sob Pad Health Station (Mae Mo District)	1996	2539	LAP2
	3. Ta Si Health Station (Mae Mo District)	1997	2540	LAP3
	4. Mae Mo Waterworks Authority Office	1997	2540	LAP4
Lamphun	1. Lamphun PAO Sport Stadium	2009	2552	LPH1
Mae Hong Son	1. MNRE Provincial Office	2008	2551	MHS1
Nan	1. Nan Municipality Office	2009	2552	NAN1
Phrae	1. TMD Provincial Office	2010	2553	PH1
Phayao	1. Phayao Knowledge Park	2010	2553	PY1

1.6 Outline of the thesis

Structure of this thesis is divided into six principal chapters along with three complementary appendices. Brief details of each chapter are as follows.

Chapter I provides problem background and significances of the study along with the objectives, scope and limitations and benefits of the study, and also general description on some aspects of the study area.

Chapter II provides knowledge on several topics relating to aerosol pollution study including: (1) basic knowledge of aerosol pollution and its principal impacts, (2) concept of AQI development and implementation, (3) standard methods for AOD and PM concentration determination, (4) descriptions of MODIS and BAER retrieval methods for AOD assessment, and (5) basic knowledge on working concepts of some atmospheric dispersion models and their main applications.

Chapter III provides information of the conceptual framework for entire study and also the research methodologies, which is separated into three parts in accordance with the proposed objectives stated in Section 1.2. In addition, preliminary analysis on some topics including PM10 pollution situation, sensitivity of MODIS Bands 1-7 to the aerosol pollution variation and details of the BAER retrieval method in use was performed and the obtained results are reported in this chapter.

Chapter IV provides conclusive results achieved for the first two objectives of the thesis along with the discussion or interpretation of these obtained results.

Chapter V provides the results obtained from the applications of the HYSPLIT model to the simulation of smoke plume's trajectory and dispersion pattern.

Chapter VI provides overall conclusions of main results achieved in this study and some recommendations for the development of further studies.

CHAPTER II

LITERATURE REVIEW

This chapter provides fundamental knowledge on several topics including: (1) aerosol pollution, (2) AQI development/implementation, (3) Determination of AOD and PM concentration, (4) MODIS and BAER retrieval methods for AOD assessment, and (5) atmospheric dispersion models. Their specific details are as follows.

2.1 Aerosol pollution

Air pollution is typically defined as the atmospheric condition in which the air is contaminated or polluted with sufficient harmful substances that can interfere with human health or welfare, or produce other harmful environmental effects (US-EPA, 2006). The incidence is currently regarded as one of the prime environmental threats to human life and the fertility of pristine nature (WHO, 2006a; 2006b; Kampa and Castanas, 2008; Fenger, 2009; Lim et al., 2012). According to the US-Environmental Protection Agency (US-EPA), there are six criteria pollutants that must be monitored by law: (1) particulate matter (PM), (2) ground-level ozone (O_3), (3) carbon monoxide (CO), (4) sulfur dioxide (SO_2), (5) nitrogen oxides (NO_x) and (6) lead (Pb) (US-EPA, 2012). Among these, great rise of PM pollutants in the lower atmosphere, both from the natural and anthropogenic sources, is found more often than other listed pollutants and has become a cause of global concern at present (WHO, 2006b; Lee, Li, Kim and Kokhanovsky, 2009; Lim et al., 2012).

Airborne particulate matter (PM) is typically referred to a mixture of tiny solid particles and liquid droplets that are suspended in the lower atmosphere with great variety in its size, composition, and origin (WHO, 2006a; US-EPA, 2013). Normally, common sizes of PM particle are ranging from 0.001 to 100 micrometers (μm) in aerodynamic diameter and dominant elementary compounds are the sulfate, nitrate, chloride, elemental/organic carbons, crustal material, and biological material (Harrison and Yin, 2000). Some of the well-known PM forms seen in nature are soot, ash, smoke, smog and dust (Figure 2.1). Based on the contributing sources, PM can be classified into two broad categories: primary and secondary type. Primary aerosols are those released directly into the earth's lower atmosphere in form of condensed solids or liquids from their contributing sources (e.g. volcanic ash, fire-induced smoke or soil dust) whereas the secondary aerosols are those originated within the atmosphere as synthesized product of complicated chemical reactions of their gaseous precursors (e.g. SO_2 or NO_x) (Jacob, 1999; Vallero, 2008).

Prominent contributing sources of the primary aerosols, as well as the gaseous precursors of the secondary aerosols, can be differentiated into two broad categories: natural processes (called the natural aerosols), e.g., windborne dust, volcanic activities and biomass burning; and human activities (called anthropogenic aerosols), e.g. fossil fuel combustion, industrial processes, nonindustrial fugitive sources (e.g. construction work), and transportation sources (e.g. automobiles). At present, the natural aerosols are found much more dominant in lower atmosphere than the anthropogenic ones on global scale (about 90% to 10% by mass in average). However, this superiority might be less obvious over certain area, e.g. highly-industrialized or highly-populated urban zones (Jacob, 1999; Chin, Kahn, and Schwartz, 2009; Voiland, 2010).

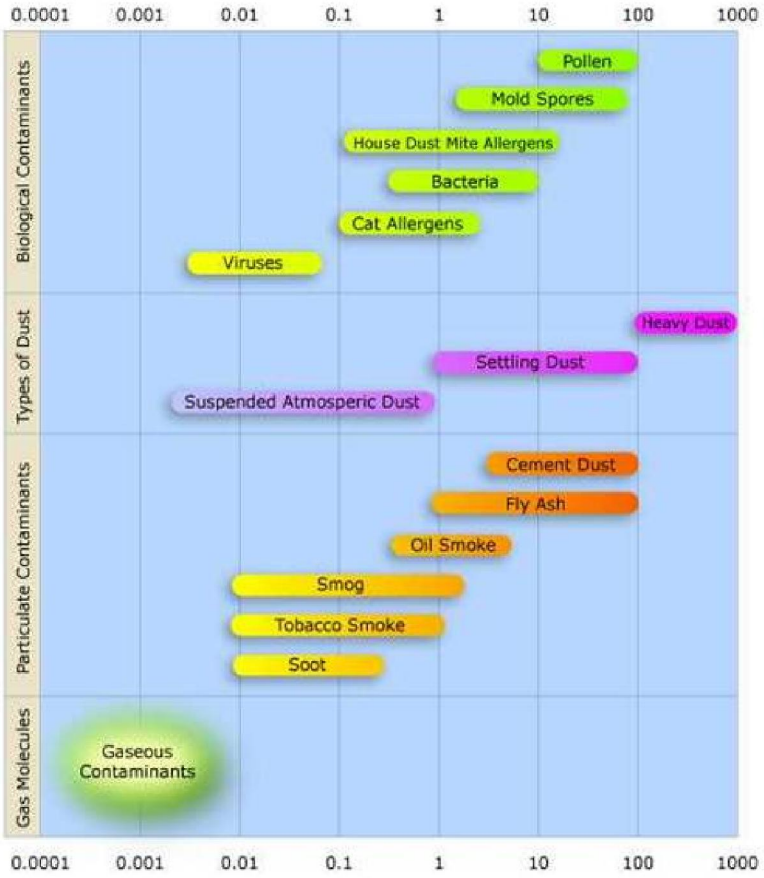

Figure 2.1 Diagram showing size distribution in micrometers (μm) of various types of atmospheric particulate matter (PM).

Source: http://en.wikipedia.org/wiki/File:Airborne-particulate-size-chart.jpg.

Though possible sizes of the PM particles might be much larger than 10 μm, however, only those with size of less than 10 μm (called PM10) is of great interest due to their abundance in nature and their notable ability to get pass natural defenses in the nose and throat before travelling into the lung that might be able to cause harmful health effect afterwards. At present, three categories of aerosol are traditionally classified: coarse (2.5-10 μm), fine (< 2.5 μm) or PM2.5, and ultrafine (< 0.1 μm) or PM0.1. In addition, the term "TSP" (total suspended particulate) is also

applied to represent all presented aerosol particles regardless to their size (WHO, 2006a; US-EPA, 2013).

Major sources of the found fine particles include motor vehicles, power plants, residential wood burning, forest fires, agricultural burning, and some industrial and combustion processes. For coarse particles, these are crushing or grinding operations, and dust stirred up by vehicles traveling on roads. In general, smaller/lighter particles tend to stay longer in the air after their formation. For large particles, they can settle to the ground more quickly by influence of gravity (maybe in a matter of hours) whereas very small particles can stay in the atmosphere for weeks and are mostly removed by precipitation eventually. These particles are suitable for the long-range transportation of the aerosol pollution (McClellan, 2002).

In reality, the 10-µm size does not represent a strict boundary between respirable and non-respirable particles, but it has been agreed upon for the monitoring of airborne particulate matter by most known regulatory agencies (along with PM2.5). At present, standard safety values (24hr average) for PM2.5 and PM10 recommended by the US-EPA are 40.4 µg/m^3 and 154 µg/m^3 respectively (Table 2.1a). In Thailand, the critical value for PM10 concentration is currently set at 120 µg/m^3 (24hr average) by the PCD (Pollution Control Department) (Table 2.1b). However, WHO guidelines have proposes critical value for PM10 (24hr average) at 50 µg/m^3 (WHO, 2006b).

2.1.1 Aerosol impacts on human health

PM is now regarded as being one of the fundamental pollutants that lead to the building up of the critical air pollution experienced around the world (Fenger, 2009). If inhaled beyond certain limits, these particles can introduce severe health problems

related to the respiratory system, e.g., aggravated asthma, respiratory symptoms, lung diseases, chronic bronchitis, or cardiovascular issues. Effects of inhaling particulate matter on human health have been extensively studied, e.g., Pearce and Crowards, 1996; Beeson, Abbey and Knutsen, 1998; Brunekreef and Holgate, 2002; Kan and Chen, 2004; Langkulsen, Jinsart, Karita and Yano, 2006; O'Connor et al., 2008; Jiménez, Linares, Rodriguez, Bleda and Diaz, 2009; Ruckerl, Schneider, Breitner, Cyrys, and Peters (2011). As reported in Lim et al. (2012), current air pollution (especially that arisen from fine PM particles) has contributed an estimate of more than three million premature deaths each year.

Size of the PM particle is a main determinant of where in the respiratory tract it will come to rest when being inhaled. Large particles are usually filtered out within nose and throat and do not cause much problem, but PM smaller than 10 μm (PM10) can settle in the bronchi and lungs while particles smaller than 2.5 μm (PM2.5) tend to penetrate into the gas-exchange region of the lungs and cause more severe problem (Figure 2.2). Moreover, very small particles (e.g. < 0.1 μm or PM0.1) may traverse pass through the lungs to affect other inner organs also (Englert, 2004). Fine particles are considered significantly dangerous for young children with developing lungs, the elderly, and all people who have asthma, bronchitis, other respiratory problems, and cardiovascular disease. In a recent study, due to the prolonged high concentrations of PM2.5 pollution over the city area, estimation of about 8,572 premature deaths were reported in four major Chinese cities in 2012 (Greenpeace, 2012).

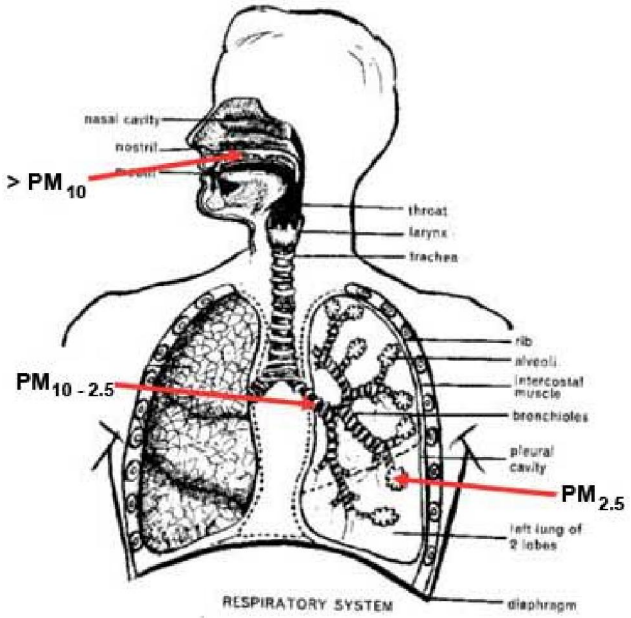

Figure 2.2 Penetration of airborne particulates into the respiratory system.

Source: http://shutthedoorhaveaseatblog.blogspot.com/2011/11/particulate-matter.

2.1.2 Aerosol impacts on climate

In addition, aerosol is also believed to have an important role in the controlling of some fundamental climatic mechanisms, like rainfall formation or global radiation balancing (Charlson et al., 1992; Levin and Cotton, 2009; Andreae and Rosenfeld, 2008; Tao et al., 2012). According to Charlson et al. (1992), radiative influences of the aerosols on climate can be classified as direct and indirect. The direct influence is associated to scattering and absorption of radiation by aerosol particles themselves whereas indirect influence is associated to influence of aerosol on cloud radiative properties. The direct influence of aerosol on climate has been known for decades to affect earth's radiation balance directly. The dominant processes are scattering and absorption of shortwave solar radiation that might reduce its intensity in the

atmosphere considerably during daytime. Aerosol particles can also absorb the earth's longwave (or infrared) radiation but this impact is relatively small in nature.

The indirect influence of aerosols on climate is resulted from their crucial role in the formation of cloud in the lower atmosphere. This is because the cloud particles (called cloud droplet) are normally generated by the condensation of water on existing aerosol particles, called cloud condensation nuclei (CCN). This implies that increased concentration of the CNN may result in having more clouds in the lower atmosphere. As ability of the cloud to reflect sunlight (defined by its albedo) depends critically on its thickness (or total amount of cloud particles); aerosols, therefore, inexplicitly help to reduce intensity of the incoming sunlight (shortwave portion in particular) before reaching the earth surface (through their role as an effective cloud producer). Reports of the Intergovernmental Panel on Climate Change-IPCC (2007) emphasize the significance of aerosol as a dominant source for the negative contribution to overall radiative forcing. This is in contrast to the greenhouse gases that generate net sum of the positive contribution that might lead to escalation of the global warming effect (Figure 2.3).

มหาวิทยาลัยเทคโนโลยีสุรนารี

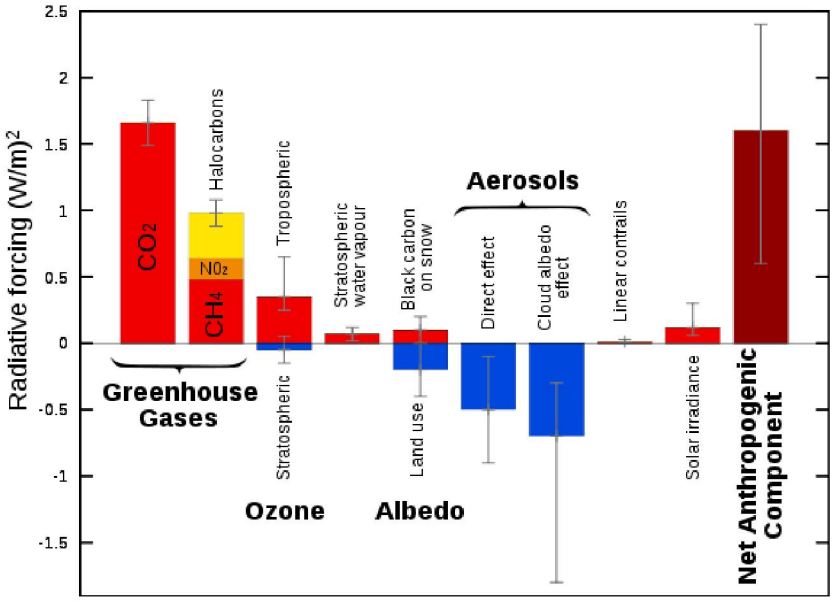

Figure 2.3 Main radiative forcing components of the earth's radiative balance system as described in the IPCC reports in 2007.

Source: http://en.wikipedia.org/wiki/File:Radiative-forcings.svg

However, precise roles of aerosols in the earth's radiative forcing contribution are still a subject of curious debate and through investigations are still in progress. This is because aerosol concentrations in the atmosphere are highly variable in space and time. This variability is largely due to the much shorter lifetime of aerosols in the air compared to the important greenhouse gases. Spatially and temporally resolved information on the atmospheric burden and radiative properties of aerosols is needed to estimate radiative forcing. In addition to the great variability in aerosol concentrations, several crucial aspects of the aerosol influences on cloud processes must be accurately modeled also (IPCC, 2007; US-CCSP, 2009; Tao et al., 2012).

2.2 AQI development and implementation

Air quality index (AQI) is a standard measure used to report daily ambient air quality over a particular area (US-EPA, 2009a). The AQI data are normally released by the government's environmental agencies on a daily basis to inform public on level of air pollution severity based on observed amount of some hazardous pollutants in the atmosphere (e.g., CO, SO_2, NO_2, Ozone, PM2.5 or PM10) and their associated health impacts. Higher value of the AQI commonly indicates greater level of the concerned air pollution and, as a consequence, higher risk of having adverse health effects to the population. In general, different names and developing methods of the AQI have been applied in different countries, e.g., the Air Quality Health Index (AQHI) in Canada, Air Pollution Index (API) in China or Malaysia, or Pollutant Standards Index (PSI) in Singapore. Comprehensive reviews on the AQI development and implementation are given in Shooter and Brimblecombe (2009) and Wai (2012).

As different countries often apply different standards, or criteria, to formulate their AQI system and to establish its specific meaning related to health issue; these differences might cause somewhat confusion if air pollution reports based on different indices are compared and interpreted for daily-life implementation. These differences primarily originate from two sources: the local differences in nature of the prevalent air quality problems and fundamental differences in concepts of the approach (Elshout and Léger, 2006). For examples, the UK (and European) index is focused primarily on monitoring air quality with PM10 concentration < 100 $\mu g/m^3$ as acute air pollution situations are rarely evidenced in the country. On the contrary, the US-EPA index was developed to accommodate wider range of aerosol intensity as detailed in Table 2.1a (for PM10 density of about 0-600 $\mu g/m^3$).

2.2.1 Derivation of AQI

AQI data are normally reported in terms of discrete numbers of certain range, e.g. from 0 to 500. These numbers are traditionally classified into several categories (or bands) indicating degradation level of air quality as defined by the known amount of the concerned air pollutants in the atmosphere. Standard formula to calculate AQI values in this format is as follows (US-EPA, 2009b):

$$I = \frac{I_{high} - I_{low}}{C_{high} - C_{low}}(C - C_{low}) + I_{low} \quad (2.1)$$

where I = Air Quality Index (AQI), C = the pollutant concentration,

C_{low} or C_{high} = the concentration breakpoint that is $\leq C$ or $\geq C$,

I_{low} or I_{high} = the index breakpoint corresponding to C_{low} or C_{high}.

The breakpoint data are specifically defined for each considered pollutant by the responsible agencies. Examples for those used by the Thailand- PCD and the US-EPA along with the associated health concerns are displayed in Tables 2.1a-c. Air quality index in some countries, like UK or Canada, is reported in terms of the defined level of air pollution severity directly (from low to high) in which amount of the concerned air pollutant is divided into several divisions ranked in order from 1 onward (e.g. from 1 to 10). These classified AQI levels are then grouped to represent predefined health risk categories as seen in Tables 2.2a-b for examples (for UK index).

Table 2.1a Breakpoint data for AQI calculation by the US-EPA (US-EPA, 2009b).

AQI value	Ozone (8 hr)	CO (8 hr)	SO_2 (1 hr)	NO_2 (1 hr)	PM10 (24 hr)	PM2.5 (24 hr)
	ppb	ppm	ppb	ppb	$\mu g/m^3$	$\mu g/m^3$
0-50	0-59	0-4.4	0-35	0-53	0-54	0-15.4
51-100	60-75	4.5-9.4	36-75	54-100	55-154	15.5-40.4
101-150	76-95	9.5-12.4	76-185	101-360	155-254	40.5-65.4
151-200	96-115	12.5-15.4	186-304	361-649	255-354	65.5-150.4
201-300	116-374	15.5-30.4	305-604	650-1249	355-424	150.5-250.4
301-500	-	30.5-50.4	604-1004	1250-2049	425-604	250.5-500.4

Table 2.1b Breakpoint data for AQI calculation by the Thailand-PCD (PCD, 2013).

AQI value	Ozone (1 hr)	CO (8 hr)	SO_2 (24 hr)	NO_2 (1 hr)	PM10 (24 hr)
	ppb	ppm	ppb	ppb	$\mu g/m^3$
0-50	0-51	0-4.48	0-25	0-85	0-40
51-100	52-100	4.49-9.00	26-120	86-170	41-120
101-200	101-203	9.01-14.84	121-305	171-600	121-350
201-300	204-405	14.85-29.69	306-610	601-1202	351-420
301-400	406-509	29.70-40.17	611-802	1203-1594	421-500
401-500	510-611	40.18-50.21	803-100	1595-1993	501-600

Table 2.1c AQI categories and meaning adopted by the US-EPA and Thailand PCD.

Air Quality Index Levels of Health Concern	Numerical Value	Meaning
Good	0-50	Air quality is considered satisfactory, and air pollution poses little or no risk.
Moderate	51-100	Air quality is acceptable; however, for some pollutants there may be a moderate health concern for a very small number of people who are unusually sensitive to air pollution.
Unhealthy for Sensitive Groups	101-150	Members of sensitive groups may experience health effects. The general public is not likely to be affected.
Unhealthy	151-200	Everyone may begin to experience health effects; members of sensitive groups may experience more serious health effects.
Very Unhealthy	201-300	Health alert: everyone may experience more serious health effects.
Hazardous	> 300	Health warnings of emergency conditions. The entire population is more likely to be affected.

Table 2.2a Breakpoint data for AQI calculation in the UK (DEFRA, 2012).

AQI band	AQI scale	Ozone (8 hr)	SO_2 (15 min)	NO_2 (1 hr)	PM10 (24 hr)	PM2.5 (24 hr)
		$\mu g/m^3$	$\mu g/m^3$	$\mu g/m^3$	$\mu g/m^3$	$\mu g/m^3$
Low	1	0-33	0-88	0-66	0-16	0-11
	2	34-65	89-176	67-133	17-33	12-23
	3	66-99	177-265	134-199	34-49	24-34
Moderate	4	100-120	266-354	200-267	50-58	35-41
	5	121-140	355-442	268-334	59-66	42-46
	6	141-159	443-531	335-399	67-74	47-52
High	7	160-187	532-708	400-467	75-83	53-58
	8	188-213	709-886	468-534	84-91	59-64
	9	214-239	887-1063	535-599	92-99	65-69
Very high	10	≥ 240	≥ 1064	≥ 600	≥ 100	≥ 70

Table 2.2b AQI categories and meaning adopted by the UK-DEFRA (2012).

AQI scale	AQI band	Accompanying health messages	
		At-risk individuals	General population
1-3	Low	Enjoy usual outdoor activities.	Enjoy usual outdoor activities.
4-6	Moderate	Adults/children with lung or hearth problems, who experience symptoms, should consider reducing strenuous physical activity, particularly outdoors.	Enjoy usual outdoor activities.
7-9	High	Adults/children with lung or hearth problems, should reduce strenuous physical exertion, particularly outdoors, and particularly if they experience symptoms. People with asthma may find they need to use their reliever inhaler more often. Older people should also reduce physical exertion.	Anyone experiencing discomfort such as sore eyes, cough or sore throat should consider reducing activity, particularly outdoors.
10	Very high	Adults/children with lung or hearth problems, and older people, should avoid strenuous physical activity. People with asthma may find they need to use their reliever inhaler more often.	Reduce physical exertion, particularly outdoors, especially if you experience symptoms such as cough or sore throat.

In addition, an index called CAQI (Common Air Quality Index) was devised for general use in the EU countries. To enable comparison between cities, three types of the index are developed: hourly index, daily index, annual index. The CAQI is used on www.airqualitynow.eu where air quality condition of nearly 100 cities is reported. For hourly and daily indices, pollution level is reported using an index scale ranging from 0 (very low) to > 100 (very high) as detailed in Table 2.3. These values present relative measure of the severity of air pollution. The calculation is primarily based on the three pollutants of major concern: PM10, NO_2, and O_3. The pollutants PM2.5, CO and SO_2 can be taken into account if their data are available for the analysis. In order to make the index more applicable, two situations are defined:

(1) City Background, telling general air quality within the city (based on urban background monitoring sites),

(2) Roadside, telling air quality in streets (based on roadside stations).

Main aim of CAQI is to raise awareness and make air quality condition comparable from one city to another, not to become a health-based index as usual (EU, 2012).

มหาวิทยาลัยเทคโนโลยีสุรนารี

Table 2.3 Breakpoint data for AQI calculation in the EU countries (EU, 2012).

Index class	Grid	Traffic						City Background							
		core pollutants			pollutants			core pollutants				pollutants			
		NO_2	PM_{10}		$PM_{2.5}$		CO	NO_2	PM_{10}		O3	$PM_{2.5}$		CO	SO_2
			1-h.	24-h.	1-h.	24-h.			1-h.	24-h.		1-h.	24-h.		
Very low	0	0	0	0	0	0	0	0	0	0	0	0	0	0	0
	25	50	25	15	15	10	5000	50	25	15	60	15	10	5000	50
Low	25	50	25	15	15	10	5000	50	25	15	60	15	10	5000	50
	50	100	50	30	30	20	7500	100	50	30	120	30	20	7500	100
Medium	50	100	50	30	30	20	7500	100	50	30	120	30	20	7500	100
	75	200	90	50	55	30	10000	200	90	50	180	55	30	10000	350
High	75	200	90	50	55	30	10000	200	90	50	180	55	30	10000	350
	100	400	180	100	110	60	20000	400	180	100	240	110	60	20000	500
Very High*	>100	>400	>180	>100	>110	>60	>20000	>400	>180	>100	>240	>110	>60	>20000	>500

NO_2, O_3, SO_2 : hourly value / maximum hourly value in $\mu g/m^3$
CO 8 hours moving average / maximum 8 hours moving average in $\mu g/m^3$
PM_{10} hourly value / daily value in $\mu g/m^3$
*An index value above 100 is not calculated but reported as * >100*

2.2.2 WHO guidelines on aerosol regulation

To reduce impact of air pollution to public health in general, the World Health Organization (WHO) has generated its air quality guidelines for the regulation of four common air pollutants: PM, O_3, NO_2 and SO_2. Details of the guideline for PM targets are shown in Table 2.4 both for the 24-hour average and annual mean concentration (WHO, 2006b). Although data of the PM10 as a whole is more widely reported, the impact of PM2.5 in particular on public health is of the more concern to the WHO and the guidelines were designed to address this issue elaborately. The PM2.5 guideline values are converted to the corresponding PM10 guideline values by application of a PM2.5/PM10 ratio of 0.5 which is typical for urban areas in developing country and is at the bottom range found in developed country urban areas (0.5-0.8). When setting local standards, and assuming the relevant data are available, a different value for this ratio that better reflects local conditions may be employed instead.

Table 2.4a WHO air quality guideline and the interim targets for particulate matter (PM) based on the observed 24-hour concentrations (WHO, 2006b).

Target level	PM10 ($\mu g/m^3$)	PM2.5 ($\mu g/m^3$)	Basis for the selected level
Interim target-1 (IT-1)	150	75	Based on published risk coefficients from multi-centre studies and meta-analyses (about 5% increase of short-term mortality over the AQG value).
Interim target-2 (IT-2)	100	50	Based on published risk coefficients from multi-centre studies and meta-analyses (about 2.5% increase of short-term mortality over the AQG value).
Interim target-3 (IT-3)	75	37.5	Based on published risk coefficients from multi-centre studies and meta-analyses (about 1.2% increase in short-term mortality over the AQG value).
Air quality guideline (AQG)	50	25	Based on relationship between 24-hour and annual PM levels.

Table 2.4b WHO air quality guideline and the interim targets for particulate matter (PM) based on the annual mean concentrations (WHO, 2006b).

Target level	PM10 ($\mu g/m^3$)	PM2.5 ($\mu g/m^3$)	Basis for the selected level
Interim target-1 (IT-1)	70	35	These levels are associated with about a 15% higher long-term mortality risk relative to the AQG level.
Interim target-2 (IT-2)	50	25	In addition to other health benefits, these levels lower the risk of premature mortality by approximately 6% [2–11%] relative to the IT-1 level.
Interim target-3 (IT-3)	30	15	In addition to other health benefits, these levels reduce the mortality risk by approximately 6% [2-11%] relative to the IT-2 level.
Air quality guideline (AQG)	20	10	These are the lowest levels at which total, cardiopul-monary and lung cancer mortality have been shown to increase with more than 95% confidence in response to long-term exposure to PM2.5.

2.3 Determination of AOD and PM concentration

In the past, knowledge of the PM concentration in both temporal and spatial aspects was mostly contributed from its data records obtained from network of the air quality monitoring stations situated within a particular area or measuring campaigns that entail high implementation and maintenance costs and are rather limited in terms of spatial coverage. However, at present, such limitations can be minimized through the continuous observation of the atmospheric aerosol intensity by a wide range of the satellite-based sensors that can be used as complementary sources to the conventional ground-based data (Lee et al., 2009). Satellite-based observations have been proved to become very useful in the analysis of spatial structure and concentration distribution of the aerosol pollution and its impacts at global to local scales (Kaufman et al., 2002; Gupta, Christopher, Wang, Gehrig, Lee and Kumar, 2006; Gupta and Christopher, 2008; Kokhanovsky and Leeuw, 2009; Tsai, Jeng, Chu, Chen, Chang, 2011; van Donkelaar et al., 2011)

2.3.1 Definition and derivation of aerosol optical depth (AOD)

The key quantity frequently reported in the satellite-based PM observations is aerosol optical depth (AOD), or alternatively called aerosol optical thickness (AOT). AOD is a dimensionless parameter developed to quantify degree to which the aerosols prevent the transmission of sunlight (at a specific wavelength) through the atmosphere by absorption or scattering mechanisms. This can be expressed by the relation,

$$\mathrm{AOD}(\lambda) = \int_{z_{min}}^{z_{max}} \sigma(\lambda, z)\mathrm{d}z \qquad (2.2a)$$

or

$$\mathrm{AOD}(\lambda) = \int_{z_{min}}^{z_{max}} \sigma(\lambda)\mathrm{f}(z)\mathrm{d}z \qquad (2.2b)$$

where $\sigma(\lambda)$ is the aerosol extinction coefficient for wavelength λ, z is altitude, f(z) is vertical distributing function of the considered aerosol, and z_{min}, z_{max} are the lower and upper altitude of air thickness to be included in the integration (where a given aerosol type can be found), respectively (Kuśmierczyk-Michulec, 2011).

By definition, the extinction coefficient is the fractional depletion of the solar radiance per unit path length (e.g. per kilometer) while propagating in the atmosphere due to two common mechanisms, absorption and scattering, induced by air molecules. The AOD determined along vertical direction is also called normal optical thickness (compared to optical thickness along slant path length). This parameter is retrieved routinely from numerous satellite-based sensors as detailed in Table 2.5 for examples. Normally, optical depth of < 0.05 shall indicate clear sky with relatively low aerosol concentration, whereas a value of 1 indicates hazy conditions. Optical depths greater than 2 or 3 often represent very high concentrations of aerosol in lower atmosphere. Aerosol monitoring sensors also measure single scattering albedo (SSA) parameter which is fraction of light being scattered compared to the total. Typical values range from about 0.7 for very absorbing particles to 1 for aerosols that only scatter light.

In theory, depending on particle size distribution, the spectral dependence of the AOD can be approximately given by the following relation (Ångström, 1964):

$$\text{AOD}(\lambda) = \beta\lambda^{-\alpha} \qquad (2.3)$$

where AOD (λ) is the AOD at wavelength λ. The parameter β is called the Ångström turbidity coefficient which equals to the AOD at 1 μm and corresponds to the particle load. The constant α is a well-known parameter called the Ångström exponent (also known as Ångström coefficient or Ångström parameter). For molecules, it is about 4 and varies between about 0 and 2 for particles (Wagner and Silva, 2008).

From Eq. 2.3, the relationship of the AOD data at two different wavelengths, λ and λ_0, for a particular aerosol can be expressed as:

$$\frac{\mathrm{AOD}(\lambda)}{\mathrm{AOD}(\lambda_0)} = \left(\frac{\lambda}{\lambda_0}\right)^{-\alpha} \tag{2.4a}$$

or,
$$\mathrm{AOD}(\lambda) = \mathrm{AOD}(\lambda_0) \cdot \left(\frac{\lambda_0}{\lambda}\right)^{\alpha} \tag{2.4b}$$

According to Eq. 2.4, if the AOD at one wavelength and the corresponding Ångström exponent are known, the AOD data at different wavelengths can then be determined automatically. In practice, the Ångström exponent is usually determined first based on prior knowledge of the AOD at two different wavelengths using the relation:

$$\alpha = -\frac{\log \frac{\tau_{\lambda_1}}{\tau_{\lambda_2}}}{\log \frac{\lambda_1}{\lambda_2}} = -\frac{\log \tau_{\lambda_1} - \log \tau_{\lambda_1}}{\log \lambda_1 - \log \lambda_2} \tag{2.5}$$

where $\tau_{\lambda 1}$ and $\tau_{\lambda 2}$ represent AOD (λ_1) and AOD (λ_2), respectively. The found value of α is then used to derive AOD data at all other wavelengths (using Eq. 2.4b) within the range of validity of this formula.

The Ångström exponent is inversely related to the average size of the aerosol particles: the smaller the particles, the larger the exponent. Thus, it is a useful quantity to assess particle size of atmospheric aerosols or clouds, and wavelength dependence of the aerosol/cloud optical properties. This parameter is routinely estimated by the AERONET sensors at present. More details of the aerosol size distribution and related optical parameters are described in Appendix A.

Table 2.5 Notable satellite-based sensors for global aerosol observations.

Sensor	Satellite	Temporal coverage (month/year)		Product resolution (Approximated)	Wavelength data
		Begin	End		
AVHRR	NOAA	06/1987	-	110 km	630 and 830 nm
POLDER	ADEOS-1	11/1996	06/1997	18.5 km	670 and 865 nm
	ADEOS-2	04/2003	10/2003		
	PARASOL	12/2004	-		
TOMS	Earth Probe	07/1996	12/2005	1 x 1.25 degree	331, 340, 360, and 380 nm
MODIS	Terra/Aqua	03/2000	-	10 km	470, 550 and 660 nm
MISR	Terra	02/2001	-	17.6 km	446, 558, 667 and 862 nm
MERIS	ENVISAT	07/2002	-	1 km (local)/ 9 km (global)	412, 442, 510, 665, 779, 865 nm
OMI	Aura	10/2004	-	13 km x 24 km	360/380 nm and 331-500 nm
CALIOP	CALIPSO	06/2006	-	5 km	532 and 1064 nm

2.3.2 Satellite-based measurement of AOD data

Aerosol properties over land and ocean are normally retrieved using passive optical satellite techniques. However, it is well known that this is a very complex task as an observed radiance by satellite can be written as a summation of 3 sources;

$$I(\text{observed}) = I(\text{surface}) + I(\text{atmosphere}) + I(\text{cloud}) \quad (2.6a)$$

where, $$I(\text{atmosphere}) = I(\text{aerosol}) + I(\text{other gases}). \quad (2.6b)$$

Here, I(observed) is amount of radiance observed at satellite's sensor, I(surface) is the contribution from land/sea surface reflection (or background effect), I(atmosphere) is contribution from scattering or absorption processes in the atmosphere, like Rayleigh scattering process, initiated by air particles (two groups: aerosol and other gases), and I(cloud) is contribution from the cloud portion in the atmosphere (Lee, Kim, Kim, Kim and von Hoyningen-Huene , 2005)

Therefore, to identify aerosol contribution to the satellite's observed radiance, other three associated terms appeared in Eq. 2.6 also; which are I(surface), I(cloud) and I(other gases), must be known. The difficulty then lies in the process of separation these four terms from each other. In practice, influence of the surface term is typically reduced by using the so-called "dark target" background like ocean whose reflectance is minimal or vanished at the NIR or MIR bands, and the cloud impacts can be readily avoided by choosing the cloud free image. However, retrieving of the AOD overland was proved much more complicated due to often strong influence of the surface term on the radiance observed by the satellite-based sensors (especially at visible/NIR/MIR bands). Several retrieval methods were applied to find proper value of AOD along the identified air column [see a review in Kokhanovsky and Leeuw (2009)].

In essence, most algorithms primarily assume that influence of the aerosols on the observed radiance in the MIR portion is negligible. Therefore, the explicit ground surface reflectance can be directly gained at the MIR wavelengths, (e.g., at 2.1 μm for MODIS) by only correcting for the Rayleigh scattering and gaseous absorption in the atmosphere. The known correlation between the MIR ground reflectance and those in visible bands (where aerosol scattering is significant) is then employed to estimate the corresponding reflectance for the selected visible bands under aerosol-free condition. The associated AOD information can then be identified using reference look-up table (LUT) prepared in advance based on knowledge of estimated and observed radiance information of the used visible bands along with observing geometry of the satellite-based instrument under the given solar illumination environment.

The AOD data have been measured routinely from numerous past and present satellite-based sensors (as detailed in Table 2.5 for examples). The first instrument of

this kind is AVHRR onboard NOAA satellite which starts to retrieve the AOD data over ocean using radiance measurement in the visible and NIR bands since late 1970s. Over the subsequent decades, several advanced instruments have been developed to quantify the AOD and the near-ground air pollution over both land and sea territories such as the Multi-angle Imaging Spectroadiometer (MISR) onboard NASA's Terra satellite (Martonchik, Kahn and Diner, 2009) and the Moderate Resolution Imaging Spectroradiomer (MODIS) onboard the Terra and Aqua satellites (Remer et al., 2005). These devices can view aerosols at several angles and spectral wavelengths, providing more accurate results (Figure 2.4). Newer instruments can also provide insight into aerosol properties, i.e., the CALIOP sensor, uses a laser-based technology to construct vertical profiles of aerosol plumes and clouds (Kacenelenbogen et al., 2011).

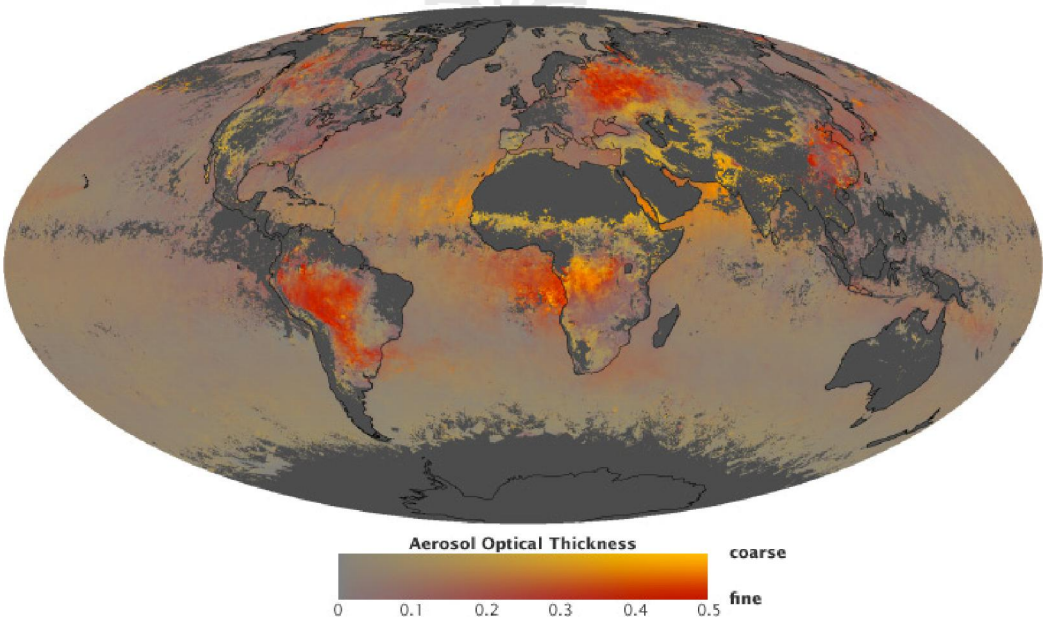

Figure 2.4 Global maps of the satellite-based AOD for the aerosols both in fine and coarse modes derived from the MODIS data.

Source: http://earthobservatory.nasa.gov/Features/Aerosols/page2.php

2.3.3 AERONET Network

Satellites provide a critical global perspective for understanding how aerosols originate, distribute and affect earth's climate, however, they still need ground-based data accumulated by the network of air quality measuring stations to validate merit of their data and to attain the most accurate measurements of AOD available. One of the well-known networks of this kind is the AERONET (the Aerosols Robotic Network). Comprehensive information of the AERONET project is provided in the AERONET website (at http://aeronet.gsfc.nasa.gov) and some contents are summarized here.

AERONET is a global network of solar radiance measurement established by NASA and France's PHOTONS group (Univ. of Lille 1, CNES, and CNRS-INSU). It has been in operation since 1993 until present for the observation of AOD around the world from expansive network of ground-based sun photometers. These obtained AOD data can provide crucial information of aerosol property necessary for the quantification of its impact on current climate variation and on public health deterioration. At present, the network consists of nearly 600 ground stations located in all continents as listed in its website. The three primary objectives of the AERONET project are:

(1) Characterization of aerosol optical properties,

(2) Validation of the satellite and model aerosol retrievals,

(3) Synergism with satellite-based or other kinds of AOD observation.

During their operation, the sun photometers carry out two different measuring modes for two important parameters; the direct solar irradiance and the sky radiance. The direct measurements of solar irradiance typically take place every 15 minutes at eight wavelengths in UV, Visible, and NIR regions (340, 380, 440, 500, 675, 870, 940

and 1020 nm). The atmospheric optical depth (AOD) at each wavelength is calculated from spectral extinction of direct beam radiation whereas attenuation due to Rayleigh scatter, and absorption by ozone, and gaseous pollutants is also estimated and then removed during the retrieval process. The acquired AOD data can be used to compute columnar water vapor (or precipitable water) and estimate the aerosol size using the Angstrom parameter relationship.

As stated earlier, in addition to the direct measurements of the solar irradiance, AERONET instruments also measure the sky radiance in four spectral bands (440, 670, 870 and 1020 nm) along the solar principal plane (i.e., at constant azimuth angle, with varied scattering angles) up to nine times per day and along the solar almucantar (i.e., at constant elevation angle, with varied azimuth angles) up to six times per day. The approach is to acquire sky radiance data through a large range of scattering angles from the sun through a constant aerosol profile to retrieve relevant information of size distribution, phase function and aerosol optical depth. Sky radiance measurements are inverted with the Dubovik and Nakajima inversions to provide aerosol properties of size distribution and phase function over the particle size range of 0.1 to 5 um.

Two data versions (Versions 1 and 2) at three quality levels are prepared and distributed for each product, which are,

(1) Level 1.0 (unscreened for clouds),

(2) Level 1.5 (cloud-screened), and

(3) Level 2.0 (cloud-screened and quality-assured).

The Levels 1.0 and 1.5 data are provided in near real-time but there is some delay of 12-month or longer (due to final calibration and manual inspection) for the Version 2

of Level 2 product to ensure highest quality. Version-2 AOD data now include fine and coarse mode AOD as well as fine mode fraction.

The estimated uncertainty in derived AERONET-AOD Level 2, due primarily to calibration uncertainty, is approximately 0.010-0.021 for field instruments (which is spectrally dependent with the higher errors in the UV). For wavelengths > 400 nm, the AERONET-AOD uncertainty is about 0.01-0.015 for the Level 2 data (includes both pre-and post- deployment calibrations). Due to their relatively high accuracy and assured quality, AERONET-AOD data are widely used as a standard reference for validating most satellite-based AOD retrieval (as listed for examples in Table 2.6).

Table 2.6 Reports of correlation between satellite-based AOD and AERONET-AOD.

Variable		Relationship form	Correlation level		Sensor	Source
x	y		R	R^2		
500-A	500-S	y = 0.95x + 0.20	-	0.73	MODIS	Van Donkelaar et al. (2011)
550-A	550-S	y = 1.102x+0.110	0.948	-	MODIS	Qi, Ge, and Huang (2013)
550-A	550-S	y = 0.63x + 0.09	0.790	-	MODIS	Sanjay, Kumar, Gupta, Devara, and Aher (2013)
558-A	558-S	y = 0.71x + 0.05	-	0.93	MISR	Jiang, Liu, Yu, and Jiang (2007)
440-S	443-A	y = 1.05 + 0.04	0.830	-	MISR	Vidot, Santer, and Aznay (2008)
675-A	640-S	y = 0.764 + 0.041	0.861	-	AVHRR	Mei1 et al. (2013)

Note: A ≡ AERONET-AOD and S ≡ satellite-based AOD. Numbers for (x,y) are the corresponding wavelengths in nm.

In Thailand, there are 9 AERONET instruments currently in use (Figure 2.5); one located in central Bangkok (at Chulalongkorn University as seen in Figure 2.6), one situated in Nakhon Patom Province (at Silpakorn University), and the rest are installed in other provinces. Among these, three are located in Chiang Mai Province (one in Omkoi District and the other two in downtown area of Mueang District) and one each situated in Mugdahan, Hua-Hin/Prajuab Kirikhan, Ubon Ratchathani and in Pimai District of Nakhon Ratchasima Province (Garivait, 2009).

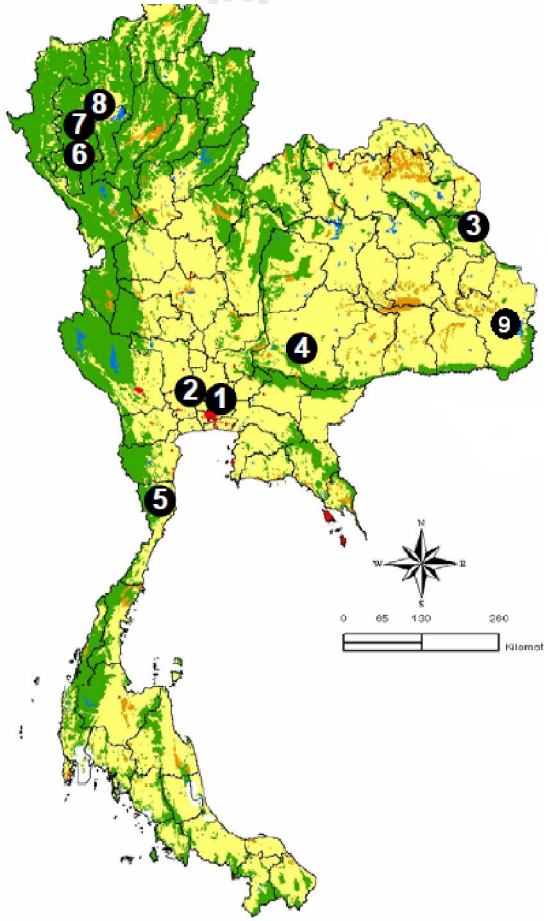

Figure 2.5 Locations of the AERONET instruments in Thailand (Garivait, 2009).

Figure 2.6 AERONET instruments at Chulalongkorn University in Bangkok.

Source: http://aeronet.gsfc.nasa.gov/THAILAND_AERONET.pdf

2.3.4 Relationship between AOD and observed PM data

In general, the PM concentration decreases following an exponential fashion in the vertical direction, but it was frequently found that there is a linear correlation between the observed AOD and measured near-surface aerosol density (as described for examples in Table 2.7 and Figure 2.7). This relationship can be written as follows:

$$PM = a_1(AOD) + a_2 \quad (2.7)$$

where a_1 and a_2 are proper constants which are in close relation to type of the aerosol particle (relevant theoretical basis of Eq. 2.7 is detailed in Appendix A).

Thus, taking advantages of the strong linear correlation between the derived AOD and PM density, the implementation of the satellite-based retrieved AOD data (e.g. MODIS-AOD) for aerosol pollution motoring at local to global scale has become a promising approach for the current aerosol pollution research field. However, the

common coarse resolution of most satellite-based AOD mapping is still a great limit to the formulation of PM concentration map at fine scale (e.g. < 1 km).

Various studies have reported empirical relations between AOD and observed PM10 or PM2.5 data over several locations around the world (as listed in Table 2.7) with promising results in general (regarding to the moderate to high correlation level). However, relatively low correlation has also been evidenced in some reports.

General conclusion arisen from these studies is that variations in local meteorological conditions, occurrence of multiple aerosol layers, and variations in aerosol chemical composition are likely to play an important role in determining the strengths of such correlations. In short, the relationship between AOD and PM should be determined regionally to account for its specific conditions.

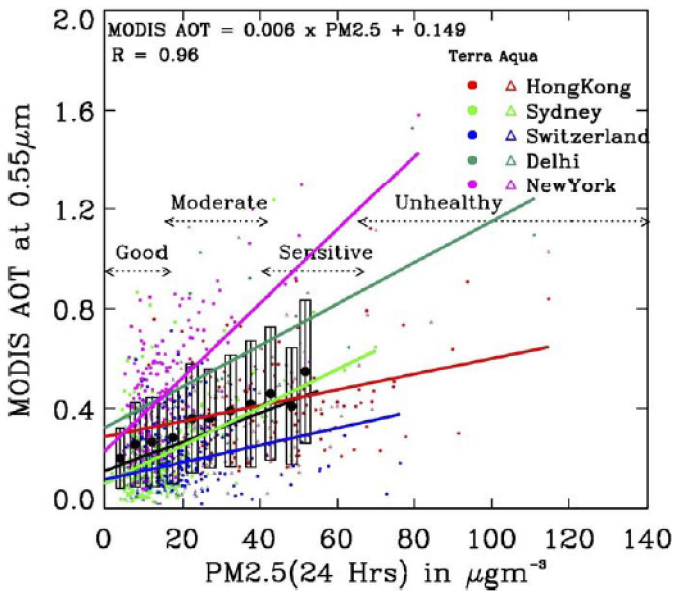

Figure 2.7 The linear relationship between MODIS-AOT and observed PM 2.5 data at several cities around the world (Gupta et al., 2006).

Table 2.7 Reports of linear relationship between AOD and near-ground PM.

Variable		Relationship	Correlation		Sensor	Source
x	y		R	R^2		
AOD	PM10	y = 302.3x - 54.4	0.82	-	MODIS	Li, Lau, Mao, and Chu (2005)
AOD	PM10	y = 219.6x-10.9	-	0.77	MODIS	Grosso, Ferreira, Mesquita, Carlos and Eberhard (2007)
AOD	PM10	y = 109.4x + 38.46	-	0.72	MODIS (Chiang Mai)	Chew et al. (2007)
AOD	PM10	y = 69x + 20.0	0.57	-	MODIS	Dinoi, Perrone and Burlizzi (2010)
AOD	PM10	y = 195.7x +14.5	-	0.83	MERIS	Retalis and Sifakis (2010)
AOD	PM10	y = 119.09x +22.684	-	0.75	MODIS (summer)	Zha, Gao, Jiang, Lu and Huang (2010)
AOD	PM10	y = 90.413x +52.368	-	0.22	MODIS (winter)	
AOD	PM2.5	y = 29.69x + 7.55	0.24	-	GOES	Chudnovsky, Lee, Kostinski, Kotlov, Koutrakis (2012)
AOD	PM2.5	-	0.65	-	MODIS	Tsai et al. (2011)
PM2.5	AOD	y = 0.0057x + 0.11	-	0.59	MODIS	Glantz, Kokhanovsky, von Hoyningen-Huene, Johansson (2009)
PM2.5	AOD	y = 0.0052x+0.064	-	0.58	MERIS	
PM2.5	AOD	y = 0.013x+0.2242	0.98	-	MODIS (Location 1)	Hutchison et al. (2008)
PM2.5	AOD	y = 0.0092x+0.367	0.47	-	MODIS (Location 2)	
PM2.5	AOD	y = 0.006x+0.149	0.96	-	MODIS	Gupta et al. (2006)

2.4 MODIS and BAER retrieval methods for AOD assessment

MODIS is a prime instrument aboard NASA's EOS-Terra and Aqua satellites, being launched into orbit in 1999 and 2002 respectively. The instrument is working in the near-earth sun-synchronous polar-orbit from a nominal altitude of 705 km and was designed to cross the equator at approximately 10:30 a.m. (for Terra-descending orbit) and 1:30 p.m. (for Aqua-ascending orbit) local time, respectively (Remer et al., 2005). These properties are summarized in Table 2.8.

2.4.1 MODIS sensors and their standard products

MODIS sensors detect incoming radiance data in 36 spectral bands ranging in wavelength from 0.4 to 14.4 μm. (Table 2.9) and be able to view the entire Earth's surface every 1-2 days due to large cross-tract swath. The measurements are operated at three different spatial resolutions: 250 m (bands 1-2), 500 m (bands 3-7), and 1 km (bands 8-36). There are 44 standard MODIS-based products available at present to support interests of users (called MOD 01-44). These products can be grouped into two broad categories: daily MODIS images (Level 1) and derived products (Level 2).

The daily MODIS images can be obtained since February 2000 at the spatial resolution of 1 km. The image data are digital numbers which can be converted to be radiance values, surface reflectance values, and/or brightness/temperature values as appropriate before performing the analysis. Terra image file names shall begin with MOD021KM and Aqua file names begin with MYD021KM. MODIS images are recorded both in the morning (Terra-MODIS) and in the afternoon (Aqua-MODIS) up to four times per day altogether. In addition, the night time data are also available in the thermal range of the spectrum.

Table 2.8 Major properties of the MODIS sensors.

Property	Details
Orbit	705 km, 10:30 a.m. descending node (Terra) or 1:30 p.m. ascending node (Aqua), sun-synchronous, near-polar, circular
Scan rate	20.3 rpm, cross track
Swath dimensions	2330 km (cross track) by 10 km (along track at nadir)
Quantization	12 bits
Spatial resolution (SR)	250 m (bands 1-2), 500 m (bands 3-7), 1000 m (bands 8-36)

Source: http://modis.gsfc.nasa.gov/about/specifications.php.

Table 2.9 List of MODIS spectral bands and their proposed primary uses.

Band	Bandwidth (nm)	SR (m)	Primary use	Band	Bandwidth (μm)	SR (m)	Primary use
1	620 - 670	250	Land/Cloud/ Aerosols boundaries	20	3.660 - 3.840	1000	Surface/Cloud temperature
2	841 - 876			21	3.929 - 3.989		
3	459 - 479	500	Land/Cloud/ Aerosols properties	22	3.929 - 3.989		
4	545 - 565			23	4.020 - 4.080		
5	1230 - 1250			24	4.433 - 4.498		Atmospheric temperature
6	1628 - 1652			25	4.482 - 4.549		
7	2105 - 2155			26	1.360 - 1.390		Cirrus clouds water vapor
8	405 - 420	1000	Ocean Color/ Phytoplankton/ Biogeochemistry	27	6.535 - 6.895		
9	438 - 448			28	7.175 - 7.475		
10	483 - 493			29	8.400 - 8.700		Cloud properties
11	526 - 536			30	9.580 - 9.880		Ozone
12	546 - 556			31	10.780 - 11.280		Surface/Cloud temperature
13	662 - 672			32	11.770 - 12.270		
14	673 - 683			33	13.185 - 13.485		Cloud top altitude
15	743 - 753			34	13.485 - 13.785		
16	862 - 877			35	13.785 - 14.085		
17	890 - 920		Atmospheric water vapor	36	14.085 - 14.385		
18	931 - 941						
19	915 - 965						

Source: http://modis.gsfc.nasa.gov/about/specifications.php.

The MODIS derived products (Level 2) can be separated into five categories based on their purposes of application: Calibration, Atmosphere, Land, Cryosphere, and Ocean. Examples of these products relevant to this study are MOD 04 (Aerosol Product), and MOD 14 (Thermal Anomalies-Fires and Biomass Burning). Typically, the MODIS Aerosol Product monitors the ambient aerosol optical thickness (AOT) globally over both the oceans and the continents. In addition, the aerosol size distribution and the aerosol type are also determined over specified regions. Daily MOD 04-Level 2 data are produced at spatial resolution of a 10x10 1-km (at nadir)-pixel array.

The MODIS Thermal Anomalies product includes fire occurrence (day/night), fire location, the logical criteria used for the fire selection, and an energy calculation for each identified fire. This product also includes the composite 8-day-and-night fire occurrence (full resolution), composite monthly day-and-night fire occurrence (full resolution), gridded 10-km summary per fire class (at daily/8-day/monthly scale), and a gridded 0.5° summary of fire counts per class (daily/8-day/ monthly). The Level 2 product includes various fire-related parameters including the occurrence of day and nighttime thermal anomalies which are flagged and grouped into different temperature classes with emitted energy from the fire. These stated parameters are retrieved daily at 1-km resolution. More detailed information of the MODIS mission and applications in atmospheric research are available at MODIS website (http://modis.gsfc.nasa.gov) and MODIS-Atmosphere website (http://modis-atmos.gsfc.nasa.gov).

2.4.2 MODIS-AOD retrieval algorithm

One of the notable applications of MODIS product is the derivation of AOD data at regional/global scales using its blue (0.47 μm), red (0.65 μm) and mid-infrared

(2.13 μm) bands. The retrieved results are then reported at 10-km resolution at nadir. Basically, the core retrieval algorithm exploits information of atmospheric reflectance ratios (corrected for the Rayleigh scattering) between the 0.47 and 2.13 μm channels along with the 0.65 and 2.13 μm channels to develop the AOD product. AOD values measured from the ground may range from near zero in pristine environments up to two or more in the heavily polluted urban areas or dust storms (see Gupta et al., 2006; Jiang et al., 2007; Hutchison, Faruqui, and Smith. 2008; Péré, Pont, Mallet, and Bessagnet, 2009 for examples). However, upper bound of 3.0 is set in the MODIS AOD retrieval process to minimize cloud contamination. Both Terra/Aqua MODIS-AOD retrievals overland are highly correlated with ground truth and present little bias (Remer et al., 2008).

A brief description of the conventional MODIS aerosol algorithm is as follows (also see work flowchart in Figure 2.8) (Chu et al., 2002; Remer et al., 2005). The used MODIS-AOD retrieval algorithm was developed based on the "dark-object" method in which the essential assumption is that if the surface is densely vegetated, the MIR surface reflectances of MODIS band 7 are linearly related to reflectances of MODIS band 3 (blue band) and band 1 (red band). Since most aerosol sizes are smaller than the MIR wavelength, aerosol effects in band 7 are typically negligible and its surface reflectance can then be readily approximated. Based on several surface measurements, Kaufman et al. (1997a) established the following empirical formulae:

$$\frac{\text{R1(Red)}}{\text{R7(MIR)}} = 0.50; \quad \frac{\text{R3(Blue)}}{\text{R7(MIR)}} = 0.25 \tag{2.8}$$

From Eq. 2.8, the surface reflectances at MODIS's red and blue bands (R1 and R3), can be conveniently estimated from the known reflectance at the MIR band (R7) and

the associated AOD at bands 1 and 3 can then be determined using the look-up tables. MODIS-AOD is retrieved at four wavelengths: 0.47 μm (blue), 0.55 μm (green), 0.66 μm (red), and 2.12 μm (MIR).

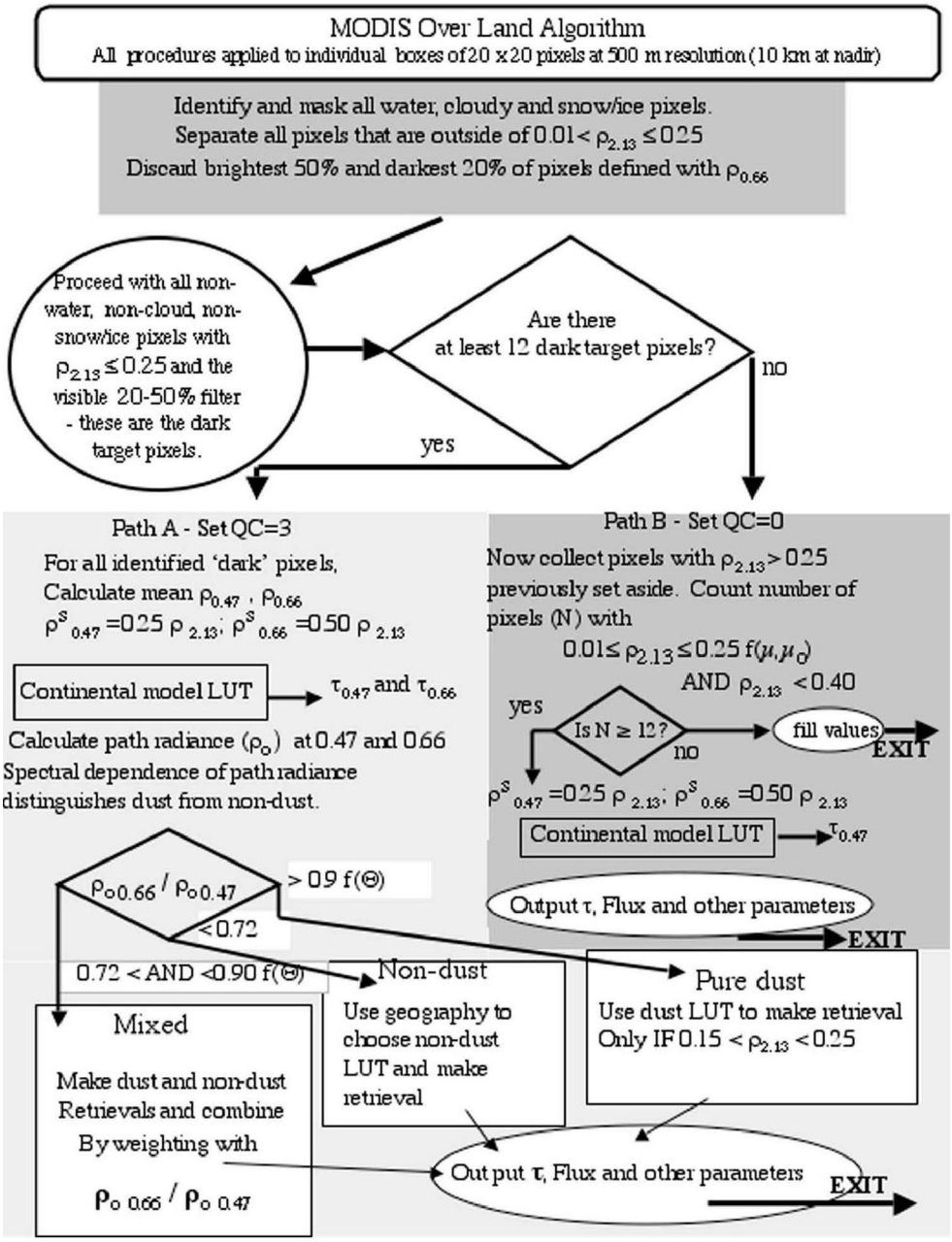

Figure 2.8 Flowchart of MODIS's aerosol retrieval algorithm (Remer et al., 2005).

The look-up tables are prepared for each aerosol models that are pre-defined for a given location and time. There are two key requirements for this method:

(1) existence of large homogeneous dense vegetation in the scene;

(2) stable empirical relationships of the surface reflectance R7 and R1, R3.

The first requirement implies inaccurate reflectance retrieval of surface with nondense vegetation canopies. To meet the second requirement, dense vegetation canopies have to be distinguished from other dark objects, such as wet soil and water. For non-dense vegetation surfaces (e.g., snow/ice, desert, agricultural lands before/after the growing peak), MODIS-AOD products are not accurate because of no aerosol correction with the actual retrieval; which results in large errors in the downstream products, such as snow/desert albedo and canopy leaf area index. After examining the MODIS aerosol optical depth product around the world, it was found that in many cases (mainly off growing season) that the MODIS algorithm fails to retrieve aerosol optical depth over land because the surfaces are not covered by dense vegetation canopies.

In the normal retrieving process, 10 km x 10 km grid boxes (cloud-free pixels) are first selected using the multi-spectral MODIS cloud mask (Ackerman et al., 2006). And to minimize errors, the MODIS aerosol retrievals over land are limited to those pixels with $R7 < 0.25$. Snow/ice and water covered surfaces are also excluded because the empirical relationships (described in Eq. 2.8) are invalid over those regions. The selected cloud-free dark pixels in the grid box may still be partially contaminated by the sub-pixel clouds, snow/ice, or soil types that do not fit the empirical relationship. Thus only part of the MODIS measured radiances is used, e.g. at 20-50% brightness range. The overall retrieval error is usually large for dust particle as oppose to that of the urban/industrial and biomass burning aerosols. To distinguish between dust and

non-dust aerosols, the ratio of aerosol path radiance at 0.66 and 0.47 μm is used. The sulfate and smoke aerosols that cannot be identified by the path radiance ratio are then separated a priori according to the geographic locations and seasons of their emission sources. More details of the MODIS's aerosol retrieval method (including the mixture of different aerosols) can be found, for examples, in Kaufman et al. (1997b); Chu, Kaufman, Ichoku, Remer, Tanré, and Holben, (2002), and Remer et al. (2005).

2.4.3 BAER-AOD retrieval algorithm

Apart from the well-known MODIS's "dark-object" method described earlier, another promising AOD retrieval method that attains wide interest in recent years is the Bremen Aerosol Retrieval (BAER) method. The method was originally developed by the University of Bremen as a new aerosol retrieval tool for the SCIAMACHY and MERIS instruments onboard the EU's ENVISAT satellite (von Hoyningen-Huene, Freitag and Burrows, 2003). However, this method has been later successfully applied for the AOD data retrieval of several instruments, e.g., SeaWiFS, MODIS, AVHRR (Lee et al., 2005; von Hoyningen-Huene, Kokhanovsky, Burrows, Bruniquel-Pinel, Regner, and Baret , 2006; 2010; Kokhanovsky, Breon, Cacciari, Carboni, and Diner, 2007; Lee, Kim, von Hoyningen-Huene, and Burrow, 2007; Song et al., 2008; Rohen, von Hoyningen-Huene, Kokhanovsky, Dinter, Vountas, and Burrows, 2011; Mei, Xue, Kokhanovsky, von Hoyningen-Huene, Leeuw, and Burrows, 2013).

In principle, working concept of the BAER method follows classic procedure of the satellite-based AOD retrieval discussed in Section 2.3.2 (see Figure 2.9 for its standard work flowchart). Here, AOD data are retrieved from the top-of-atmosphere (TOA) radiance measured by the nadir viewing instruments like MERIS or MODIS.

These instruments measure the upwelling, or TOA, radiance, $I_{TOA}(\lambda)$, along with the apparent solar extraterrestrial irradiance $E_0(\lambda)$ in visible wavelengths. Normalization of the $I_{TOA}(\lambda)$ to the solar illumination conditions for each wavelength λ is defined as being TOA reflectance (ρ_{TOA}):

$$\rho_{TOA}(\lambda) = \frac{\pi I_{TOA}(\lambda)}{E_0(\lambda)\cos(\theta)} \tag{2.9}$$

where θ is the solar zenith angle (Glantz et al., 2009).

Intensity of the TOA reflectance given in Eq. 2.9 depends on several factors, i.e., background surface reflectance, atmospheric scattering or absorption effects, and geometry of the instrument's observing pattern and solar illumination. This fact can be described by the simple relation:

$$\rho_{TOA}(\lambda) = \rho_{ATM}(\lambda) + \rho_{SF}(\lambda) = [\rho_{RL}(\lambda) + \rho_{AS}(\lambda)] + \rho_{SF}(\lambda) \tag{2.10}$$

where ρ_{ATM} is the total reflectance contributed by the earth's atmosphere as a whole and ρ_{SF} is reflectance contributed by the earth's surface. Influence of the atmosphere in this case typically originates from two main sources: the Rayleigh reflectance (ρ_{RL}) by air molecules and the aerosol reflectance (ρ_{AS}) by aerosol particles.

Therefore, the aerosol reflectance can be readily determined by subtracting the known Rayleigh reflectance (ρ_{RL}) and surface reflectance (ρ_{SF}) data from the relevant TOA reflectance (ρ_{TOA}) data (von Hoyningen-Huene et al., 2003):

$$\rho_{AS}(\lambda) = \rho_{TOA}(\lambda) - \rho_{RL}(\lambda) - \rho_{SF}(\lambda) \tag{2.11}$$

For the conversion of the aerosol reflectance data into associated AOD data, the pre-determined look-up-tables (LUT) either between TOA reflectance and AOD or aerosol reflectance and AOD are required. For the preparation of necessary LUT, radiative transfer modeling is performed based on knowledge of aerosol and surface characteristics, Rayleigh scattering pattern and the geometry of solar illumination and instrument's observation pattern. Aerosol characteristics are usually explained by an aerosol phase function, the spectral single scattering albedo and a range of AOD, for instance 0.03-2.5.

The Rayleigh scattering term can be derived from the DEM and the standard model atmosphere. According to Bucholtz (1995), the Rayleigh path reflectance can be determined based on the atmospheric pressure at altitude *z*, or *p(z)*, in each pixel:

$$\rho_{\mathrm{RL}}(\lambda) = A\lambda^{-(B+C\lambda+D/\lambda)} \cdot \frac{p(z)}{p_0} \tag{2.12}$$

where A, B, C and D are the constants for the total Rayleigh scattering cross-section at standard atmosphere: A = 3.01577x10^{-28}, B = 3.55212, C = 1.35579, D = 0.11563 (for λ = 0.2-0.5 μm); A = 4.01061x10^{-28}, B = 3.99668, C = 1.10298, D = 2.71393x10^{-2} (for λ > 0.5 μm). The atmospheric pressure at altitude z (in km), or p(z), can be estimated by the barometric equation (von Hoyningen-Huene et al., 2003):

$$p(z) = p_0 \cdot \exp\left[\frac{-(29.87g)\cdot(0.75z)}{8.315(T_{\mathrm{SF}} - 0.75g\cdot z)}\right] \tag{2.13}$$

where g is the gravity acceleration (9.807 m/s^2), p_0 is the reference pressure data at the mean level (p_0 = 101325 pascal) and T_{SF} is the surface temperature (in K).

The surface reflectance (ρ_{SF}) is typically defined as follows:

$$\rho_{SF}(\lambda) = \frac{T_{Tot}(\theta_0) \cdot T_{Tot}(\theta_S)}{1 - A_{SF} \cdot r_{Hem}} \cdot A_{SF}(\lambda) \quad (2.14)$$

where θ_0 and θ_S are solar and satellite zenith angles, respectively. The parameter T_{Tot} is total transmission along illumination and viewing geometry (θ_0 and θ_S), and γ_{Hem} is the hemispheric reflectance. These parameters can be approximated from the radiative transfer calculations (Kokhanovsky et al., 2007; von Hoyningen-Huene et al., 2006). The parameter A_{SF} is the surface reflectance at the considered wavelength. In general, influence of the hemispheric reflectance term over low reflecting surfaces (e.g. ocean or vegetation in the blue spectral region) is typically low and able to be negligible in the calculation in Eq. 2.14. However, its influence over bright surfaces, like desert, is fairly high and could not be ignored.

For the calculation of surface reflectance, the BAER method uses a vegetation index for the estimation of the preferred surface reflectance (A_{SF}) by the linear mixing model (LLM) as follows (von Hoyningen-Huene et al., 2003):

$$A_{SF}(\lambda) = F \cdot \left[C_{Veg} \cdot \rho_{Veg}(\lambda) + (1 - C_{Veg}) \cdot \rho_{Soil}(\lambda) \right] \quad (2.15)$$

where $\rho_{Veg,}$ ρ_{Soil} are the spectral reflectances of "green vegetation" and "bare soil", respectively, and C_{Veg} is the chosen vegetation index while F is the scaling factor used to adapt the spectral surface model to the conditions within the scene:

$$F = \frac{\rho_{TOA}(0.67) - \rho_{RL}(0.67) - \rho_{AS}(0.67)}{C_{Veg} \cdot \rho_{Veg}(0.67) + (1 - C_{Veg}) \cdot \rho_{Soil}(0.67)} \quad (2.16)$$

Thus, for visible channels, the surface reflectance over land can be estimated per pixel basis assumed that values of all required parameters are known. First version of BAER method uses NDVI (Normalized Difference Vegetation Index) to represent

vegetation data in each target pixel. However, NDVI was found to be substantially sensitive to the presence of the aerosol in the atmosphere which makes it unsuitable for predicting vegetation impact under polluted air environment. To reduce sensitivity issue of NDVI, an alternative index called AFRI (Aerosol Free Vegetation Index) was introduced in some works as a replacement for the NDVI, for examples, in Lee et al., (2005) , Lee, Kim, von Hoyningen-Huene, Burrow (2007) and Song et al. (2008).

Definition of AFRI is as follows (Lee et al., 2005):

$$AFRI = \frac{\rho_{\mathrm{NIR}} - 0.5\rho_{2.1}}{\rho_{\mathrm{NIR}} + 0.5\rho_{2.1}} \quad . \tag{2.17}$$

Using this relationship, *AFRI* is able to estimate vegetation fraction with low aerosol effect because aerosol scattering is very weak in the MIR region.

มหาวิทยาลัยเทคโนโลยีสุรนารี

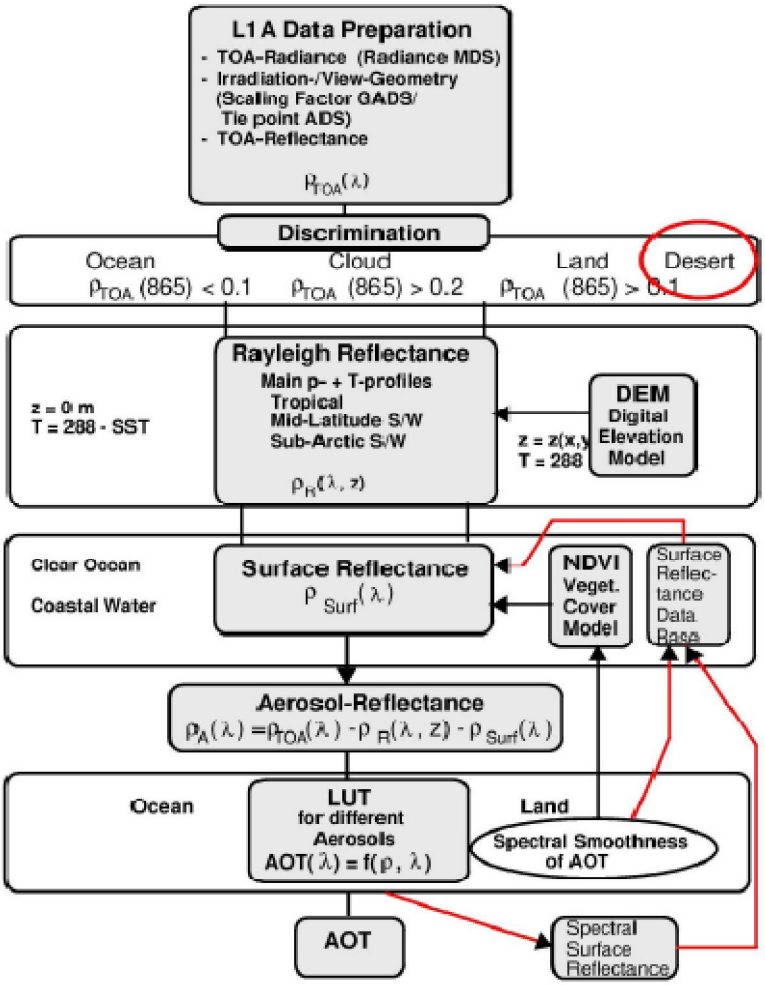

Figure 2.9 Original AOD retrieval procedure of the BARE method (von Hoyningen-Huene et al., 2003).

Figure 2.9 presents work flowchart of original AOD retrieval procedure of the BARE method described in von Hoyningen-Huene et al. (2003). The main steps are to select the required data for solar and viewing geometry, geographic coordinates, TOA radiance, extraterrestrial solar irradiance and prepare the TOA reflectance for the retrieval. Knowledge of the surface reflectance term (from Eq. 2.12) is used for initialization of the iterative determination of the spectral AOD: (a) determination of aerosol reflectance, (b) derivation of the AOD by the selected LUT, (c) analysis of the

smoothness spectral AOD by RMSD between retrieved and the Angstrom power law approximation and (d) correction of spectral surface reflectance until RMSE < 0.005 or return to step (a). Figure 2.10 demonstrates example of the LUT's relationship between the derived aerosol reflectance (ρ_{AS}) and observed AOD (at 0.412 μm) given in von Hoyningen-Huene et al. (2003).

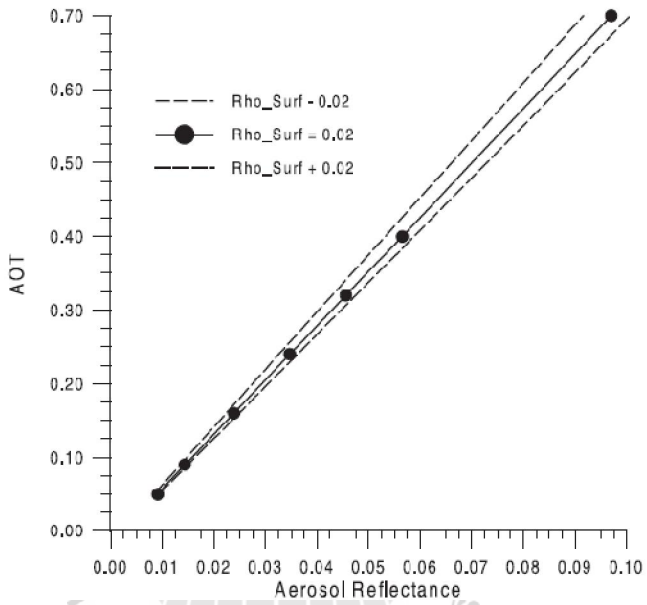

Figure 2.10 Example of the LUT for the relationship between the aerosol reflectance and AOT (for 0.412 μm) at different values of surface reflectance (0.02±0.02).

2.5 Atmospheric dispersion models

Atmospheric (or air) dispersion modeling is the mathematical simulation of how airborne pollutants disperse (after the emission) in specific ambient atmosphere. The dispersion models are normally implemented to describe pattern of the downwind concentration of air pollutants emitted from the contributing sources under influences of the assumed atmospheric conditions (local wind speed in particular). These sources

can be divided into four broad categories: point source (e.g. factory stack), line source (e.g. roadway), area source (e.g. forest fire), and volume source (e.g. open sand pile).

The process of air pollution assessment by most models usually contains four fundamental stages: data input (e.g. emission property/atmospheric condition/terrain condition), dispersion calculations (based on the assumed dispersion pattern), deriving concentration data (over specific area or at a particular location), and analysis/report of the obtained results. Air dispersion models are very important to the governmental agencies responsible for the protection and improving of ambient air quality as they are able to realistically simulate air pollution situation over the concerned area and offer crucial information for effective air pollution control strategies. Comprehensive reviews of dispersion modeling are given in Daly and Zannetti (2007) and Popović (2011).

2.5.1 Types of air dispersion models

A variety of air dispersion models have been developed so far mostly for the use in the analysis of air pollution distribution over a particular region from regional to global scale. These models are traditionally developed based on the pre-determined concept of the air dispersion nature under the given atmospheric condition from which four broad categories of them can be listed as follows.

(1) Box model. This is the simplest form of dispersion model which assumes that the airshed (i.e. a given volume of atmospheric air in a geographical region) is in the shape of a rectangular box and the air pollutants inside the box are well-mixed and homogeneously distributed. The aerosol concentration level in this case is assumed to be in the steady state (i.e. constant over a specific time period). For the analysis of

urban air pollution, the dimensions of this conceptual box are determined by the length of urban area upwind of a receptor (L) and the height of the mixing boundary layer (H) (Figure 2.11). Main source of the existing aerosol is the emission from ground-based contributors at assumed constant rate of Q (called the area source strength and defined by amount of pollutant mass released/ unit surface area/unit time, e.g. in $\mu g/m^2 \cdot s$).

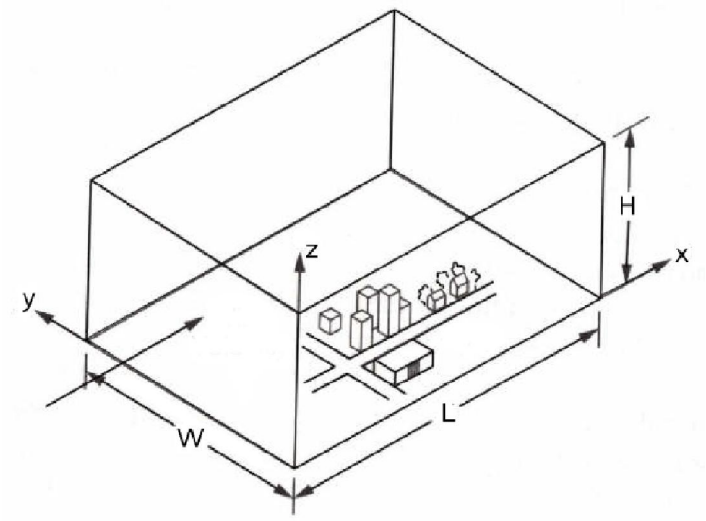

Figure 2.11 Conceptual presentation of the box dispersion model (Noor, 2003).

The released pollutants are instantaneously mixed throughout the defined box under influence of the predominant wind with mean speed u. Under the assumption of steady state condition, the mean pollutant concentration in the box can be determined using the following relation (Noor, 2013):

$$c = \frac{QL}{uH} + b \tag{2.18}$$

where *b* is the background concentration. Although useful, this model is still very limited in its ability to accurately predict dispersion of air pollutants in reality due to its often unrealistic assumption of the homogeneous pollutant distribution within the defined box for each study case (especially within severely-polluted city).

(2) Gaussian plume model. This is the most prominent type of air dispersion model which assumes that the dispersion of air pollutants within the smoke plume has Gaussian form, meaning that it has a normal probabilistic distribution along specified directions as the plume propagates in the atmosphere.

In essence, Gaussian models primarily try to simulate the dispersion pattern of smoke plume (originating from the identified source) under the assumed steady-state atmosphere over a time period of the analysis (often an hour). Distributing pattern of the pollutant concentration of the traveling plume is assumed to have Gaussian form along two referred axes (crosswind and vertical direction) as illustrated in Figure 2.12. Note that, the downwind movement of the plume (along x-axis) is critically depended on wind speed and hence the dispersion along this direction is not in Gaussian form. From the figure, the origin of the coordinate system is placed at the base of the smoke stack with the x-axis aligned in the downwind direction. The polluted smoke plume rises from the smoke stack and then propagates along x direction under influence of the assumed uniform wind along that direction and gradually spreads in the y (cross-wind) and z (vertical) direction as it travels. The smoke plume naturally rises higher over the smoke stack due to its higher temperature than the surrounding atmosphere and its inertial vertical velocity after releasing.

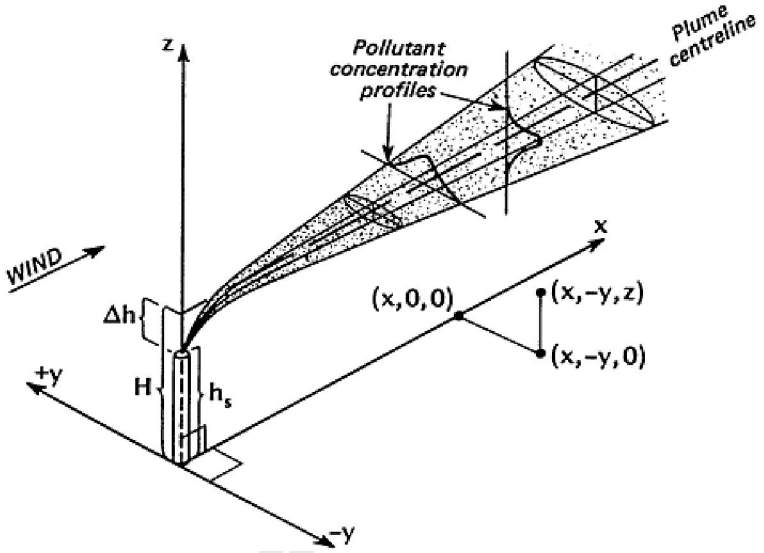

Figure 2.12 Dispersing pattern of air pollutant plume in the Gaussian models.

Source: http://www.mfe.govt.nz/index.html.

For the calculations, the plume is assumed to be emitted at coordinate (0, 0, H) where H is effective stack height which is the summation of the physical stack height and plume rise (Δh). The emitted smoke at the point source is assumed to travel along x direction under support of the constant horizontal wind velocity u. According to this concept, value of aerosol concentration at a particular point *(x,y,z)* can be estimated through the relation (Srivastava and Rao, 2011):

$$C(x,y,z) = \frac{Q}{2\pi.u.\sigma_y.\sigma_z} e^{\frac{-y^2}{2\sigma_y^2}} . \left[e^{\frac{-(z-H)^2}{2\sigma_z^2}} + e^{\frac{-(z+H)^2}{2\sigma_z^2}} \right] \qquad (2.19)$$

where *C(x,y,z)* is aerosol concentration at the preferred location on the downwind side (g/m^3), Q is source emission rate (g/s), u is horizontal wind speed (m/s), H is effective

stack height (m), σ_y and σ_z are standard deviations of air pollutant distribution along the cross-wind horizontal (y-axis) and vertical (z-axis) directions, respectively (m). Values of σ_y and σ_z depend mainly on the downwind distance from source (along x-axis) and the air stability level.

The Gaussian models are often used for predicting dispersion of continuous, buoyant air pollution plumes originating from the ground-level or elevated sources under the steady-state atmosphere (as shown in Figure 2.10). However, these models may also be applied for the prediction of the dispersion pattern of non-continuous air pollution plumes (called puff models). Due to initial assumptions stated earlier, the Gaussian models are not suitable for prediction long range dispersion (e.g. greater than 50 km), that frequently under control of the non-steady state atmosphere, and also the analysis of smoke plume distribution under relatively calm atmosphere (with $u \approx 0$) (Pasquill, 1974; Holmes and Morawska, 2006 and Srivastava and Rao, 2011).

(3) Lagrangian model. Apart from the popular Gaussian models stated earlier, another approach to air dispersion simulation that gains more attention in recent years is the so-called Lagrangian model. These models try to describe the transportation and diffusion pattern of the smoke plume (or puff) under the ambient turbulence based on statistical analysis of the random movement of a large number of the pollution plume (or puff) particles with respect to a moving frame of reference that follows along with the plume movement. This approach is much more applicable nowadays due to the support of advanced computing technology that makes the tracing of the trajectory of individual aerosol particles (within a plume) can be performed more realistically as well as the distribution pattern after a certain time elapse (Srivastava and Rao, 2011).

The Lagrangian approach was proved very promising in the evaluation of air pollution dispersion pattern in the non-steady state atmosphere which is still not much fulfilled by the classic Gaussian plume models. This approach also benefits for the long-range prediction of air pollution under gradual changes in atmospheric condition like the turbulence or wind velocity as mentioned in Bellasio, Scarpato, Bianconi, and Zeppa (2012).

(4) Eulerian model. This model has similar concept to that of the Lagrangian model in that it tracks moving path of a large number of pollution plume parcels as they gradually move away from their initial location. The most important difference between these two groups of the models is that the Eulerian model uses a fixed three-dimensional Cartesian grid as a frame of reference for describing movement of plume particles rather than a moving frame of reference that follows along the travelling path of these particles preferred in the Lagrangian model. More details of these two types of dispersion models are given in Srivastava and Rao (2011).

มหาวิทยาลัยเทคโนโลยีสุรนารี

2.5.2 Prominent air dispersion models

Plenty of the air dispersion models exist at present to serve the growing needs in field of air pollution assessment. Among theses, some are recommended for the use by the US-EPA as detailed below (SCRAM-EPA, 2012).

(1) AERMOD (AMS/EPA Regulatory Model). This is a widely-used steady-state dispersion model designed for short-range (up to 50 kilometers) dispersion of air pollutant emissions from stationary industrial sources. It was developed as joint work of the American Meteorological Society (AMS) and the US-EPA during 1990s period and was officially adopted by the EPA for operating short-range dispersion analysis as

a replacement for its predecessor ISC3 (Industrial Source Complex) model in 2000. AERMOD simulates the dispersion of air pollutants under different conditions of the atmospheric boundary layer turbulence and terrain characteristics based on Gaussian dispersion framework for the stable atmospheric conditions (i.e., with low turbulence) and on non-Gaussian dispersion for unstable conditions (high turbulence). Algorithms for plume depletion by wet and dry deposition are also included in the model.

The AERMOD modeling system consists of two pre-processor components called the AERMET and AERMAP, and the core dispersion model called AERMOD. During the operation, the AERMET shall provide AERMOD with the meteorological information needed to characterize atmospheric condition while the AERMAP shall characterize terrain and generate receptor grids for the dispersion model (AERMOD). More details of the AERMOD model are given in US-EPA (2004).

(2) CALPUFF (California Puff). This is an advanced, integrated Gaussian and Lagrangian model for the simulation of atmospheric pollution dispersion of the smoke puff under the non-steady state atmosphere. It has been developed and distributed by the Atmospheric Studies Group at TRC Solutions and was recommended for the use in far-field (> 50 km) air quality assessment by the EPA in 2003 and for near-source (< 50 km) analysis in 2005.

The CALPUFF model was designed to simulate dispersion of buoyant, puff or the continuous point, area, or line sources. Its modeling system consists of three main components called the CALMET (a diagnostic 3-dimensional meteorological model for preparing input meteorological data), CALPUFF (an air quality dispersion model), and CALPOST (a post-processing package). Each of these programs has independent graphical user interface (GUI). In addition to these components, there are numerous

other processors that may be used to prepare geophysical (land use and terrain) data in many standard formats as well as the relevant meteorological data (surface, upper air, precipitation). More information is given in Scire, Strmaitis and Yamartino (2000).

(3) CALINE (California Line Source Model). This model was developed by the California Department of Transportation and the US Federal Highways Agency for assessing roadway traffic emissions. The first version (CALINE1) was released in 1972 and its latest available version is CALINE4. The model adopts classic Gaussian diffusion theory (as in the Gaussian plume model) to explain the gradual expansion of the traffic-induced air pollution plume and predict concentration of the air pollutants over a particular area located within 500 meters of the roadway (CO, NO_2 and PM).

CALINE4 works by partitioning the examined traffic line into several small sections which are treated as a separated emission point source of a pollutant plume that shall subsequently disperse downwind under influence of the uniform horizontal wind. Pollutant concentrations at any specific location can be determined using total contribution from the overlapping pollution plumes originating from the sequence of roadway links. Each CALINE run allows the prediction of up to eight one-hour mean concentrations. Therefore it is useful for investigating one-hour concentrations of NO_2 and CO and eight-hour concentrations of CO. However, CALINE4 was not designed to emulate changing emission rate from decelerating, idling and accelerating vehicles (i.e. emission rate for each given roadway element in the model is an hourly average). In this case, some CALINE-based model designed specifically to evaluate intersection dispersion such as the CAL3QHC (CALINE3 with queuing and hot spot calculations) may be more appropriate. More CALINE information is available in Caltrans (1989).

2.5.3 The HYSPLIT dispersion model

In this thesis, application of the interested dispersion model called HYSPLIT (HYbrid Single-Particle Lagrangian Integrated Trajectory) was carried out to evaluate the forward and backward trajectories and distributing patterns of the fire-induced smoke plumes observed over the study area. The model was developed by joint effort of NOAA's Air Resources Laboratory (ARL) and Australia's Bureau of Meteorology. The first version (1.0) was introduced in 1982 and latest version (4.9) was released in 2009, where the global Eulerian model (grid-in-plume) was integrated, and is able to be acquired free of charge at website: http://www.arl.noaa.gov/HYSPLIT_info.php.

The HYSPLIT model is now attracting more interest as a powerful tool for the simulation of air parcel trajectory for the regional or long-range transport, dispersion, and deposition of air pollutants. Its applications typically focus in three main topics: (1) air trajectory mapping, (2) plume dispersion simulation and (3) air concentrations and deposition quantification. The following description of the model presented here is mostly based on Draxler (2004; 2011). The model's processing method is a hybrid between the Lagrangian approach that uses a moving frame of reference to locate movements of individual air parcels and the Eulerian approach, which uses a fixed 3D grid as frame of reference (Figure 2.13). In the model, advection/diffusion processes are performed in Lagrangian framework following the transport of air parcels while the calculation of pollutant concentrations are evaluated on fixed grid. The dispersion of air pollutants in HYSPLIT model is simulated by assuming either puff or particle dispersion concept, or as an integration of both (hybrid method).

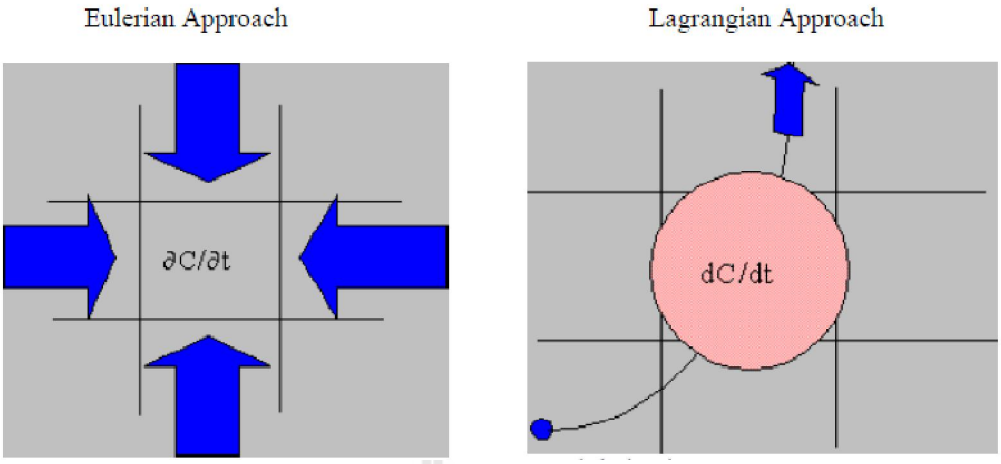

Figure 2.13 The Eulerian and Lagrangian approach used in the HYSPLIT model (ARL, 2013).

In the particle model, a fixed number of particles are released from original source with mean and random motion. They are advected about the model domain by mean wind field and spread by a turbulent component. Under this condition, a cluster of particles released at the same point (from contributing source) shall be expanded in space and time simulating the dispersive nature of the atmosphere. The smoke plume trajectory is then identified by time integration of the position of an air parcel as it is transported by the 3D winds that results in temporal 3D particle distribution map that can be further used as required.

In a puff model, the source is simulated by releasing pollutant puffs at regular intervals over the duration of the release with either a Gaussian or top-hat horizontal density distribution. The puff will be advected according to the trajectory of its center position while the size of the puff (both horizontally and vertically) expands in time to account for the dispersive nature of a turbulent atmosphere. These puffs will expand (in 3D configuration) until they exceed definite size of meteorological grid cell (either

horizontally or vertically), then split into several new puffs, each with its share of the pollutant mass. Regardless of which approach, the turbulent component of the motion is needed to be computed from the meteorological data.

The hybrid method integrates both puff and particle methods assuming a puff distribution in horizontal and particle dispersion in the vertical direction. The resulting calculation may be started with a single particle. As its horizontal distribution expands beyond the meteorological grid size, it will split into multiple particle-puffs, each with their respective fraction of the pollutant mass. In this way, the greater accuracy of the vertical dispersion parameterization of the particle model is combined with advantage of having an expanding number of particles represent the pollutant distribution as the spatial coverage of the pollutant increases and therefore a single particle can represent relatively lower concentrations. Both forward and backward trajectories can be found by the HYSPLIT model. By moving backward in time, the back trajectory indicates air volume arriving at a given point at a specific time, thus can inform source region.

Determination of air concentration

Air concentrations are computed by summing each particle's mass as it passes over the concentration grid, which is often defined by latitude-longitude intersections. Simultaneous multiple grids with different horizontal resolutions/temporal averaging periods can be defined for each simulation. Each considered pollutant species is summed independently on each grid. In the particle-based mode, the concentration grid is treated as a matrix of cells, each with a volume defined by the grid dimensions. Therefore, the air concentration is just the particle mass divided by the cell volume. In the puff calculation, however, the defined concentration grid is considered as a matrix of sampling points, such that the puff only contributes to the concentration as it passes

over the sampling point. In the puff calculation mode, it is possible for a puff to pass between points and not be shown on the display. Examples of concentration maps the particle and puff distributions are shown in Figure 2.14. Note that the puff distribution is smoother but much broader as, for this particular case; the horizontal puff growth equations give larger values than the particle expansion.

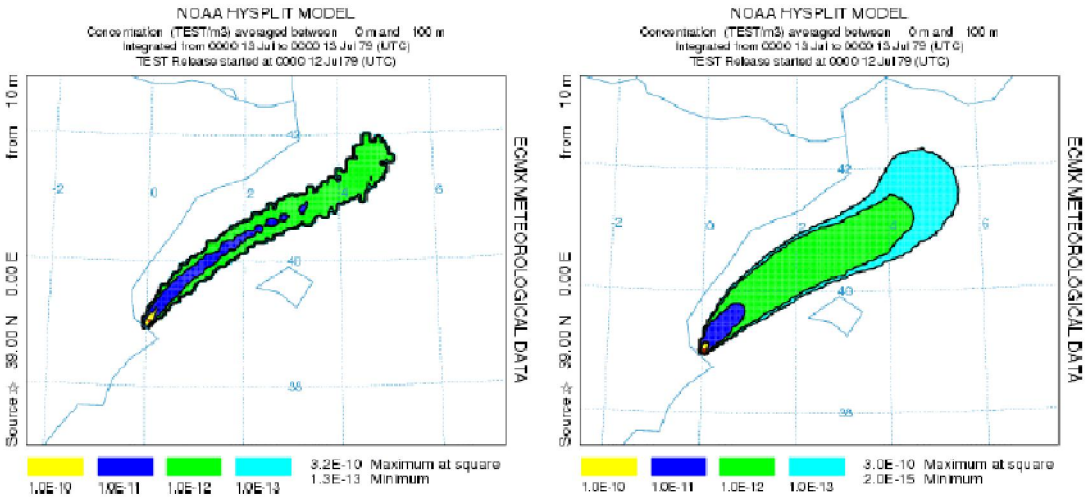

(a) particle-based (b) puff-based

Figure 2.14 Examples of (a) particle-based and (b) puff-based concentration maps produced by the HYSPLIT model (ARL, 2013).

Input/output data

Apart from the pollutant emission information, knowledge on gridded fields of the meteorological variables is required at regular temporal interval. The time interval between fields should be constant for each predefined grid. The meteorological data file should consist of direct-access, fixed-length records, one record per variable per level. These data field may be provided using one of four different vertical coordinate

systems, which are, the pressure-sigma, pressure-absolute, terrain-sigma, or a hybrid absolute-pressure-sigma. At a minimum, the model requires at least horizontal wind components, temperature, height or pressure, and the pressure at the surface. If wet deposition is to be included, the model also requires the rainfall field. Two basic types of the model output are available: trajectories (as ASCII files) and air concentrations or depositions (as binary files). Contoured plots could be generated using similar post-processing programs. More HYSPLIT information is given in ARL (2013).

The HYSPLIT model has been successfully utilized in several reported works, for examples, Ma and Choi (2007) used the model to identify area source of the dust storm experienced at Fukuoka, Japan, during springtime of 2005 and found that it was driven mainly from the Chinese continent. Pongkiatkul and Oanh (2007) applied both trajectory analysis and monitoring data to assess potential contribution of long range transportation to PM pollution found in Bangkok Metropolitan Region (BMR). The 10-day backward trajectories of air masses arriving at BMR from January 2002 to December 2004 were identified and categorized by k-means clustering into 6 clusters with different associated PM levels. Highest average PM10 and PM2.5 levels were found in long-distance air mass that moved over populated South East Asia (SEA).

Lee, Park, Kim and Kim (2008) investigated impact of air mass trajectories on the PM2.5 mass. It was found that during the Asian dust (AD) periods when air mass passed over Korean peninsula, Asian dust and secondary organic carbon accounted for 25.2 and 23.0% of the PM2.5 mass, respectively, whereas Asian dust contributed only 10.8% to the PM2.5 mass during the AD event when the air mass passed over the Yellow Sea. Contribution of biomass burning to the PM2.5 mass during the biomass burning (BB) event was about 63.8%.

Liu, Kahn, Chaloulakou and Koutrakis (2009) studied the impact of Greek forest fires in August 2007 on air quality in Athens, Greece, from which two pollution episodes were identified by ground-based PM10 measurements between August 23 and September 4. It was concluded that, for the first episode, Evia and Peloponnese fires contributed substantially to air pollution levels in Athens. In the second episode, transport of industrial pollution from Italy and Western Europe as well as forest fires in Albania contributed greatly to the air pollution levels recorded in Athens.

Shan, Yin, Lu, and Liang (2009) analyzed the ozone episodes experienced in 2004 at the Jinan city of East China. The meteorological conditions of episode days and non-episode days were compared and examined and categorization of 6 groups in total of the backward trajectories was performed. It was concluded that most episodes were caused by the local photochemical production and the pollutant accumulation. In addition, the transport of pollutants from highly polluted regions could significantly influence air quality at the ground-based measuring site.

Kaskaoutis, Kosmopoulos, Kambezidis, and Nastos (2010) applied the model at Athens, Greece, to identify back trajectories at three altitudes to investigate relation between AOD550-FM (fine mode) and wind sector. Obtained results indicate that, the accumulation of the local pollution is favored in spring linked to air masses at lower altitudes originating from Eastern Europe and the Balkan. Clean maritime conditions are rare over the Athens, limited in winter season and associated with air masses from western or northwestern sector. In summer, northern sector dominates, while in the other season of the year (especially spring), the air masses belong to southern sector enriched with Saharan dust aerosols.

Cheng et al. (2013) examined impact of trans-boundary air pollutant transport on regional air quality based on a combination of the HYSPLIT trajectory model, the CAMx air quality model, and the MM5 meteorological model, in Guangzhou city of southern China. Their results illustrated that trans-boundary PM10 transport played a critical role in the formation of PM10 pollution events in the Guangzhou, with a mean contribution ratio of nearly 49%. In particular, two air mass clusters originated from Guangzhou's surrounding regions were found to be the main pollutant transport.

CHAPTER III

METHODOLOGY AND PRELIMINARY ANALYSIS

3.1 Conceptual framework

This work comprises of three main parts in accordance with three objectives stated in Section 1.2 as detailed in work flowchart displayed in Figure 3.1. The first part is devoted to the examination of relationships among MODIS radiances (in blue, green, red, and MIR bands), MODIS-AOD, BAER-AOD, AERONET AOD, NDAI, and the reference PM10 data accumulate from the ground-based measuring stations situated in the study area (as listed in Table 1.1). The found relationships are reported along with their corresponding R^2. The main objectives of this part are to find mutual relationship among parameters under consideration and to identify a parameter that attains optimal correlation to the reference PM10 data and could be used for further derivation of daily PM10 maps over the entire area done in the following part.

The second part is contributed to the derivation and implementation of the fine-scale maps (at 500m spatial resolution) of NDAI, PM10, and AQI data on some specific dates of interest during 2010 fire season. The PM10 maps were developed from the preferred method found in the first part as mentioned earlier. Subsequently, the associated AQI maps were generated from the PM10 maps using standard method adopted in Thailand, UK, and USA. In addition, the newly-proposed method for AQI classification was also applied to be an alternative option for doing this work.

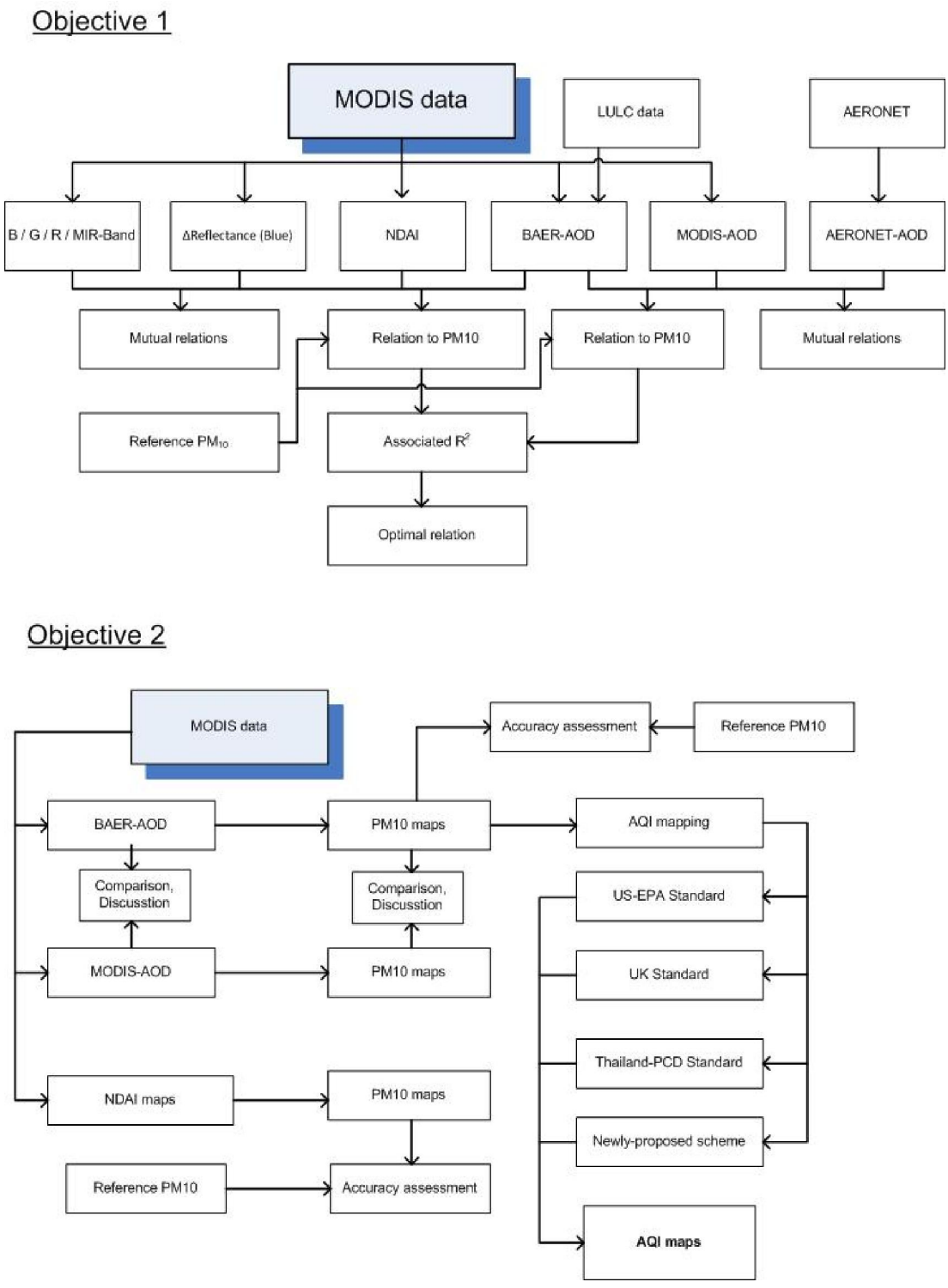

Figure 3.1a Conceptual framework of the study for Objectives 1 and 2.

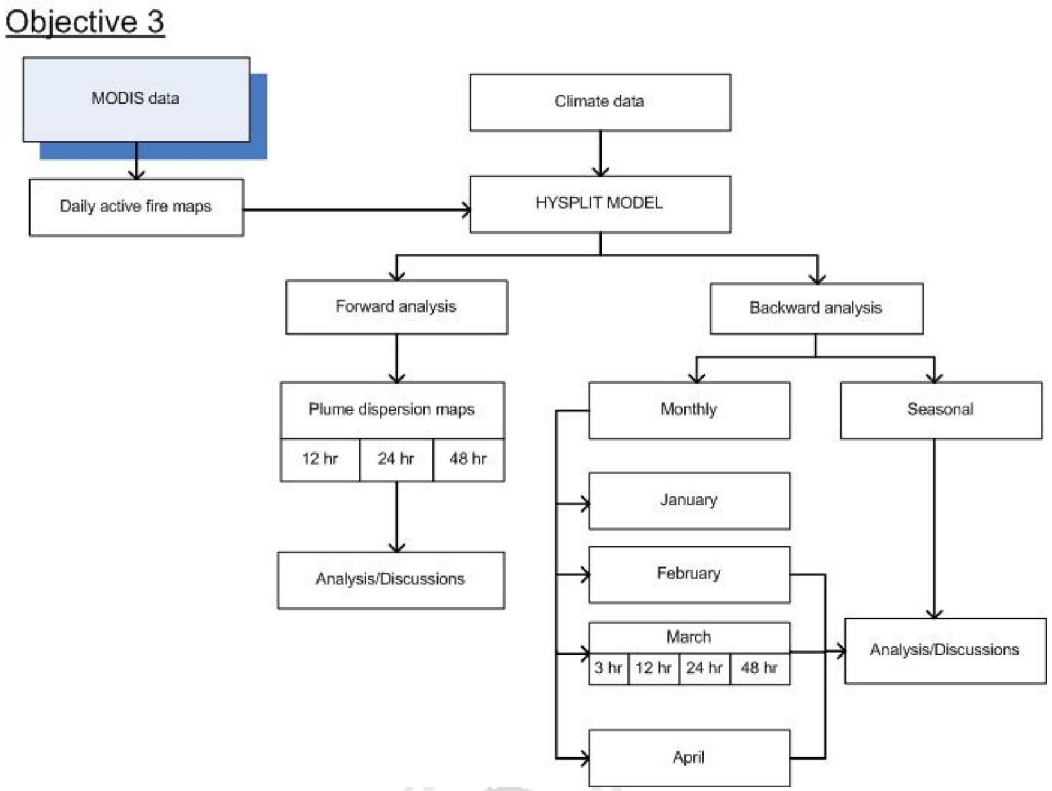

Figure 3.1b Conceptual framework of the study for proposed Objective 3.

Table 3.1 Information of required input data and their contributing sources.

Data Type	Distributor
MODIS imagery (Terra satellite)	USGS's LP- DACC website, AIT-ACRoRS
MODIS AOD	LAADS website (MOD04-Level 2)
Active fire data	Derivation based on MOD14 dataset
AERONET-AOD	AERONET website
Reference PM10 data	Pollution Control Department (PCD)
Meteorological data	NASA-ARL meteorological data center
LULC, DEM, Administrative map	Land Development Department (LDD)

Note: MODIS imagery was mostly processed by ERDAS-Imagine software while the relevant GIS-based dataset (input/output) were mainly processed by appropriate ArcGIS softwares.

NDAI is a new index introduced here to be a primary indicator of the aerosol pollution severity experienced over the area based on the observed MODIS radiance data in the blue and MIR bands. It was intended to be used as a simple index for the quantification on amount of aerosol pollutant in lower atmosphere similar to the use of NDVI to represent amount of vegetation cover over a particular area. In addition, PM10 data maps derived from conventional MODIS-AOD data (at 10-km resolution) were also presented and compared to their associated fine-scale ones. Main purposes of work carried out in this part are to produce NDAI, PM10 and AQI maps at 500-m scale to implement for the monitoring and assessment of aerosol pollution situation over the entire study area on daily basis over some certain period (with reported high aerosol pollution) during the 2010 fire season (4^{th}-9^{th} April).

The final part focuses on application of the chosen atmospheric dispersion model (HYSPLIT) to the simulation of the fire-induced smoke plume trajectory and distributing pattern as it is moving away from the originated location (within the study area and beyond). This is called the forward analysis of the model. The other task was to trace back trajectories of smoke plumes (based on predicted local air mass moving path) observed at some chosen PCD's aerosol measuring stations over a prescribed period of time (3, 12, 24, and 48 hours). Principal objective of this part is to formulate better understanding on impact of fire locations on aerosol pollution distribution and accumulation observed over the entire study area during 2010 fire season, especially, those long-distance smoke plumes that were contributed by the forest and agricultural fires located in the neighboring countries like Myanmar or Laos which has never been explored systematically before for the area.

3.2 Data preparation

There are five main groups of the data required for this study. These data were acquired from different sources or from developing procedures as listed in Table 3.1 and their initial details are as follows.

(1) MODIS-based data. Three types of the primary data for this category were derived from the original MODIS imagery: (a) reflectance radiance information for several bands of interest; i.e. Band 1-Red, Bands 2-NIR, Band 3-Blue, Band 4-Green and Band 7-MIR (as detailed in Table 2.9); (b) MODIS-AOD data at a standard scale of 10 km provided at the NASA's Level 1 and Atmosphere Archive and Distribution System (LAADS) website (http://ladsweb.nascom.nasa.gov/index.html); (c) MODIS active fire maps. These maps were constructed from the MOD14 module provided by the MODIS website. Concepts of the MODIS fire detection algorithms were reported in several works, e.g., Kaufman et al. (2002); Justtice et al. (2002); and Giglio, Descloitres, Justice, and Kaufman (2003).

The crucial original MODIS imagery were acquired directly from the official USGS's Land Processes Distributed Active Archive Center (LP-DAAC) website (https://lpdaac. usgs.gov). These images were undergone proper georectifying process using reference data given at the LP-DAAC website. Major cloud elements visible on the images were filtered off beforehand using the cloud filtering method developed by the MODIS Cloud Mask Team as detailed in Ackerman et al. (2006).

(2) AERONET-AOD data (Level 2) recorded at the active AERONET station situated in Chiang Mai's central area. These dataset were downloaded directly from the AERONET website (at http://aeronet.gsfc.nasa.gov). The temporal resolution of the acquired data is 15 minutes.

(3) Reference recorded near-ground PM10 data (hourly and daily scales). These data were accumulated from the Pollution Control Department (PCD) for the stations of interest situated in the study area (as listed in Table 1.1).

PM10 samples were divided into two groups of data, during January to April 2009 and January to March 2010. The data were used for model construction while PM10 samples in April 2010 were used to validate the model.

(4) Meteorological data required by the HYSPLIT model, e.g., local wind speed/direction, mixing height (PBL), air pressure, air temperature. These data were acquired from the NASA-Air Resources Laboratory (ARL) meteorological data center for the HYSPLIT applications.

(5) Main auxiliary data required in the study include:

5.1 Land use and land cover (LULC) data in 2010 for the entire study area was provided by LDD as well as the associated administrative map of the area. Five main LULC classed were subsequently identified: forest (68.9%), agriculture (25.2%), urban/built-up (3.0%), water body (1.2%) and others (1.7%) as detailed in Figure 3.2 and Table 3.2. In addition, three subclasses of forest were also identified: evergreen forest (11.6%), deciduous forest (56.9%) and plantation forest (0.4%).

5.2 Topography data (10 m-DEM) of the study area were contributed from the Land Development Department (LDD) as shown in Figure 1.1. The elevations were found ranging from about 100 to 2,600 m. above mean sea level.

Table 3.2 Proportion of the LULC distribution presented in Figure 3.2.

Area	LULC								Total
	FOR				AGR	U/B	WAT	MIS	
	EVG	DCD	PLT	Total					
km^2	10,292	50,274	348	60,914	22,257	2,632	1,061	1,506	88,370
%	11.6	56.9	0.4	68.9	25.2	3.0	1.2	1.7	100.0

Note: FOR ≡ Forest, EVG ≡ Evergreen forest, DCD ≡ Deciduous forest, PLT ≡ Plantation forest, AGR ≡ Agriculture, U/B ≡ Urban/Build-up, WAT ≡ Water body MIS ≡ Miscellaneous

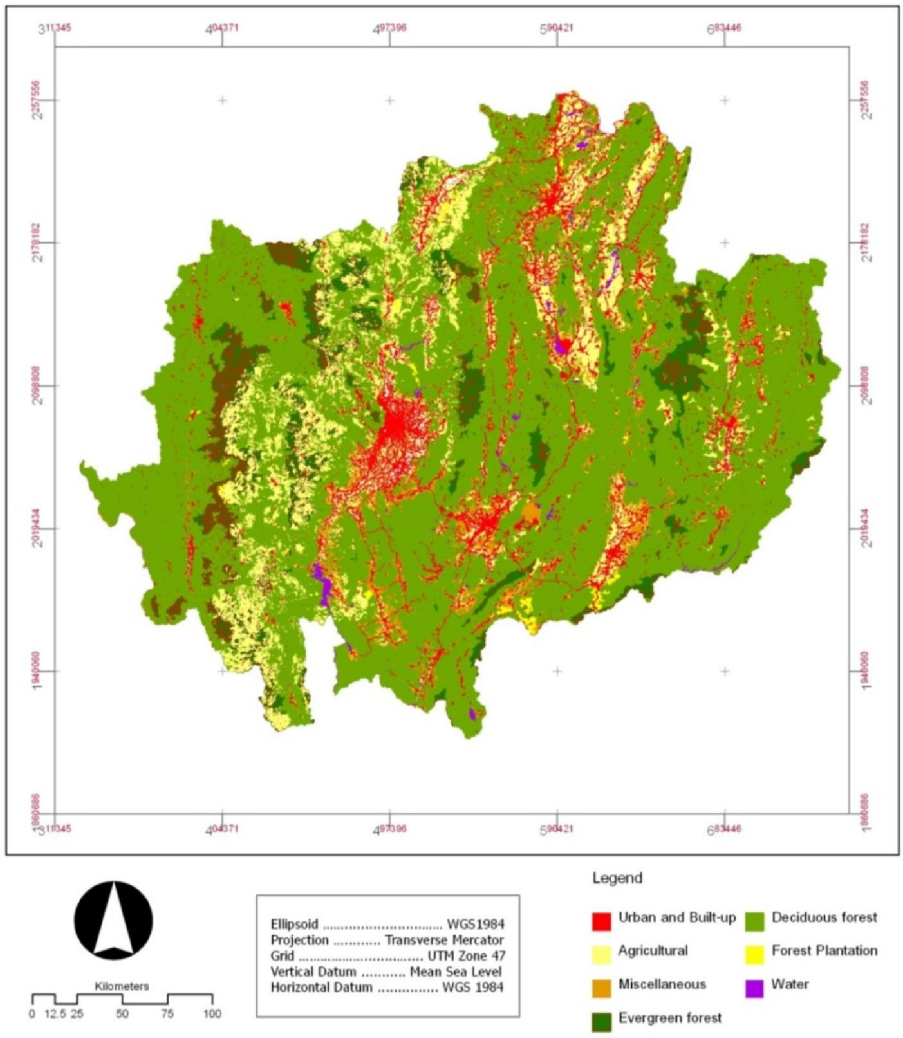

Figure 3.2 Classified LULC map of the study area. (LDD, 2007)

3.3 Research procedure

The research procedure is divided into three main parts in accordance with the three proposed objectives stated in Section 1.2 as follows.

3.3.1 Relationship analysis of MODIS-based parameters and PM10 data

(1) MODIS reflectance radiances of blue, green, red, and MIR bands were extracted (at a pixel-based scale) from original MODIS images during 2009 and 2010 fire seasons. These images were mostly chosen from those dates which have moderate to high PM10 pollution reported over the area.

(2) Data of the interested MODIS-based parameters (MODIS-AOD, BAER-AOD, ΔR [blue], NDAI) and AERONET-AOD were prepared from the original data acquired from their official contributing sources or generated from the associated MODIS spectral radiance data compiled in step (1) using appropriate methods. More details are as follows.

2.1 MODIS-AOD maps (at standard 10km spatial scale) were prepared from the acquired original data (MOD04-Level 2) provided at the LAADS website.

2.2 The BAER-AOD maps (at 500m spatial scale) were produced using the proposed method described in Chapter 2 (Section 2.4.3). This method was developed based on reports about recent applications of the BAER method on AOD retrieval over land from satellite imagery, for examples, von Hoyningen-Huene et al. (2003); Lee et al. (2005); Lee, Kim, von Hoyningen-Huene and Burrow (2007). To achieve this stated task, some prior assumptions were introduced to assist the AOD determination by the BAER method as described later in Section 3.4.4, especially, the

fundamental relationship of the computed aerosol reflectance (ρ_{AS}) and observed AOD data.

2.3 Pixel-based radiance difference data (ΔR) of MODIS's blue band (Band 3) were calculated from the differences in reflectance radiance data of this band on the polluted dates of interest with those on the reference pollution-free date, or,

$$\Delta R(\text{blue}) = R(PD) - R(PFD) \tag{3.1}$$

where R(PD) and R(PFD) are radiance values of the MODIS-Band 3 on the polluted date and the reference pollution-free date respectively. The blue radiance was chosen due to its highly sensitive nature to variation of PM10 concentration level as found in the preliminary analysis (in Section 3.4.3).

2.4 The proposed Normalized Difference Aerosol Index (NDAI) was computed using the following relation:

$$NDAI = \frac{\text{Blue} - 0.25\text{MIR}}{\text{Blue} + 0.25\text{MIR}} \tag{3.2}$$

where Blue and MIR are measured radiance intensity of the MODIS's blue band (Band 3) and mid-infrared band (Band 7), respectively. The constant term (0.25) was chosen as indicated by results of the preliminary analysis on the established relation between the blue and MIR bands (Figure 3.10) to make the NDAI becomes close to zero on the aerosol-free date (PM10 $\approx$ 0).

Example of the MODIS-visible image on 6th April 2010 (polluted date) along with its associated MODIS-AOD, BAER-AOD, and NDAI maps are presented in Figure 3.3. The appearance of smoke plume over the entire area is clearly noticeable in the VIS image and its intensity can be approximated by the AOD and NDAI maps.

Information of these parameters for other dates of the 2010 fire season is presented in Chapter 4 and Appendix B, respectively.

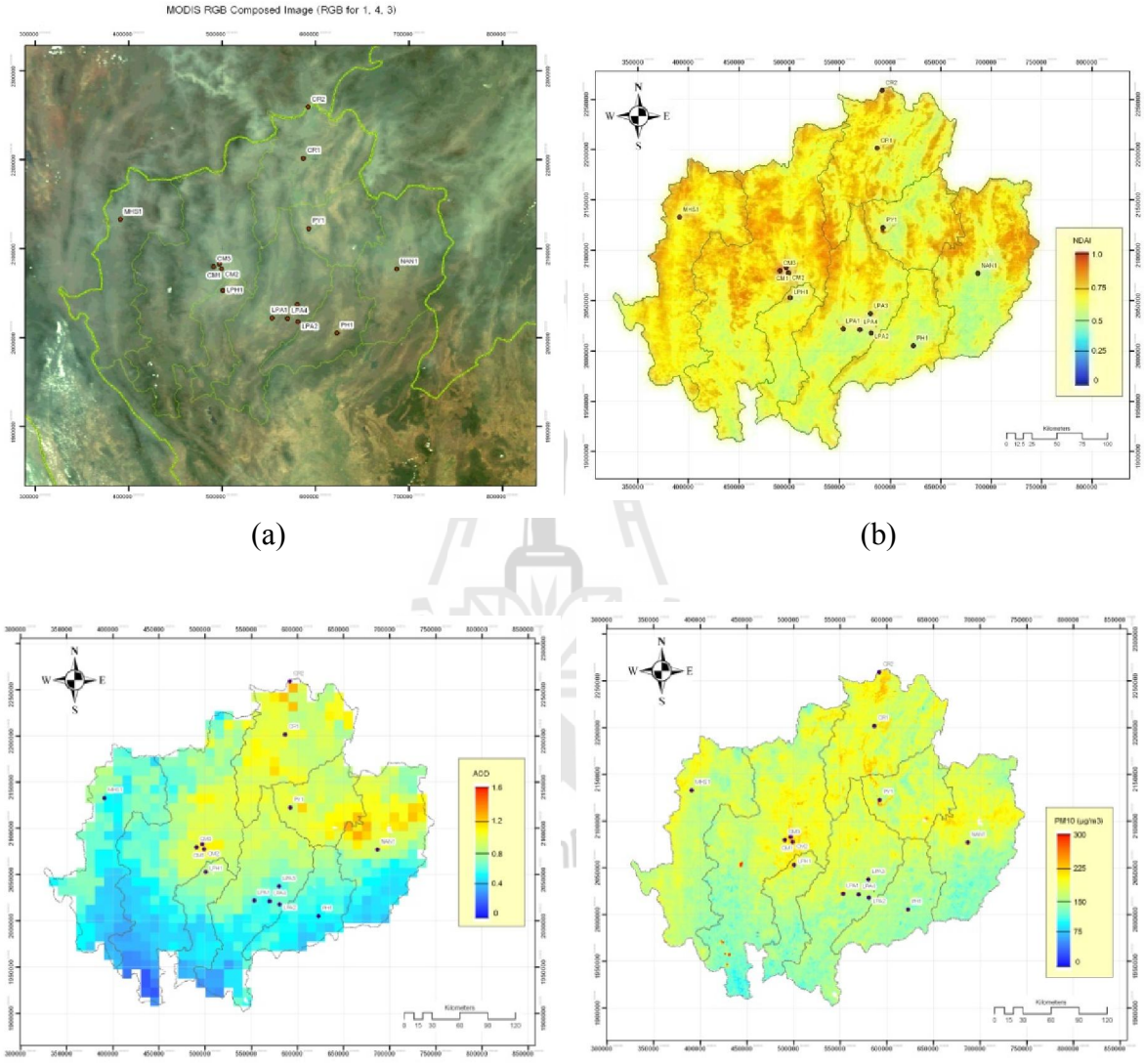

Figure 3.3 Example of derived MODIS-based data maps on 6th April 2010 including (a) MODIS-Visible image (true color), (b) derived NDAI map, (c) MODIS-AOD map and (d) BAER-AOD map.

(3) The apparent relationships between each parameter [MODIS radiances in B/G/R/MIR bands, ΔR (blue), MODIS-AOD, BAER-AOD, NDAI, and AERONET-AOD] with reference ground-based PM10 data were evaluated. The linear regression relation was assumed and the coefficient of determination (R^2) was determined to identify the correlation level seen in each found relationship. The output with highest value of R^2 (except for the MODIS-AOD and AERONET-AOD) was considered an optimal parameter which was subsequently taken to produce predicted PM10 maps (at 500-m scale) over the entire area in later study. The MODIS-AOD data were excluded due to the coarse resolution (10 km) and the AERONET-AOD data were not in favor due to their very limited locations available which are not sufficient for the producing associated PM10 maps for the whole area. However, their apparent high correlation to the observed PM10 data is very useful as they might be applicable for the preliminary assessment of PM10 pollution severity over the entire study area (for the MODIS-AOD) and in the Chiang Mai's central area in particular (for the AERONET-AOD). Moreover, the mutual relationships between some pair of parameters listed above were also examined and reported along with their corresponding R^2.

Note that, due to the rather differences in spatial scale and observing time of the MODIS-based data, AERONET data, and PM10 data; a pair of the dataset to be assessed their potential relationship must be accumulated from the specific pixels or locations that have less space/time discrepancy as much as possible to each other. For example, the MODIS-AOD pixels whose centers positioned closest to the PM10 measuring stations in use were employed in conjunction with the used PM10 data recorded within ±30 minutes of the satellite over passing time.

3.3.2 Development of the fine-scale maps of NDAI, PM10, and AQI data

(1) Maps of the NDAI were constructed for the entire area on the chosen dates with relatively high PM10 pollution severity (4^{th}-9^{th} April 2010) based on the formula given in Eq. 3.2. Results were then interpreted and discussed.

(2) Maps of the PM10 concentration on chosen dates (4^{th}-9^{th} April 2010) were derived from MODIS images using optimal method identified in the earlier analysis. Accuracy of these developed maps was assessed using the concurrent reference data measured at the ground stations situated within the area. The assessment results are reported in terms of the mean absolute error (MSE) and R^2 value, respectively.

(3) The derived PM10 map obtained in Step (2) were compared to those maps generated from the MODIS-AOD data on the same dates and to the derived NDAI maps in Step (1) to identify the existing notable similarity or differences.

(4) The associated air quality index (AQI) maps for the chosen dates were formulated from their corresponding PM10 density maps gained in Step (2) based on three chosen methods (as listed in Table 3.3). The output maps obtained from each considered method were compared and discussed. The methods under consideration here are as follows:

4.1 PCD standard (for Thailand). Its current criteria were modified from those introduced by the US-EPA as reported in 1999 (Table 2.1b). The conversion of the original PM10 data into the equivalent AQI data was performed in according to the formula given in Eq. 2.1 where six classes (or bands) of AQI data were identified (from good to hazardous level for AQI data ranging from 0 to 500).

4.2 US-EPA standard. Its current criteria were introduced and effective since 2006 (Table 2.1a). Conversion of the original PM10 data into the equivalent

AQI data was conducted using a formula in Eq. 2.1 and six classes of AQI data were identified (from good to hazardous level for AQI data ranging from 0 to 500).

4.3 UK standard. This is currently in use for making daily report on PM10 situation in the United Kingdom by the Department for Environment Food and Rural Affairs (DEFRA) (Table 2.2a). This system divides the observed PM data into 10 principal classes (or band) which are grouped to form four distinct PM10 severity levels (from low to very high) in which only PM10 density of about 0 to 100 $\mu g/m^3$ are mostly monitored as no further indexing is made for PM10 data of > 100 $\mu g/m^3$. The UK classifying method is also implemented (with some modifications) in some countries of the Commonwealth like Canada and Australia (COMEAP, 2011).

มหาวิทยาลัยเทคโนโลยีสุรนารี

Table 3.3 Classifying criteria of the PM10 (24-hour running mean concentration) and associated AQI data used in the three applied methods (PM10 unit: $\mu g/m^3$).

Thailand-PCD		**Air quality category**
AQI	PM10	
0-50	0-40	Good
51-100	41-120	Moderate
101-200	121-350	Unhealthy
201-300	351-420	Very Unhealthy
301-400	421-500	Hazardous
US-EPA		**Air quality category**
AQI	PM10	
0-50	0-54	Good
51-100	55-154	Moderate
101-150	155-254	Unhealthy (for sensitive group)
151-200	255-354	Unhealthy
201-300	355-424	Very Unhealthy
301-500	425-600	Hazardous
UK-DEFRA		**Category**
AQI Band	PM10	
1	0-16	Low
2	17-33	
3	34-49	
4	50-58	Moderate
5	59-66	
6	67-74	
7	75-83	High
8	84-91	
9	92-99	
10	≥ 100	Very High

3.3.3 Newly-proposed method for AQI map

Newly-proposed method. It was established to accommodate WHO guide lines on the PM10 regulations (Table 2.4a) and to act as a compromise between current EPA-standard (whose AQI bands are rather broad in terms of the associated PM10 range) and the UK standard (whose AQI bands are rather narrow in terms of the associated PM10 range). There are twelve AQI bands proposed at present in total which are associated to the PM10 density ranging from 0 to 400 $\mu g/m^3$ mostly. Among these, five bands were allocated for the PM10 data of 100-300 $\mu g/m^3$ which were found to be most dominant (over 90% of the total derived PM10 data) during period of the study (as seen in Figure 4.9).

Under the criteria taken by the newly-proposed method, the known PM10 data are segmented into twelve bands (with different bandwidths) to establish six AQI categories as listed in Table 3.4 (from low to extremely high). Main interest of the design was focused on the "Low" and "Moderate" categories (PM10 of 0-150 $\mu g/m^3$) that are expected to occur the most during the year of the study area. There are two AQI bands contributed to the "Low" category of the observed PM10 data (Band 1-2) with the assigned bandwidth of 25 $\mu g/m^3$ each. At this level, it is still considered safe for the human health in general (equivalent to the "Good" category of the EPA and PCD standards and the "Low" category of the UK standard). Upper bound of this category (at 50 $\mu g/m^3$) was set to reflect ultimate target for the surface PM10 volume proposed by the WHO (AQG).

Table 3.4 Classifying criteria of the PM10 (24-hour running mean concentration) and associated AQI data used in the Newly-propose method (PM10 unit: $\mu g/m^3$).

AQI Band	This study (proposed)		
	PM10	WHO/PCD	Category
1	0-25	-	Low
2	26-50	Target (50)	
3	51-75	IT-3 (75)	Moderate
4	76-100	IT-2 (100)	
5	101-120	PCD (120)	Relatively High
6	121-150	IT-1 (150)	
7	151-200	-	High
8	201-250	-	
9	251-300	-	Very High
10	301-350	-	
11	351-400	-	
12	≥ 400	-	Extremely High

Note: IT ≡ Interim target for the PM10 regulation proposed by the WHO.

The moderate and relatively high portions of PM10 data (50-150 $\mu g/m^3$) were defined to be primary stages of the concern for the possible health impact caused by the increase of PM10 pollutant in the lower atmosphere. This is resembled to the "Moderate" category of the EPA and PCD standards but with better details and to the "Moderate" and "High" categories of the UK-DEFRA standard (for Bands 3 and 4, respectively) with coarser details. Health warning associated to the PM10 data at this level can be adapted from these responsible agencies, or from the WHO guidelines earlier stated in Section 2.2.2. The upper bound value of 75 $\mu g/m^3$ (for Band 3), 100 $\mu g/m^3$ (for Band 4), and 150 $\mu g/m^3$ (for Band 6) were set to equal the interim target for the near-ground PM10 volume proposed by the WHO. And the 120 $\mu g/m^3$ (for

band 5) was chosen to represent the critical value for having severe PM10 pollution used by the PCD at present.

The "High" category (for PM10 of 151-250 $\mu g/m^3$) is divided into two AQI bands (Band 7-8). It was defined to indicate high level of the PM10 volume in the atmosphere that might be harmful for the sensitive group (like children or people with respiratory or lung diseases) which is similar to the "Unhealthy (for sensitive group)" category adopted in the US-EPA standard. The "Very High" category (for PM10 of 251-400 $\mu g/m^3$) is divided into three AQI bands (Bands 9 to 11). This group was established to signify serious danger of the PM10 pollution that might affect health of most people, not only for those in the sensitive group and general public should be alerted of potential health impact frequently arisen under this situation. Regarding to the affixed PM10 density, Band 9 and 10 are fairly comparative to the "Unhealthy" category and Band 11 is broadly equivalent to the "Very Unhealthy" category adopted in the US-EPA standard.

Finally, the "Extremely High" category (for PM10 of $\geq$ 400 $\mu g/m^3$) was introduced to represent rare occasion that amount of the PM10 volume in the air is unusually high and all lives are under threat of having serious health problem if the prolonged inhaling of the polluted air is undergone. This is broadly equivalent to the "Hazadous" category of the US-EPA standard at which all physical activity outdoors should be avoided and strong caution must bear in mind for all people in preventing themselves from exposing to the polluted air for too long. Note that, according to US-EPA standard, the AQI value terminates at 500 for the PM10 data of about 600 $\mu g/m^3$ only and no formal consideration is given to the PM10 data lying beyond this limit.

However, under this new system, any PM10 amount of ≥ 400 μg/m^3 is considered being in the "Extremely High" situation.

3.3.4 Applications of the HYSPLIT model

(1) Accumulated active fire locations during the period 4^{nd}-8^{th} April 2010 was mapped based on the obtained daily MODIS data.

(2) The forward analysis was carried out in which the dispersion patterns of observed smoke plumes originated at some specific locations (both inside and outside the country) were evaluated using the HYSPLIT model. Here, the moving time-step of each independent analysis (the smoke plume concentration mapping) was set to be every 12 hours (from 12 to 48 hours). Correlation of the acquired daily concentration maps and their associated PM10 maps was also considered.

(3) Backward analysis was operated in which movement of the air masses arriving at a particular PM10 measuring station (e.g. the CM1 or MHH1 stations) at altitude of 500 m above ground during a time period of interest (e.g. 1 month) were individually traced backwardly in time to portray their back trajectories over a certain timescale (e.g. every 12 hours). The study was divided into 2 main parts:

3.1 All air mass trajectories arriving at each considerred measuring stations of each provinces were mapped for each month of the 2010 fire season at specific time steps of 3, 12, 24, and 48 hours backward.

3.2 Mean trajectories of all air masses arriving at the preferred stations (at each province) at 48-hours time step during each month of the 2010 fire season, and for the entire season, were extracted and mapped. Results are reported here in form of trajectory maps representing major moving directions and information of their

associated air mass number (in percent) along each identified direction. There are six major clusters of the trajectories being identified for each province.

3.4 Preliminary analysis

The preliminary analysis was carried out to gain some crucial information in nature of the aerosol air pollution occurrences experienced over the study area in recent years (especially during the 2010 fire season) as well as the crucial knowledge on relationship between the MODIS radiances of Band 3 (blue) and Band 7 (MIR). In addition, working process of the BAER retrieval method applied in this thesis is also presented in this section. All knowledge achieved at this stage is necessary for the preparation and implementation of relevant works required in Objectives 1 and 2 as described earlier in Section 3.3.

3.4.1 General situation of PM10-based air pollution

According to PCD reports on the PM10 pollution situation over the study area during 1996-2012 (as illustrated in Tables 3.4 and 3.5 and Figures 3.4-3.5), it was found that, in general, PM10 pollution is worst during fire season (January-April) for all provinces with peak values often occurred in March and April while the minimum values mostly found during monsoon season especially in August and September. Large variation of the monthly-mean PM10 data is also readily observed from which the peak values in March are usually about eight times higher than the bottom values in August . Sharp increase of PM10 concentration experienced during February-April each year is traditionally contributed to the dramatic rise in number of the vegetation fires originated both within and beyond the study area (mainly from forest product gathering and agricultural land preparation activity). The most severe years regarding

to level of aerosol pollution are 1999, 2004, 2007, 2010, 2012 and the highest record of the average 24hr data found in the area is 505.5 µg/m^3 at Mae Hong Son in 2010.

Table 3.5 Monthly-mean PM10 data during 1996-2012 (unit: µg/m^3).

Province	Month											
	JAN	FEB	MAR	APR	MAY	JUN	JUL	AUG	SEP	OCT	NOV	DEC
Chiang Mai	44.6	72.5	115.9	104.3	38.1	27.1	21.5	20.4	21.2	22.6	45.9	37.1
Chiang Rai	88.2	89	159.7	116.4	34.4	24.0	20.8	18.7	21.6	28.0	49.6	49.4
Lampang	40.7	85.0	103.2	73.4	30.4	27.4	15.4	14.4	20.8	22.0	38.6	36.6
Lamphun	54.0	110.8	142.2	112.0	42.1	27.2	21.4	21.0	20.1	29.1	65.2	54.8
Mae Hong Son	35.4	76.2	190.8	106.6	44.3	37.1	28.7	19.6	10.4	16.0	30.8	22.8
Nan	36.0	69.8	123.7	84.1	32.5	25.7	17.2	12.6	16.3	22.8	45.9	41.8
Phayao	49.6	100.7	145.3	109.6	43.7	11.2	15.1	6.8	13.4	21.5	72.2	71.9
Phrae	42.4	64.4	74.3	53.9	32.3	22.3	14.7	16.9	22.1	26.2	56.3	55.2
Average	43.9	83.5	131.9	95.0	37.2	25.2	19.4	16.3	18.2	23.5	50.6	46.2

Note: PM10 data for each province were averaged from the available PM10 data at every measuring station situated in the province as listed in Table 1.1.

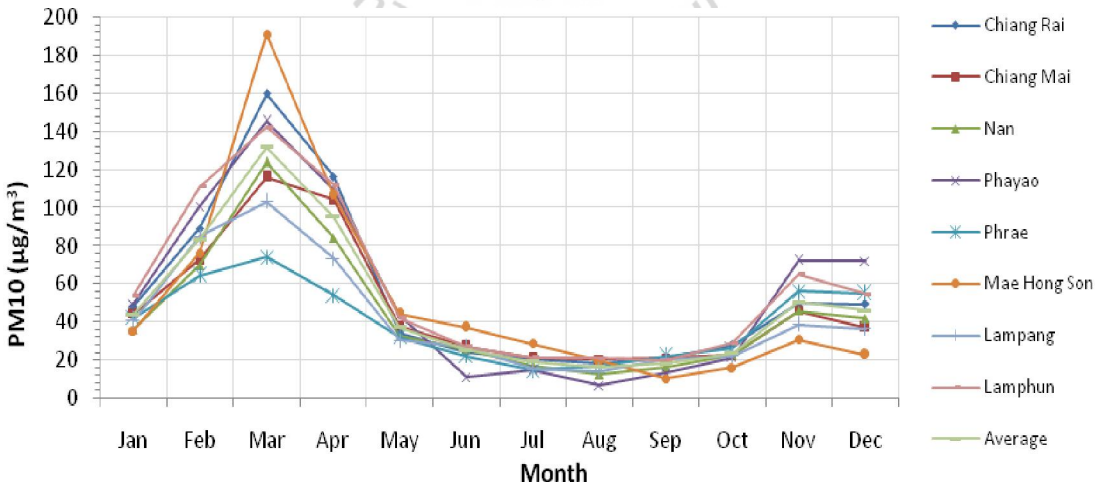

Figure 3.4 Variation of the monthly-mean PM10 data in the area. The maximum and minimum values occur in March and August, respectively (from Table 3.5).

Table 3.6 24 hr-average and 24hr-maximum measured PM10 data for annual fire seasons during 1996-2012 (unit: $\mu g/m^3$).

Province	**PM data**	**1996**	**1997**	**1998**	**1999**	**2000**	**2001**
Chiang Mai	24 hr-average	130.8	170.4	166.1	202.2	129.8	109.7
	24hr-max	213.0	278.1	285.8	403.2	285.6	151.5
Lampang	24 hr-average	122.9	162.8	165.7	185.8	159.7	156.0
	24hr-max	347.7	264.2	296.8	271.6	267.2	192.3
Province	**PM data**	**2002**	**2003**	**2004**	**2005**	**2006**	**2007**
Chiang Mai	24 hr-average	154.9	65.2	217.7	127.8	122.2	162.5
	24hr-max	245.2	155.9	274.6	206.9	237.0	396.4
Lampang	24 hr-average	141.3	85.6	187.8	137.8	103.5	126.4
	24hr-max	230.4	165.6	231.3	234.4	152.9	255.3
Province	**PM data**	**2008**	**2009**	**2010**	**2011**	**2012**	-
Chiang Mai	24 hr-average	99.9	118.4	120.2	54.3	106.2	-
	24hr-max	178.9	219.0	291.1	94.3	195.0	-
Chiang Rai	24 hr-average	-	159.0	159.7	59.4	174.0	-
	24hr-max	-	286.4	267.1	149.9	293.4	-
Lampang	24 hr-average	104.6	154.5	113.4	62.4	125.6	-
	24hr-max	192.2	292.8	188.2	127.5	202.5	-
Lamphun	24 hr-average	-	-	142.2	68.9	118.1	-
	24hr-max	-	-	343.0	116.2	245.5	-
Mae Hong Son	24 hr-average	-	151.8	190.8	68.5	221.7	-
	24hr-max	-	264.9	505.5	162.7	354.8	-
Nan	24 hr-average	-	-	123.8	61.4	125.9	-
	24hr-max	-	-	388.0	99.6	218.0	-
Phayao	24 hr-average	-	-	145.3	91.4	138.7	-
	24hr-max	-	-	327.0	129.8	274.6	-
Phrae	24 hr-average	-	91.5	74.3	81.0	124.5	-
	24hr-max	-	263.0	156.0	121.5	249.0	-

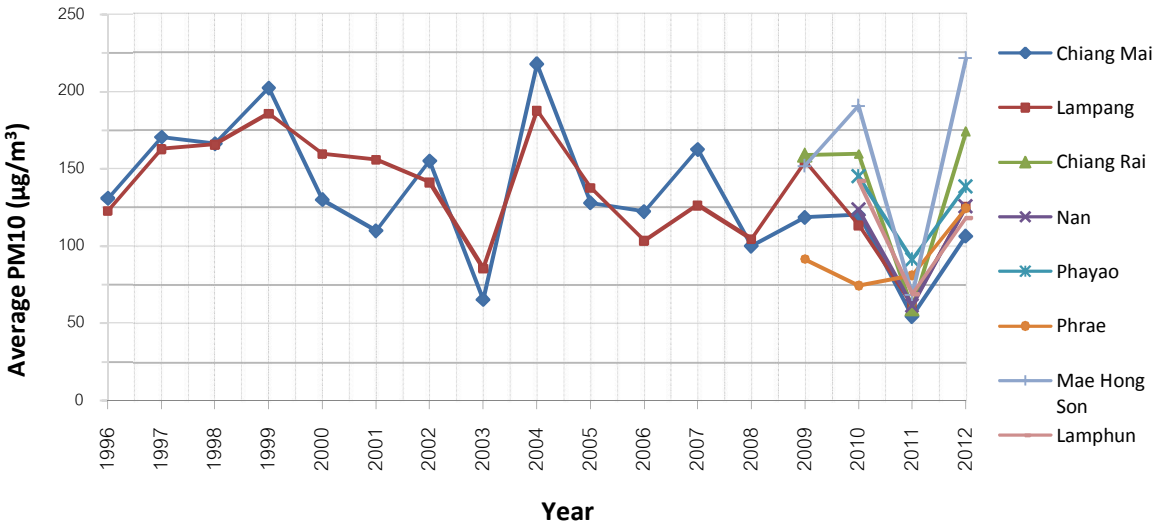

Figure 3.5a 24 hr-average observed PM10 data in the area for annual fire seasons during 1996-2012 (from Table 3.6).

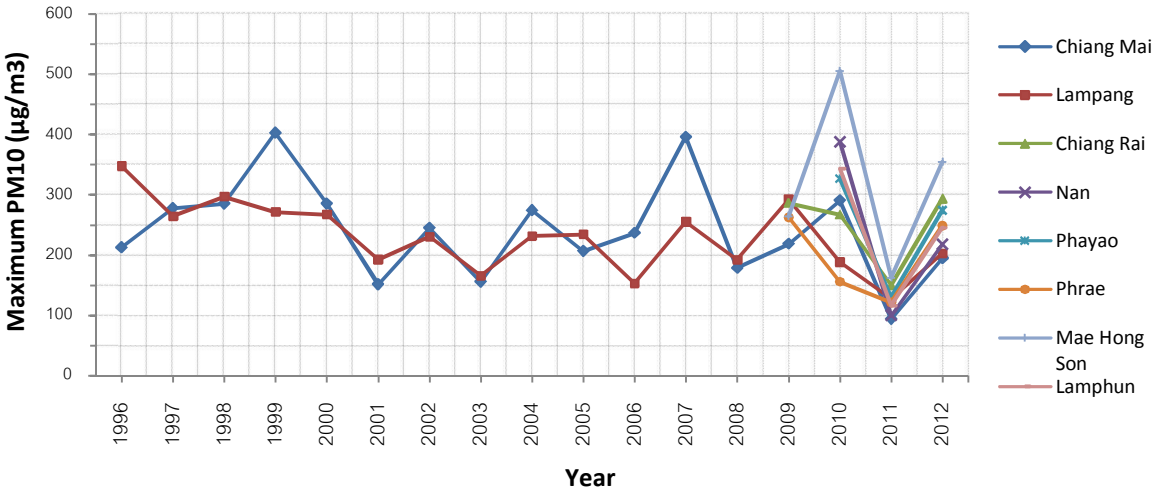

Figure 3.5b Variation of the 24hr-maximum PM10 data for annual fire seasons during 1996-2012 (from Table 3.6).

Table 3.7 Daily PM10 data during 2010 fire season recorded at the CM1 station in Chiang Mai Province (unit: $\mu g/m^3$). Note: PM10 >120 $\mu g/m^3$ are highlighted.

JAN	PM10	FEB	PM10	MAR	PM10	APR	PM10
1	31.6	1	41.3	1	70.0	1	101.5
2	27.8	2	43.2	2	93.2	2	112.8
3	21.3	3	41.0	3	101.6	3	127.0
4	33.8	4	40.7	4	89.8	4	139.7
5	47.3	5	43.0	5	92.3	5	127.6
6	48.5	6	37.9	6	101.7	6	140.4
7	52.3	7	51.3	7	112.8	7	156.0
8	31.0	8	50.9	8	106.5	8	176.6
9	29.5	9	66.5	9	132.3	9	131.8
10	40.2	10	60.7	10	162.2	10	111.0
11	40.1	11	58.0	11	83.1	11	122.5
12	37.8	12	68.6	12	95.2	12	133.7
13	43.2	13	56.4	13	80.4	13	123.3
14	62.3	14	58.4	14	124.9	14	109.4
15	56.2	15	77.5	15	167.8	15	84.3
16	57.6	16	76.7	16	220.5	16	106.8
17	49.8	17	87.0	17	268.4	17	91.96
18	52.9	18	70.7	18	179.1	18	84.7
19	52.5	19	58.5	19	88.7	19	109.5
20	54.3	20	65.5	20	57.8	20	80.1
21	47.3	21	85.1	21	73.5	21	79.1
22	56.1	22	83.8	22	84.2	22	89.4
23	58.8	23	108.2	23	82.6	23	99.2
24	42.7	24	60.5	24	96.3	24	54.1
25	26.5	25	88.5	25	123.2	25	53.3
26	33.0	26	111.8	26	179.8	26	68.2
27	25.3	27	111.5	27	107.2	27	57.3
28	33.0	28	83.5	28	66.4	28	59.8
29	27.6	-	-	29	72.2	29	65.8
30	25.2	-	-	30	62.9	30	62.3
31	30.5	-	-	31	77.8	-	-

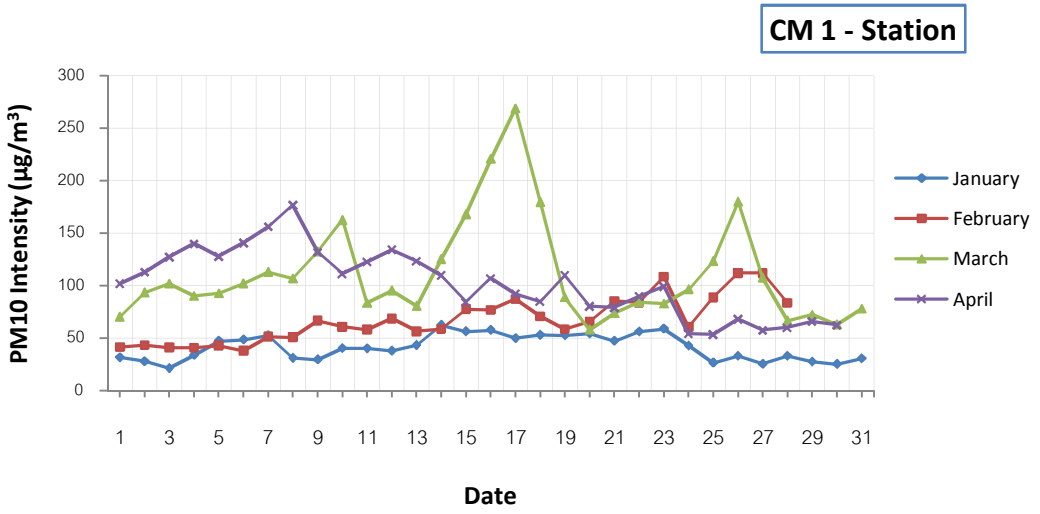

Figure 3.6 Daily PM10 data in 2010 fire season recorded at the CM1 station.

Selection of proper dates for PM10 and AQI mapping analysis

During the 2010 fire season, the worst situation for Chiang Mai Province appeared around the middle and late March and early April periods (as detailed for example in Table 3.7 and Figure 3.6 for the measurement at the CM1 station). These periods were of particular concern to having public health degradation due to the prolonged severe air pollution situation and had become prime dates for the conducting of the NDAI, PM10 and AQI mapping and analysis by the preferred method found in this research (as detailed in Section 3.3.2). However, due to the low quality of MODIS images for most candidate dates during March (too much cloud cover), only six dates during early April (4^{th}-9^{th} April 2010) were selected for further study. Figure 3.7 depicts the MODIS-visible images for all chosen dates stated earlier. Note that, not full scenes of the images on 7^{th} and 8^{th} April were acquired from the original source.

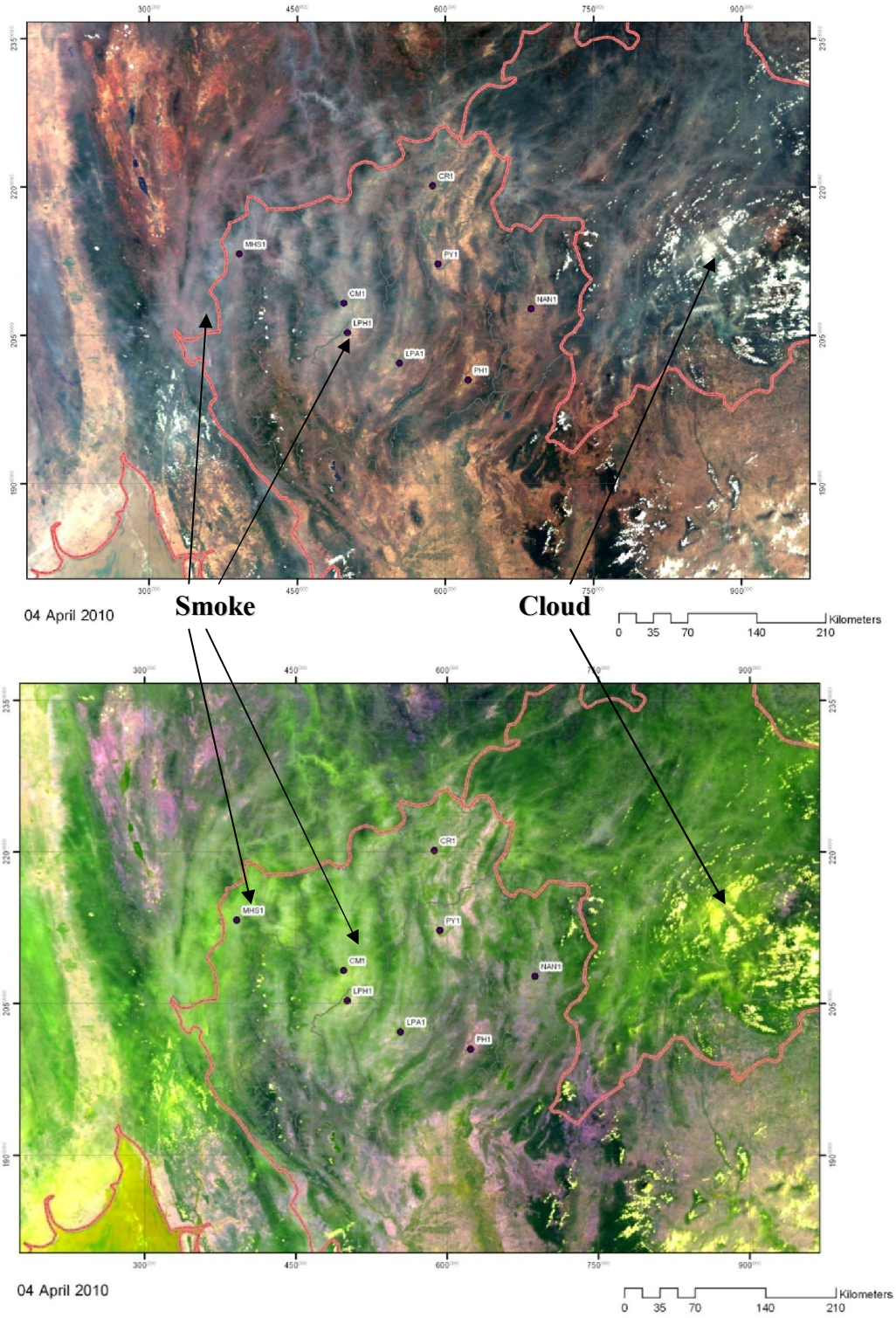

Figure 3.7 Composite MODIS images taken during 4th-9th April 2010 including the visible image [RGB: 1(red)/4(green)/3(blue)] and Mid-IR image [RGB: 1/3/7(MIR)] where green tone indicates smoke plume area on the latter image.

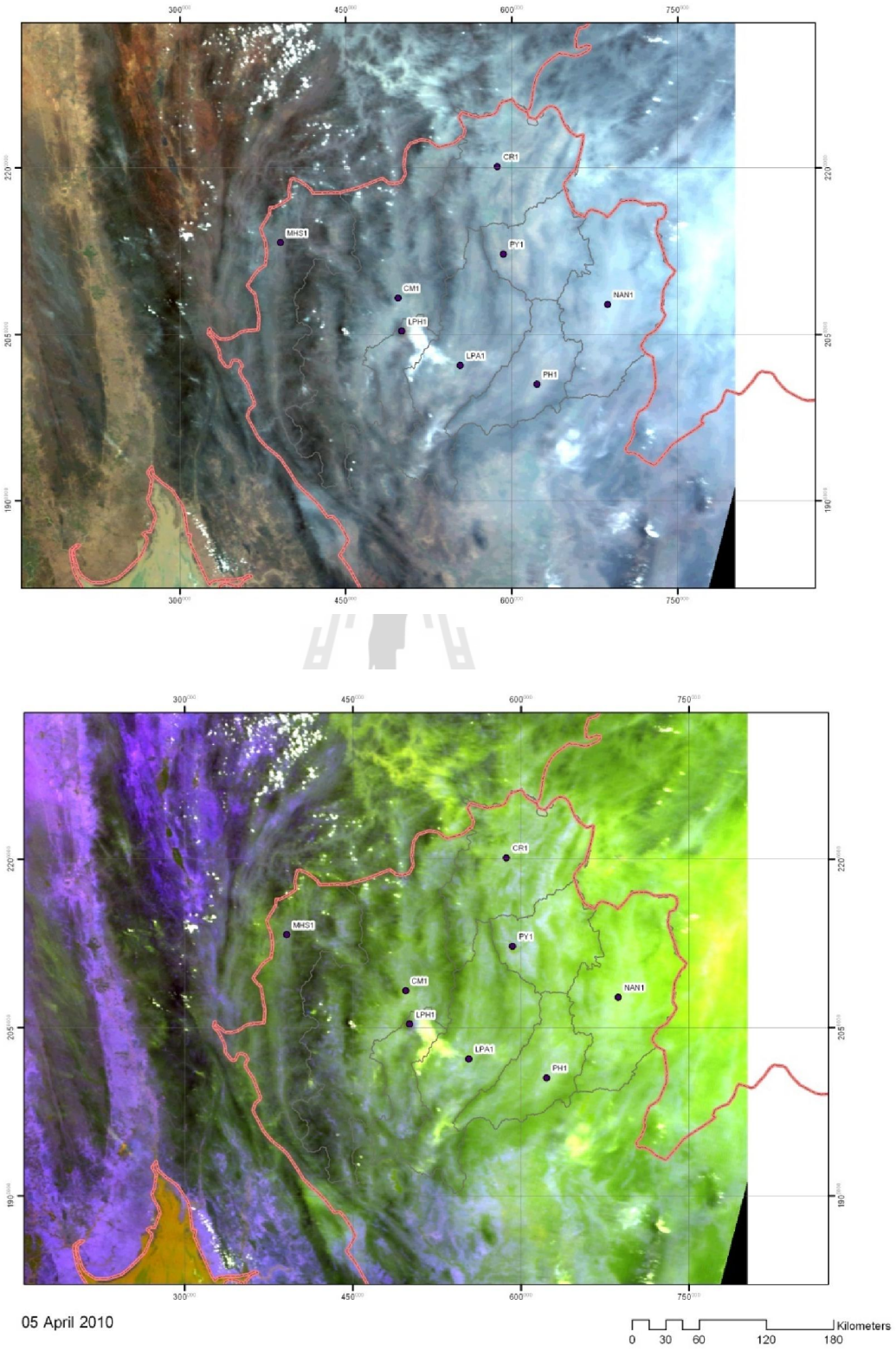

Figure 3.7 (Continued -For 5th April 2010).

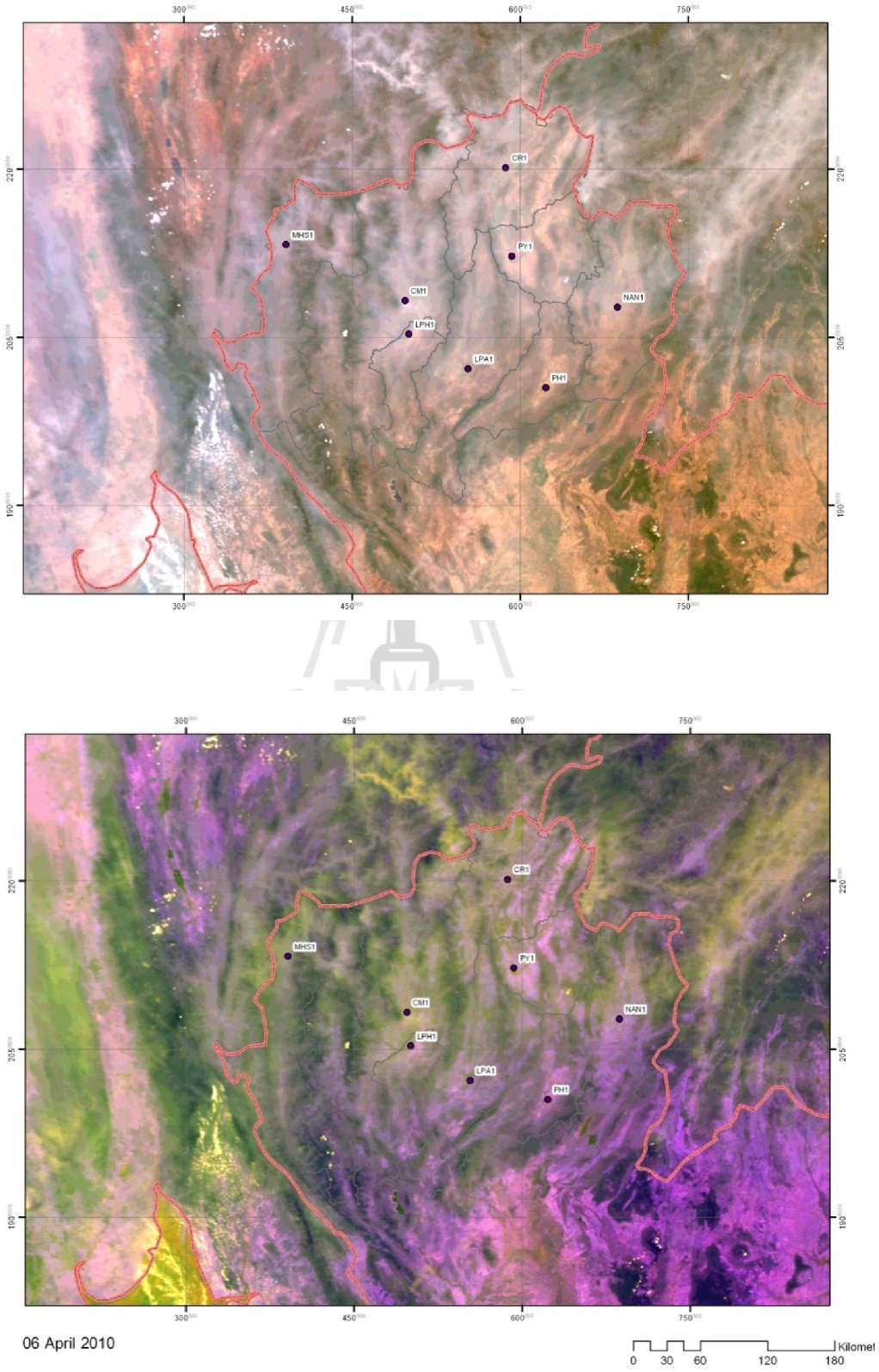

Figure 3.7 (Continued -For 6th April 2010).

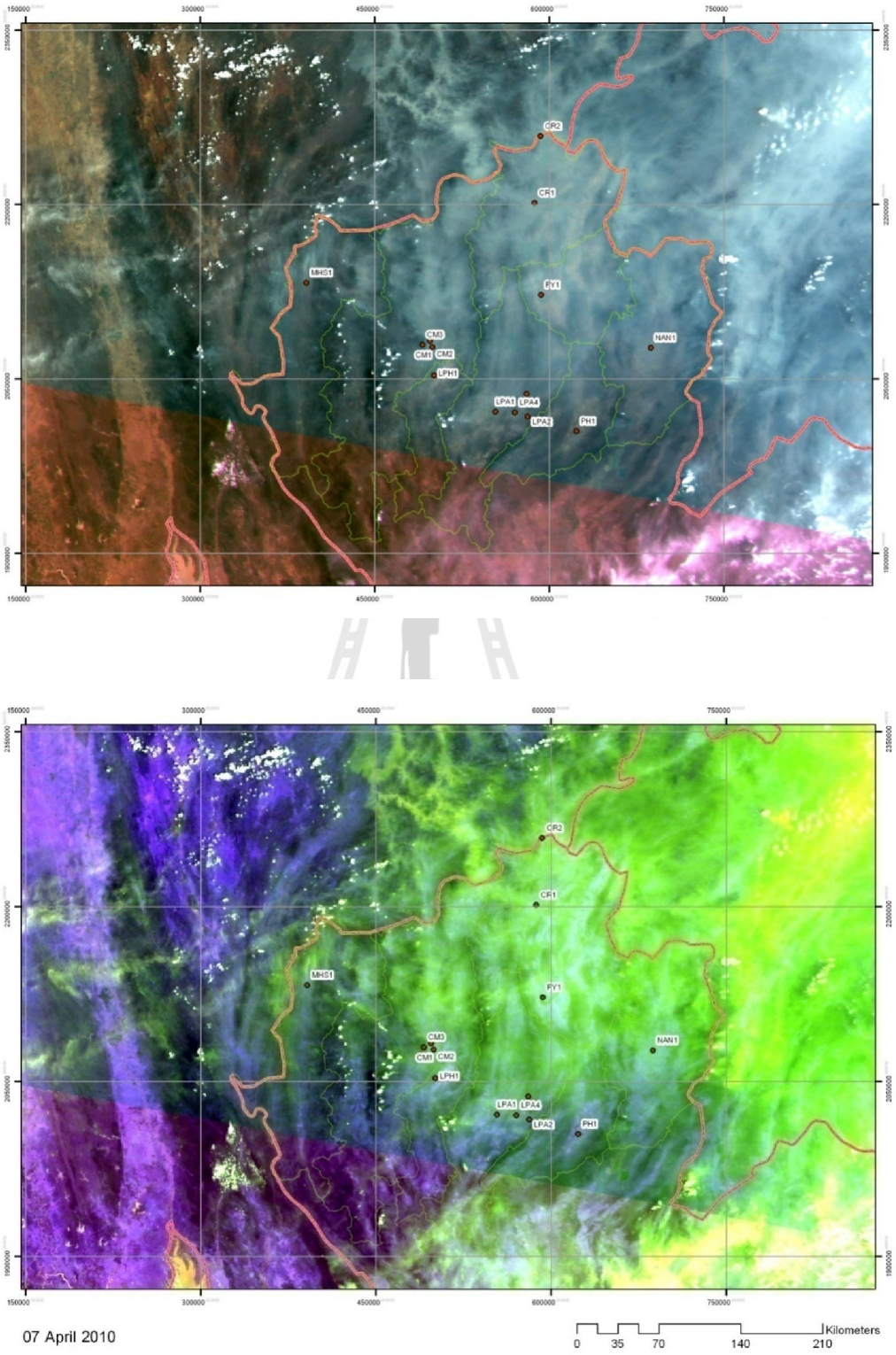

Figure 3.7 (Continued -For 7th April 2010).

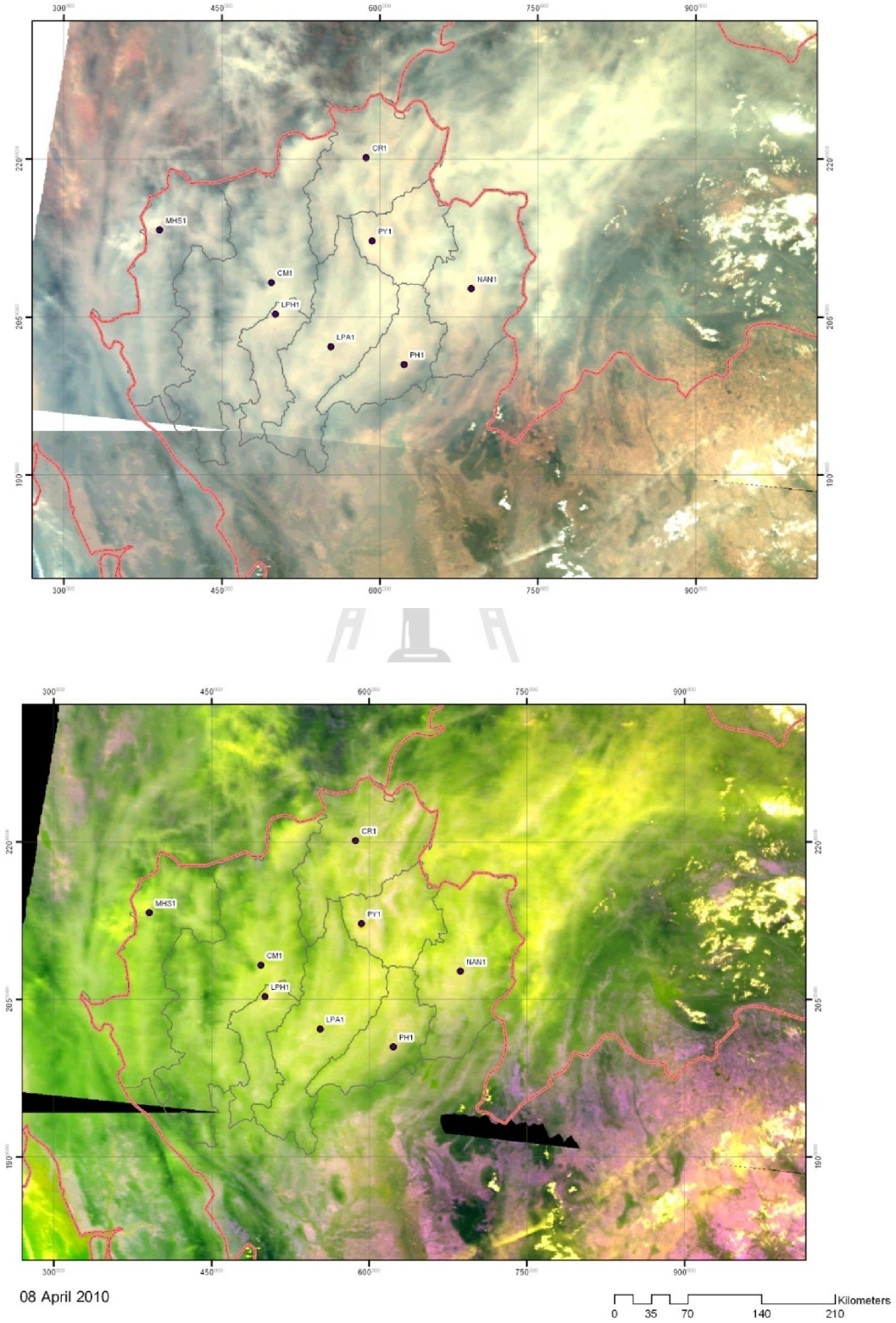

Figure 3.7 (Continued -For 8th April 2010).

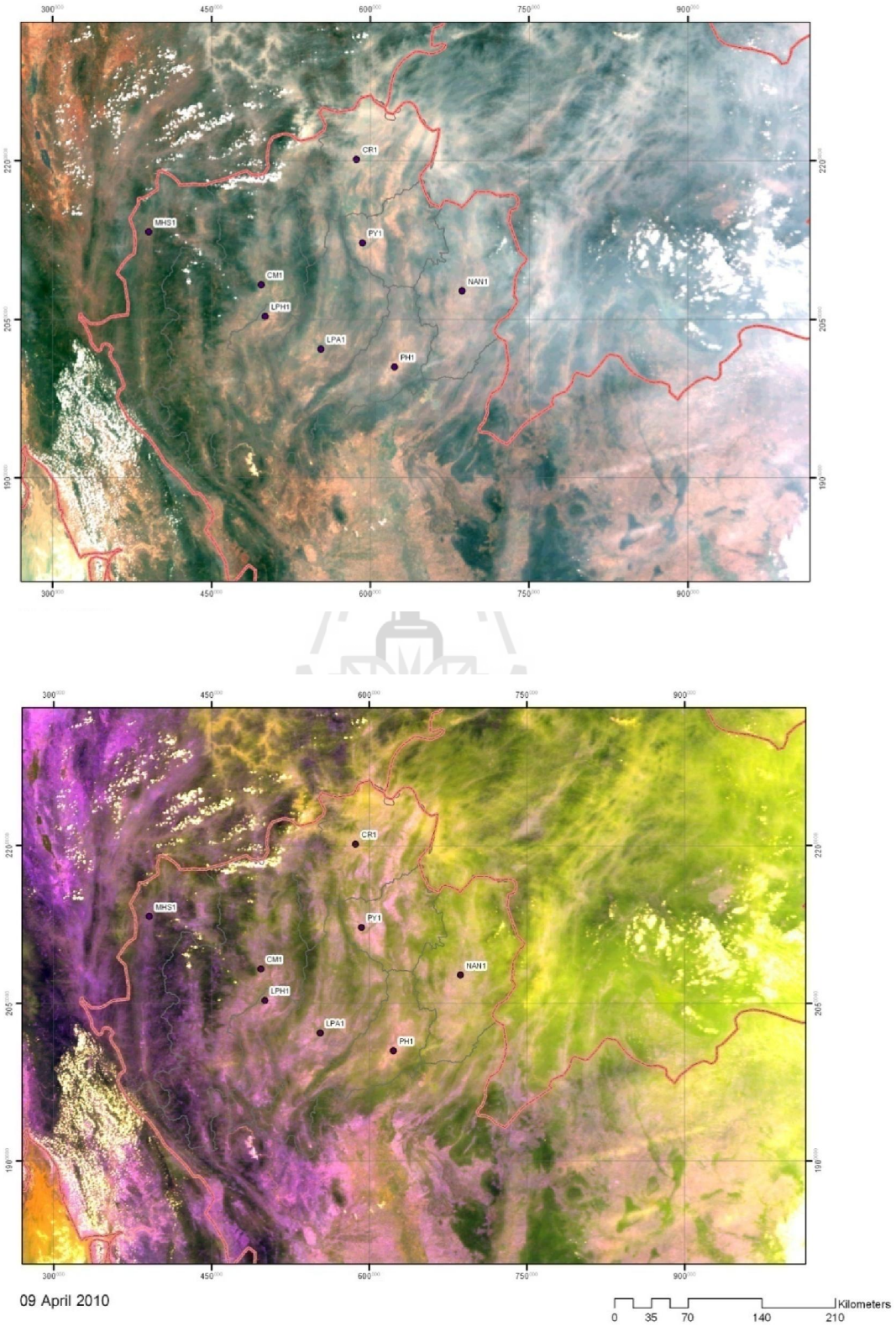

Figure 3.7 (Continued -For 9th April 2010).

Table 3.8 Daily observed PM10 data during 4th-9th April 2010 (unit: μg/m3).

Date	Province								Average (Date)
	CM	CR	NAN	PY	PH	MHS	LPA	LPH	
4th April	172	150	109	142	100	184	140	176	146.63
5th April	163	182	111	138	-	114	89	141	134.00
6th April	220	236	120	170	-	223	143	208	188.54
7th April	199	280	117	136	-	171	104	179	169.43
8th April	239	324	183	225	-	270	159	236	233.71
9th April	178	245	157	189	-	221	120	184	184.86
Average (Province)	195.2	236.2	132.8	166.7	100.0	197.2	125.8	187.3	176.19

Note: CM ≡ Chiang Mai, CR ≡ Chiang Rai, NAN ≡ Nan, PY ≡ Phayao, PH ≡ Phare,

MHS ≡ Mae Hong Son, LPA ≡ Lampang, and LPH ≡ Lamphun

Table 3.9 Hourly variations of the observed PM10 data during 4th-8th April 2010 at Chiang Mai Province (average from stations CM1 and CM2) (unit: μg/m3).

4th April		5th April		6th April		7th April		8th April		9th April	
Time	PM10	Time	PM10	Time	PM10	Time	PM10	Time	PM10	Time	PM10
1:00	125	1:00	159	1:00	163	1:00	185	1:00	178	1:00	170
2:00	133	2:00	139	2:00	145	2:00	195	2:00	171	2:00	150
3:00	120	3:00	131	3:00	140	3:00	151	3:00	175	3:00	138
4:00	118	4:00	136	4:00	142	4:00	157	4:00	158	4:00	136
5:00	123	5:00	141	5:00	143	5:00	163	5:00	162	5:00	139
6:00	137	6:00	136	6:00	161	6:00	191	6:00	169	6:00	148
7:00	146	7:00	148	7:00	186	7:00	197	7:00	185	7:00	161
8:00	176	8:00	163	8:00	203	8:00	231	8:00	219	8:00	185
9:00	194	9:00	166	9:00	223	9:00	258	9:00	231	9:00	201
10:00	209	10:00	163	10:00	220	10:00	216	10:00	224	10:00	195
11:00	162	11:00	141	11:00	208	11:00	191	11:00	239	11:00	171

Table 3.9 (Continued.)

4th April		5th April		6th April		7th April		8th April		9th April	
Time	PM10	Time	PM10	Time	PM10	Time	PM10	Time	PM10	Time	PM10
12:00	170	12:00	121	12:00	159	12:00	167	12:00	211	12:00	145
13:00	156	13:00	103	13:00	97	13:00	147	13:00	151	13:00	123
14:00	117	14:00	109	14:00	148	14:00	149	14:00	137	14:00	106
15:00	110	15:00	61	15:00	121	15:00	86	15:00	177	15:00	83
16:00	66	16:00	67	16:00	99	16:00	124	16:00	164	16:00	77
17:00	105	17:00	83	17:00	105	17:00	134	17:00	156	17:00	138
18:00	134	18:00	102	18:00	102	18:00	95	18:00	148	18:00	158
19:00	139	19:00	139	19:00	135	19:00	91	19:00	162	19:00	119
20:00	157	20:00	108	20:00	177	20:00	157	20:00	160	20:00	106
21:00	127	21:00	198	21:00	230	21:00	196	21:00	160	21:00	120
22:00	144	22:00	184	22:00	173	22:00	177	22:00	181	22:00	117
23:00	143	23:00	153	23:00	186	23:00	153	23:00	165	23:00	108
24:00	141	24:00	199	24:00	161	24:00	182	24:00	155	24:00	99

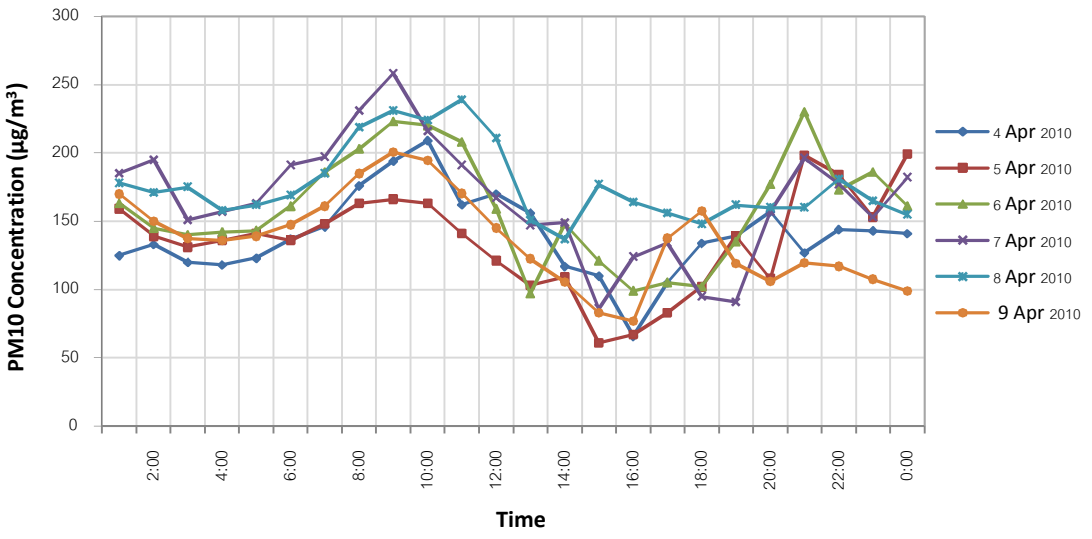

Figure 3.8 Time sequences of the PM10 concentrations during 4th-9th April 2010 at Chiang Mai Province (average from stations CM1 and CM2) (from Table 3.9). Note that, 4th April 2010 is Sunday and 6th April is public holiday.

3.4.2 General PM10 information of the preferred dates

Apart from Chiang Mai, most provinces in the area were also experienced prominent air pollution during the chosen dates (4^{th}-9^{th} April 2010) according to data described in Table 3.8. During this period, Chiang Rai had endured the worst situation with amount of PM10 concentration in 24-average of 234.4 $\mu g/m^3$, followed by Chiang Mai and Mae Hong Son with average PM10 concentration of about 198.6 and 192.4 $\mu g/m^3$, respectively. Notable variation of the measured PM10 data during each preferred date was also clearly visible as shown, for example, in Figure 3.8 for the average PM10 data recorded at two Chiang Mai stations (CM1 and CM2). Note that, only data on 4^{th} April at Phrae station (PH1) was available for the use in this study and date with worst situation in general was 8^{th} April for all the listed provinces in Table 3.8 (except Phrae).

It was found that diurnal variations of the observed PM concentration for each day have similar patterns with two apparent peak values; mid-morning (or daytime) peak appears around 8:00-11:00 in the morning and the evening (or nighttime) peak often seen around 20:00-22:00. The lowest part of each daily record was evidenced in mid-afternoon around 14:00-16:00. This distinct feature of the PM10 diurnal variation is well acknowledged as detailed in several reports, e.g. Alföldy et al. (2007); Krecl, Strom, Johansson (2008); Azri, Mabrouk, and Medhioub (2009); Feng et al. (2010) and Trompetter, Davy and Markwitz (2010). The origin of this phenomenon is often attributed to the complicated combination of two associated factors: total amount of the released PM pollutants (or PM emission) within the area and the prevailed atmospheric condition during the day, especially, local wind speed and thickness of

the mixing layer height (MLH) as most pollutants shall be trapped under this MLH after being released into the atmosphere.

The mid-morning peak is normally believed to be resulted from the build-up morning traffic under the still relatively low MLH boundary while the evening peak is developed from the afternoon and evening traffic and the burning of solid fuels for domestic purposes (e.g. wood, coal, charcoal). The evening peak is most pronounced in fire season during the cold, calm, dry nights as the ground-based PM emission tends to have limited vertical dispersion and shall mostly be contained in the near-ground atmosphere for long period of time. Moreover, the formation of temperature inversion layer might also greatly amplify the air pollution situation over the area; it is thus necessary to be taken into account for the investigation of the seen PM diurnal variation pattern as appropriate. The notably low recorded PM density during mid-afternoon is probably due to the prominent rise of the MLH during daytime that can substantially reduce the near-ground PM concentration as a consequence (Azri et al., 2009; Trompetter et al., 2010).

มหาวิทยาลัยเทคโนโลยีสุรนารี

3.4.3 MODIS radiance response to PM10 pollution severity

As discussed in Section 2.3, in theory, the MODIS radiances observed at different bands should act differently to the variation of the PM10 concentration in lower atmosphere. Bands with shorter wavelengths should be more sensitive to changes in PM10 amount than those with longer wavelengths. This conventional believe was confirmed in the preliminary study as illustrated in Figure 3.9. In this work, MODIS radiances in the visible (red/green/blue), NIR and MIR bands were accumulated from dates with different levels of the PM10 severity (as suggested by averaged value of MODIS-AOD). Four categories of PM10 severity were primarily

assigned: very low (AOD < 0.05), low (AOD = 0.05-0.1), medium (AOD = 0.4-0.45), and high (AOD > 0.55).

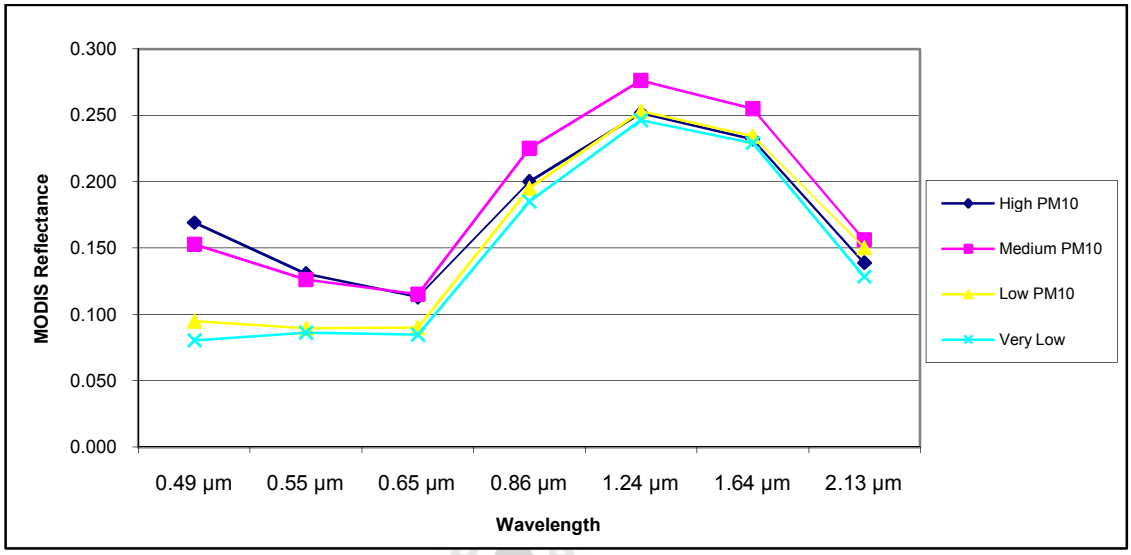

Figure 3.9 Averaged reflectance values of MODIS Bands 1-7 at different levels of PM10 pollution severity from very low to high (based on MODIS-AOD data).

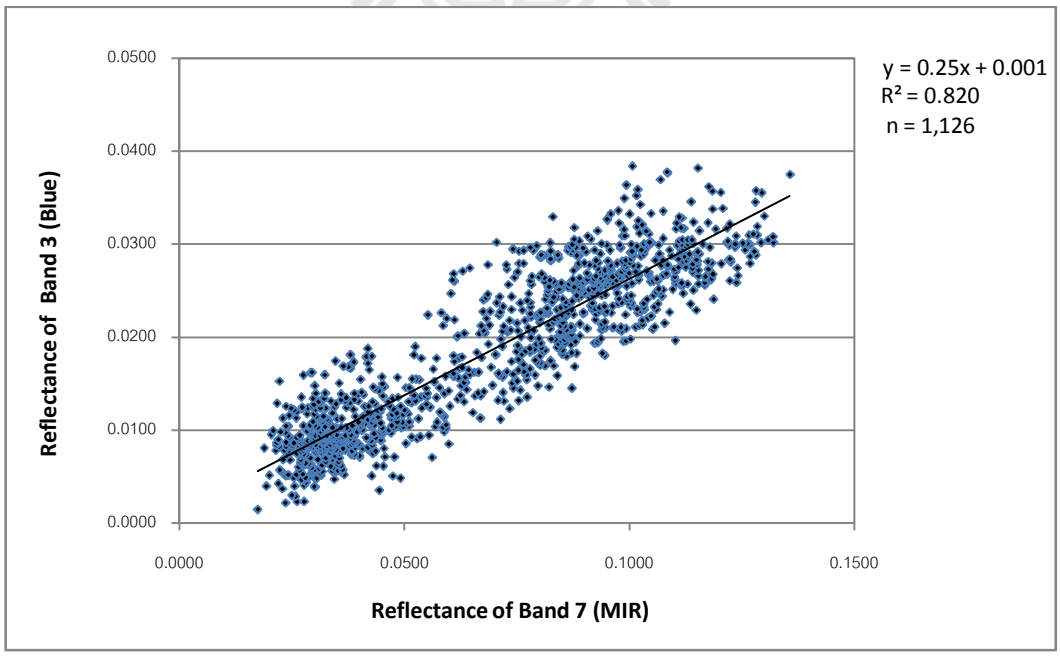

Figure 3.10 Linear relationship of reflectance data in MODIS-Band 3 (blue) and Band 7 (MIR) over the study area with $R^2 = 0.82$.

Results of the study (Figure 3.9) indicate that sensitivity of the observed radiance to PM10 density change is generally reduced as its spectral wavelength increases. This means MODIS-blue band (at 0.49 μm) should exhibit the highest sensitivity level and MIR band (at 2.13 μm) should express the least sensitivity (see Table 4.1 for more information). As a consequence, the blue and MIR bands were primarily selected for the formulation of the ΔR and NDAI parameters (as described in Eqs. 3.1 and 3.2, respectively). In addition, strong linear relation between MODIS radiances band 3 (B3-blue) and band 7 (B7-MIR) on some pollution-free dates over the area was also obtained with $R^2 = 0.820$ (Figure 3.10) with the expressed formula: B3 = 0.25(B7) + 0.001. This enables opportunity to compute spectral reflectance of the MODIS-blue band (B3) using that of the MODIS-MIR band (B7) directly. The obtained band ratio (Band3/Band 7) of 0.25 is similar to that used in the standard MODIS-AOD retrieval method described in Kaufman et al. (1997) and Kaufman, Gobron, Pinty, Widlowski, and Verstraete (2002).

3.4.4 Applied details of the BAER retrieval method

General concept of the BAER retrieval method was previously explained in Section 2.4.3 and its specific details being used in this thesis are presented here while the achieved results will be discussed later in Chapter 4. Figure 3.11 shows original work flowchart of the modified BAER method used in Song et al. (2008) where AFRI was replaced the normal NDVI parameter for the calculation of surface reflectance value (ρ_{SF}). This index was introduced to reduce effects of the aerosol presence on VI calculation of the BAER method. This flowchart was also adopted in this study with some modifications as subsequently detailed.

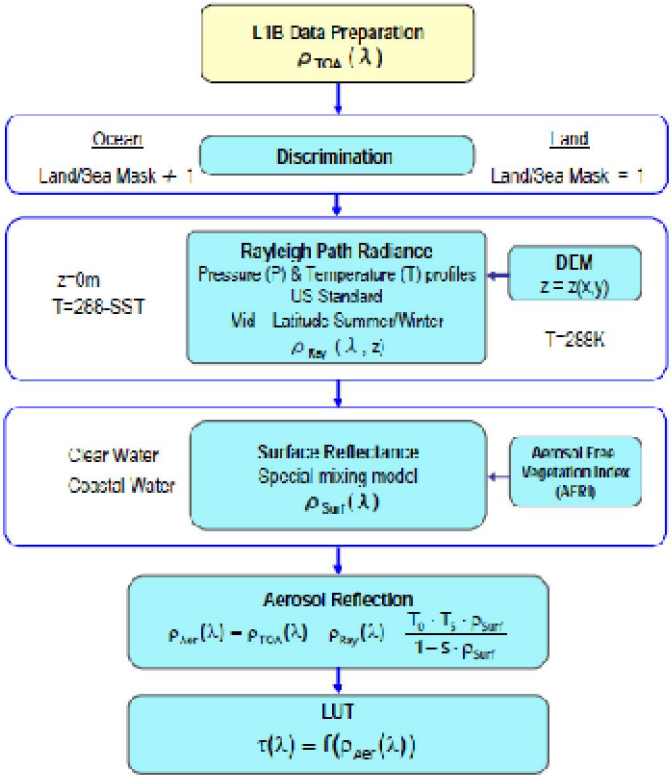

Figure 3.11 Modified BAER-AOD retrieval algorithm used in Song et al. (2008) and was adopted for the study in this thesis (with some modifications).

Determination of the BAER-AOD (pixel-based value) in this research was carried out based on the following the procedure:

(1) Preparing TOA reflectance data maps (ρ_{TOA}) of the MODIS-blue band from the MODIS-TOA data covering the entire study area on the specific dates of interest. Definition of ρ_{TOA} was given in Eq. 2.9.

(2) Calculation of the Rayleigh reflectance (ρ_{RL}) for each particular pixel. This was performed using a formula described by Eq. 2.12 in which the required surface pressure p(z) was determined directly from the relation stated in Eq. 2.13 and the surface temperature (T_{SF}) was extracted from the MOD11 dataset.

(3) Determination of the surface reflectance value (ρ_{SF}). This was utilized based on Eq. 2.14 in which the surface reflectance term, A_{SF}, was prepared first for each month based on the linear mixing model described in Eq. 2.15 and results are presented in Figure 3.12. In addition, the term $A_{SF} \cdot \gamma_{Hem}$ was ignored ($A_{SF} \cdot \gamma_{Hem} = 0$) which gives $\rho_{SF} = T_{Tot}(\theta_0) \cdot T_{Tot}(\theta_S) \cdot A_{SF}$. The transmittance term, $T_{Tot}(\theta_0) \cdot T_{Tot}(\theta_S)$, was assumed to be constant over the area for each month of interest and was considered having maximum value of 1 in this study to attain simple relation: $\rho_{SF} = A_{SF}$.

(4) Derivation of aerosol reflectance value (ρ_{AS}). This factor was determined under the prior stated assumptions using the following relation (from Eq. 2.11):

$$\rho_{AS}(\lambda) = \rho_{TOA}(\lambda) - \rho_{RL}(\lambda) - \rho_{SF}(\lambda). \quad (3.3)$$

(5) Determination of the AOD data. The pixel-based AOD data were derived from the known relationship between the obtained aerosol reflectance (ρ_{AS}) calculated from Eq. 3.3 (at wavelength of 470 nm) and the observed ground-based AERONET-AOD (at 440 nm). This relationship was found empirically as shown in Figure 3.13 and can be expressed in general form as follows:

$$y = 20.25x \; ; (R^2 = 0.801) \quad (3.4)$$

where y is the derived AOD (at 440 nm) and x is the defined aerosol reflectance (ρ_{AS}) (at 470 nm) computed for each pixel of relevant MODIS image as detailed in Eq. 3.3. The AOD derived from Eq. 3.4 is called the BAER-AOD which is equivalent to the corresponding AERONET-AOD computed at 440 nm.

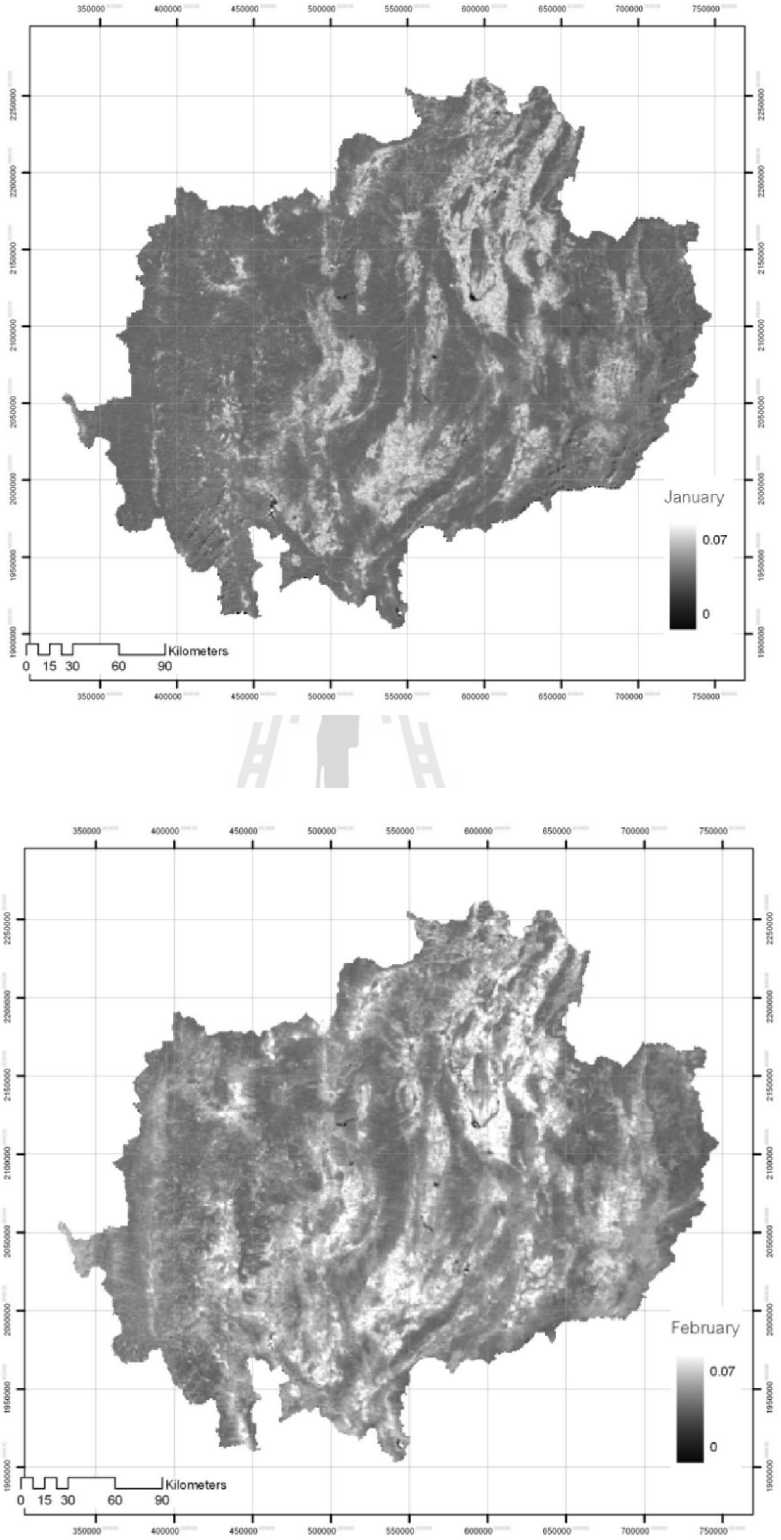

Figures 3.12 Derived monthly surface reflectance maps (A_{SF}) for January-April 2010.

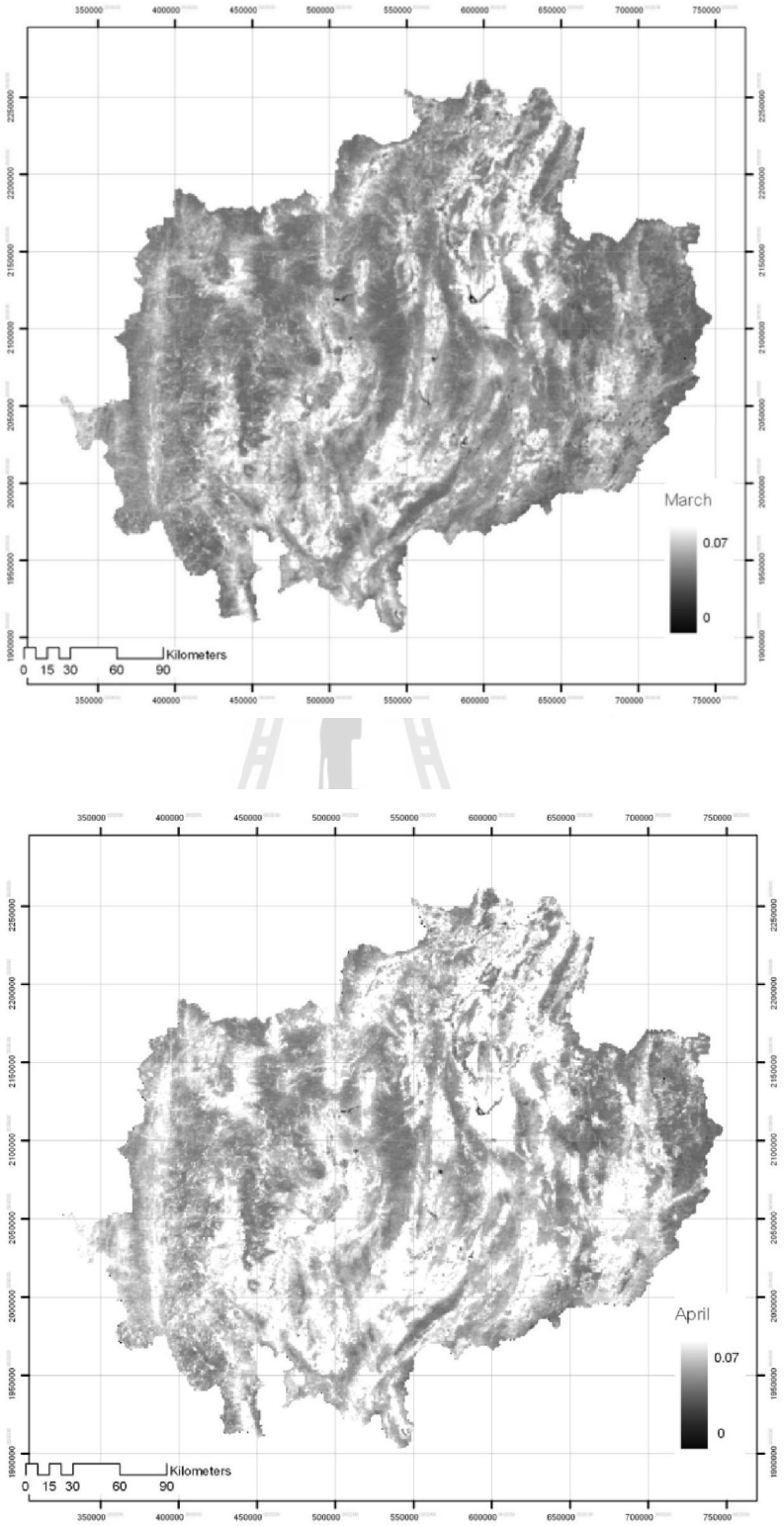

Figures 3.12 (Continued -For March and April).

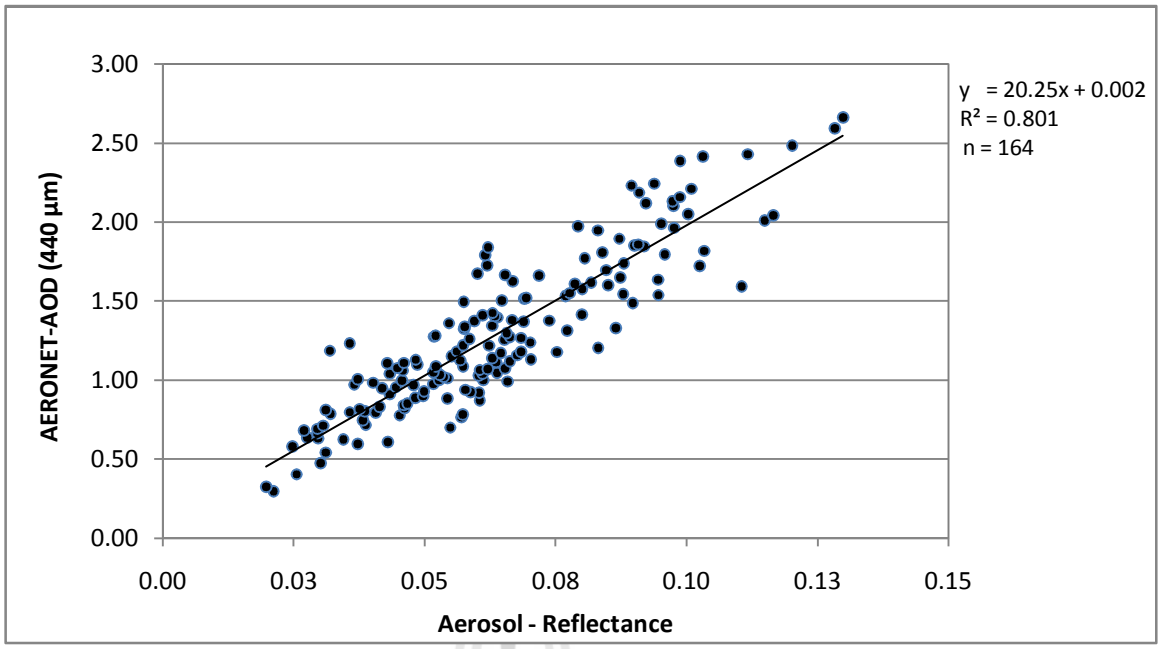

Figure 3.13 Established relationship between the AERONET-AOD (at 440 nm) and defined aerosol reflectance (ρ_{AS}) (at 470 nm) found in this study.

มหาวิทยาลัยเทคโนโลยีสุรนารี

CHAPTER IV

PM10 AND AQI DETERMINATION AND MAPPING

This chapter reports main results achieved for the Objectives 1 and 2 stated in Chapter 1 followed the research framework detailed in Chapter 3. The main content is divided into three main parts: (1) evaluation on apparent relationship of the MODIS-based parameters and AERONET data with the reference PM10 data, (2) derivation of daily NDAI maps and PM10 maps (developed from through the BAER method) for the entire study area and (3) formulation of AQI maps based on four selected methods including the newly-proposed one to assess aerosol pollution situation over the area.

4.1 Relationships of MODIS-based parameters and PM10 data

This section is divided into three subsections involving evaluation of proper relation functions of the MODIS radiances and parameters (and AERONET data) and the reference PM10 data, and also among themselves. Relevant details are as follows.

4.1.1 Relationships of MODIS radiances with the reference PM10 data

The first task processed in this part was to investigate apparent relations of the MODIS radiances (in blue/green/red/MIR band) to the reference PM10 data observed at ground stations listed in Table 1.1. The obtained results are reported along with the corresponding R^2 as described in Table 4.1a and Figures 4.1a-d. In theory, the MIR band should be not sensitive much to changes of aerosol amount in lower atmosphere

due to its relatively long wavelength compared to those in the visible region. On the contrary the blue band should exhibit most sensitivity to the PM10 variation due to its shortest wavelength which makes it most vulnerable to the aerosol-induced scattering effect. This assumption was discovered in several works on the AOD dependency on wavelength, e.g., Eck et al. (1999); Kant et al. (2000); Kaskaoutis and Kambezdis (2006); Ranjan, Ganguly, Joshi and Iyer (2007) and Tian and Chen (2010).

Similarly to those reports, it was found in this study that the observed MODIS reflectance radiance increases continuously with rise of the reference aerosol data in distinguish linear fashion (for the visible region) but precise detail of each relation depends on the observed radiance wavelength. In terms of the blue band (B3) was found to gain the highest value at 0.710 followed by the green and red bands with R^2 of 0.616 and 0.563, respectively (Figures 4.1a-c). These results indicate the possibility of using B3 radiance data as an indicator of PM10 pollution over the entire study area due to its relatively good relation to the observed PM10 concentration data. And in terms of the sensitivity, the blue wavelength also exhibits the highest strength compared to the other visible bands. For the MIR band (B7), no obvious linear pattern of the relationship was found with extremely low significant level (R^2=0.029) was evidenced (Figure 4.1c). It should be noted that, on the PM10 free date (PM10 ≈ 0), the blue reflectance data is still at 0.038 while that of red band is about 0.003 only.

Table 4.1a Found linear relationships between the reference PM10 data and different MODIS-radiance.

Parameter		Found relationship (y = ax+b)	R^2	Sensitivity (Δy/Δx)	Scale (m)	n	Figure
x	y						
Radiance (Blue)	PM10	y = 1920x - 72.04	0.710	1920	500	192	4.1a
Radiance (Green)	PM10	y = 1851x - 54.190	0.616	1851	500	192	4.1b
Radiance (Red)	PM10	y = 1620x - 5.062	0.563	1620	250	192	4.1c
Radiance (MIR)	PM10	y = -543.0x+165.6	0.029	-	500	192	4.1d

Note: 1. PM10 has unit of $\mu g/m^3$.

2. Sensitivity (Δy/Δx) indicates amount of the PM10 concentration change (in unit of $\mu g/m^3$) per a unit change of the reflected radiance.

3. n ≡ number of data pair in use

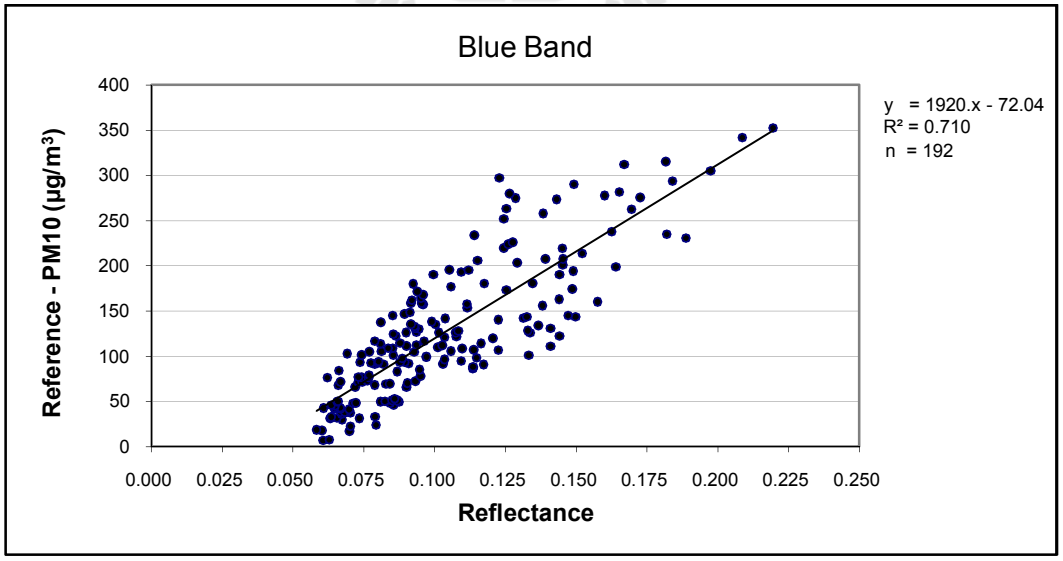

Figure 4.1a Linear relationship of the reflectance data for blue band (Band 3) and reference PM10 data ($R^2 = 0.710$).

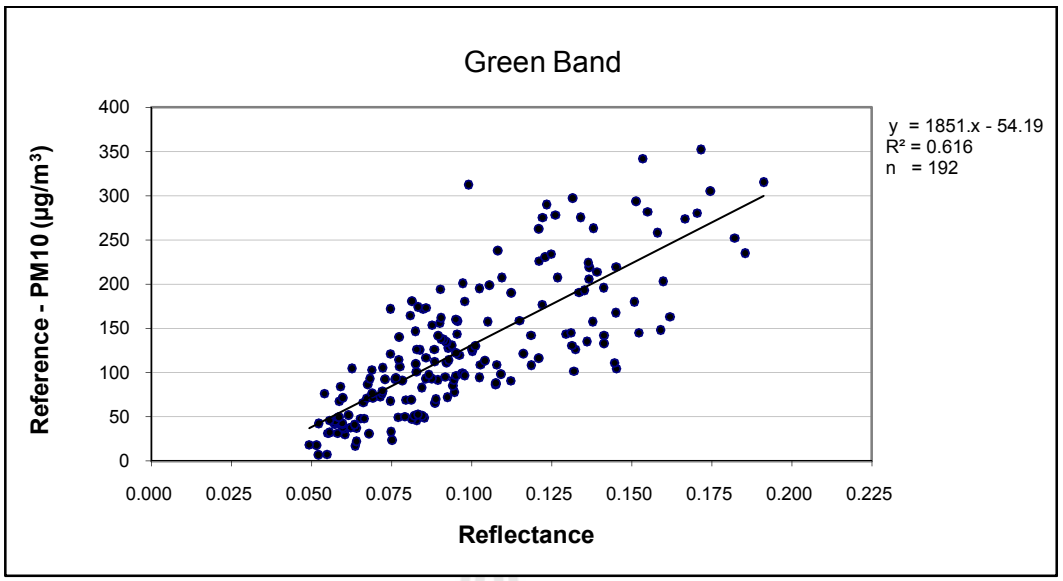

Figure 4.1b Linear relationship of the reflectance data in green band (Band 4) and measured PM10 data ($R^2 = 0.616$).

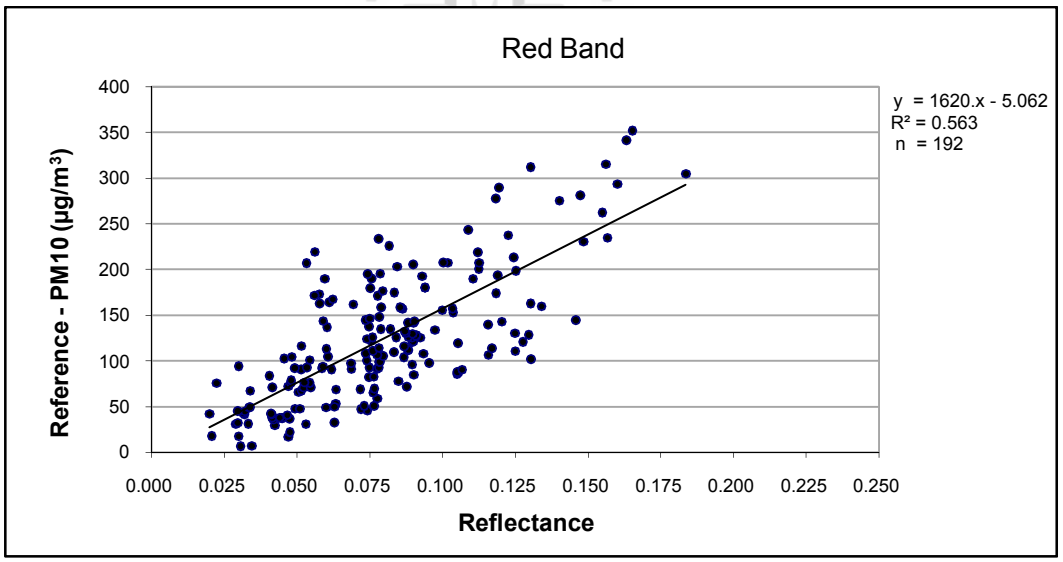

Figure 4.1c Linear relationship of the reflectance data in red band (Band 1) and reference PM10 data ($R^2 = 0.563$).

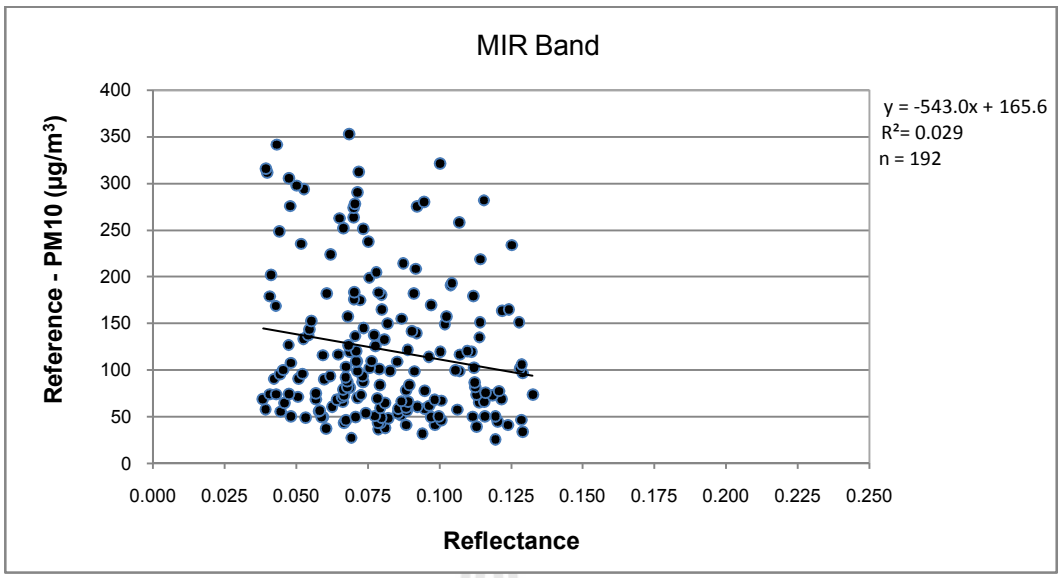

Figure 4.1d Linear relationship of the reflectance data in MIR band (Band 7) and reference PM10 data ($R^2 = 0.029$).

4.1.2 Relationships of the MODIS-based parameters and AERONET-AOD with reference PM10 data

After the relationships between MODIS radiances and reference PM10 data were examined, more study was performed based on four MODIS-based parameters: ΔR(blue), NDAI, MODIS-AOD, BAER-AOD, and AERONET-AOD. The obtained results are presented in Table 4.1b and Figures 4.2a-e, respectively.

In this work, ΔR was found to be most sensitive to the assumed changes of the PM10 data with R^2 of 0.667. It also exhibits small bias in producing PM10 data at the low values because, if ΔR = 0, the resulted PM10 data would become 26.92 µg/m^3, close to the ideal value of ≈ 0 µg/m^3 (on the reference aerosol-free date defined in Eq. 3.1). By definition, merit of this parameter in predicting PM10 data is equivalent to that of the actual blue radiance discussed earlier (as described in Figure 4.1) except

the background blue radiance (estimated from the reference pollution-free dates) must be subtracted first from the original observed radiance on a particular day of interest.

For NDAI, it shows rather strong relation to the reference PM10 data in use ($R^2 = 0.661$) with minimal bias at low values in predicting PM10 data as at NDAI = 0, the output PM10 data would become 4.527 $\mu g/m^3$, highly close to the ideal value of 0 $\mu g/m^3$ expected from its definition illustrated in Eq. 3.2. Also, its possible values are limited to just -1 to 1 (by definition) with prospective values of ≥ 0 in reality. These stated properties make the potential use of NDAI as a proxy for the PM10 pollution severity look very promising (similar to the use of NDVI for quantifying vegetation abundant over the area). However, the found relationship for NDAI stated in Figure 4.2b indicates that it is valid at PM10 data less than about 300 $\mu g/m^3$ only (as NDAI must be always ≤ 1). This fact is not a serious deficiency of this parameter as amount of the PM10 data observed in the area were mostly less than 300 $\mu g/m^3$ in general at all concerned provinces (see Table 3.4 for more information).

Table 4.1b Found linear relationships between the reference PM10 data and different MODIS-based parameters and AERONET-AOD data.

Parameter		Found relationship (y = ax+b)	R^2	Sensitivity ($\Delta y/\Delta x$)	Scale (m)	n	Figure
x	y						
ΔR (Blue)	PM10	y = 1306x - 26.92	0.667	1306.0	500	440	4.2a
NDAI	PM10	y = 300.6x + 4.527	0.661	300.6	500	240	4.2b
MODIS-AOD	PM10	y = 267.9x - 12.03	0.720	267.9	10,000	104	4.2c
BAER-AOD	PM10	y = 135x + 17.38	0.784	364.5	500	256	4.2d
AERONET-AOD	PM10	y = 90.89x + 13.01	0.860	90.89	-	228	4.2e

Note: DN, ΔR, NDAI, AOD are unitless

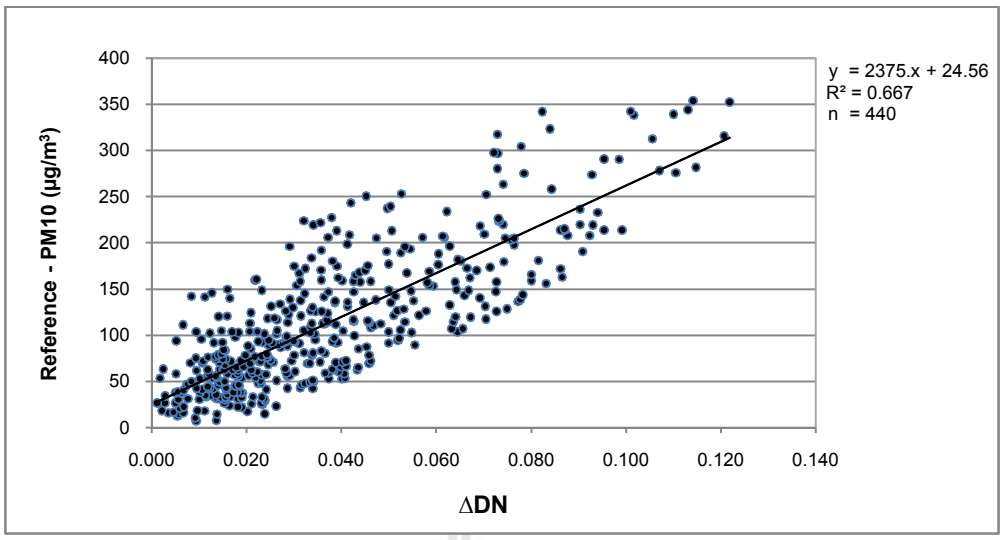

Figure 4.2a Linear relationship of ΔR and reference PM10 data ($R^2 = 0.667$).

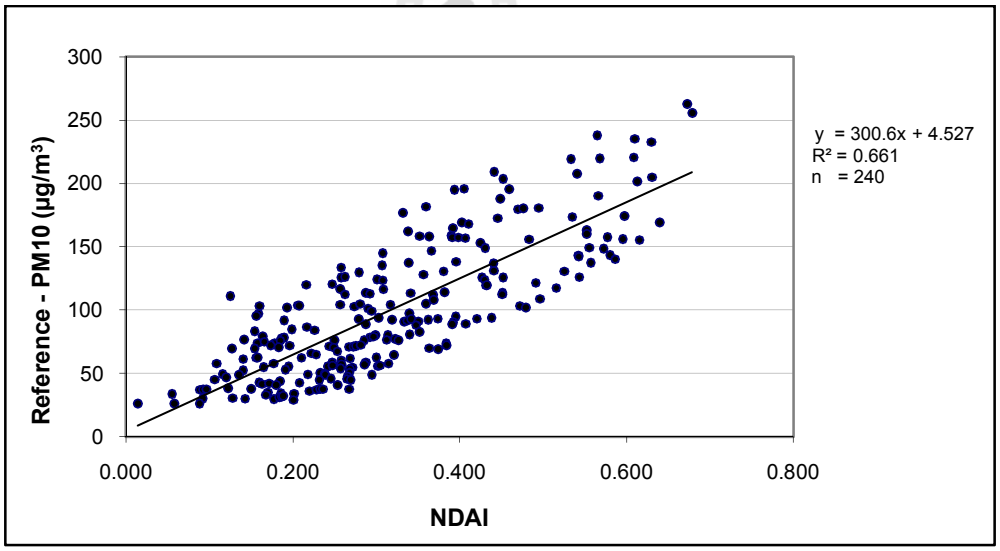

Figure 4.2b Linear relationship of NADI and reference PM10 data ($R^2 = 0.661$).

The third MODIS-based parameter being assessed here is the MODIS-AOD (550 nm) which has relatively high relation to the reference PM10 data ($R^2 = 0.72$) with small bias seen at AOD = 0. These findings correspond well to several reports on apparent relations of the MODIS-AOD to estimate near-ground PM10 data (see those listed in Table 2.7 for examples). The obvious advantage of using MODIS-AOD for

being PM10 predictor is its availability as the data can be readily acquired from the LAADS website as mentioned in Chapter III. However, two crucial drawbacks of this approach are the coarse resolution (of 10 km) of the standard MODIS-AOD products and the uncertainty on their relations with the observed PM data (as evidenced from details shown in Table 2.7). The coarse resolution makes them adequate for studying synoptic and regional-scale characteristics of aerosol pollution but normally not good enough to explore spatial variation of aerosol pollution at provincial or watershed scales, especially over the complex urbanized regions, which need better resolution of MODIS-AOD to effectively fulfill this task (Li, Lau, Mao, and Chu, 2005; Kumara, Chub, and Fosterc 2007; Wong, Lee, Nichol, and Li, 2010 and Munchak et al., 2013).

And on the second issue, it was often found that relation tendency between the MODIS-AOD and observed PM data varies significantly with place and time due mostly to local meteorological conditions, especially mixing layer height (MLH) and relative humidity (RH) (Schaap, Apituley, Timmermans, Koelemeijer, and de Leeuw, 2009; Zha, Gao, Jiang, Lu and Huang, 2010 and Tsai, Jeng, Chu, Chen, Chang, 2011). As a consequence, experiments conducted under different meteorological conditions might yield notably different results.

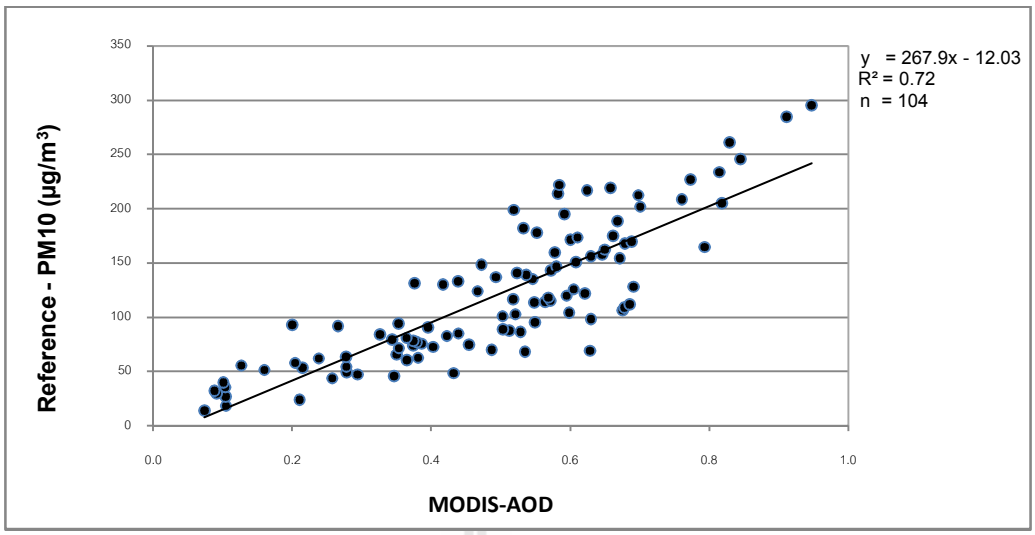

Figure 4.2c Linear relationship of MODIS-AOD (at 550 nm) and the reference PM10 data (with $R^2 = 0.720$).

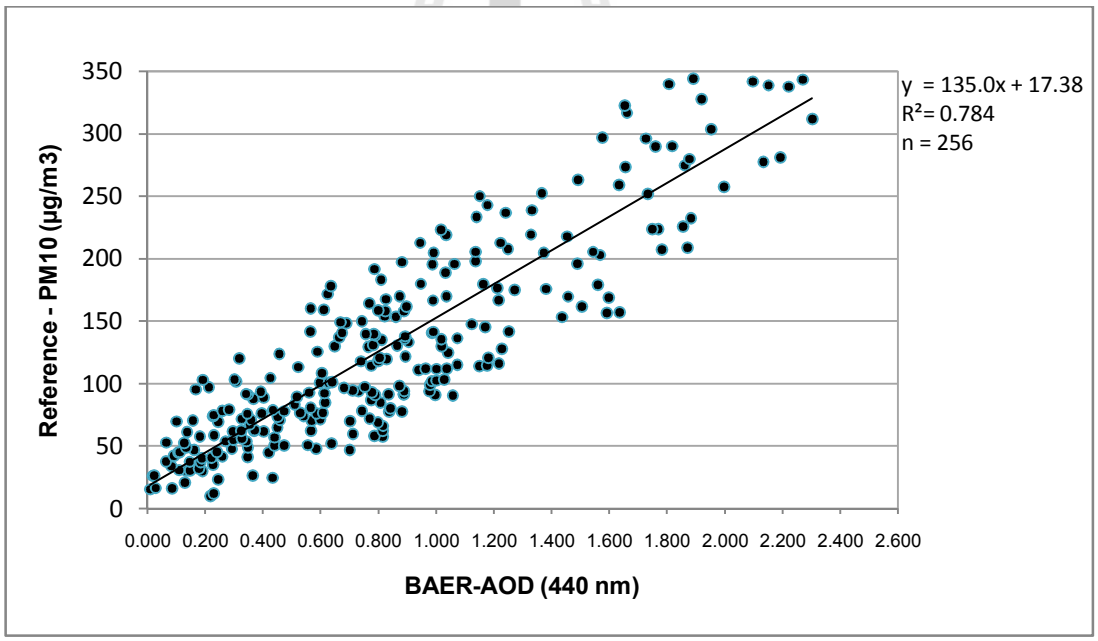

Figure 4.2d Linear relationship of the BAER-AOD (at 440 nm) and the reference PM10 data (with $R^2 = 0.784$).

To achieve better spatial resolution of AOD map developed from the original MODIS data, in this thesis, attention was paid on the application of the BAER-AOD derived from the MODIS data (as detailed in Chapters II and III) to predict the surface PM10 concentration at 500-m resolution. As illustrated in Table 4.1 and Figure 4.2d, the BAER-AOD (at 440 nm) attains impressive relation to reference PM10 data (R^2 = 0.784) with small deviation appeared at AOD = 0 (with PM10 = 17.11 $\mu g/m^3$). Regarding to all these found outstanding properties, the BAER-AOD was chosen to prepare the temporal PM10 maps for entire study area as described in Section 4.3.2.

Another work accomplished here was to establish the distinguish relationship between the AERONET-AOD (440 nm) from station in Chiang Mai downtown and the averaged PM10 data observed at the two measuring stations nearby (CM1 and CM2). Result of the study indicates relatively high relation between AERONET-AOD and reference PM10 data (R^2 = 0.86) with small offset at AOD = 0 (with PM10 = 13 $\mu g/m^3$). This finding is notably better than those reported in some earlier works, e.g. Koelemeijer, Homan, Matthijsen (2006) (R = 0.58); Péré, Pont, Mallet, Bessagnet (2009) (R = 0.69) and Kalivitis et al. (2007) (R^2 = 0.6). This achieved result implies that AERONET-AOD data might be applied as a respective indicator of the concerned PM10 pollution occurring over Chiang Mai central area with timescale of about 15 minutes which is significantly better than the 1-hour timescale of regular PM10 measuring at most PCD stations. However, due to its limited locations, the AEONET-AOD is not suitable for the production of PM10 maps over the entire area.

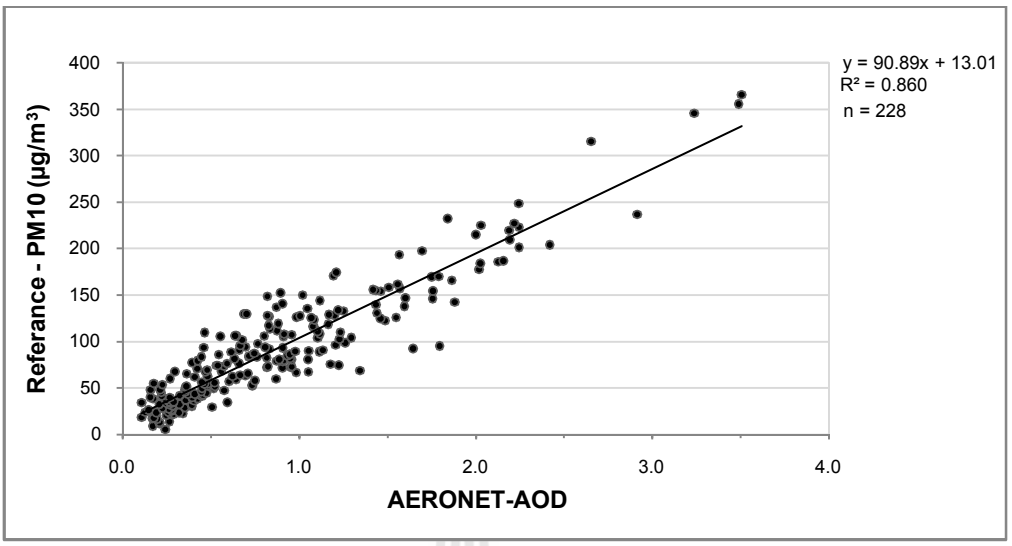

Figure 4.2e Linear relationship of AERONET-AOD (at 440 nm) and reference PM10 data (with $R^2 = 0.86$).

4.1.3 Mutual relations of MODIS-based parameters and AERONET-AOD

In this work, the mutual relations among some MODIS-based parameters and AERONET-AOD were investigated. These include relations between NDAI and ΔR (Blue), AERONET-AOD and MODIS-AOD, and AERONET-AOD and BAER-AOD. It was found that all these pair of parameters express quite notable relations to each other ($R^2 = 0.803$-0.832) as reported in Table 4.1c and Figures 4.3a-c. The rather high relation between NDAI and ΔR (with $R^2 = 0.803$) means these two newly-proposed parameters are potentially interchangeable as being a promising PM10 predictor for the study area. Also, good agreement between the AERONET-AOD and the MODIS-AOD (with R^2 of 0.832) achieved here supports similar discoveries published earlierlike those listed in Table 2.6. Note that, these AOD dataset were computed at different wavelengths that led to the noticeable discrepancy in their actual values.

Table 4.1c Found linear relationships between MODIS-NADI and AERONET-AOD data.

Parameter		Found relationship (y = ax+b)	R^2	Sensitivity (Δy/Δx)	Scale (m)	n	Figure
x	y						
NDAI	ΔR (Blue)	y = 0.186x - 0.025	0.803	-	-	618	4.3a
AERONET-AOD	MODIS-AOD	y = 0.55x + 0.032	0.832	-	-	83	4.3b
AERONET-AOD	BAER-AOD	y = 1.05x - 0.061	0.828	-	-	53	4.3c

Note: 1. DN, ΔR, NDAI, AOD are unitless.

2. n ≡ number of data pair in use

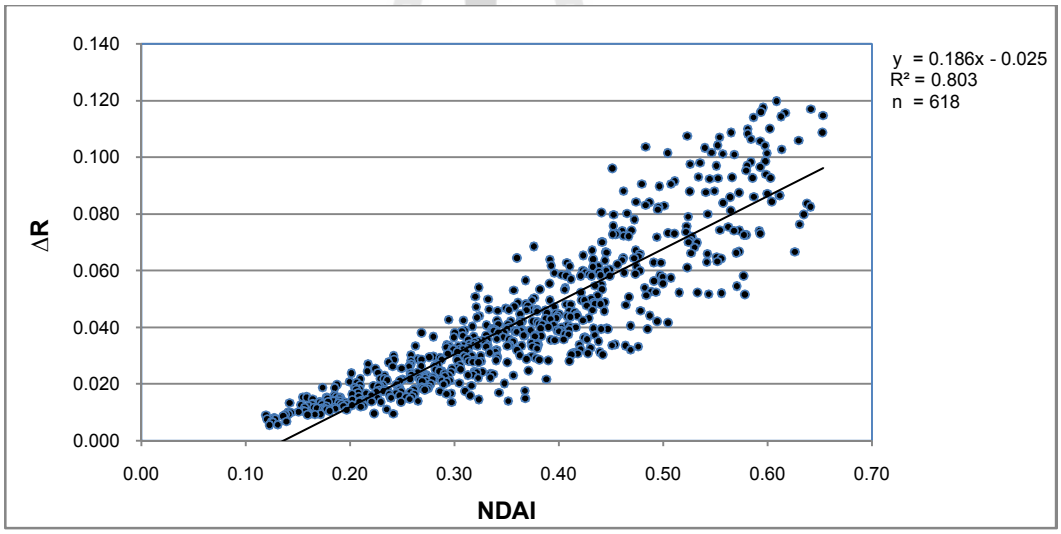

Figure 4.3a Linear relationship of NADI and ΔR (blue) data (with $R^2 = 0.803$).

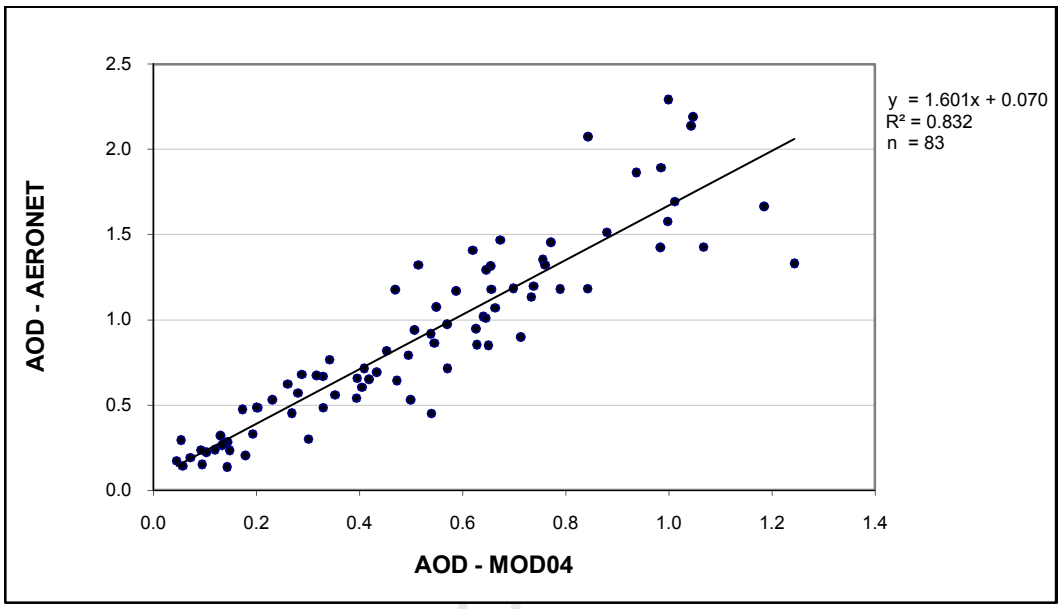

Figure 4.3b Linear relationship of the AERONET-AOD (440 nm) and MODIS-AOD (550 nm) (with $R^2 = 0.832$).

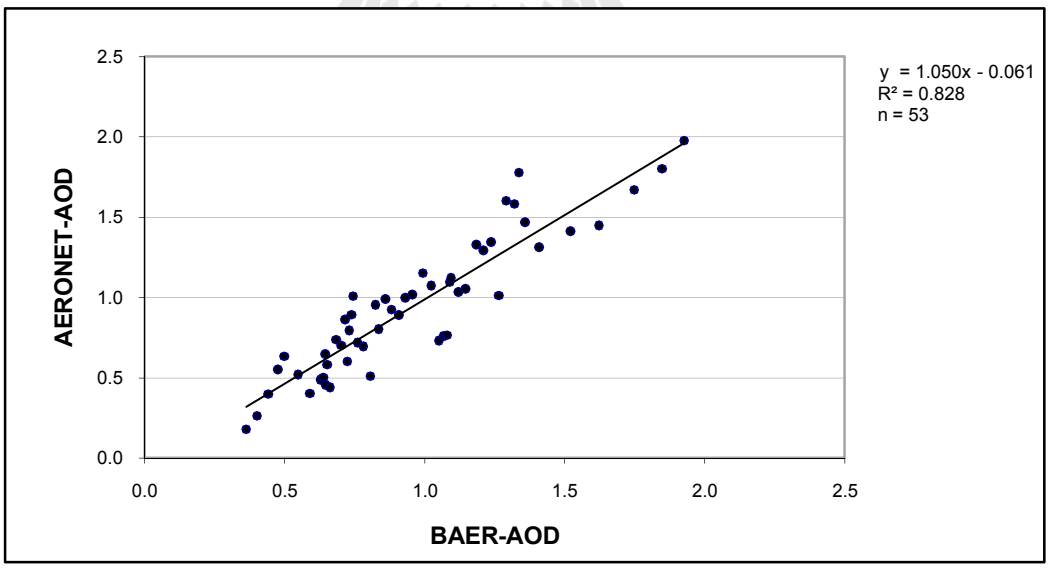

Figure 4.3c Linear relationship of the BAER-AOD (440 nm) and AERONET-AOD (440 nm) (with $R^2 = 0.828$).

Finally, relationship between BAER-AOD and AERONET-AOD was assessed and result is shown in Figure 4.3c with relatively high relation level accomplished (with $R^2 = 0.828$). The AERONET-AOD data is often believed to have high accuracy in the quantification of atmospheric AOD at a particular place and time. As a result, its high relation to the derived BAER-AOD in this work, with nearly 1:1 fit to each other (as seen in Figure 4.3c) under the relation form:

$$\text{AERONET} = 1.05(\text{BAER}) - 0.061, \qquad (4.1)$$

indicates the impressive achievement of the applied BAER-AOD derivation method. This distinguished capacity is rather essential for the formulation of PM10 maps from the BAER-AOD in the next section. In addition, R^2 of 0.828 achieved here is fairly comparable to those attained in other reports, e.g., Lee et al. (2005) (R = 0.96); Lee et al. (2007) (R = 0.90); Song et al. (2008) (R = 0.46-0.89) and Glantz, Kokhanovsky, von Hoyningen-Huene, and Johansson (2009) ($R^2 = 0.92$).

4.2 Applications of the derived NDAI, PM10 and AQI maps

This section is divided into three major parts regarding to the derivation and application of the NDAI maps, PM10 maps from the BAER-AOD data, and AQI maps from the derived PM10 maps. Their details are as follows.

4.2.1 Derivation and application of the NDAI maps

As mentioned in Section 4.1.2, the NDAI contains three interesting properties that make it become a promising candidate for being primary indicator for the PM10-led air pollution severity. These are (1) its considerable strong relation to the reference PM10 data in use ($R^2 = 0.661$), (2) its minimal bias in predicting the PM10 data at low

values, and (3) its prospective values which are limited to about 0 to 1 in reality and can be readily interpreted. The higher NDAI indicates higher PM10 concentration in a linear proportion as described by the following relationship (from Figure 4.2b):

$$PM10 = 300.6NDAI + 4.527. \quad (4.2)$$

This knowledge was applied to evaluate PM10 air pollution situation during 2010 fire season over the entire area on 4^{th}-9^{th} April and results (NDAI and associated PM10 information) are shown in Figures 4.4a-e and Table 4.2, respectively.

From Figure 4.4a (for 4^{th} April), lower values of the NDAI are dominant over most provinces except at Mae Hong Son (along Thai/Myanmar border), Chiang Mai (middle region), and Nan (eastern/ northwestern parts), that have some areas attached to relatively high values of the NDAI (e.g. > 0.4). This suggests the existence of air pollution problem over those areas (as confirmed by the associated PM10 maps).

มหาวิทยาลัยเทคโนโลยีสุรนารี

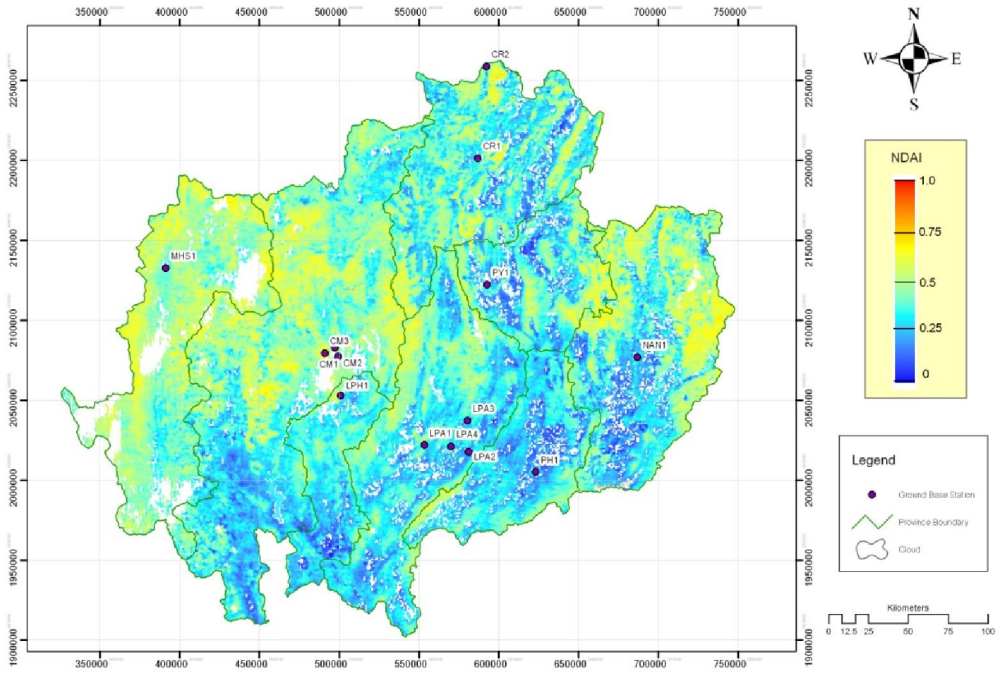

(a)

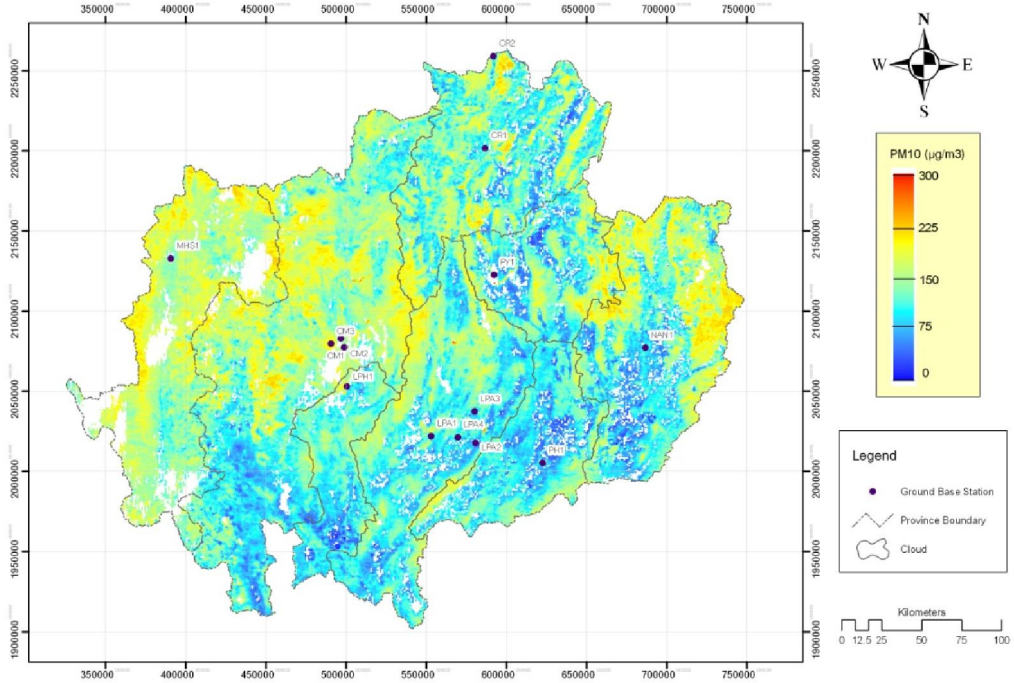

(b)

Figure 4.4a (a) NDAI and (b) the associated PM10 maps on 4th April 2010.

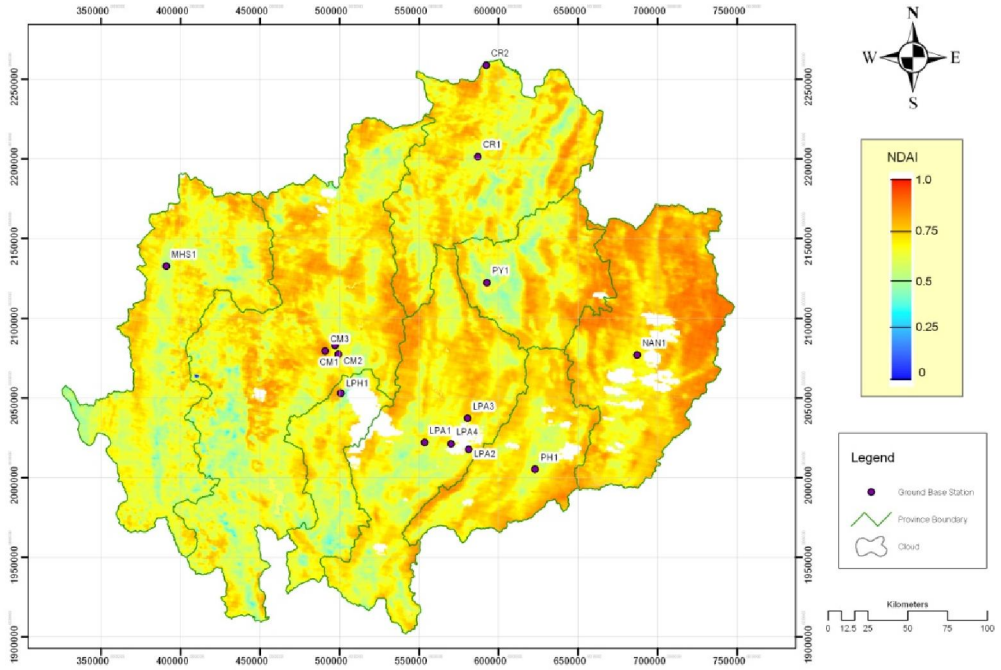

(a)

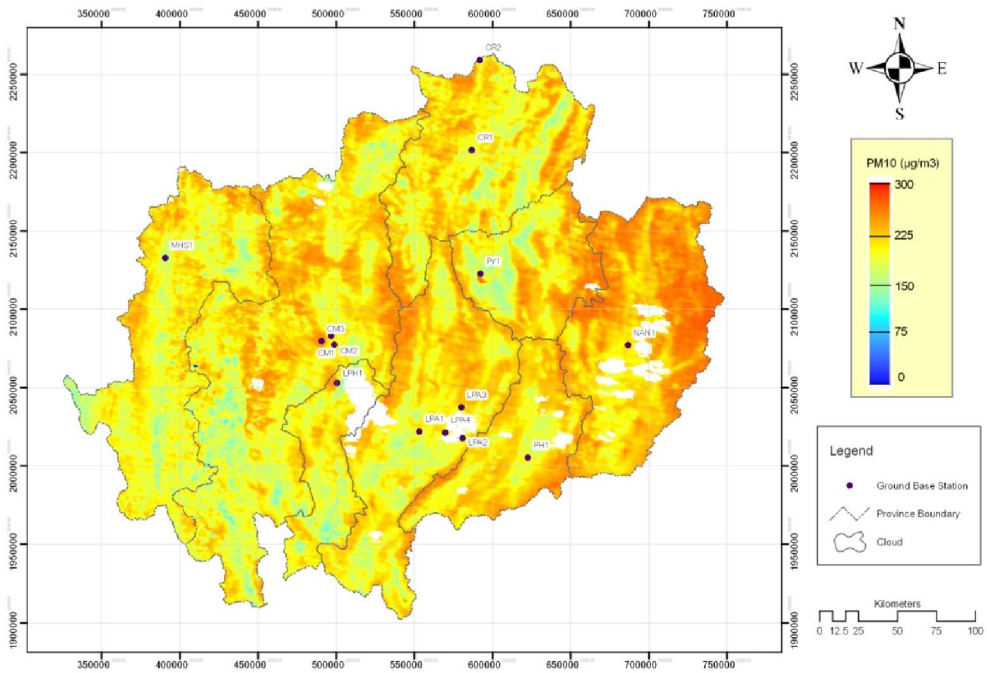

(b)

Figure 4.4b (a) NDAI and (b) the associated PM10 maps on 5th April 2010.

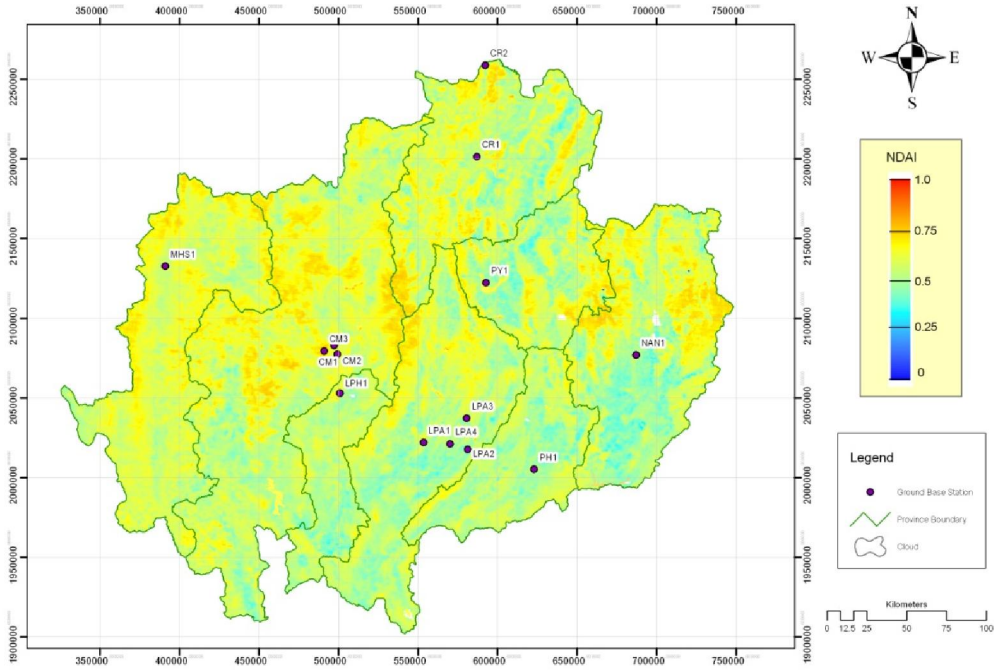

(a)

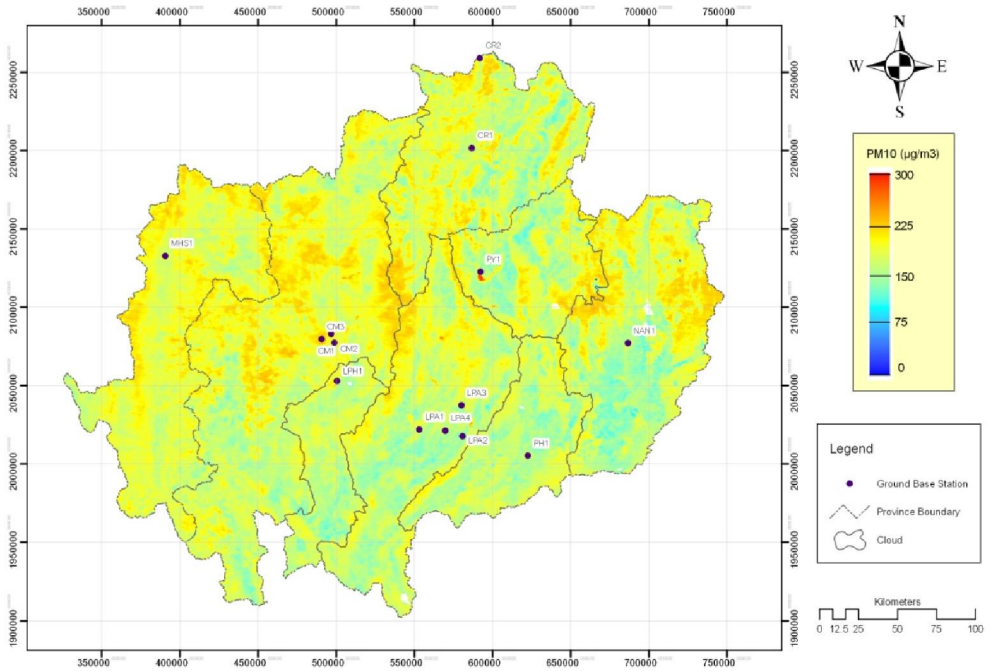

(b)

Figure 4.4c (a) NDAI and (b) the associated PM10 maps on 6th April 2010.

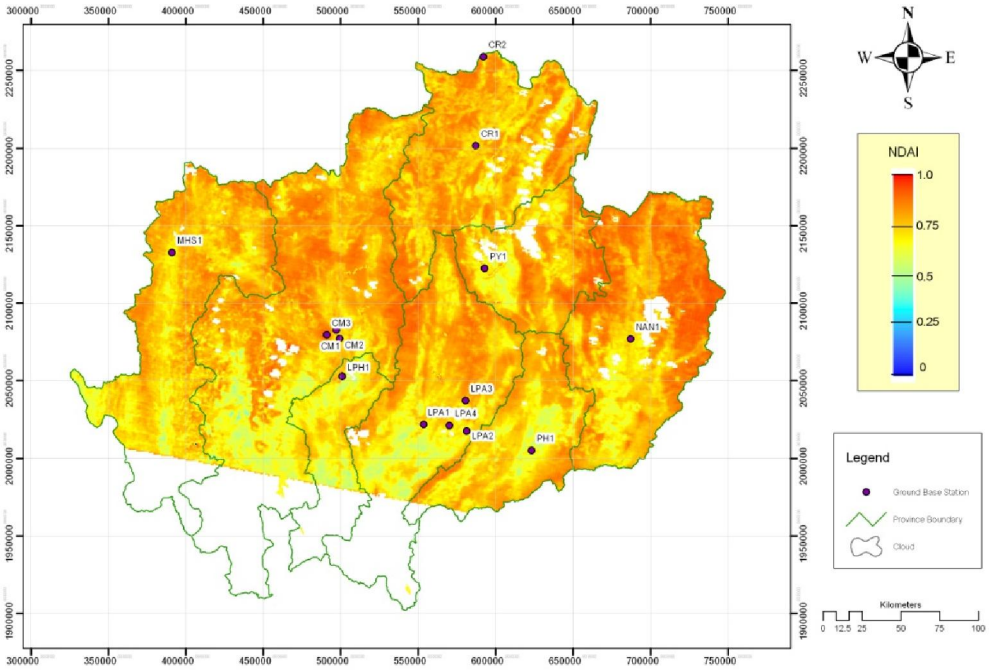

(a)

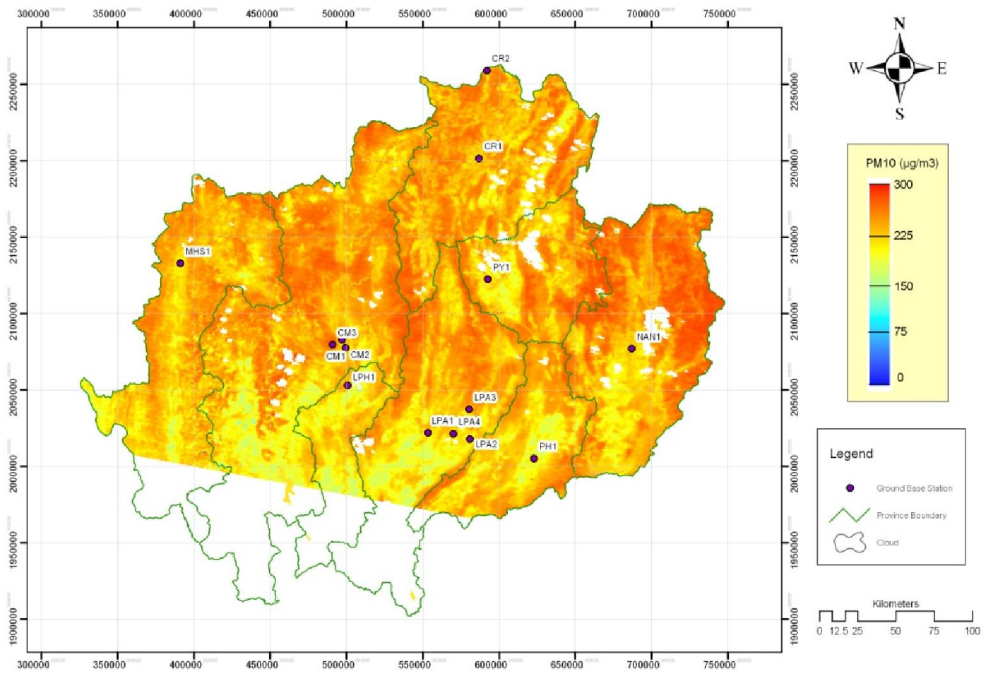

(b)

Figure 4.4d (a) NDAI and (b) the associated PM10 maps on 7th April 2010.

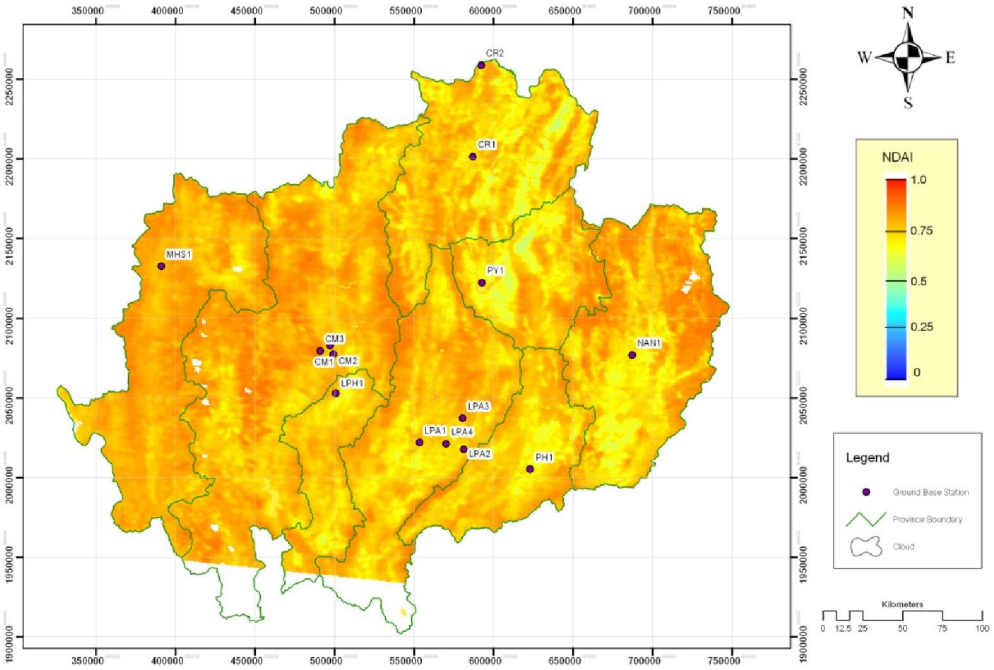

(a)

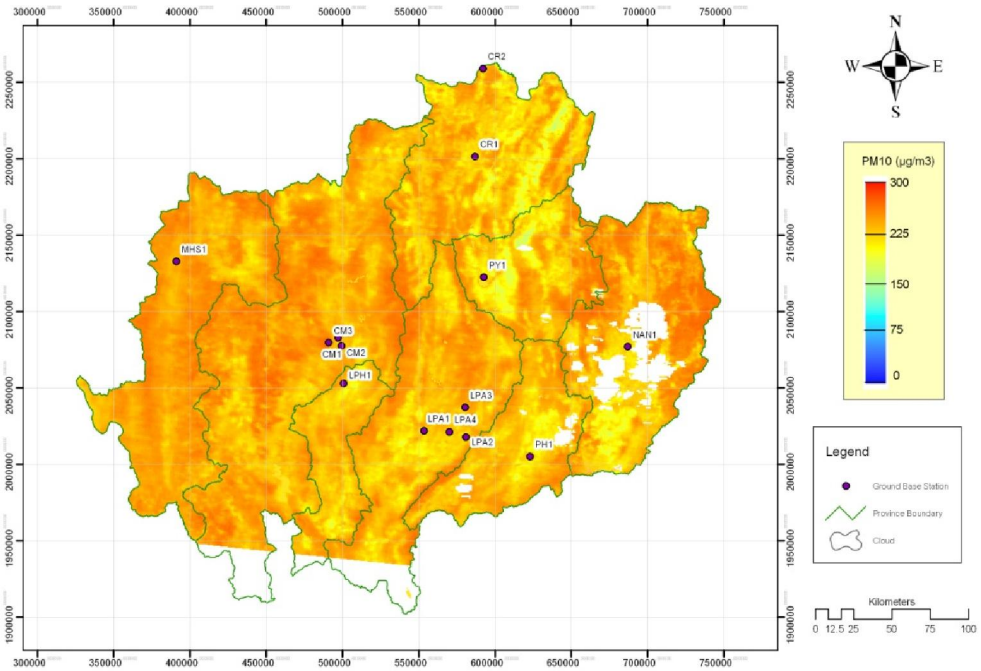

(b)

Figure 4.4e (a) NDAI and (b) the associated PM10 maps on 8th April 2010.

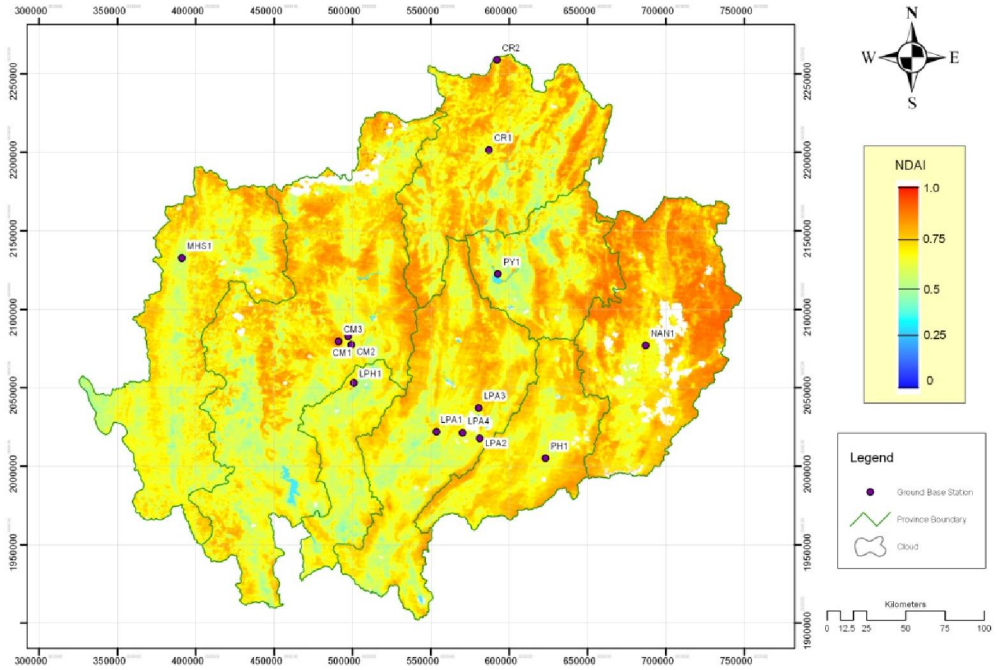

(a)

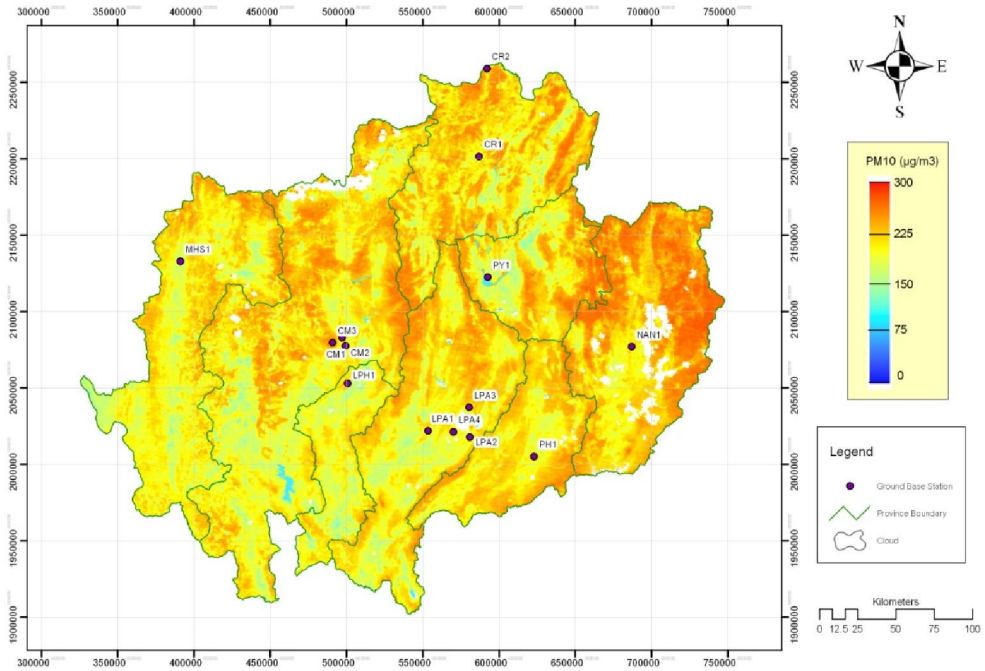

(b)

Figure 4.4f (a) NDAI and (b) the associated PM10 maps on 9th April 2010.

Table 4.2 Distribution of NDAI and PM10 concentration over the area on 4th-9th April 2010 (PM10 has unit of μg/m3).

NDAI	PM10 (Approxi-mated)	4th April		5th April		6th April	
		Area (km^2)	%	Area (km^2)	%	Area (km^2)	%
0.0-0.2	0-65	6,354	7.19	4	-	-	-
0.2-0.4	65-125	40,305	45.61	89	0.10	813	0.92
0.4-0.6	125-185	37,937	42.93	16,623	18.81	57,225	64.76
0.6-0.8	185-245	3,758	4.25	64,123	72.56	30,318	34.31
0.8-1.0	> 285	18	0.02	7,533	8.52	15	0.02
NDAI	PM10 (Approxi-mated)	7th April		8th April		9th April	
		Area (km^2)	%	Area (km^2)	%	Area (km^2)	%
0.0-0.2	0-65	-	-	-	-	-	-
0.2-0.4	65-125	-	-	-	-	9	0.01
0.4-0.6	125-185	2,289	2.59	369	0.42	13,540	15.32
0.6-0.8	185-245	49,658	56.19	63,109	71.41	64,881	73.42
0.8-1.0	> 285	27,004	30.56	22,866	25.88	9,942	11.25

The situation was getting worse on 5th with about 80% of the area having NDAI > 0.6 (or PM10 > 185 μg/m3) but this value was reduced to be about 34% on 6th April (about 64.76% having NDAI = 0.4-0.6). Pollution problem was getting worse again on 7th-9th April as majority of land having NDAI > 0.6 (in total of 87%, 99% and 85% for 7th, 8th, and 9th date respectively).

Validation of the used PM10 maps was also assessed by the determination of correlation level between the derived and reference PM10 data and the mean absolute error (MAE) of the two datasets in use calculated based on the following formula:

$$\text{MAE}\ (\%) = \frac{1}{n}\left[\sum_{i=1}^{n}\frac{\left|PM_{NDAI,i} - PM_{REF,i}\right|}{PM_{REF,i}} x100\%\right] \qquad (4.3)$$

where $PM_{NDAI,i}$ and $PM_{REF,i}$ are the i^{th} pair of the derived and reference PM10 data, respectively, while n is total number of the relevant data pairs in use (n = 70 in this case). It was found that both groups of data are correlated to each other moderately well with the R^2 of 0.678 and the mean absolute error (MAE) of 17.59% (Figure 4.5) which are fairly satisfied. More information of the MAE calculation for the NDAI-based PM10 data is reported in Appendix A.

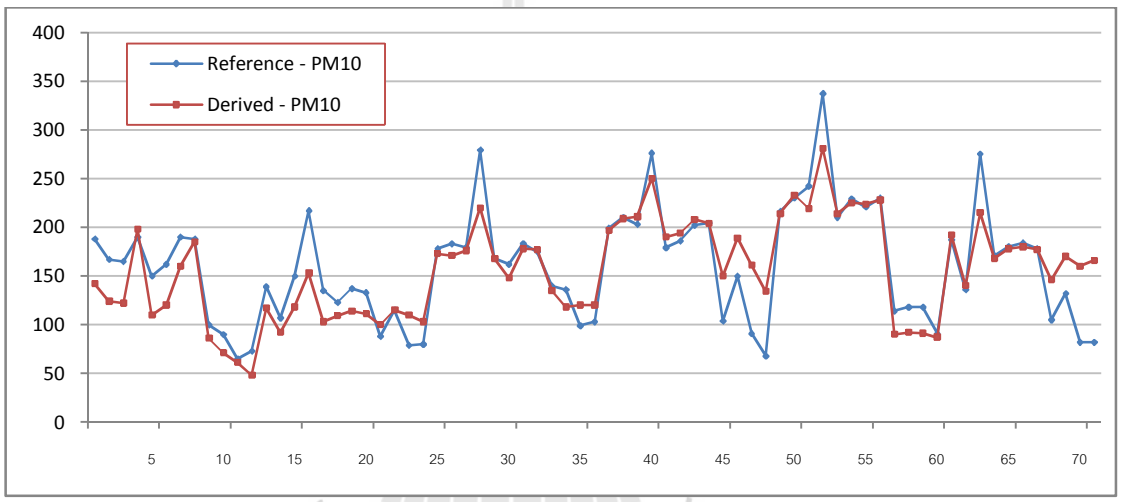

Figure 4.5a Comparison of the derived PM10 data (PM_{NDAI}) and reference PM10 data (PM_{REF}) (with MAE = 17.59%).

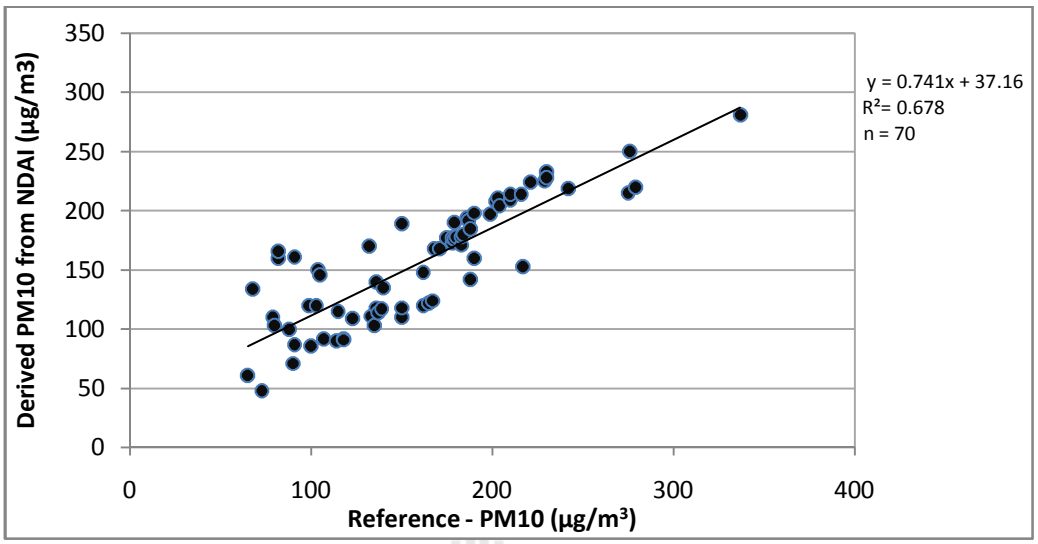

Figure 4.5b Relation of the derived PM10 data (PM_{NDAI}) and reference PM10 data (PM_{REF}) (with $R^2 = 0.678$).

4.2.2 Derivation and application of the BAER-AOD maps

As discussed earlier in Section 4.1.2, the BAER-AOD was considered as being prime candidate for the production of the PM10 density map over the study area due to its strong relation to the reference PM10 data ($R^2 = 0.78$) and low bias in predicting low PM10 data along with its fine mapping resolution (of 500 m). In this section, its merit in the preparation of associated PM10 map for the study area during 2010 fire season is assessed and discussed. Main results can be concluded as follows.

At the beginning, daily maps of the BAER-AOD during period of 4^{th}-9^{th} April 2010 were constructed based on methodology described in Chapter III. These obtained results are reported along with the corresponding MODIS-AOD map in Figure 4.6a-f, respectively (at their respective scales). The required PM10 maps were subsequently made for each date from their MODIS-AOD and BAER-AOD counterpart maps and results are summarized in Figure 4.6a-f and Table 4.3, respectively. It is apparent from these obtained figures that, in general, both AOD

maps for each date indicate high degree of conformity, however, substantial difference in their scales could make this resemblance more difficult to visualize instantly. In conclusion, the BAER-AOD maps are clearly able to provide subtle details of the atmospheric AOD variation that still seriously lack in the standard MODIS-AOD maps (about 20 times better in terms of the spatial resolution). The BAER-AOD is also obviously better than MODIS-AOD in predicting the surface PM10 data in general (with R^2 of 0.72 for the MODIS-AOD and 0.78 for the BAER-AOD, respectively, as shown in Table 4.1). Figures 4.7a-f presents maps of near-ground PM density generated from the original MODIS-AOD and BAER-AOD data for each respective date during 4^{th}-9^{th} April 2010. And like AOD maps, the yielded PM10 maps here in both cases are considerably resemble regardless of their notable difference in spatial resolutions.

These derived AOD and PM10 maps indicate that on 4^{th} April, Chiang Mai, Lamphun, and Mae Hong Son (along the Myanmar border) are suffered the most from extensive aerosol pollution. The least severity situation is presented on the lower part of the study area, especially in Chiang Mai, Lamphun, Phare and Nan. The dominant BAER-AOD scale found on this date is between 0.4-0.6 (66.37%) which is equivalent to the PM10 data of about 163-236 $\mu g/m^3$ while the second most dominant scale is 0.2-0.4 (22.87%). Note that, most polluted areas are not always situated in urban area where most of the measuring stations are located, therefore, they are very unlikely to be recognized by the traditional ground-based fixed-station measurements.

On the following date, 5^{th} April, the aerosol pollution is distributed along eastern side of the area, especially in Nan and Phayao, while on western side the PM situation is noticeably low, especially in Mae Hong Son and Chiang Mai. The most

dominant BAER-AOD scale on this date is between 0.4-0.6 (46.23%) and the second most dominant one is at 0.2-0.4 (42.48%), which is equivalent to the PM10 data of about 90-163 $\mu g/m^3$, similar to those found on the previous day. Areas with fairly serious locations with AOD > 0.6 cover about 7% of the entire area, mostly in Nan Province. However, the pollution situation is getting better on the eastern side on 6th April but thing is getting worse on the western side both in Chiang Mai and Mae Hong Son. This finding conforms well to the daily-mean PM10 data observed at the PCD stations in both provinces (shown in Table 3.7) which are 220 $\mu g/m^3$ (CM) and 223 $\mu g/m^3$ (MHS) on the 5th April but only at 163 $\mu g/m^3$ (CM) and 114 $\mu g/m^3$ (MHS) on the 4th April. The most severe situation is visible over Chiang Rai in general (with daily mean PM10 = 236 $\mu g/m^3$) and over Chiang Mai and Lamphun Provinces (in lowland regions). And highly concerned areas with AOD > 0.6 (PM10 > 236 $\mu g/m^3$) cover just about 0.1% on this date.

On 7th April, the aerosol situation has notably deteriorated over most parts of the area especially for the eastern provinces like Chiang Rai, Nan, and Phayao, but the situation is improved considerably over the lower parts of Chiang Mai and Mae Hong Son. This great degradation of air quality is reflected in apparent data of the most dominant BAER-AOD scale on this date which is at 0.6-0.8 (30.86%) followed by 0.4-0.6 (26.16%), 0.2-0.4 (19.74%) and 0.8-1.0 (18.55%). Note that, critical areas with AOD > 0.6 cover about 50% of the entire area. This pattern was also discovered taking place on 8th April but its detail was still somewhat limited due to some missing data in the acquired MODIS imagery available on that date.

Finally, on the last date of 9th April, the aerosol pollution is less visible on the western portion of the area, especially in Chiang Mai and Mae Hong Son, but the

situation is still critical in the far eastern part of the area along with the Laos border, especially in Nan and Chiang Rai. The most dominant BAER-AOD scale on this date is at 0.4-0.6 (39.87%) and the second most dominant one is 0.2-0.4 (36.30%). Critical areas with AOD > 0.6 are found covering about 20% of the entire area, mostly in those provinces bordered with Laos.

General conclusion drawn from results achieved in this part is as follows:

(1) The AOD and PM10 maps derived from BAER method and from MODIS data directly are rather similar in terms of distributing pattern despite the substantial difference in their spatial scales. However, the BAER-AOD and PM10 maps were found much superior in terms of spatial resolution (about 20 times better).

(2) Level of the aerosol pollution discovered in average during study period is quite devastated as it often far surpassed critical limit of 120 $\mu g/m^3$ to stay above the 200 $\mu g/m^3$ level. The worst date is 7th April with average data of 242 $\mu g/m^3$ followed by 8th April at 230 $\mu g/m^3$. And the eastern provinces like Nan, Payao and Chiang Rai were suffered the most from aerosol pollution in average.

(3) The critical areas with rather high values of PM10 data (e.g. > 200 $\mu g/m^3$) were spread over most parts of the study area which make it very difficult to monitor this development of the situation (both in terms of spatial coverage and PM intensity) based on aerosol data measured at a limited number of the ground-based air quality measuring stations alone. In this circumstance, the PM10 maps derived over the entire area as presented here could provide more accurate information of the situation than the ground-based data on a daily basis. However, cloud contamination might reduce the applicability level of this method substantially.

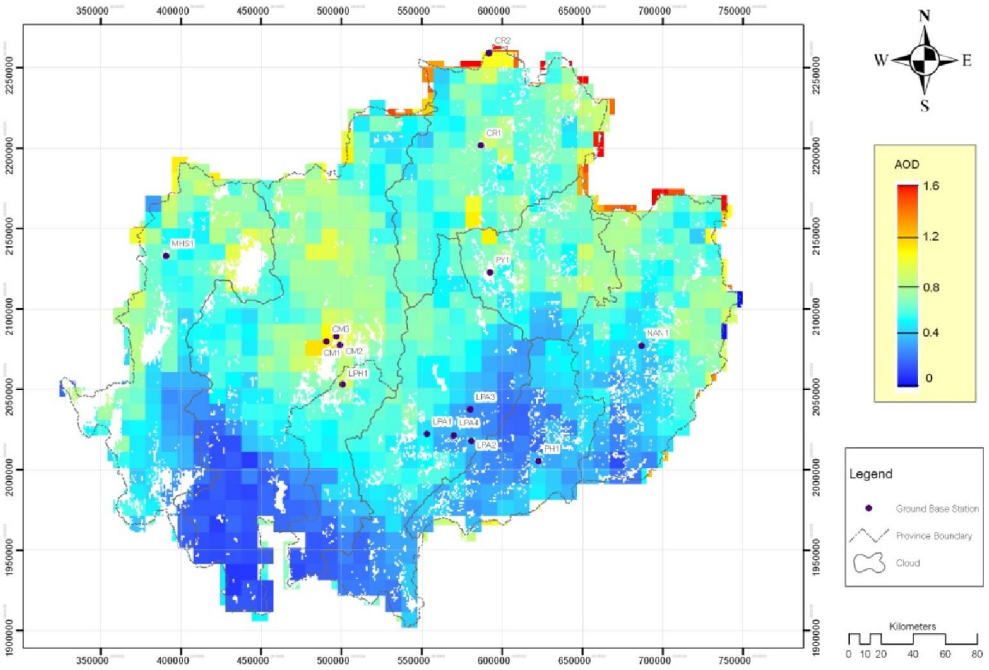

(a)

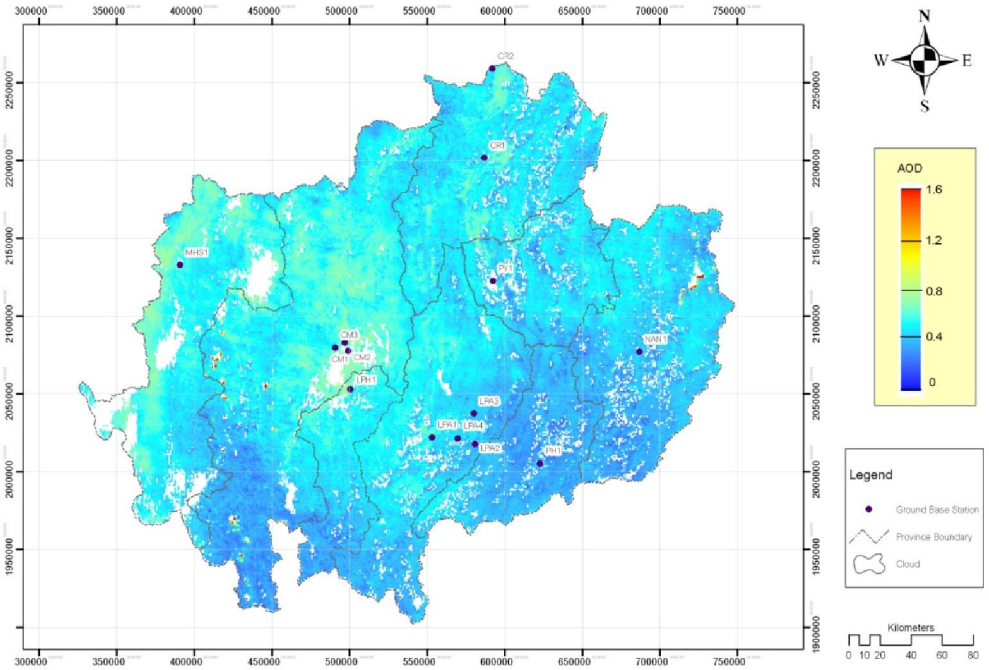

(b)

Figure 4.6a Maps of (a) MODIS-AOD and (b) BAER-AOD data on 4th April 2010.

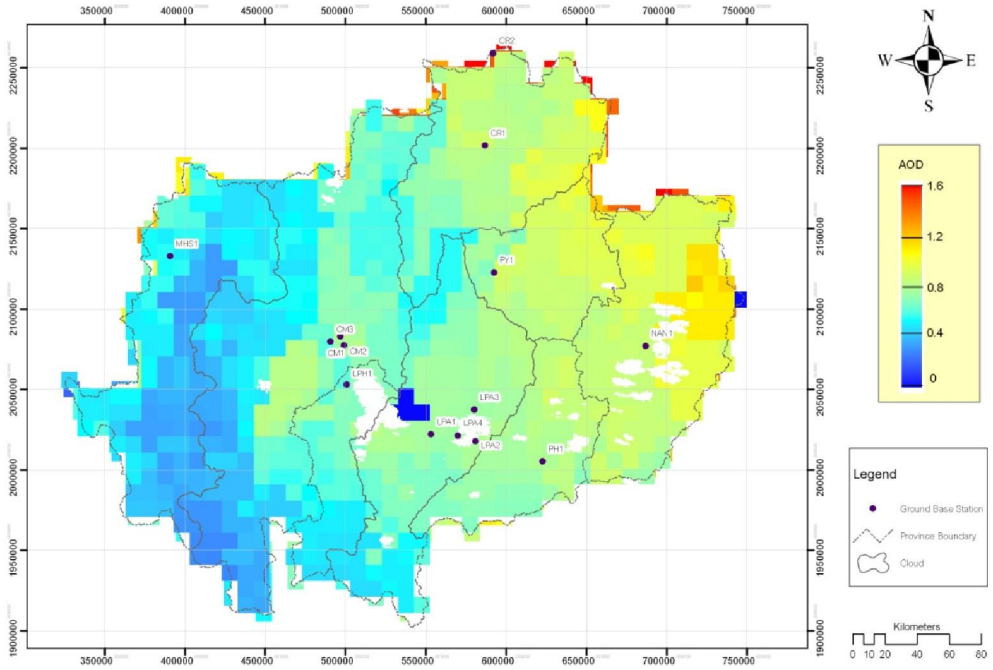

(a)

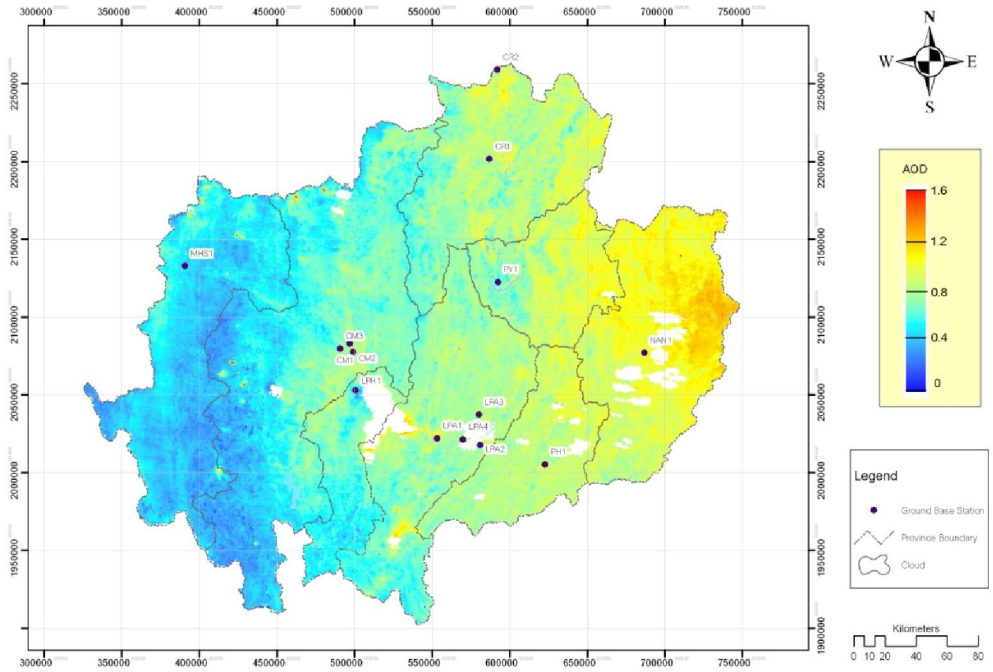

(b)

Figure 4.6b Maps of (a) MODIS-AOD and (b) BAER-AOD data on 5th April 2010.

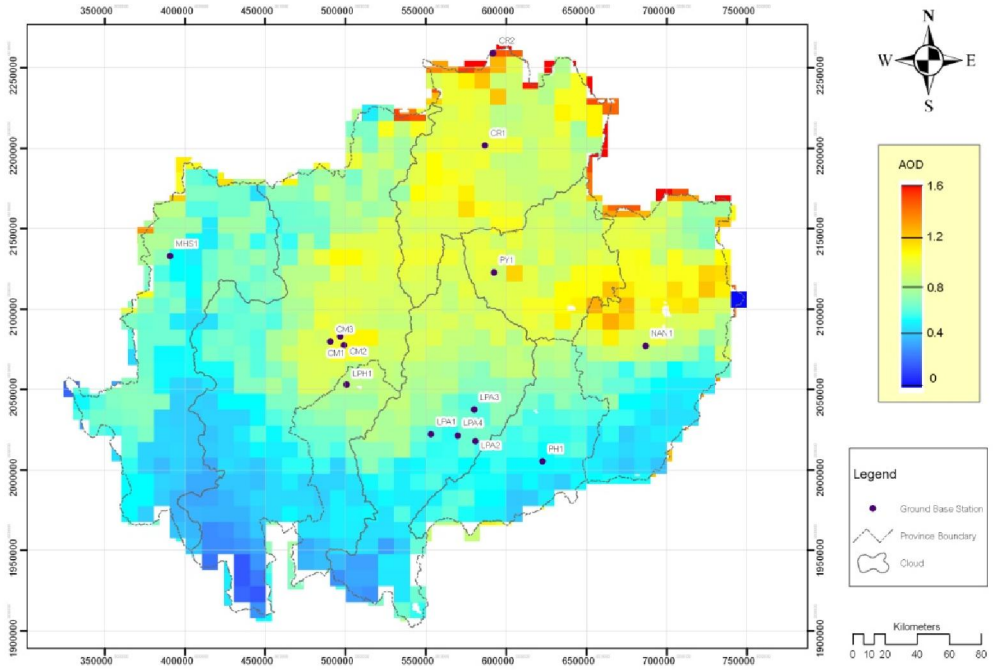

(a)

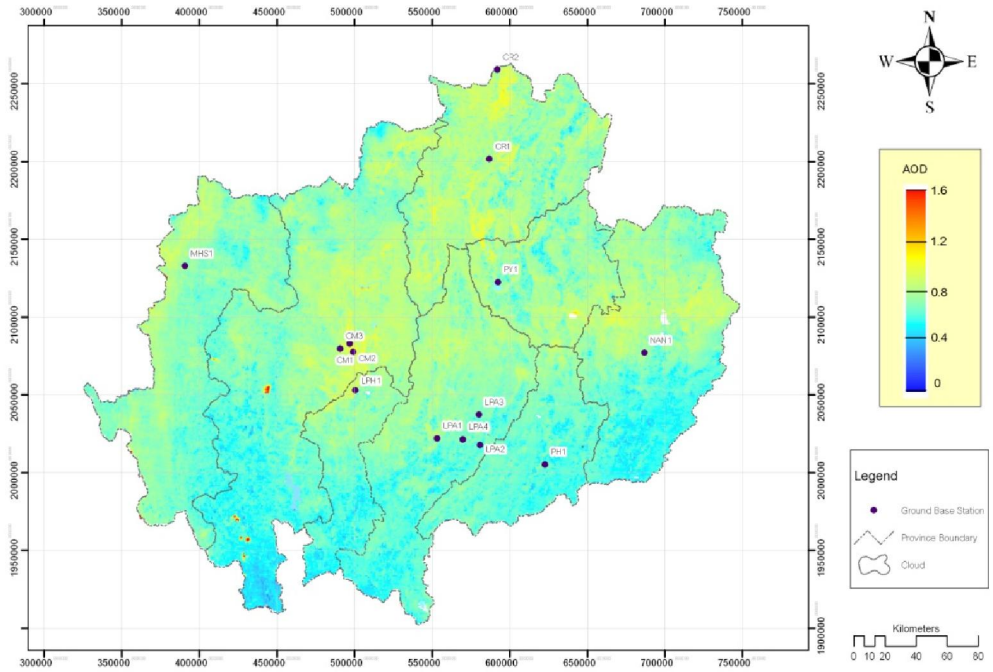

(b)

Figure 4.6c Maps of (a) MODIS-AOD and (b) BAER-AOD data on 6th April 2010.

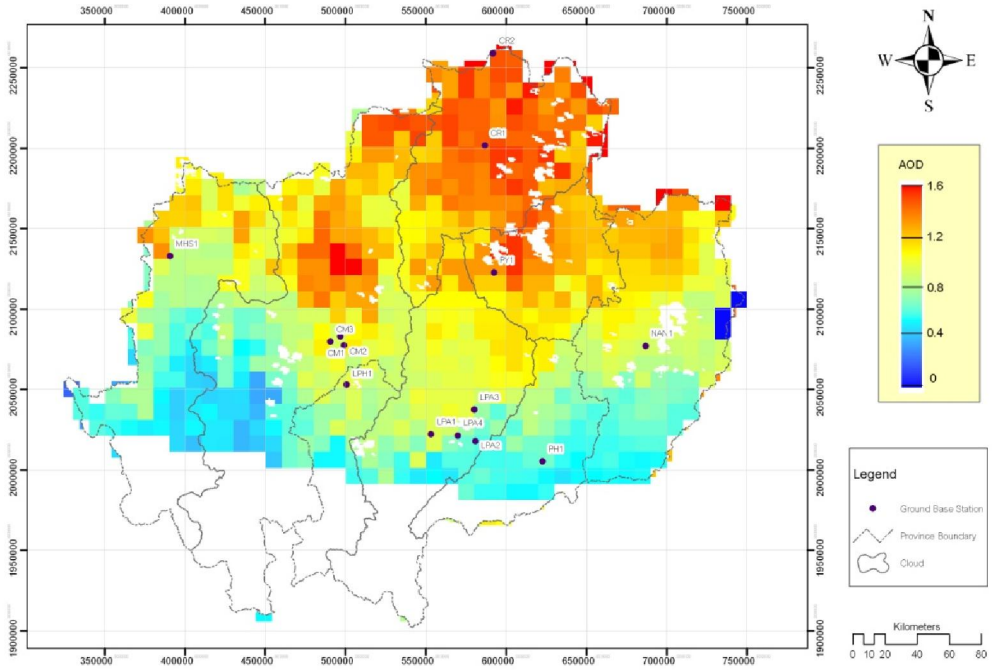

(a)

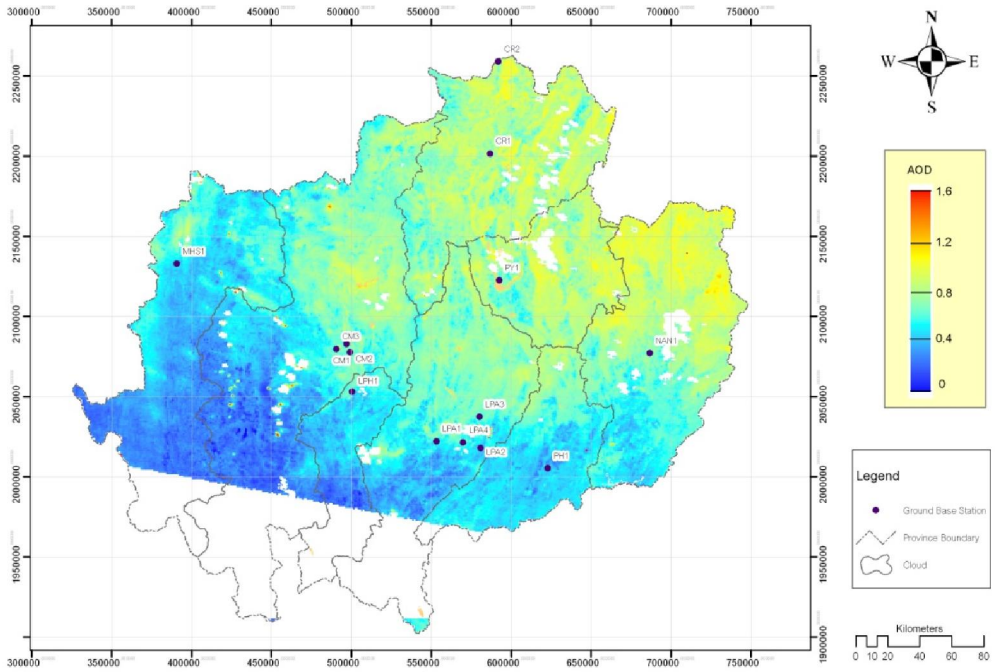

(b)

Figure 4.6d Maps of (a) MODIS-AOD and (b) BAER-AOD data on 7th April 2010.

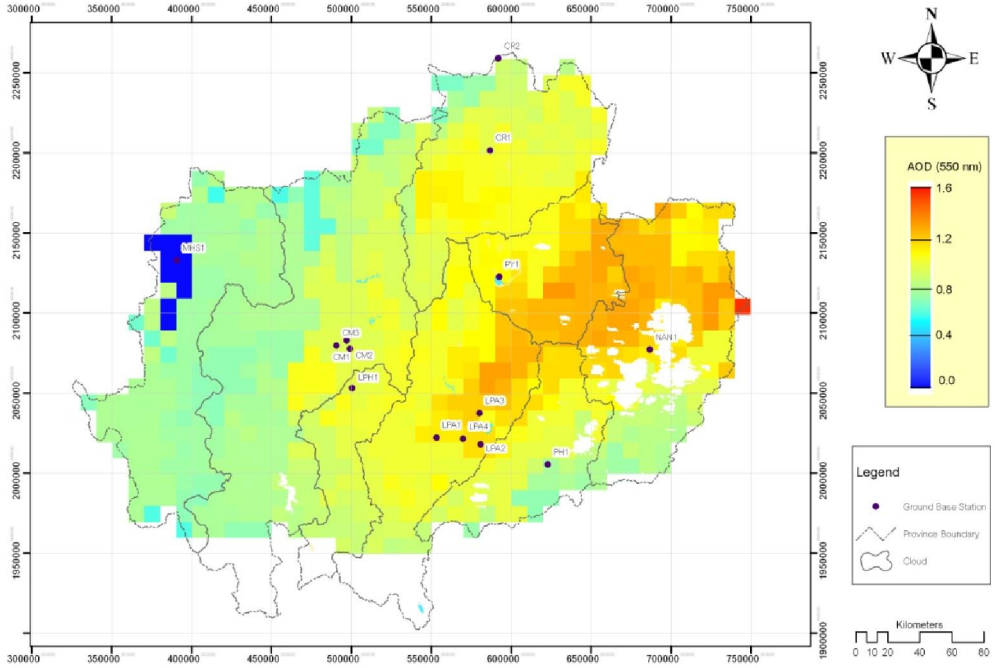

(a)

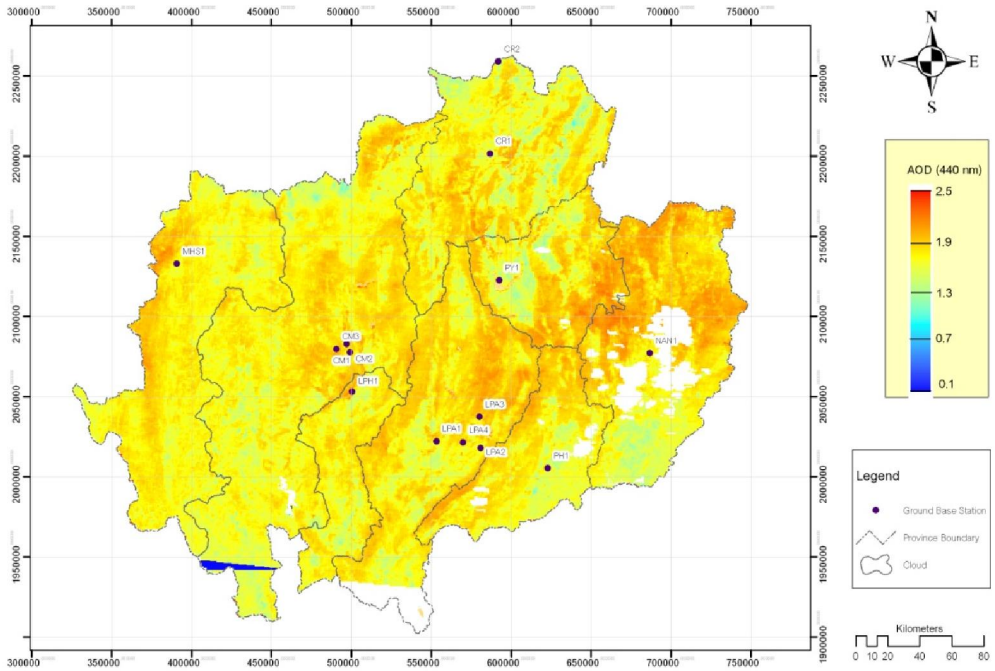

(b)

Figure 4.6e Maps of (a) MODIS-AOD and (b) BAER-AOD data on 8th April 2010.

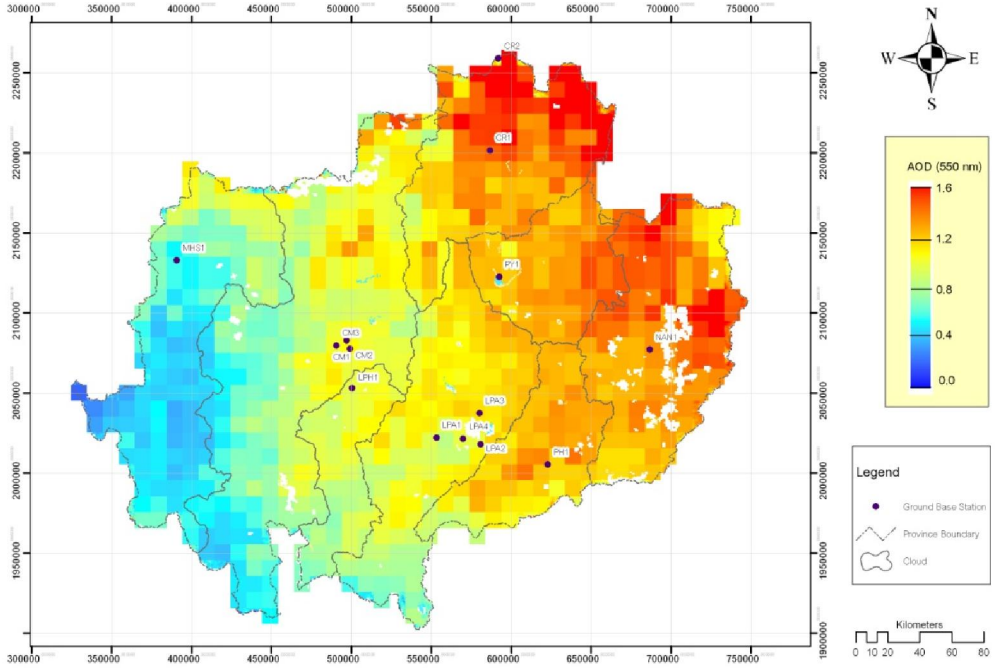

(a)

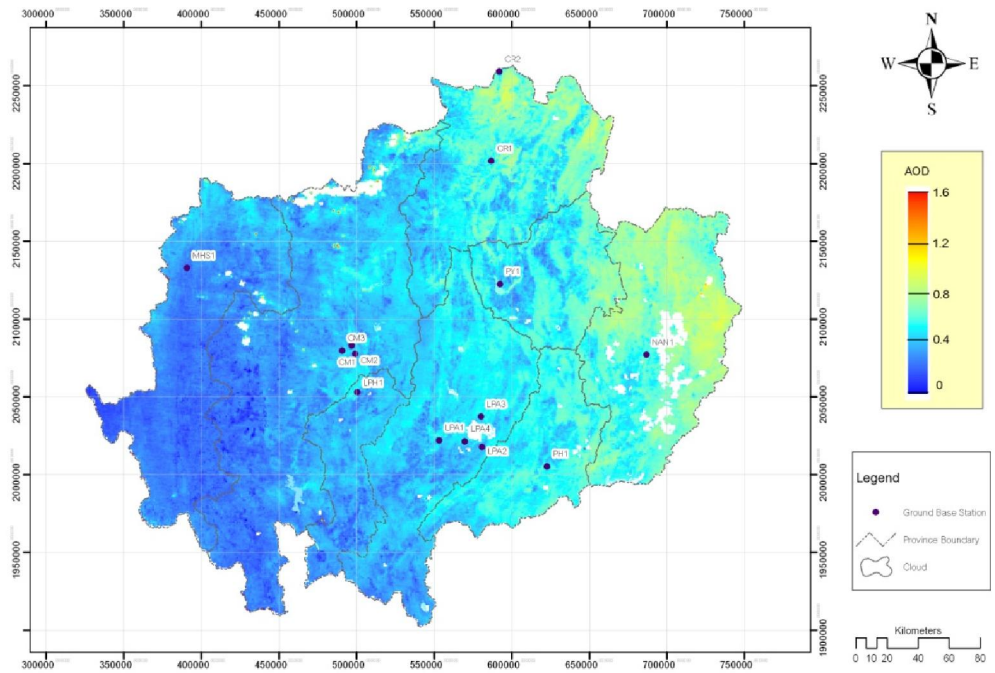

(b)

Figure 4.6f Maps of (a) MODIS-AOD and (b) BAER-AOD data on 9th April 2010.

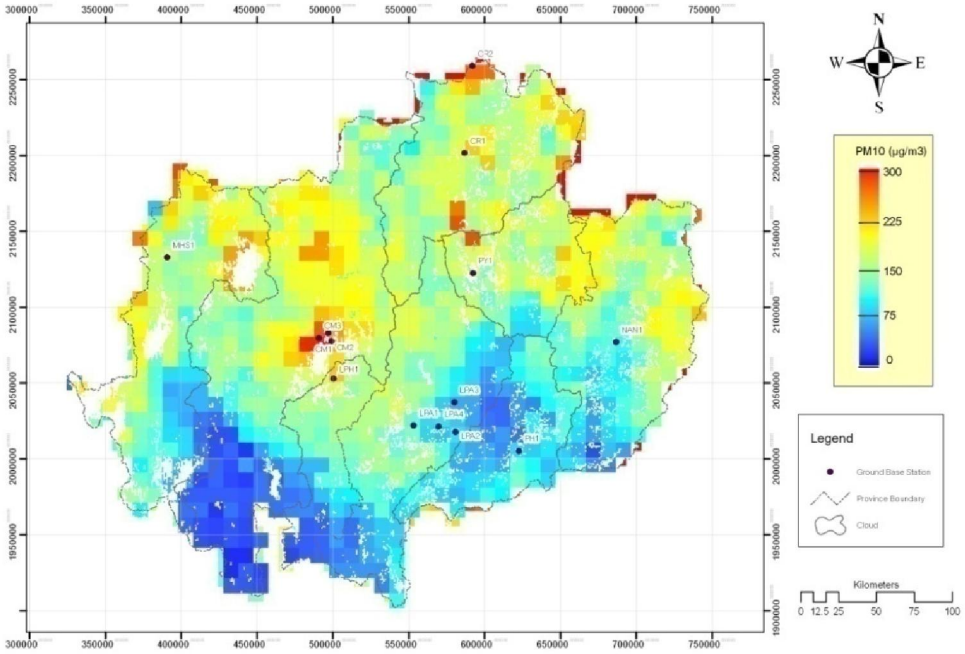

(a)

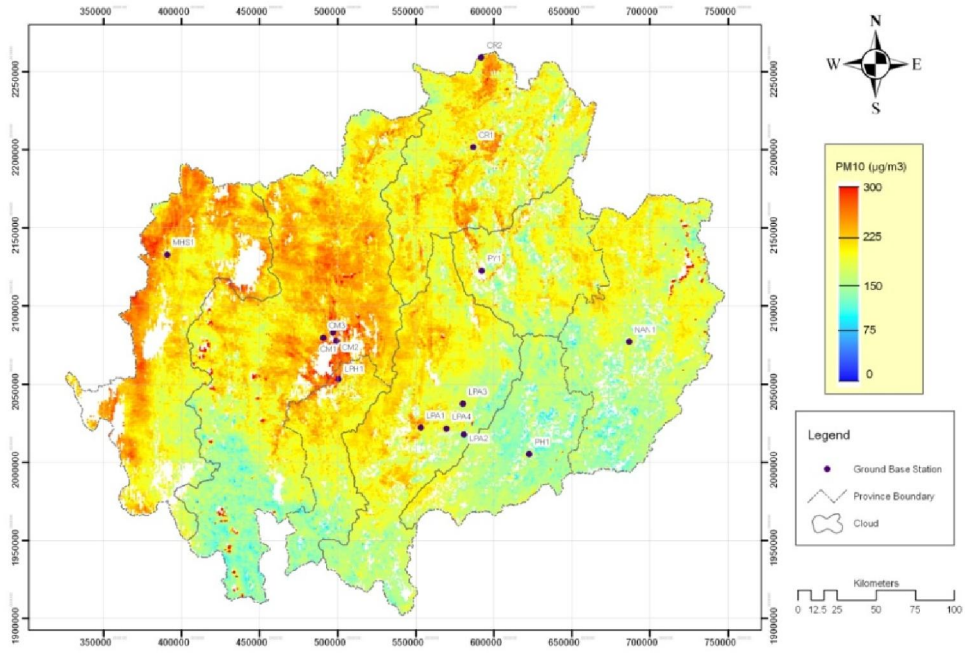

(b)

Figure 4.7a Maps of PM10 derived from (a) MODIS-AOD and (b) BAER-AOD data on 4th April 2010 (using relationships expressed in Table 4.1).

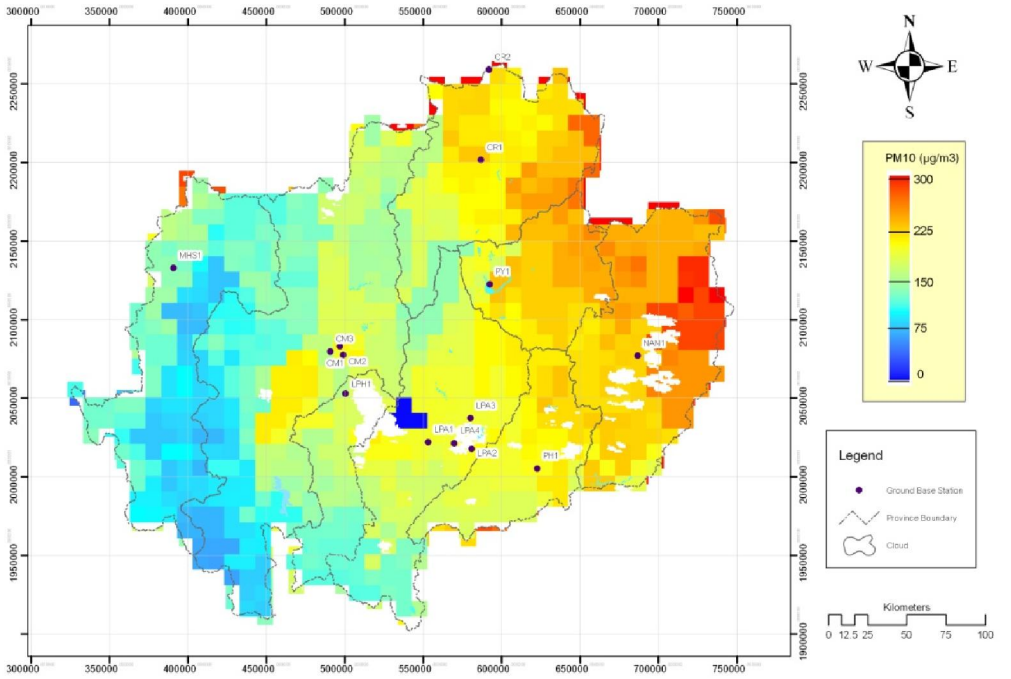

(a)

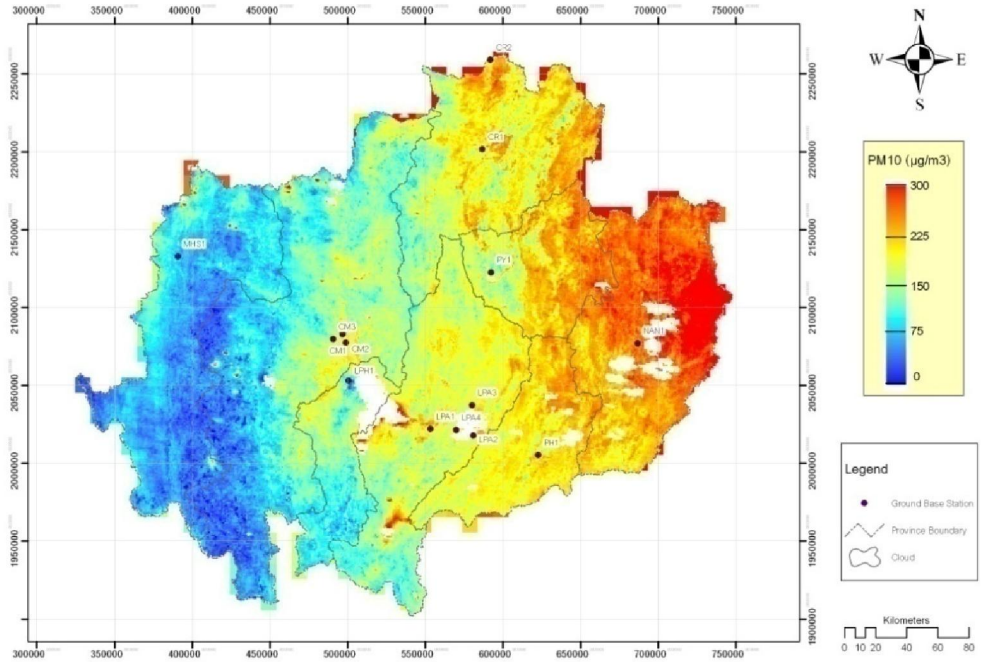

(b)

Figure 4.7b Maps of PM10 derived from (a) MODIS-AOD and (b) BAER-AOD data on 5th April 2010 (using relationships expressed in Table 4.1).

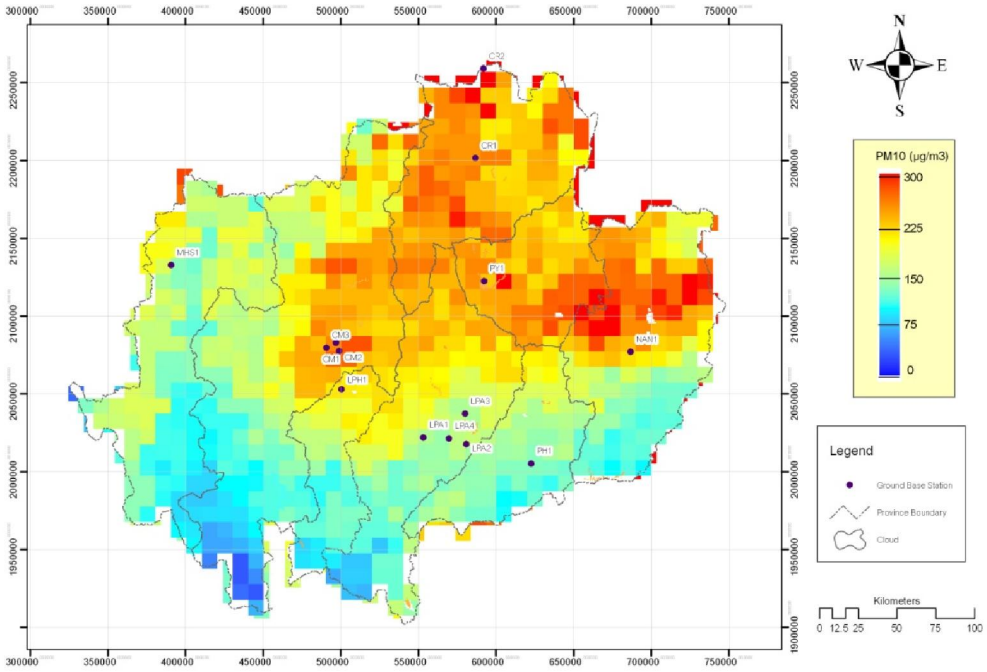

(a)

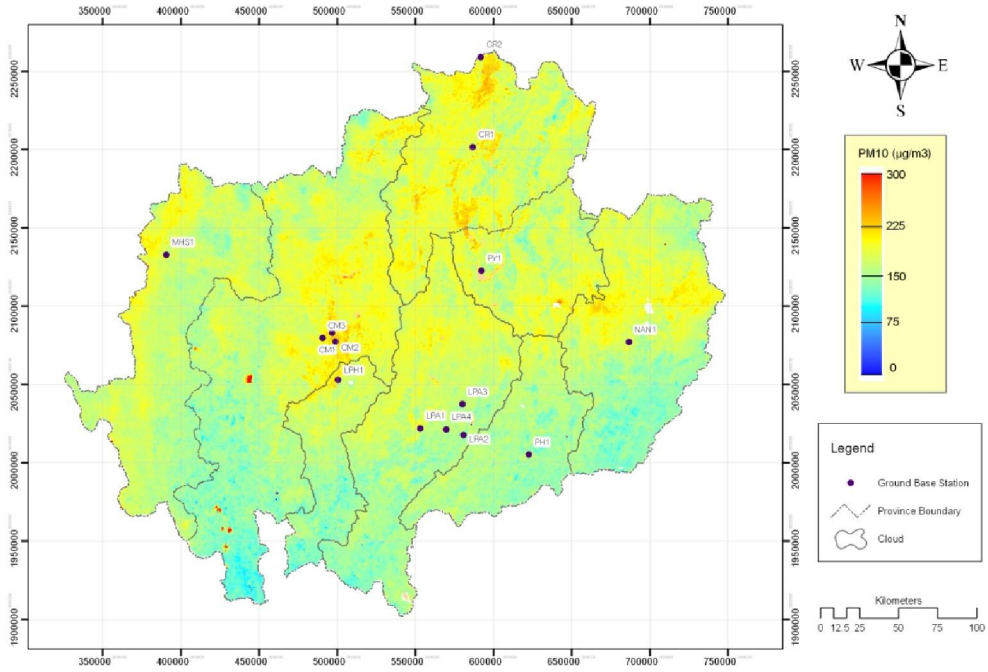

(b)

Figure 4.7c Maps of PM10 derived from (a) MODIS-AOD and (b) BAER-AOD data on 6th April 2010 (using relationships expressed in Table 4.1).

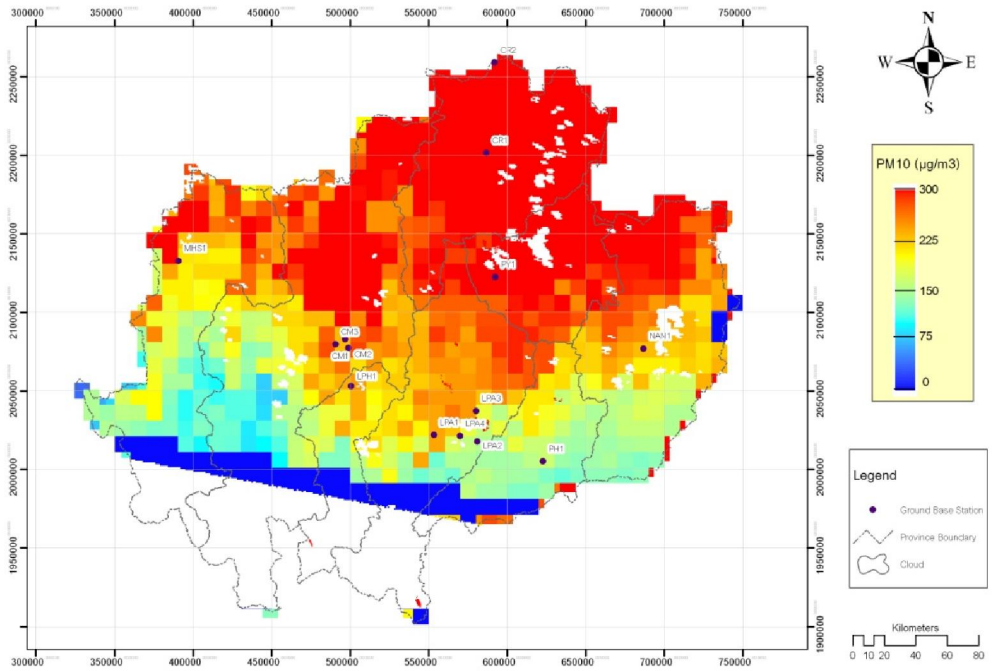

(a)

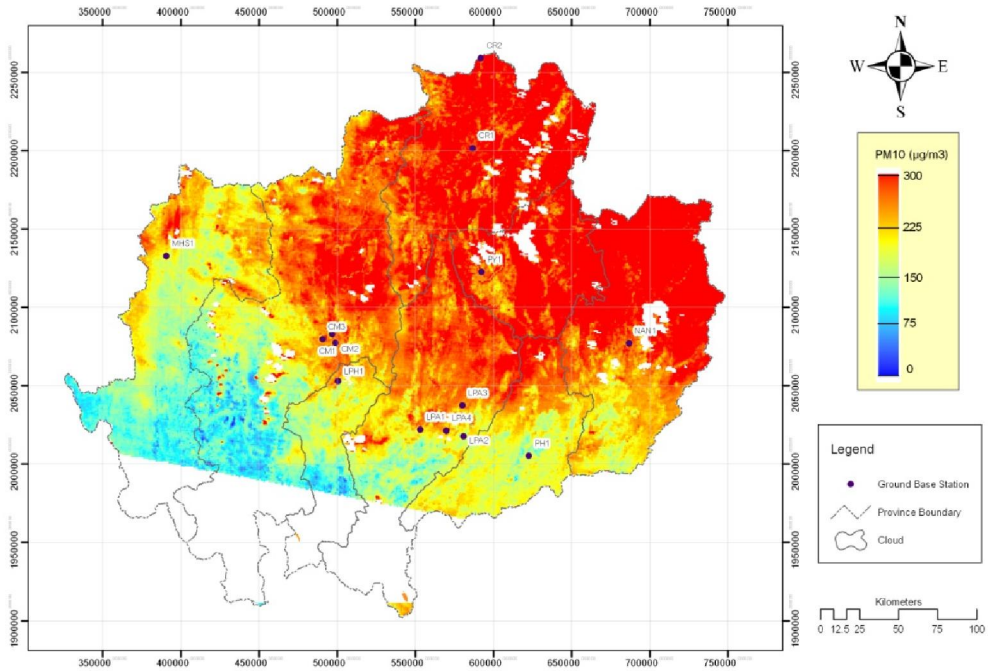

(b)

Figure 4.7d Maps of PM10 derived from (a) MODIS-AOD and (b) BAER-AOD data on 7th April 2010 (using relationships expressed in Table 4.1).

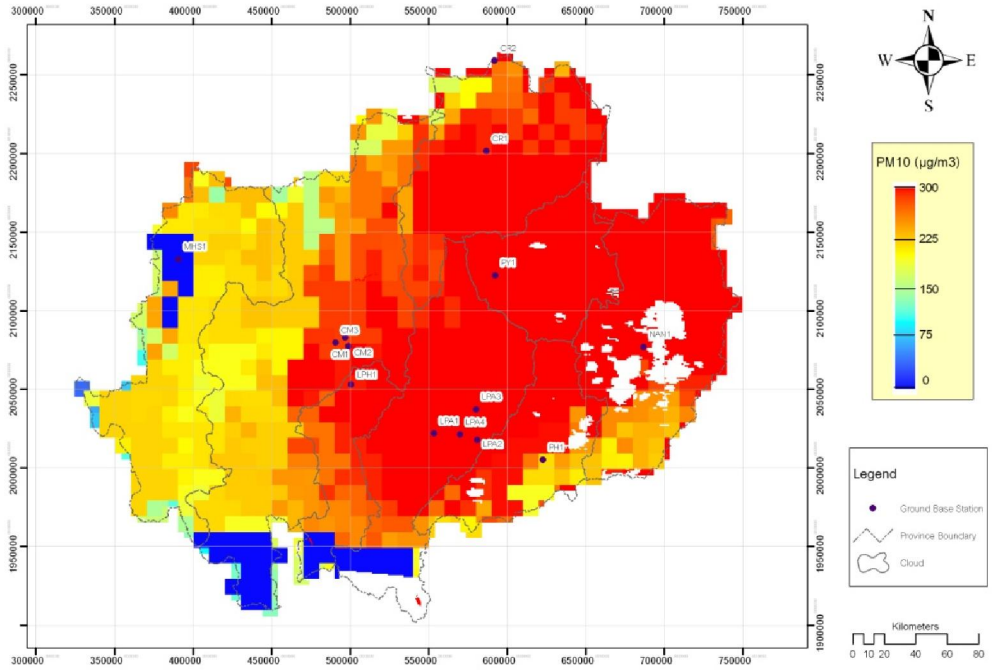

(a)

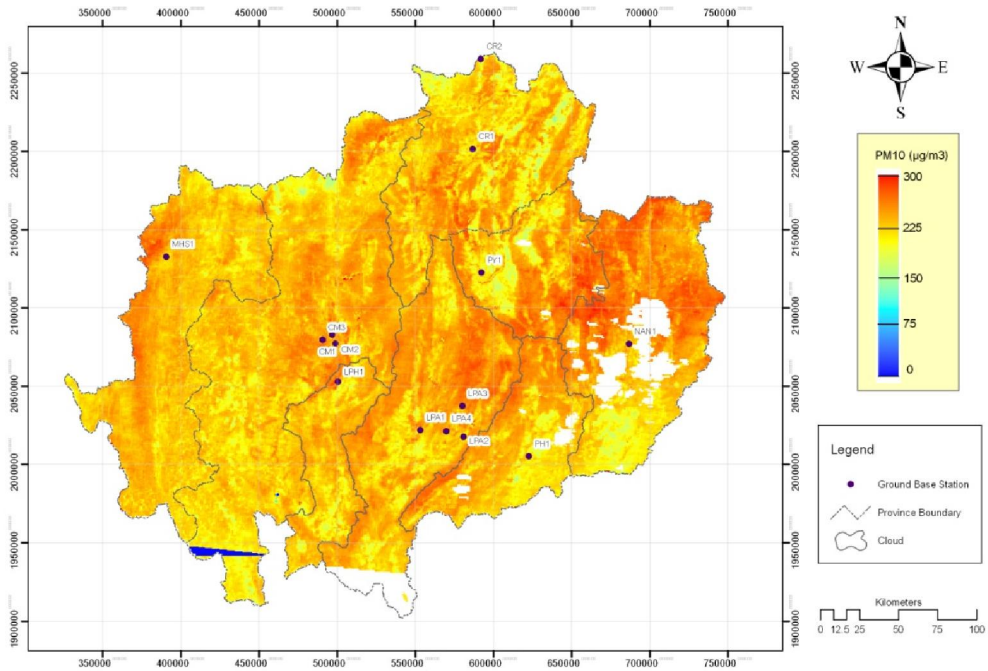

(b)

Figure 4.7e Maps of PM10 derived from (a) MODIS-AOD and (b) BAER-AOD data on 8th April 2010 (using relationships expressed in Table 4.1).

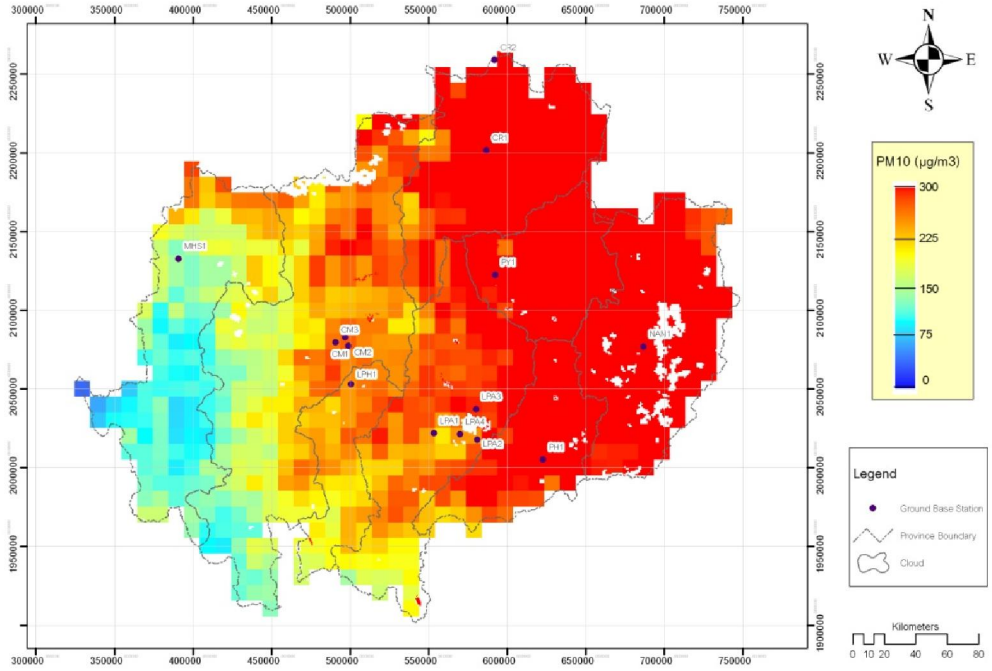

(a)

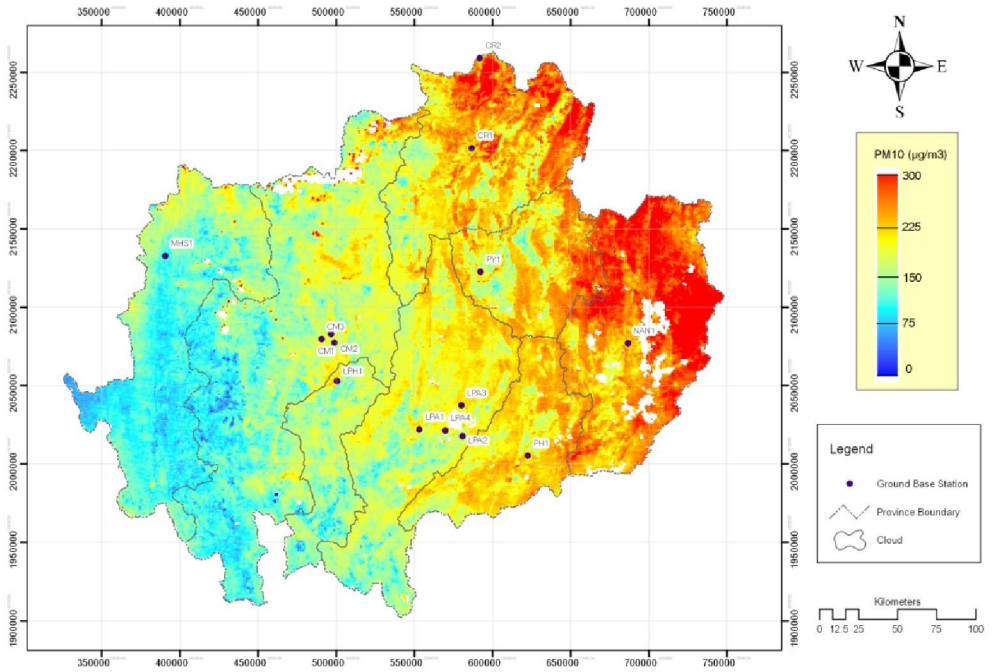

(b)

Figure 4.7f Maps of PM10 derived from (a) MODIS-AOD and (b) BAER-AOD data on 9th April 2010 (using relationships expressed in Table 4.1).

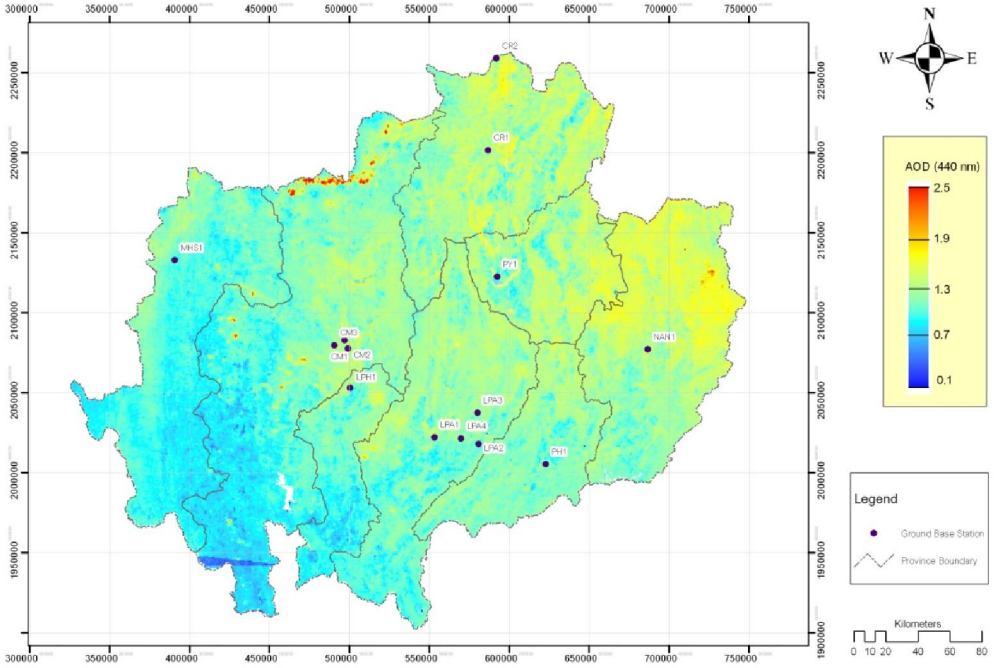

(a)

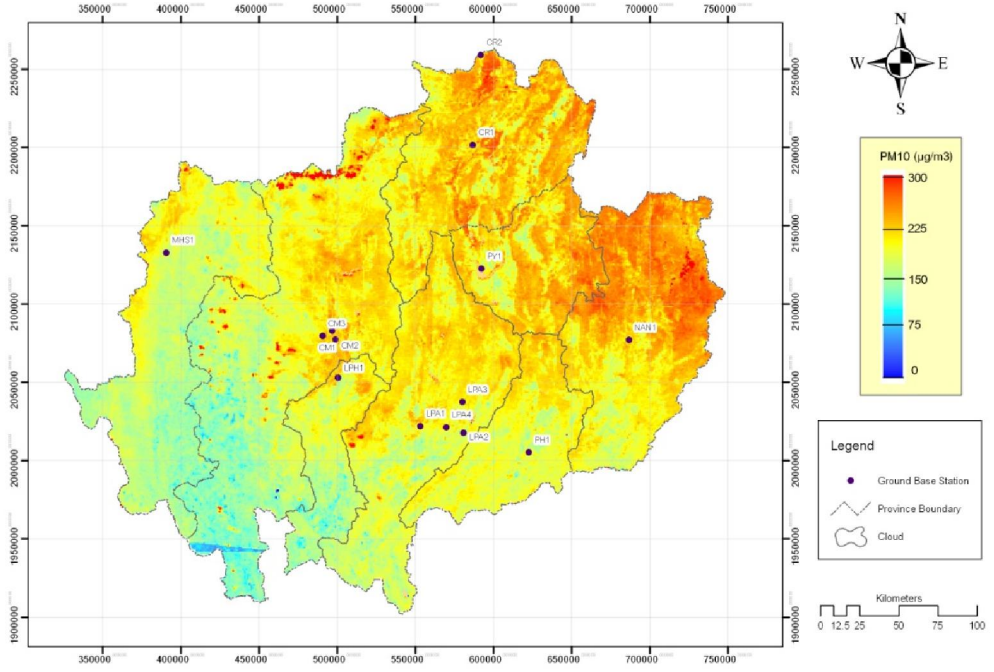

(b)

Figure 4.8 Maps of (a) the averaged AOD and (b) PM10 on period of 4th-9th April 2010 (based on AOD and PM10 maps expressed in Figures 4.6 and 4.7).

Table 4.3 Distribution of BAER-AOD and PM10 over the area on 4th-9th April.

BEAR-AOD	PM10 (μg/m3)	4th April		5th April		6th April		7th April	
		Area (km2)	%	Area (km2)	%	Area (km2)	%	Area (km2)	%
0.0-0.4	0-90	60	0.07	3,800	4.34	-	-	3,144	3.59
0.4-0.7	90-163	20,013	22.87	37,213	42.48	40,302	45.99	17,305	19.74
0.7-1.0	163-236	58,091	66.37	40,501	46.23	47,200	53.86	22,928	26.16
1.0-1.3	236-300	9,274	10.60	5,896	6.73	90	0.10	27,048	30.86
1.3-1.7	300-385	84	0.10	189	0.22	-	-	16,260	18.55
1.7-2.0	385-455	-	-	-	-	-	-	962	1.1
> 2.0	> 455	-	-	-	-	-	-	-	-
Averaged PM10/AOD		191/0.83		164/0.72		165/0.72		242/1.06	

BEAR-AOD	PM10 (μg/m3)	8th April		9th April		4th-9th April	
		Area (km2)	%	Area (km2)	%	Area (km2)	%
0.0-0.4	0-90	177	0.20	2,910	3.33	10,091	1.92
0.4-0.7	90-163	182	0.21	31,692	36.23	146,707	27.91
0.7-1.0	163-236	52,232	59.49	34,880	39.87	255,832	48.67
1.0-1.3	236-300	35,211	40.10	15,716	17.96	93,235	17.74
1.3-1.7	300-385	-	-	2,224	2.54	18,757	3.57
1.7-2.0	385-455	-	-	62	0.07	1,024	0.19
> 2.0	> 455	-	-	-	-	-	-
Averaged PM10/AOD		230/1.01		183/0.8		195/0.85	

Note: Averaged $AOD = \frac{\sum_{i=1}^{N} AOD_i}{N}$ and Averaged $PM10 = \frac{\sum_{i=1}^{N} PM10_i}{N}$, where N is the total number of pixels and i denotes pixel i of the area.

Histogram and distributing pattern of the PM10 data in average

To understand an overview of the PM10 pollution situation during period of the study more constructively, histogram of the PM10 data distribution during 0-400 $\mu g/m^3$ is presented in Table 4.4 and Figure 4.9. It was found that > 90% of the derived PM10 data are in the range of 100-300 $\mu g/m^3$ with peak values are at 175-200 $\mu g/m^3$ (17.24%), 150-175 $\mu g/m^3$ (16.19%) and 200-225 $\mu g/m^3$ (15.07%). And about 4.36% of the PM10 values exceed 300 $\mu g/m^3$ while about only 3.16% that have values less than 100. The safest location identified by the study is on the far southwestern portion of the area in the lower part of Chiang Mai, Lamphun and Mae Hong Son Provinces while the most critical one is located on the upper part of Nan Province and also in most parts of the Chiang Rai Province (Figure 4.8). These findings might be still not well perceived by the public as information of the aerosol intensity over most areas is still quite limited but this can be explicitly revealed by the satellite-based observation conducted for being example in this thesis.

Table 4.4 Proportion of PM10 data distribution at 0-400 $\mu g/m^3$.

Class	PM10 ($\mu g/m^3$)	Number of occurrences		Class	PM10 ($\mu g/m^3$)	Number of occurrences	
		Pixels	%			Pixels	%
1	0-25	242	0.01	9	200-225	317,384	15.07
2	25-50	624	0.03	10	225-250	282,217	13.40
3	50-75	7,161	0.34	11	250-275	135,682	6.44
4	75-100	56,729	2.69	12	275-300	60,747	2.88
5	100-125	125,280	5.95	13	300-325	41,611	1.98
6	125-150	229,065	10.88	14	325-350	28,524	1.35
7	150-175	340,897	16.19	15	350-375	16,247	0.77
8	175-200	363,035	17.24	16	375-400	5,577	0.26

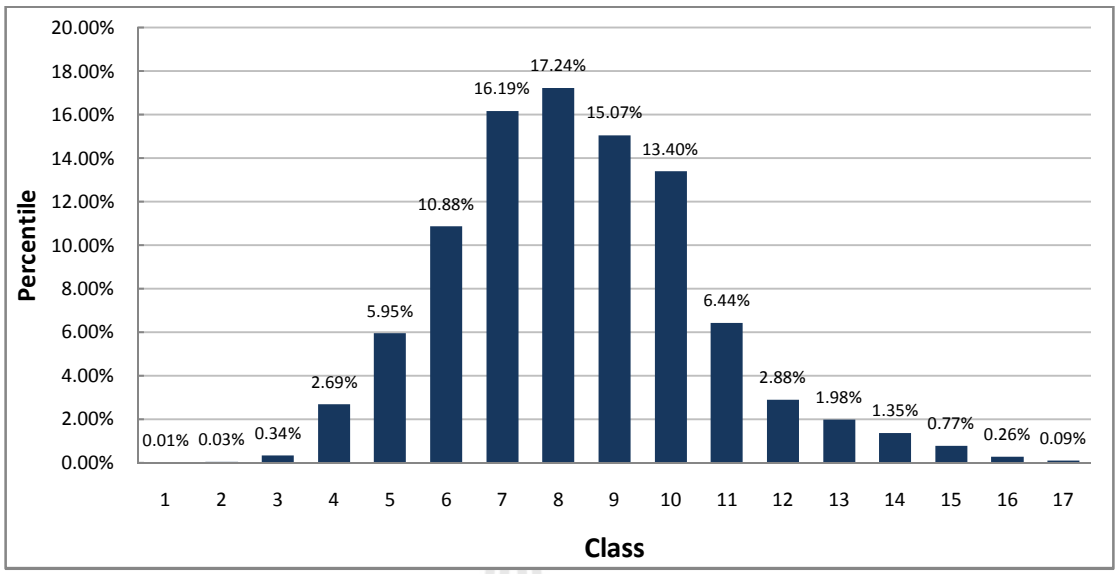

Figure 4.9 Histogram of the PM10 data occurred in the area during 4th-9th 2010.

Validation of the produced PM10 maps

Validation of the produced PM10 maps (from BAER-AOD data) shown in Figures 4.7a-f was also evaluated based on the found relation level (R^2) of derived PM10 data and reference PM10 data and the mean absolute error (MAE) of the two datasets in use as described in Eq. 4.5. Total number of the data pairs used here for the evaluating process is 126. It was found that both groups of the PM10 data are highly correlated to each other with R^2 of 0.744 and very low mean absolute error (MAE) of about 6.62% (Figures 4.10a-b). These results indicate high credential of the prepared PM10 maps (from the derived BAER AOD) which make them very useful for further applications in the monitoring and assessment of PM10-induced air pollution severity over some particular area of interest in the future or for other application implemented by researchers in this field. More information of the MAE calculation for the BAER AOD-based PM10 data is reported in Appendix C.

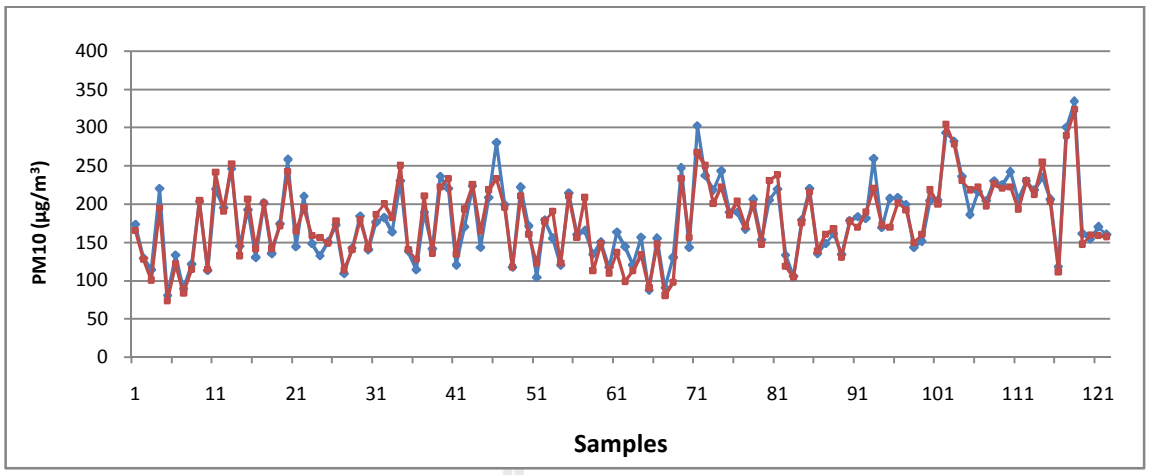

Figure 4.10a Comparison of the derived PM10 data (PM_{BAER}) and the reference PM10 data (PM_{REF}) (with MAE = 6.62%).

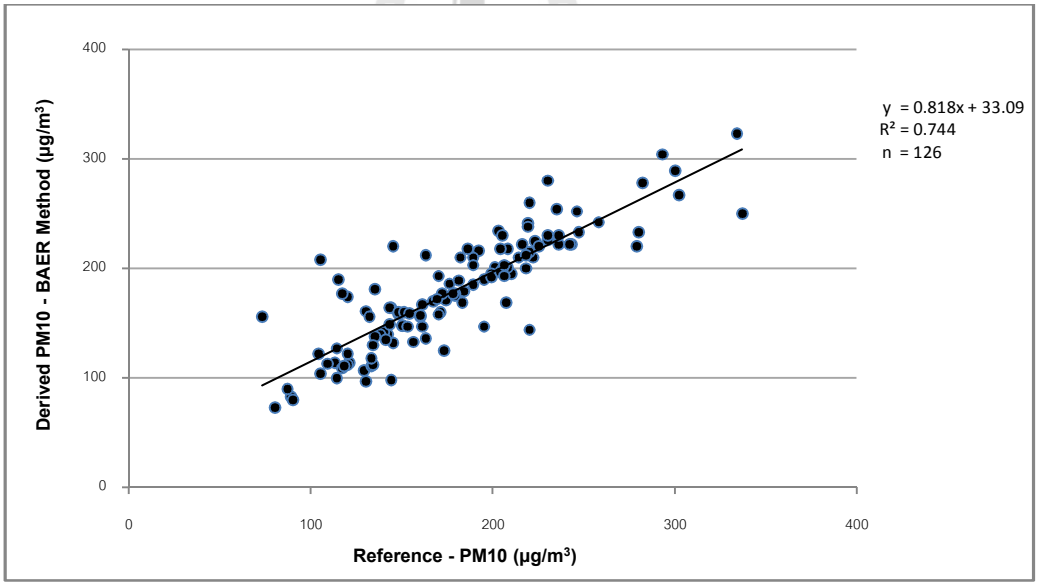

Figure 4.10b Correlation of the derived PM10 data (PM_{BAER}) and reference PM10 data (PM_{REF}) (with $R^2 = 0.744$).

Table 4.5a Averaged PM10 concentration (μg/m^3) over different LULC types (from Figure 4.8).

LULC	PM10 (μg/m^3)	Area	
		km^2	%
Forest	194.5	60,303	69.1
Agriculture	196.7	22,116	25.3
Urban	201.5	2,628	3.0
Others	190.2	2,223	2.5

Table 4.5b Averaged PM10 concentration (μg/m^3) over different altitudes (from Figure 4.8).

Altitude (m-MSL)	PM10 (μg/m^3)	Area	
		km^2	%
0 - 300	187.0	10,750	12.3
300 - 550	201.8	32,934	37.6
550 - 800	199.4	19,918	22.7
800 - 1,000	192.1	13,543	15.4
> 1,000	184.4	10,516	12.0

Relations of the PM10 distribution pattern to LULC and altitude

From the PM10 map seen in Figure 4.8, the averaged PM10 concentration over different LULC types and altitudes are as described in Table 4.5 and 4.6. Regarding to the LULC, these results indicate that the aerosol pollution was most

severe over urban area (with average PM10 data of 201.5 μg/m^3) followed by agricultural and forest lands, respectively (with average PM10 density of 196.1 and 194.5 μg/m^3). In terms of altitude, the most severe situation was found at altitude 300-550 meters (PM10 = 201.8 μg/m^3). Most areas also situate at this altitude range also (37.6%). The second worst aerosol pollution level was found as altitude of 550-800 meters (PM10 = 199.4 μg/m^3). In general, areas at higher altitudes experienced less PM pollution, the higher having the lesser, as being evidenced in case of the altitude range > 1,000 meters which has lowest level of PM10 data in average at 184.4 μg/m^3. However, this level of the PM10 density is still considered rather dangerous to human health according to the global standards proposed by renowned agencies like US-EPA or WHO (as detailed for examples in Tables 2.1-2.4)

4.2.3 Derivation and application of the AQI maps

In this thesis, four different approaches for the AQI quantification and ranking (Table 3.3) were introduced to develop AQI maps for five chosen dates (during 4th-9th April 2010) over the entire study area from the PM10 maps generated from BAER-AOD maps inherited from the previous part, BAER-method algorithm for MODIS 500 m. data is coupled with the minimum reflectance technique which is used to derive the surface reflectance images and LUT constructed from the various AERONET-AOD, sun-satellite geometries and BAER-AOD result also showed better accuracy than ΔR and NDAI method over the study area. These methods include:

(1) PCD standard (for Thailand). This was modified from the original criteria recommended by the US-EPA and in use since 1999.

(2) US-EPA standard. This was revised and in use since 2006,

(3) UK standard. This is currently in use by the UK-DEFRA for its daily AQI report, and

(4) Newly-proposed method. This was designed to support the guide lines on the PM10 targets issued by the WHO and to serve as a compromise between the EPA-standard and the UK standard as described in Table 3.3.

Details of the relevant AQI definition and ranking criteria are as described in Section 2.2 and total results of the study are reported in Figures 4.11-4.16 and Tables 4.6a-f, respectively. The color code implemented for each particular method (except the newly-proposed one) is followed the standard practice conducted by the respective agencies under consideration. In general, it was discovered that there are only two AQI conditions that dominate the PCD-based AQI maps: "Moderate" (for PM10 = 41-120 $\mu g/m^3$) and "Unhealthy" (for PM10 = 121-350 $\mu g/m^3$). And between these two states, the "Unhealthy" category is hugely predominant on every studied date with occupied area of about 76.9, 93.8, 100.0, 83.34, 100 and 83.45% of the entire area dated from 4^{th} to 9^{th} April 2010, respectively. This occurrence shall result in the monotonic shade of PM10 data illustrated on the PCD-based AQI map on most dates (in yellow tone). This found character is a direct result of the normal PM10 range determined from the derived BAER-AOD which appears at about 100-300 $\mu g/m^3$ except on the 7^{th} April that the upper bound of PM10 is located somewhat higher (as seen in Table 4.3).

This result means that the standard AQI classification adopted by the PCD at present is still not practically useful in differentiating great variation of PM10 density and its associated air quality over the entire study area during the period of interest. And, as a consequence, its potential use for health warning purpose or for air quality

monitoring over large area is also limited. Broad advice from the PCD for those live witin the “Unhealthy” zone is that people with respiratory diseases should avoid all physical outdoors and everyone else, especially children or older adults, should avoid the prolonged or heavy exertion (PCD, 2013).

Similar situation was evidenced for the classified AQI maps created based on the US-EPA standard from which only three AQI categories were mostly achieved: “Moderate” for PM10 = 55-154 $\mu g/m^3$, “Unhealthy (for sensitive group)” for PM10 = 155-254 $\mu g/m^3$ and “Unhealthy” for PM10 = 255-354 $\mu g/m^3$. The most dominant outlook of the situation is the second category, Unhealthy (for sensitive group), which occupies about 41.4, 54.9, 85.6, 51.8, and 52.1% of the total area dated from 4th to 9th April 2010, respectively. The “Moderate” category is most visible on 4th April (58.6%) and 9th April (34.5%) while the “Unhealthy” class is most prominent on 5th April (25.36%) and 7th April (20.4%). Associated health warning can be issued for a particular area followed the instruction addressed in Table 4.6, especially for people living in the “Unhealthy” or “Very Unhealthy” zones.

มหาวิทยาลัยเทคโนโลยีสุรนารี

Table 4.6 Instructions for reducing risk from aerosol pollution (US-EPA, 2009).

PM10 ($\mu g/m^3$)	AQI	Condition	Instructions for reducing health risk
0-54	0-50	Good	None
55-154	51-100	Moderate	Unusually, sensitive people should consider reducing prolonged or heavy exertion.
155-254	101-150	Unhealthy (for sensitive group)	People with heart/lung disease or children/older adults should reduce prolonged or heavy outdoor exertion. Everyone else should limit prolonged or heavy exertion.
255-354	151-200	Unhealthy	People with heart/lung disease or children/older adults should avoid all physical outdoors. Everyone else should avoid prolonged or heavy exertion.
355-424	201-300	Very Unhealthy	People with heart/lung disease or children/older adults should remain indoors and keep activity levels low. Everyone else should avoid all physical activity outdoors.
425-604	301-500	Hazardous	

In addition, it should be noted that, the AQI maps derived based on US-EPA standard and those produced under PCD standard look rather resemble to each other as both methods adopt similar rules for AQI determination and ranking. However, the color-code system used by the PCD is different from that of the US-EPA which might lead to some confusion for their interpretation (as displayed in Figure 4.11-4.16).

On the contrary to the PCD and US-EPA standards investigated earlier, the UK-DEFRA standard focuses mainly on fine classification of the PM10 data between 0-100 $\mu g/m^3$ (separated into 3 major categories and 9 sub-categories) while variation of the PM10 data of > 100 $\mu g/m^3$ is still ignored (only one category, “very high”, is

reported). This means the UK standard is suitable for reporting information of the low to moderate air pollution conditions mostly resulted from the overcrowded traffic or regular household activities (with PM10 concentration < 100 $\mu g/m^3$). However, it was proved inefficient for the creation of descriptive AQI maps during fire season for the upper northern Thailand as desired. This is during this season, typical range of PM10 data is between 100-300 $\mu g/m^3$ that is much higher than a proxy limit of 100 $\mu g/m^3$ endorsed in the UK standard. For the "very high" category, the advice for those living in the area is that (from Table 2.2b);

(1) Adults/children with lung or hearth problems, as well as older people, should avoid strenuous physical activity. People with asthma may find they need to use their reliever inhaler more often.

(2) People should reduce physical exertion, particularly outdoor activities, especially if they experience symptoms such as cough or sore throat.

In this circumstance, the PCD and US-EPA standards discussed earlier are considered more appropriate as they can accommodate PM10 concentration data of up to 600 $\mu g/m^3$ for AQI scales of 0 to 500 (Table 3.3). However, at the scale of 100 to 300 $\mu g/m^3$, both methods still has limited capability to differentiate them.

To gain more subtle knowledge on variation of the PM10-led pollution at this scale range in terms of the available AQI bands, a new AQI classification method was introduced as detailed in Table 3.3 with 12 AQI bands available, among these, five bands were prepared for the PM10 data of 100-300 $\mu g/m^3$ (Band 5-9). In general, it was found that this proposed system can inform gradual variation of the PM10 pollution found in the area well when compared to the PCD and US-EPA standards

with more details in AQI map outlook, and it did much better than the UK standard for the monitoring of PM10 pollution situation with PM10 data > 100 $\mu g/m^3$.

Under the proposed scheme, the most prominent AQI bands for the whole period are Band 7 and 8, respectively; both are in the "High" category (for PM10 of 151-250 $\mu g/m^3$) of this established system. As described earlier in Chapter III (Section 3.3.2), these two dominant AQI bands (Band 7-8) were defined to indicate high level of PM10 density in the atmosphere that might be harmful for sensitive group (like children or people with respiratory or lung diseases), similar to the "Unhealthy (for sensitive group)" category adopted in the US-EPA standard. As such, the associated warning on health concerns for those living in the "High" aerosol pollution zone defined in this system might be adapted from the guidelines recommended by the US-PGA for its "Unhealthy (for sensitive group)" category directly (Table 4.6).

The "Very High" category of Bands 9-11 (for PM10 of 251-400 $\mu g/m^3$) is also clearly evident on later dates when aerosol pollution level is relatively high over most areas (especially on 7^{th}-9^{th} April). This AQI category occupies about 49.9, 17.7 and 15.0% of total area dated from 7^{th} to 9^{th} April 2010, respectively. It signifies serious danger of the PM10 pollution that might affect health of most people, not only for sensitive groups and general public should be alerted of potential health impact under this situation. This is comparative to the "Unhealthy" category (for Band 9-10) and "Very Unhealthy" category (for band 11) adopted in the formal US-EPA standard (as detailed in Table 3.3).

According to Shooter and Brimblecombe (2009) and EU (2012), there are three fundamental roles of the established AQI systems:

(1) To link air quality condition to potential health effects (called health-based index) for contributing proper warnings or advices to the public;

(2) To condense complex data to provide an information overview e.g. for the development of policy or to check compliance with standards;

(3) To draw public's attention to air quality issues and raising awareness.

These three purposes can effectively be fulfilled by the proposed method as it can inform the public of aerosol pollution severity and its distributing pattern on daily basis at fine scale of 500 m. The obtained aerosol density maps that are classified into 12 levels (or AQI bands) of PM10 concentration under the procedure described in this thesis (as seen in Figures 4.11a-f) can be related directly to the pre-evaluated potential health effects that might be experienced by local people living within the study area. This information provides visualized map of the aerosol pollution covering the entire area which is very helpful to draw public's attention to actual situation of the aerosol pollution problem and to raise awareness on its possible impact as well.

In addition, knowledge of the aerosol distributing pattern in long-time term is also useful for the proper initiation or implementation of the aerosol pollution control policies to reduce prospect severity of the incidence or minimize its impacts on public health as much as possible.

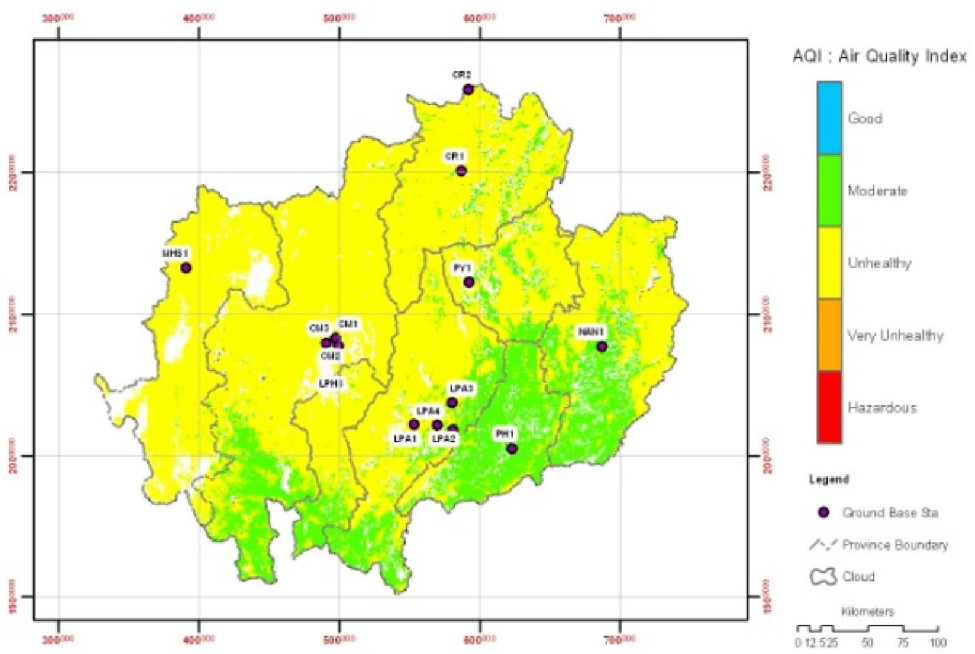

(a)

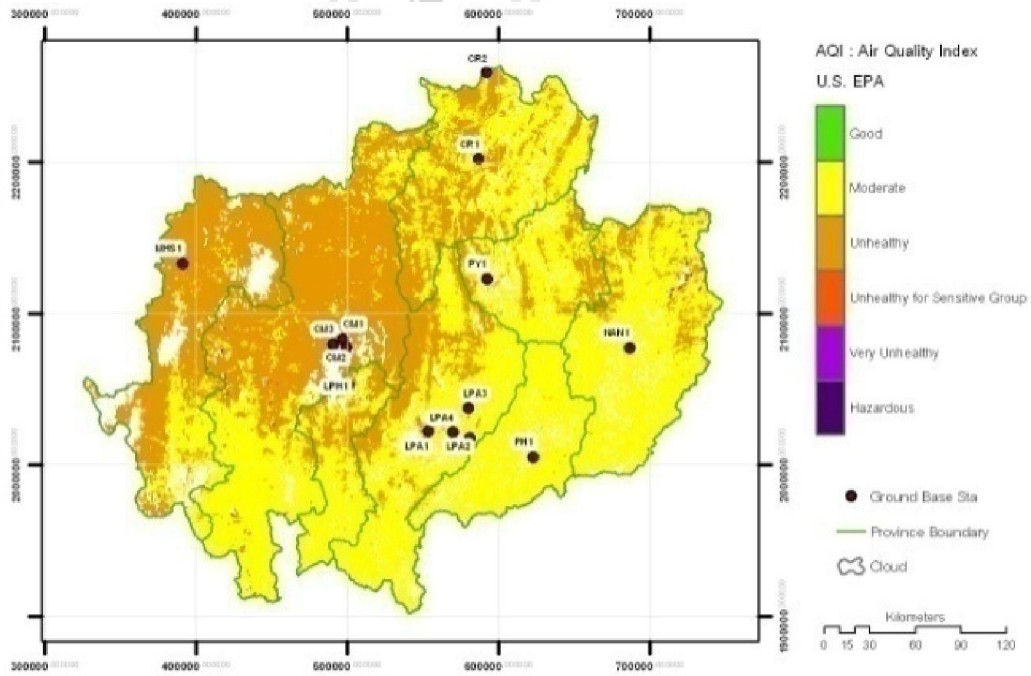

(b)

Figure 4.11 Derived AQI maps on 4th April 2010 based on (a) standards of the PCD, (b) US-EPA, (c) UK-DEFRA and (d) by the newly-proposed method.

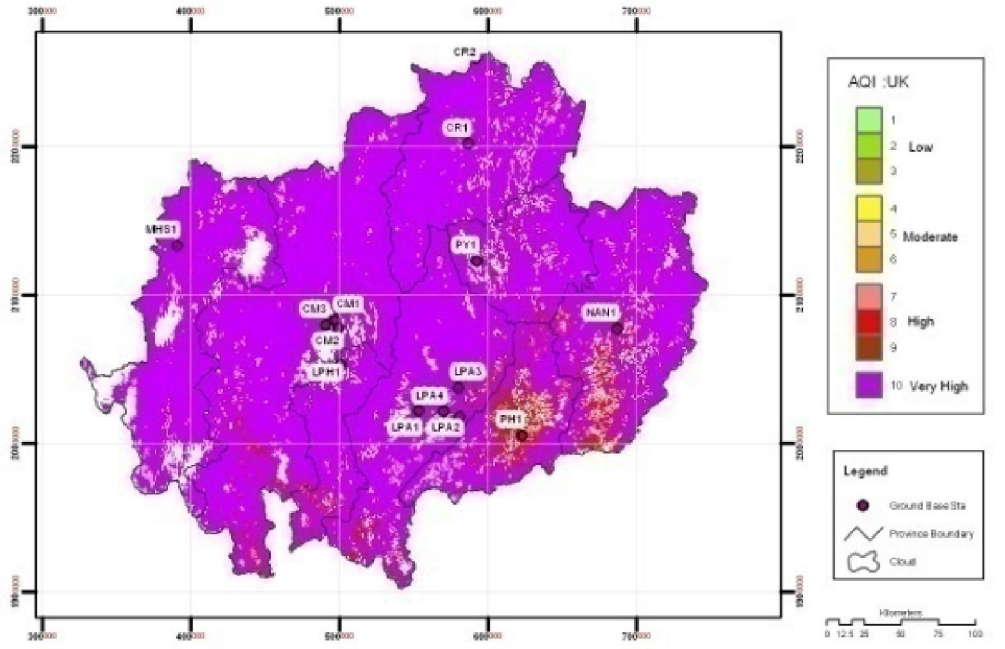

(c)

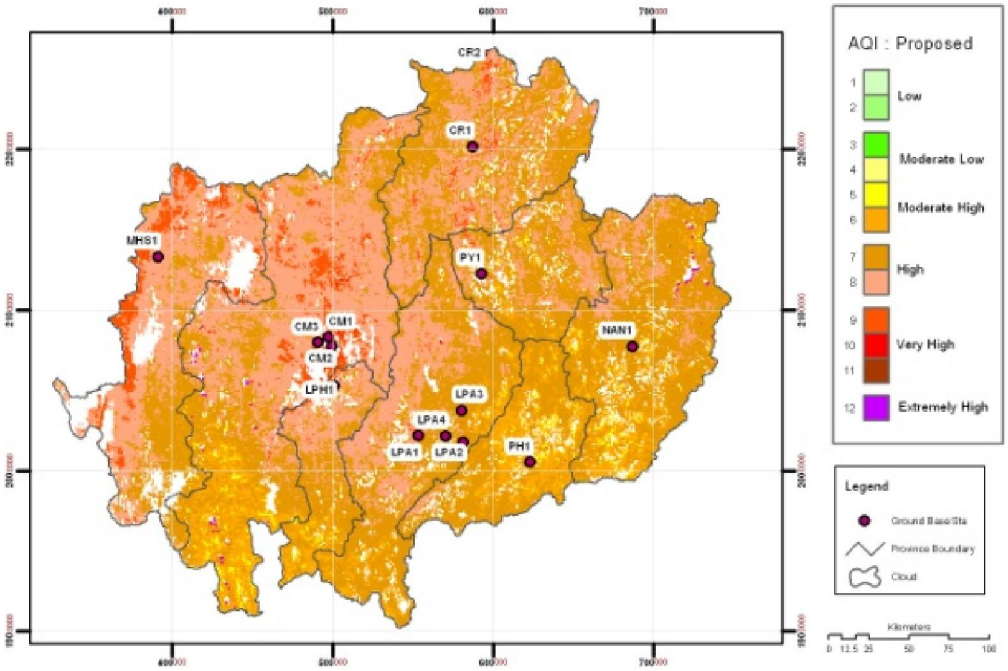

(d)

Figure 4.11 (Continued- For 4th April 2010).

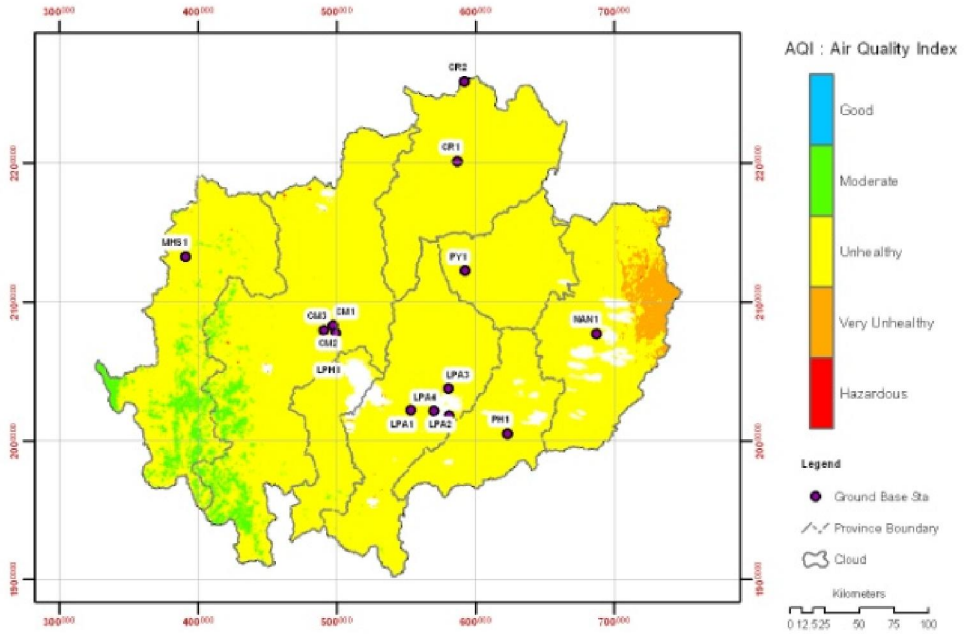

(a)

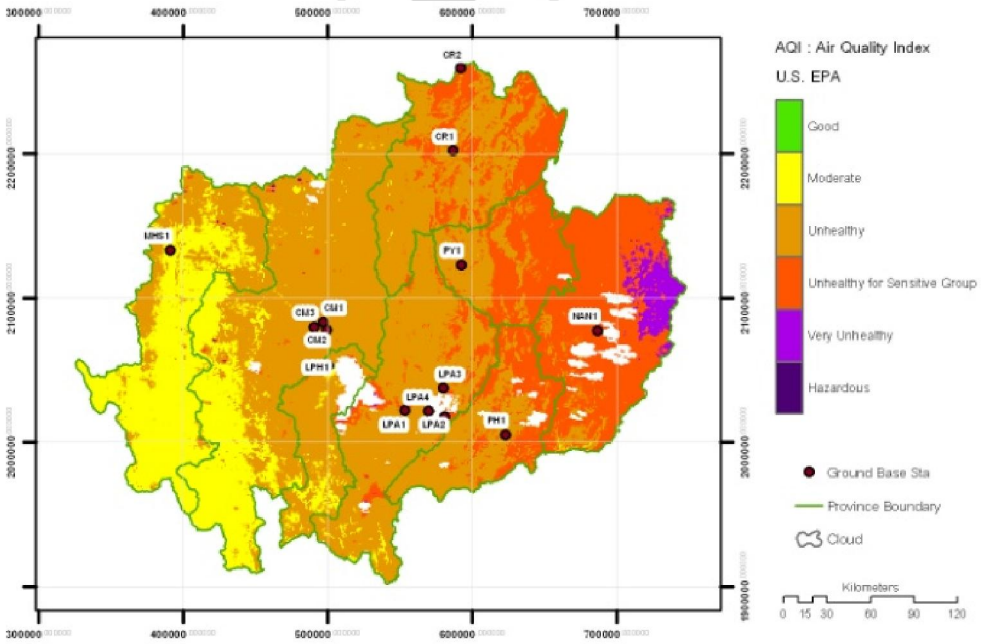

(b)

Figure 4.12 Derived AQI maps on 5th April 2010 based on (a) standards of the PCD, (b) US-EPA, (c) UK-DEFRA and (d) by the newly-proposed method.

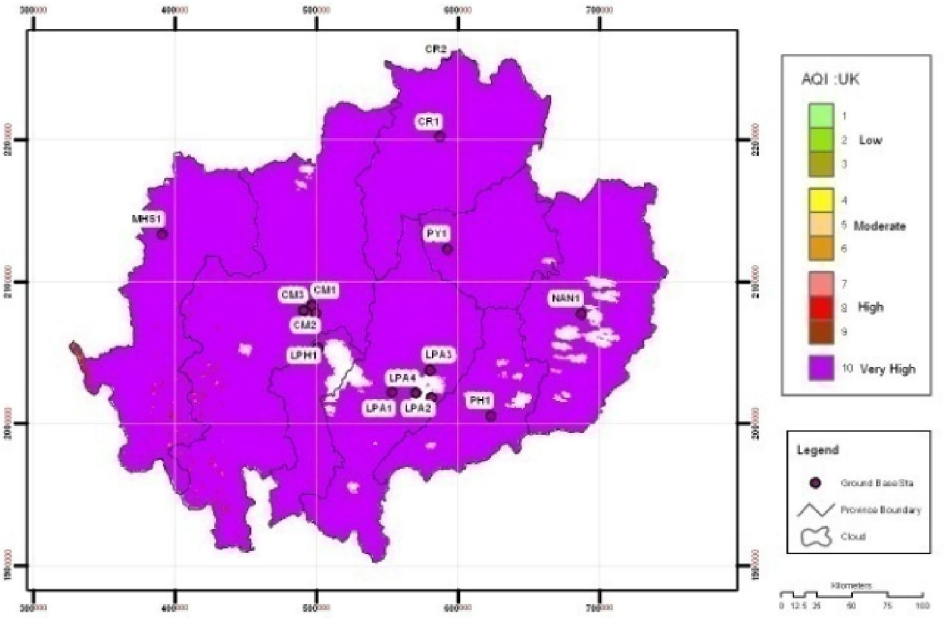

(c)

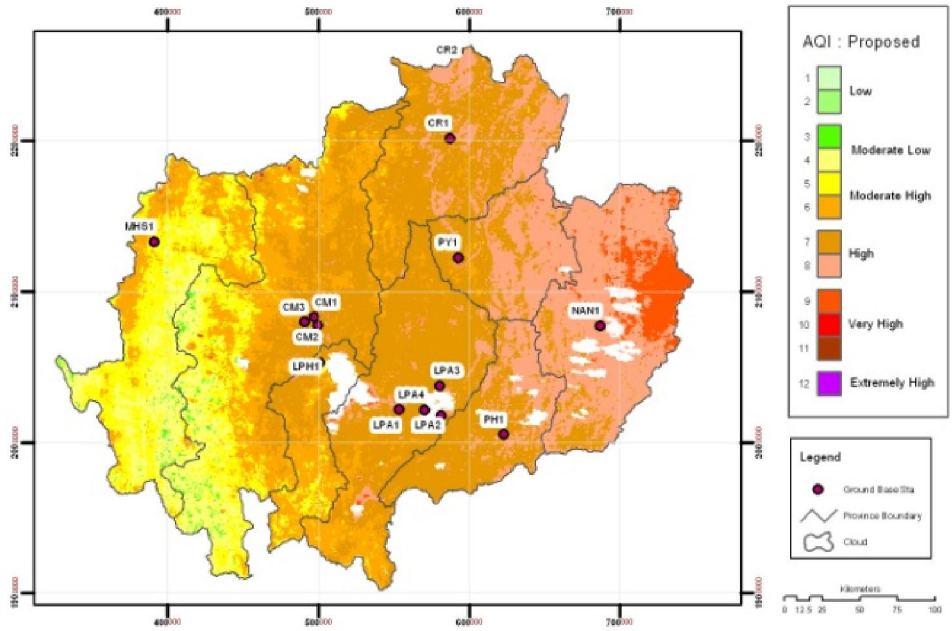

(d)

Figure 4.12 (Continued- For 5th April 2010).

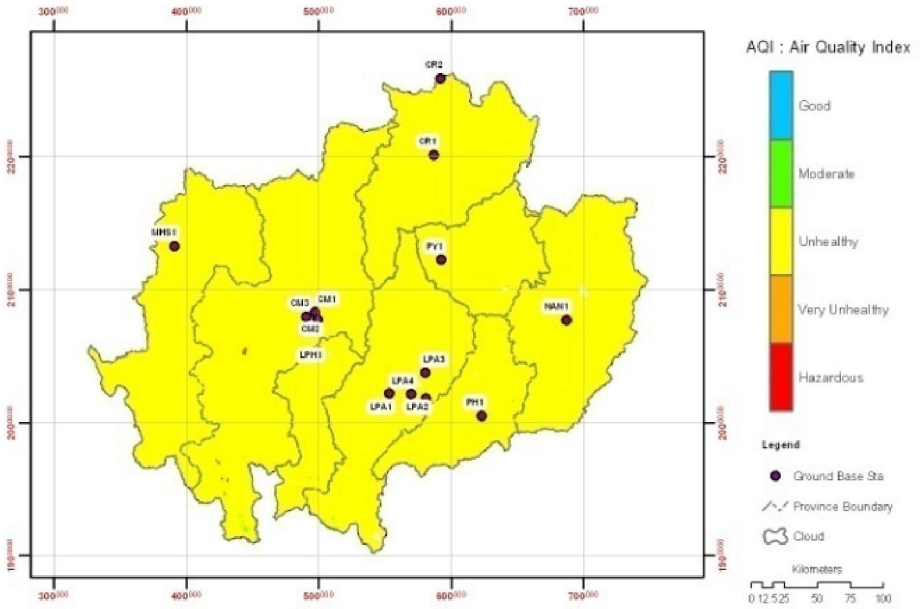

(a)

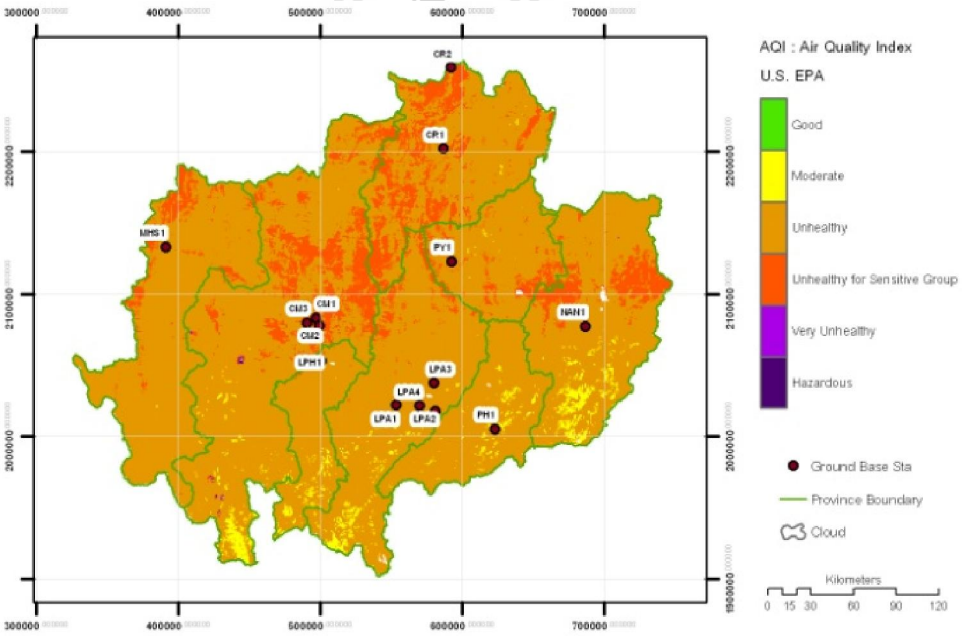

(b)

Figure 4.13 Derived AQI maps on 6th April 2010 based on (a) standards of the PCD, (b) US-EPA, (c) UK-DEFRA and (d) by the newly-proposed method.

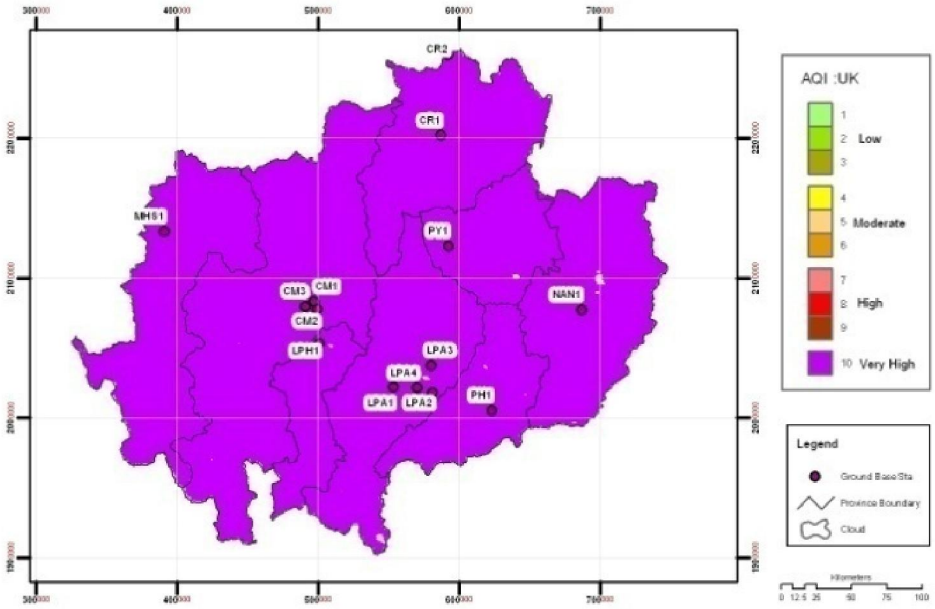

(c)

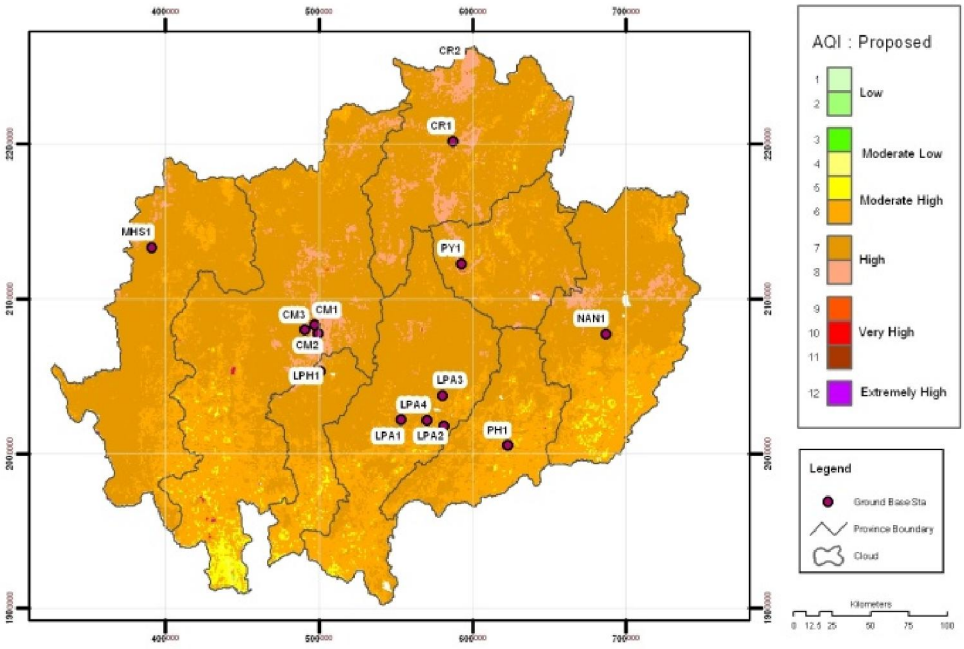

(d)

Figure 4.13 (Continued- For 6th April 2010).

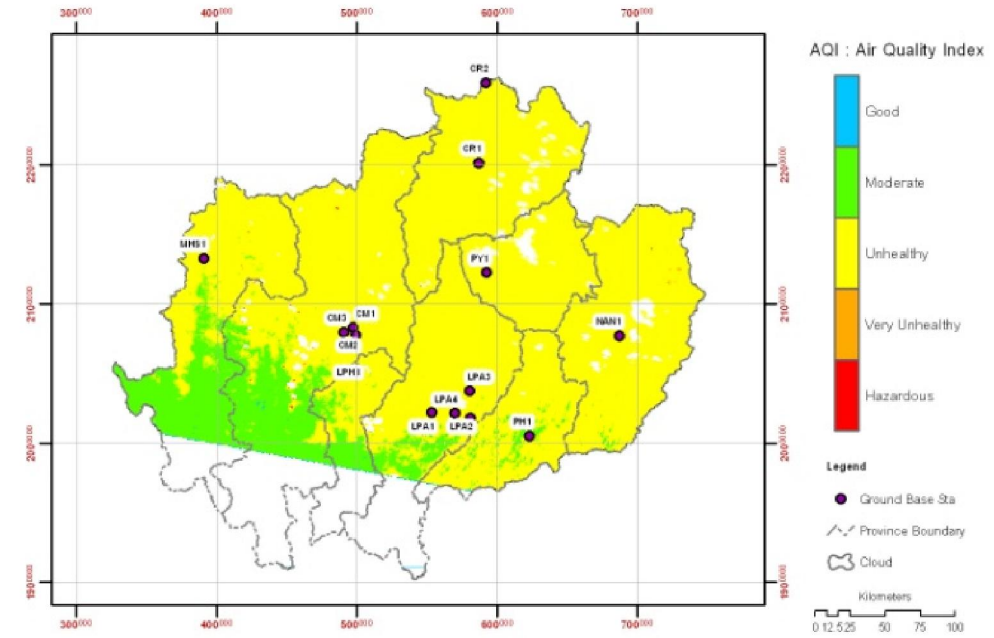

(a)

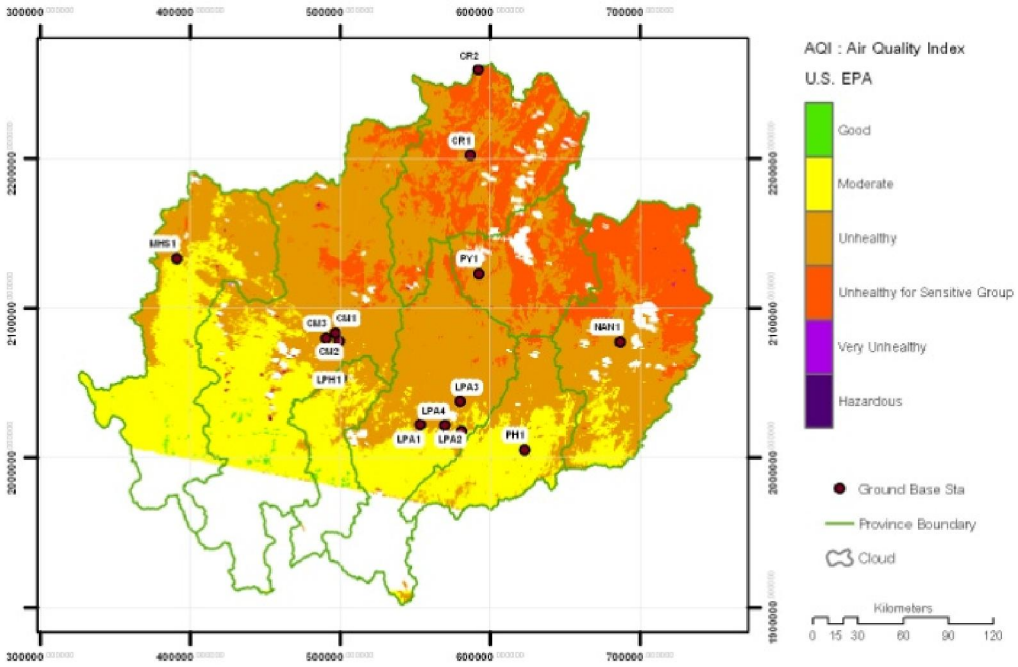

(b)

Figure 4.14 Derived AQI maps on 7th April 2010 based on (a) standards of the PCD, (b) US-EPA, (c) UK-DEFRA and (d) by the newly-proposed method.

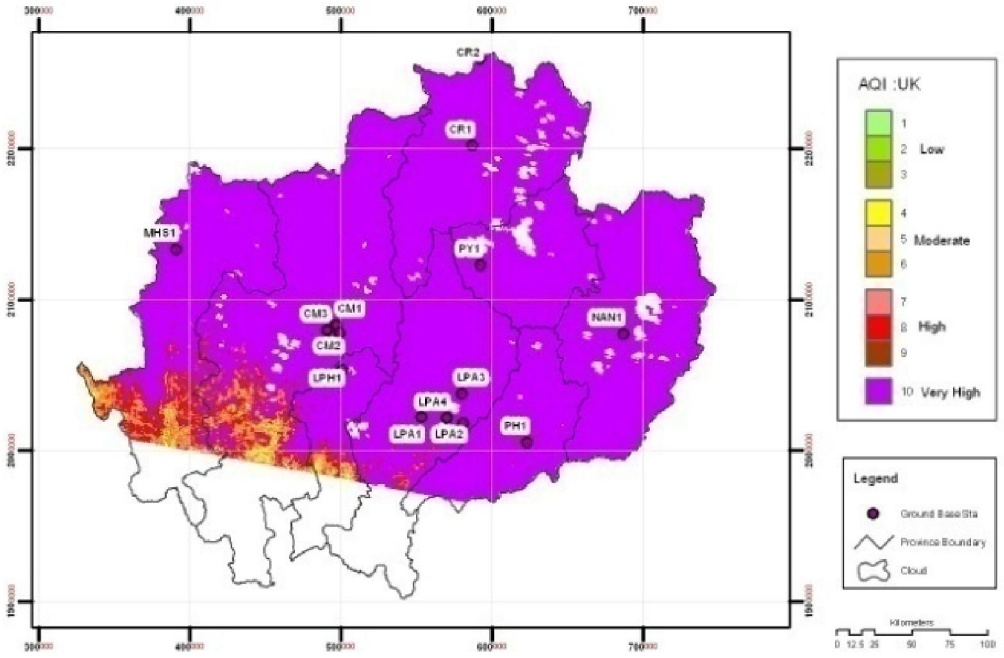

(c)

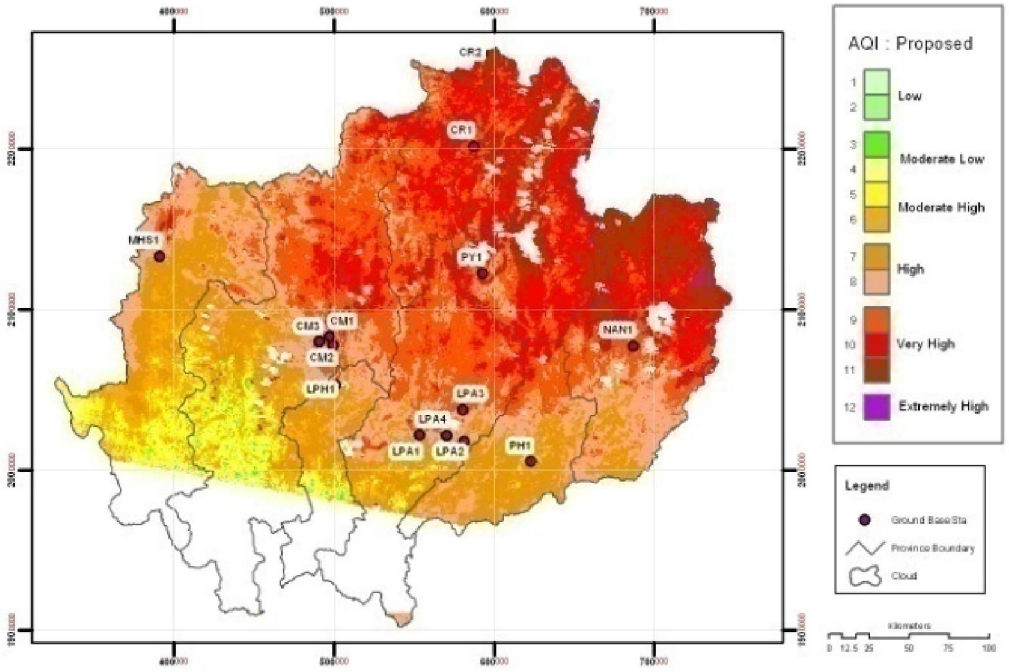

(d)

Figure 4.14 (Continued- For 7th April 2010).

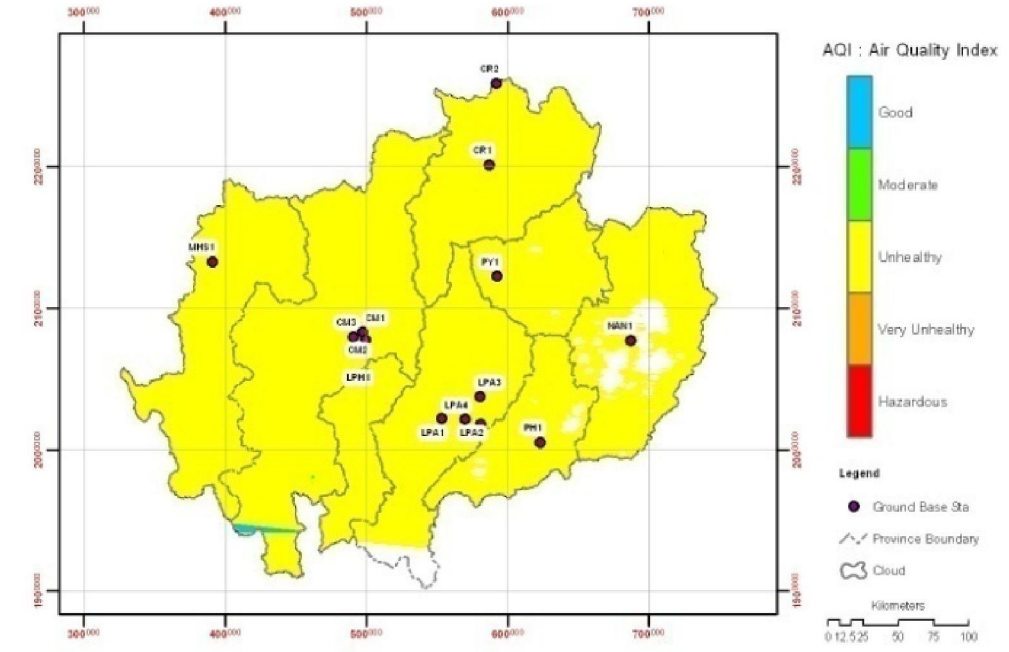

(a)

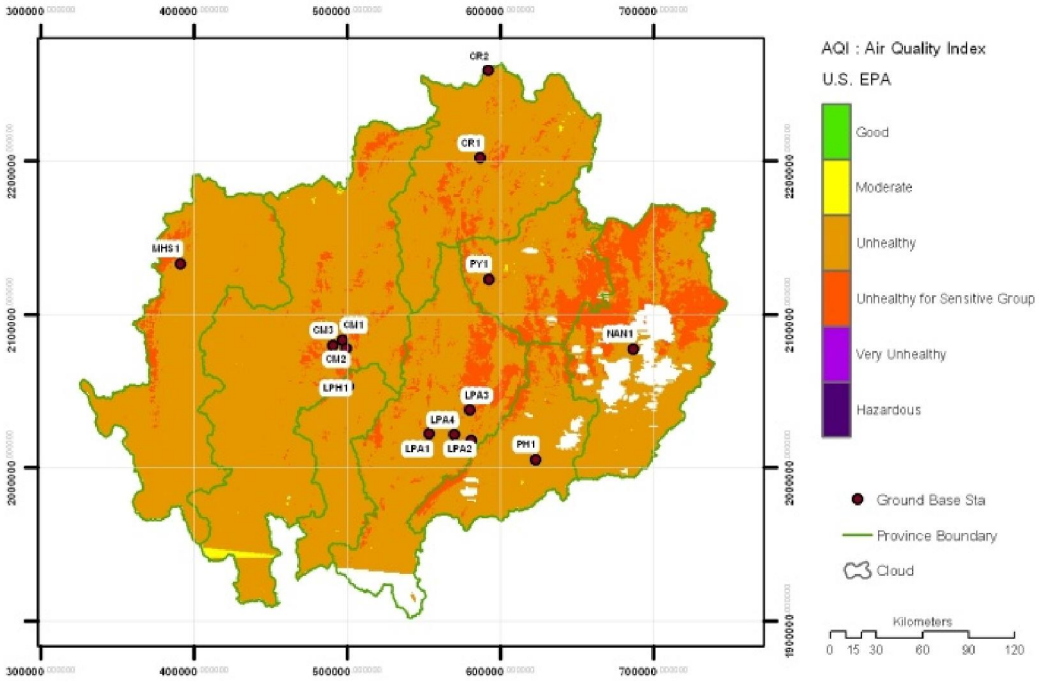

(b)

Figure 4.15 Derived AQI maps on 8th April 2010 based on (a) standards of the PCD, (b) US-EPA, (c) UK-DEFRA and (d) by the newly-proposed method.

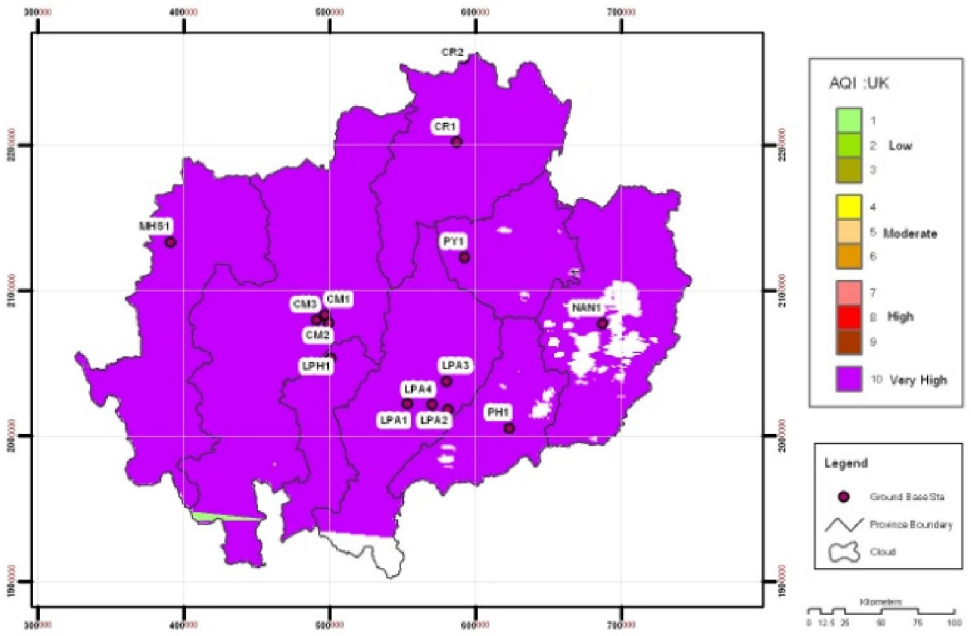

(c)

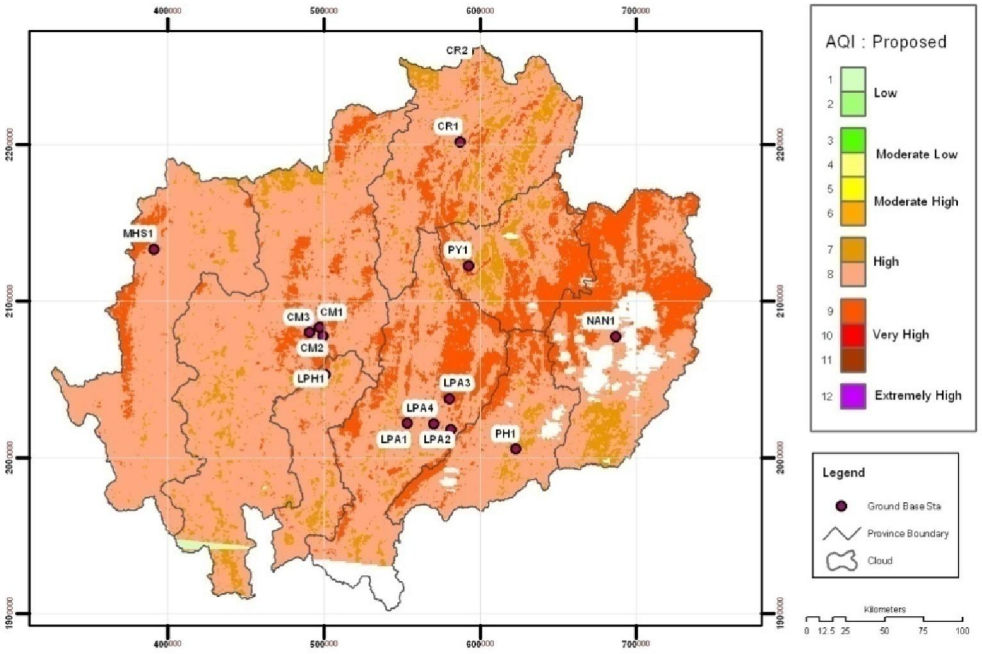

(d)

Figure 4.15 (Continued- For 8th April 2010).

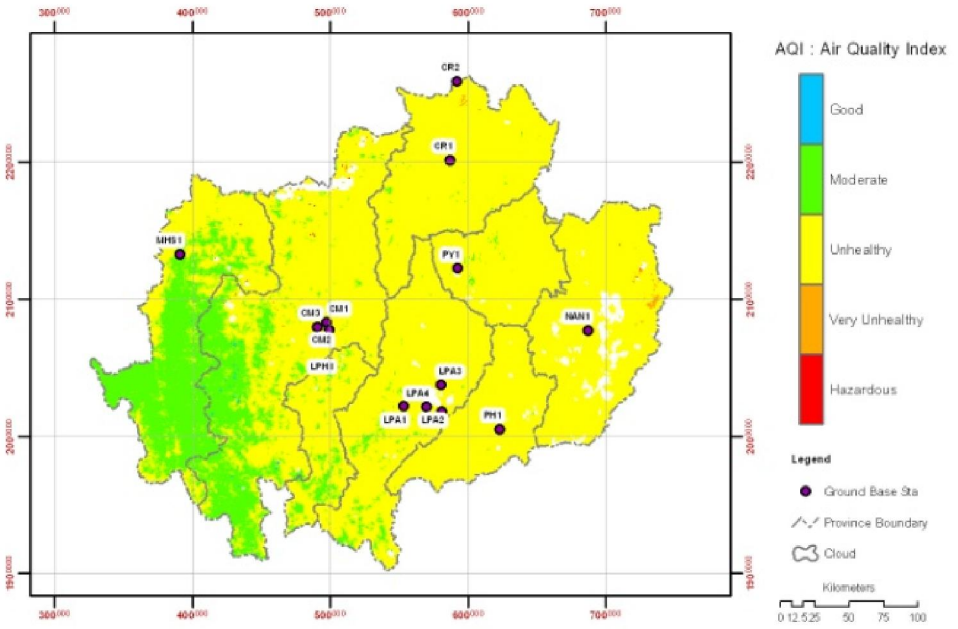

(a)

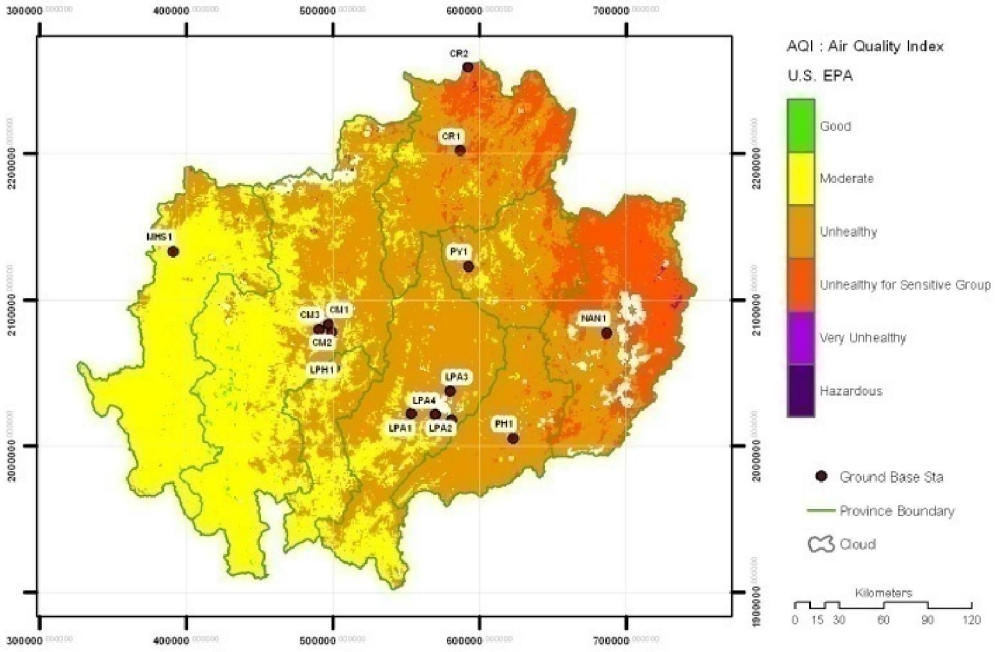

(b)

Figure 4.16 Derived AQI maps on 9th April 2010 based on (a) standards of the PCD, (b) US-EPA, (c) UK-DEFRA and (d) by the newly-proposed method.

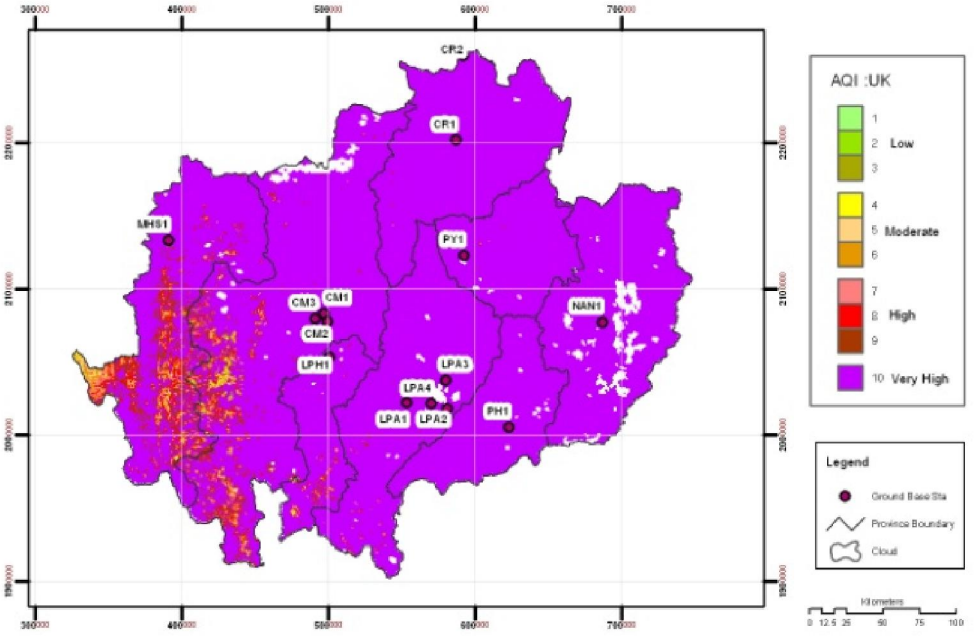

(c)

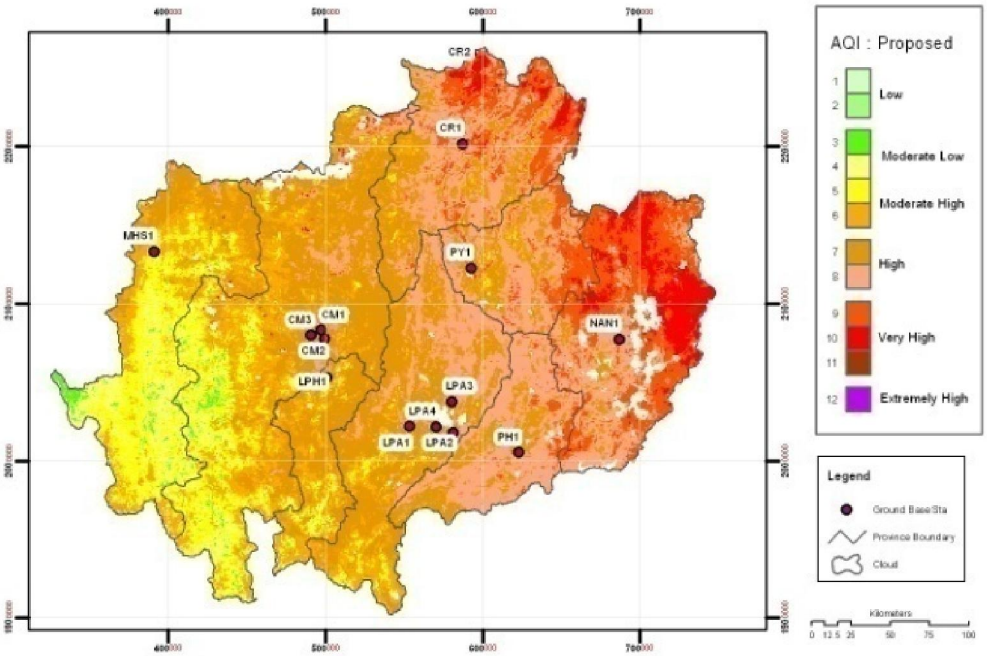

(d)

Figure 4.16 (Continued-For 9th April 2010).

Table 4.7a Distribution of the PM10 density over entire area on 4th April 2010 based on the derived AQI maps by the four chosen methods (in Figure 4.11).

Thailand-PCD				**US-EPA**			
PM10 ($\mu g/m^3$)	AQI	Area		PM10 ($\mu g/m^3$)	AQI	Area	
		km^2	%			km^2	%
0-40	0-50	-	-	0-54	0-50	-	-
41-120	51-100	20,279	23.1	55-154	51-100	51,329	58.6
121-350	101-200	67,394	76.9	155-254	101-150	36,246	41.4
				255-354	151-200	-	-
351-420	201-300	-	-	355-424	201-300	-	-
421-500	301-400	-	-	425-504	301-400	-	-
501-600	401-500	-	-	505-604	401-500	-	-
Total area		87,673	100	Total area		87,575	100
UK-DEFRA				**This study (proposed)**			
PM10 ($\mu g/m^3$)	AQI Band	Area		PM10 ($\mu g/m^3$)	AQI Band	Area	
		km^2	%			km^2	%
0-16	1	-	-	0-25	1	-	-
17-33	2	-	-	26-50	2	-	-
34-49	3	-	-	51-75	3	-	-
50-58	4	-	-	76-100	4	-	-
59-66	5	-	-	101-120	5	1,099	1.3
67-74	6	-	-	121-150	6	10,196	11.7
75-83	7	799	1.0	151-200	7	40,367	46.3
84-91	8	1,706	2.0	201-250	8	31,151	35.7
92-99	9	3,488	4.0	251-300	9	4,409	5.1
≥ 100	10	81,315	93	301-350	10	-	-
Total area		87,308	100	351-400	11	-	-
-	-	-	-	≥ 400	12	-	-
-	-	-	-	Total area		87,222	100

Table 4.7b Distribution of the PM10 density over entire area on 5th April 2010 based on the derived AQI maps by the four chosen methods (in Figure 4.12).

Thailand-PCD				**US-EPA**			
PM10 ($\mu g/m^3$)	AQI	Area		PM10 ($\mu g/m^3$)	AQI	Area	
		km^2	%			km^2	%
0-40	0-50	-	-	0-54	0-50	-	-
41-120	51-100	3,442	3.9	55-154	51-100	15,595	17.81
121-350	101-200	82,071	93.8	155-254	101-150	48,027	54.86
				255-354	151-200	22,207	25.36
351-420	201-300	2,015	2.3	355-424	201-300	1,723	1.97
421-500	301-400	-	-	425-504	301-400	-	-
501-600	401-500	-	-	505-604	401-500	-	-
Total area		87,528	100	Total area		87,552	100
UK-DEFRA				**This study (proposed)**			
PM10 ($\mu g/m^3$)	AQI Band	Area		PM10 ($\mu g/m^3$)	AQI Band	Area	
		km^2	%			km^2	%
0-16	1	-	-	0-25	1	-	-
17-33	2	-	-	26-50	2	-	-
34-49	3	-	-	51-75	3	-	-
50-58	4	-	-	76-100	4	7,908	9.1
59-66	5	-	-	101-120	5	9,586	11.0
67-74	6	-	-	121-150	6	15,417	17.7
75-83	7	-	-	151-200	7	33,108	37.9
84-91	8	-	-	201-250	8	18,707	21.4
92-99	9	-	-	251-300	9	2,595	3.0
≥ 100	10	87,291	100	301-350	10	-	-
Total area		87,291	100	351-400	11	-	-
-	-	-	-	≥ 400	12	-	-
-	-	-	-	Total area		87,321	100

Table 4.7c Distribution of the PM10 density over entire area on 6th April 2010 based on the derived AQI maps by the four chosen methods (in Figure 4.13).

Thailand-PCD				**US-EPA**			
PM10 ($\mu g/m^3$)	AQI	Area		PM10 ($\mu g/m^3$)	AQI	Area	
		km^2	%			km^2	%
0-40	0-50	-	-	0-54	0-50	-	-
41-120	51-100	-	-	55-154	51-100	1,890	2.2
121-350	101-200	87,718	100	155-254	101-150	75,130	85.6
				255-354	151-200	10,725	12.2
351-420	201-300	-	-	355-424	201-300	-	-
421-500	301-400	-	-	425-504	301-400	-	-
501-600	401-500	-	-	505-604	401-500	-	-
Total area		87,718	100	Total area		87,745	100
UK-DEFRA				**This study (proposed)**			
PM10 ($\mu g/m^3$)	AQI Band	Area		PM10 ($\mu g/m^3$)	AQI Band	Area	
		km^2	%			km^2	%
0-16	1	-	-	0-25	1	-	-
17-33	2	-	-	26-50	2	-	-
34-49	3	-	-	51-75	3	-	-
50-58	4	-	-	76-100	4	-	-
59-66	5	-	-	101-120	5	1,590	1.8
67-74	6	-	-	121-150	6	21,478	24.6
75-83	7	-	-	151-200	7	60,518	69.2
84-91	8	-	-	201-250	8	3,878	4.4
92-99	9	-	-	251-300	9	-	-
≥ 100	10	87,784	100	301-350	10	-	-
Total area		87,784	100	351-400	11	-	-
-	-	-	-	≥ 400	12	-	-
-	-	-	-	Total area		87,104	100

Table 4.7d Distribution of the PM10 density over entire area on 7th April 2010 based on the derived AQI maps by the four chosen methods (in Figure 4.14).

Thailand-PCD				**US-EPA**			
PM10 ($\mu g/m^3$)	AQI	Area		PM10 ($\mu g/m^3$)	AQI	Area	
		km^2	%			km^2	%
0-40	0-50	-	-	0-54	0-50	-	-
41-120	51-100	10,570	15.66	55-154	51-100	21,609	27.7
121-350	101-200	67,497	84.34	155-254	101-150	40,378	51.8
				255-354	151-200	15,925	20.4
351-420	201-300	-	-	355-424	201-300	-	-
421-500	301-400	-	-	425-504	301-400	-	-
501-600	401-500	-	-	505-604	401-500	-	-
Total area		78,067	100	Total area		77,912	100
UK-DEFRA				**This study (proposed)**			
PM10 ($\mu g/m^3$)	AQI Band	Area		PM10 ($\mu g/m^3$)	AQI Band	Area	
		km^2	%			km^2	%
0-16	1	-	-	0-25	1	-	-
17-33	2	-	-	26-50	2	-	-
34-49	3	-	-	51-75	3	-	-
50-58	4	-	-	76-100	4	1,824	2.4
59-66	5	-	-	101-120	5	3,263	4.3
67-74	6	993	1.27	121-150	6	5,144	6.8
75-83	7	1,185	1.52	151-200	7	12,977	17.1
84-91	8	1,468	1.88	201-250	8	14,869	19.6
92-99	9	1,836	2.35	251-300	9	18,164	23.9
≥ 100	10	72,116	92.47	301-350	10	14,419	19.0
Total area		77,598	100	351-400	11	5,324	7.0
-	-	-	-	≥ 400	12	-	-
-	-	-	-	Total area		75,984	100

Table 4.7e Distribution of the PM10 density over entire area on 8th April 2010 based on the derived AQI maps by the four chosen methods (in Figure 4.15).

Thailand-PCD				**US-EPA**			
PM10 ($\mu g/m^3$)	AQI	Area		PM10 ($\mu g/m^3$)	AQI	Area	
		km^2	%			km^2	%
0-40	0-50	-	-	0-54	0-50	-	-
41-120	51-100	-	-	55-154	51-100	-	-
121-350	101-200	87,628	100	155-254	101-150	76,974	88
				255-354	151-200	10,590	12
351-420	201-300	-	-	355-424	201-300	-	-
421-500	301-400	-	-	425-504	301-400	-	-
501-600	401-500	-	-	505-604	401-500	-	-
Total area		87,628	100	Total area		87,564	100
UK-DEFRA				**This study (proposed)**			
PM10 ($\mu g/m^3$)	AQI Band	Area		PM10 ($\mu g/m^3$)	AQI Band	Area	
		km^2	%			km^2	%
0-16	1	-	-	0-25	1	-	-
17-33	2	-	-	26-50	2	-	-
34-49	3	-	-	51-75	3	-	-
50-58	4	-	-	76-100	4	-	-
59-66	5	-	-	101-120	5	-	-
67-74	6	-	-	121-150	6	-	-
75-83	7	-	-	151-200	7	6,916	7.9
84-91	8	-	-	201-250	8	65,171	74.4
92-99	9	-	-	251-300	9	15,495	17.7
≥ 100	10	87,593	100	301-350	10	-	-
Total area		87,593	100	351-400	11	-	-
-	-	-	-	≥ 400	12	-	-
-	-	-	-	Total area		87,582	100

Table 4.7f Distribution of the PM10 density over entire area on 9th April 2010 based on the derived AQI maps by the four chosen methods (in Figure 4.16).

Thailand-PCD				**US-EPA**			
PM10 ($\mu g/m^3$)	AQI	Area		PM10 ($\mu g/m^3$)	AQI	Area	
		km^2	%			km^2	%
0-40	0-50	-	-	0-54	0-50	-	-
41-120	51-100	14,355	16.55	55-154	51-100	30,096	34.5
121-350	101-200	72,882	83.45	155-254	101-150	45,382	52.1
				255-354	151-200	11,672	13.4
351-420	201-300	-	-	355-424	201-300	-	-
421-500	301-400	-	-	425-504	301-400	-	-
501-600	401-500	-	-	505-604	401-500	-	-
Total area		87,237	100	Total area		87,150	100
UK-DEFRA				**This study (proposed)**			
PM10 ($\mu g/m^3$)	AQI Band	Area		PM10 ($\mu g/m^3$)	AQI Band	Area	
		km^2	%			km^2	%
0-16	1	-	-	0-25	1	-	-
17-33	2	-	-	26-50	2	-	-
34-49	3	-	-	51-75	3	-	-
50-58	4	-	-	76-100	4	5,637	6.5
59-66	5	-	-	101-120	5	8,650	9.9
67-74	6	-	-	121-150	6	13,320	15.3
75-83	7	1,360	1.56	151-200	7	26,185	30.0
84-91	8	1,531	1.75	201-250	8	20,306	23.3
92-99	9	2,387	2.73	251-300	9	10,002	11.5
≥ 100	10	82,051	93.96	301-350	10	3,069	3.5
Total area		87,329	100	351-400	11	-	-
-	-	-	-	≥ 400	12	-	-
-	-	-	-	Total area		87,169	100

มหาวิทยาลัยเทคโนโลยีสุรนารี

CHAPTER V

APPLICATIONS OF HYSPLIT MODEL

This chapter reports results from the applications of the HYSPLIT model to assess trajectory and distributing pattern of the smoke plume originated from the active fire sources located both within and outside the study area, especially those situated in two neighboring countries; Myanmar and Laos. The content is separated into two principal parts. The first one is contributed to the assessment of smoke plume trajectory of the propagation and evolution of its distributing pattern with time (called the forward trajectory analysis). The second one is the analysis of air mass backward trajectory characteristics (or back trajectory analysis).

5.1 Forward trajectory and dispersion analysis

In this part, potential sources of the severe air pollution observed during 4^{st}-9^{st} April 2010 were evaluated based on the simulated results of smoke plume moving trajectory and distributing pattern over 48-hour period from the identified source locations given by the HYSPLIT model (see Figure 5.1 for example). To achieve this task, the active fire maps for each particular date (4^{nd}-8^{st} April 2010) were produced from the MODIS data covering both fire-prone areas in northern Thailand and in its neighboring countries (Myanmar and Laos) and results are reported in Figure 5.2 and Table 5.1. It was found that number of the total fire spots yielded is 2540 events, among these, about 11.73% were in Thailand while the rest were found elsewhere.

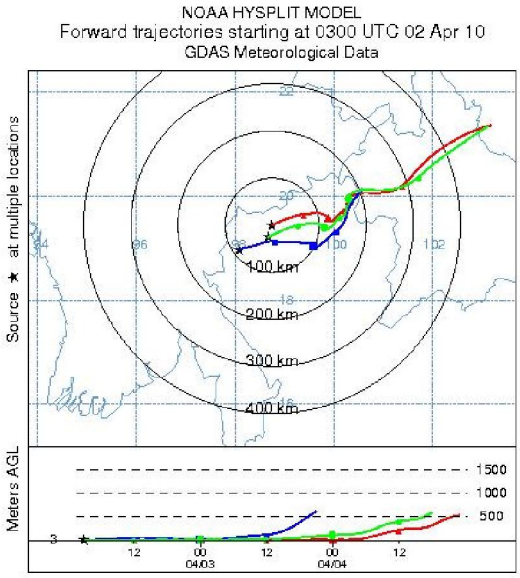

Figure 5.1 Example of the forward trajectories of smoke plumes (starting from 03.00 UTC of 2nd April 2010 onward) originated at three different locations.

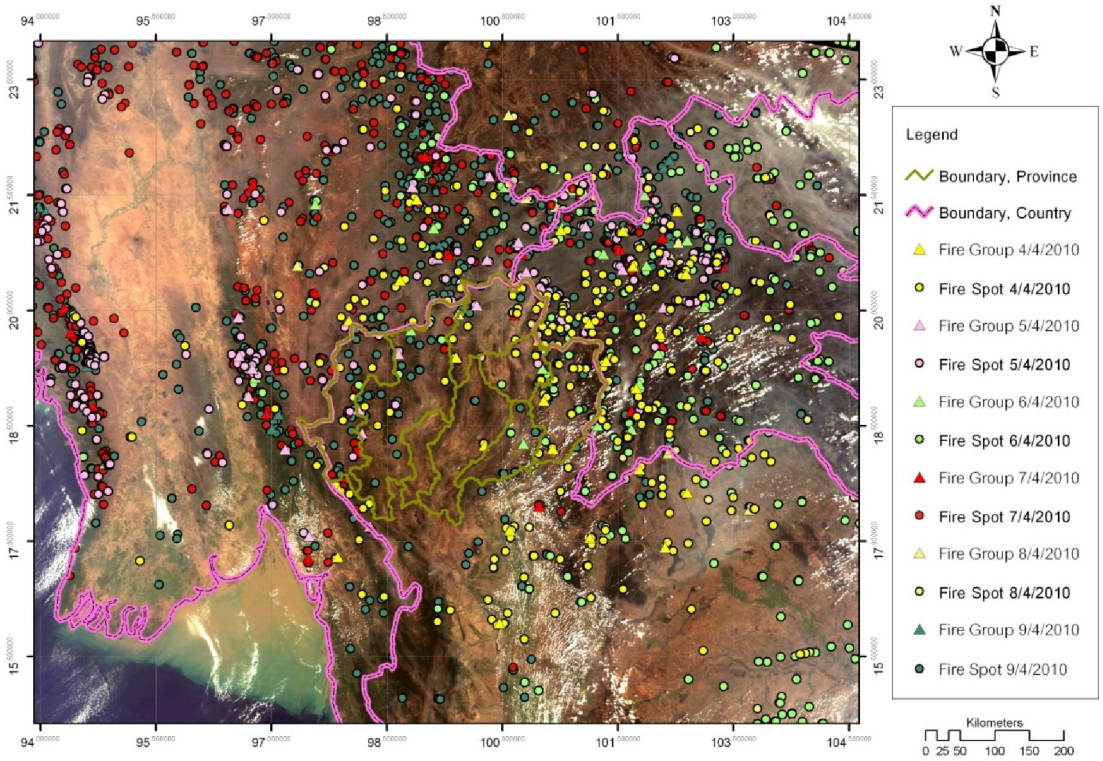

Figure 5.2 MODIS-based fire map over period of 4th-9th April 2010 and the assumed locations of fire spots for each grid cell.

Table 5.1a Location distribution of active fire spots during 4nd-8th April 2010.

Source region		Number of identified fire spots					Total (location)	
		4th	5th	6th	7th	8th	number	%
Thailand	Chiang Rai	19	3	2	9	5	38	1.50
	Chiang Mai	5	11	9	3	-	28	1.10
	Lampang	2	-	-	-	-	2	0.08
	Lamphun	-	-	-	-	-	-	-
	Mae Hong Son	5	7	1	8	2	23	0.91
	Nan	19	-	12	-	2	33	1.30
	Phayao	5	2	6	4	2	19	0.75
	Phrae	1	-	-	-	-	1	0.04
	Others	74	-	80	-	-	154	6.06
Aboard	Myanmar	74	273	90	515	38	990	38.98
	Laos	173	168	217	145	77	780	30.71
	Others	39	42	165	99	127	472	18.58
Total (date)		416	506	582	783	253	2540	100.0

Table 5.1b Location distribution of fire clusters during 4nd-8th April 2010.

Source region		Number of identified fire clusters					Total (location)	
		4th	5th	6th	7th	8th	number	%
Thailand	Chiang Rai	2	1	-	1	1	5	3.8
	Chiang Mai	-	3	1	-	-	4	3.1
	Lampang	-	-	-	-	-	-	-
	Lamphun	1	-	-	-	-	1	0.8
	Mae Hong Son	-	-	-	1	-	1	0.8
	Nan	2	-	1	-	-	3	2.3
	Phayao	1	-	1	1	1	4	3.1
	Phrae	-	-	1	1	-	2	1.5
	Others	7	1	1	1	3	13	9.9
Aboard	Myanmar	4	13	7	14	6	44	33.6
	Laos	9	9	14	8	11	51	38.9
	Others	-	-	-	-	3	3	2.3
Total (date)		26	27	26	27	25	131	100

From data given in Figure 5.1, it is obvious that on 2nd April 2010, smoke plumes released from three assumed sources in northern Thailand shall move along northeast-bound direction crossing into the Laos territory eventually. Total number of fire events recorded in Myanmar is 990 (38.98%) and in Laos is 780 (30.71%), which should be prime contributing sources of aerosol pollutants found in the area during 2010 fire season. It shall be demonstrated further in this chapter that the fire activities in Myanmar could produce serious consequence in terms of the aerosol pollution experienced over northern Thailand over the studied period. In addition, the aerosol-polluted region was remarkably extended to occupy large part of the upper Laos during that time also. Noted that, few domestic sources were identified in this study if compared to those situated abroad where the highest number is in Chiang Rai (38) followed by Nan (33), Chiang Mai (28), Mae Hong Son (23), Phayao (19), Lampang (2), Phare (1) and none in Lamphun. And by initial visual examination, most listed fire events occurred in the forest area of all the three aforementioned countries.

To reduce complexity in the simulation of smoke plume spatial dispersion and their aggregation over time, high number of the observed sources were grouped using clustering technique provided by the ArcGIS tool based on a 10 km radius criteria. Each cluster was treated as being a single contributing source located at its center and then applied as input data for the HYSPLIT simulation afterwards. This practice shall provide a broad overview of smoke plume distributing pattern over time period of interest after releasing from the assumed sources over entire study area and beyond as shown in Figure 5.3-5.7.

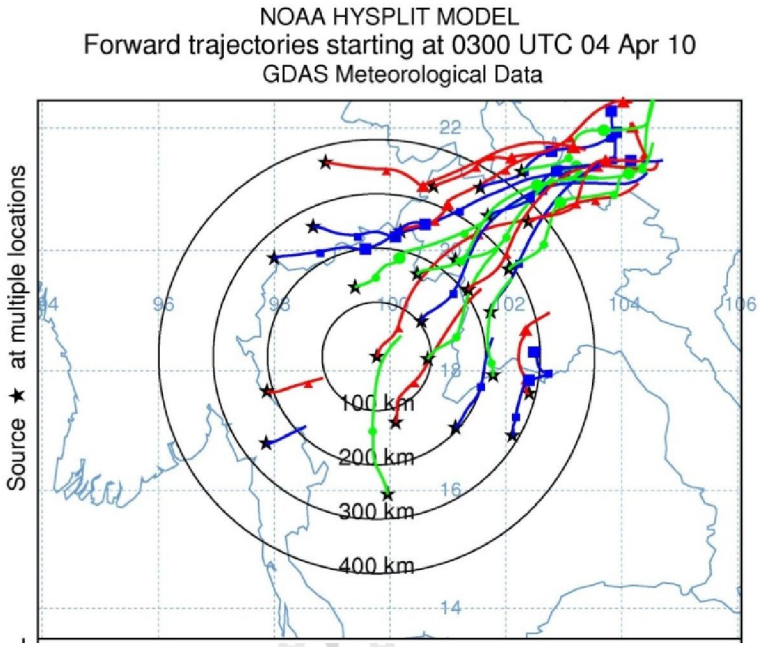

Figure 5.3a Forward trajectories of smoke plumes originated on 4th April 2010 from the pre-assigned fire clusters (starting at 03.00 UTC or 10.00 LST).

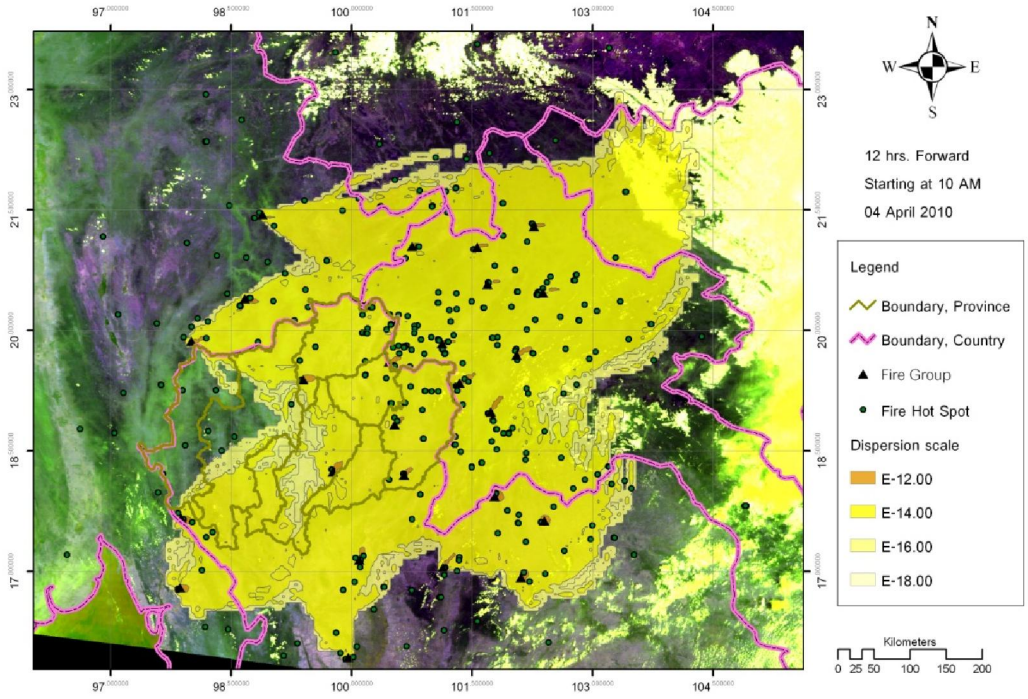

Figure 5.3b Distributing pattern of smoke plumes originated on 4th April 2010 from the pre-assigned fire clusters (12-hour forward starting at 10 AM).

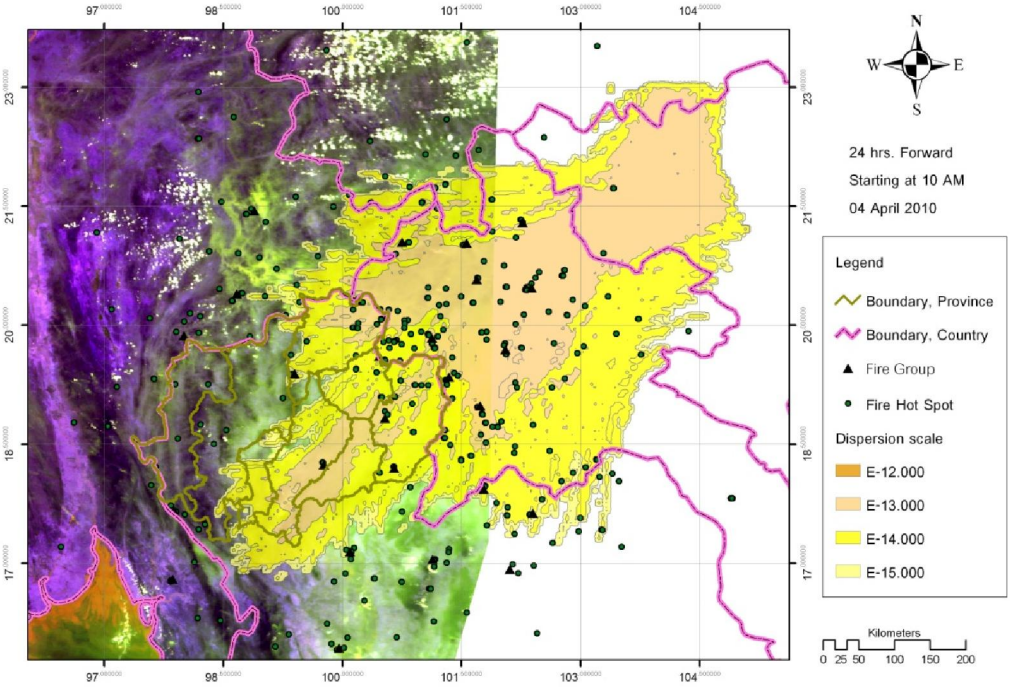

Figure 5.3c Distributing pattern of smoke plumes originated on 4th April 2010 from the pre-assigned fire clusters (24-hour forward starting at 10 AM).

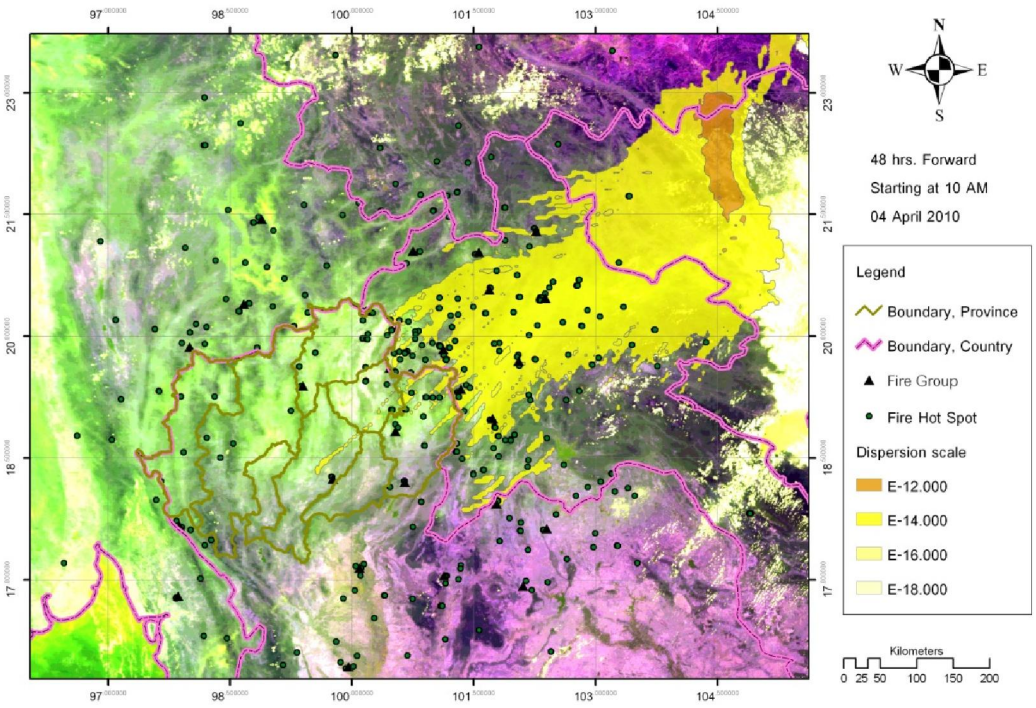

Figure 5.3d Distributing pattern of smoke plumes originated on 4th April 2010 from the pre-assigned fire clusters (48-hour forward starting at 10 AM).

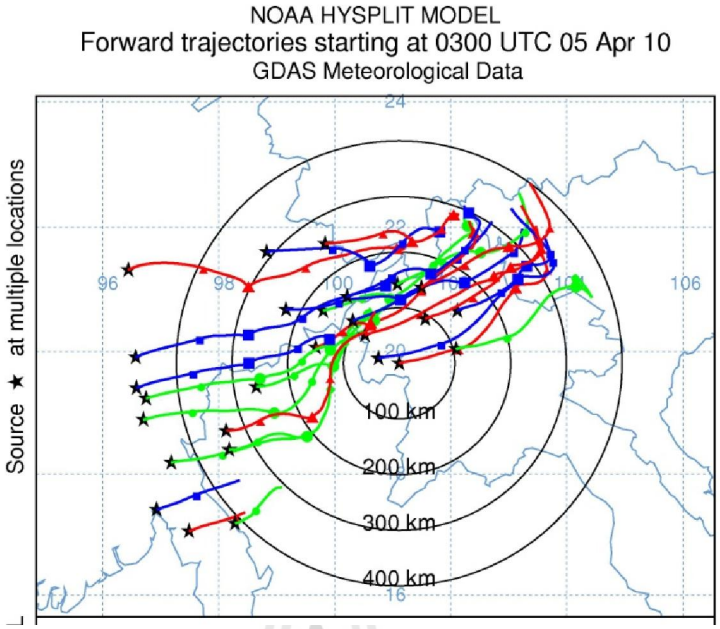

Figure 5.4a Forward trajectories of smoke plumes originated on 5th April 2010 from the pre-assigned fire clusters (starting at 03.00 UTC or 10.00 LST).

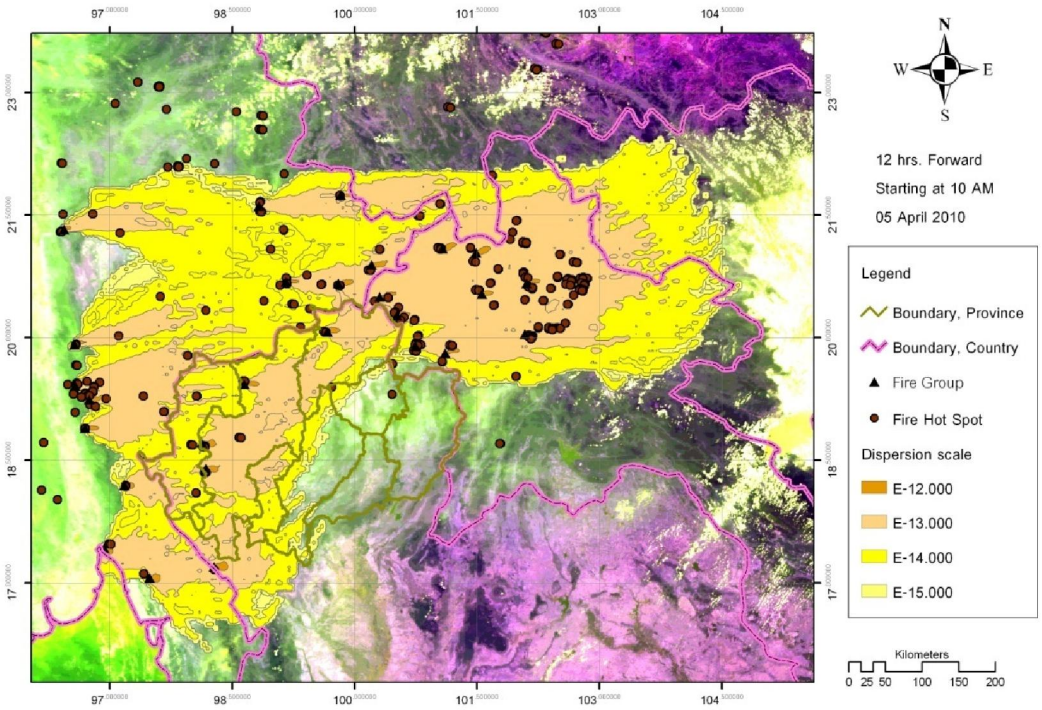

Figure 5.4b Distributing pattern of smoke plumes originated on 5th April 2010 from the pre-assigned fire clusters (12-hour forward starting at 10 AM).

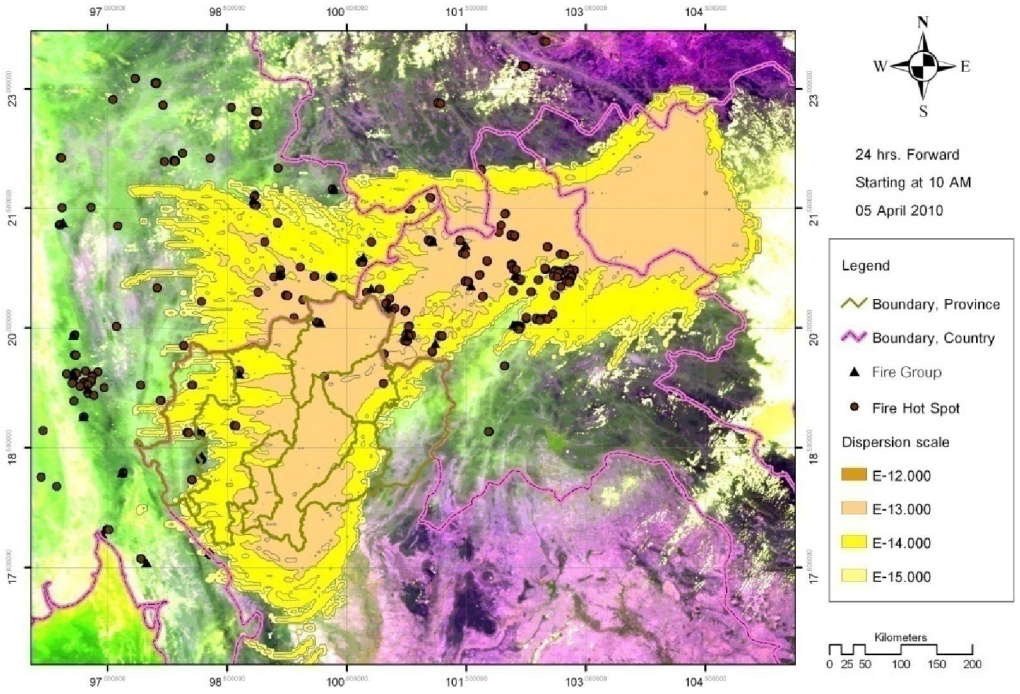

Figure 5.4c Distributing pattern of smoke plumes originated on 5th April 2010 from the pre-assigned fire clusters (24-hour forward starting at 10 AM).

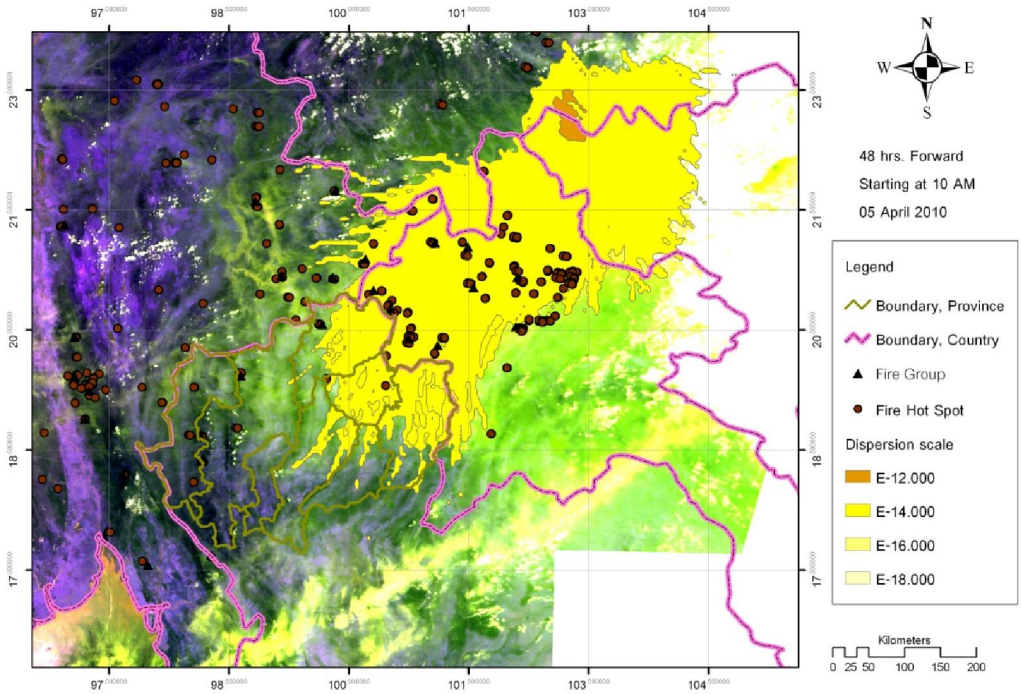

Figure 5.4d Distributing pattern of smoke plumes originated on 5th April 2010 from the pre-assigned fire clusters (48-hour forward starting at 10 AM).

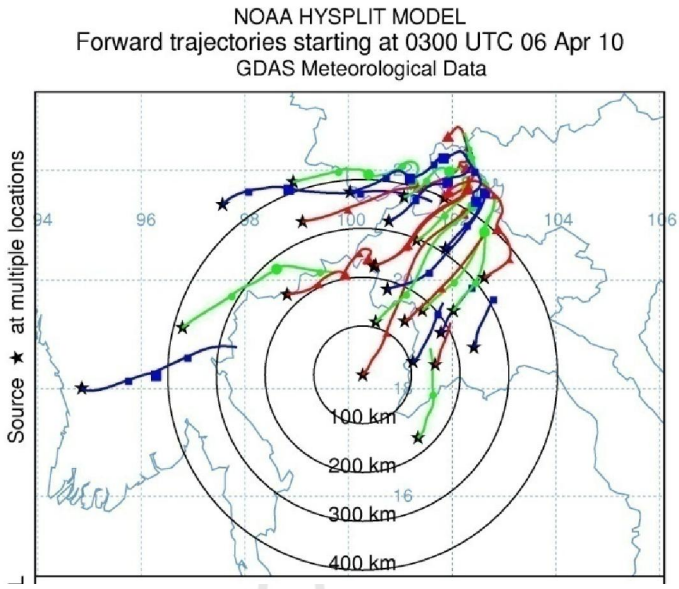

Figure 5.5a Forward trajectories of smoke plumes originated on 6th April 2010 from the pre-assigned fire clusters (starting at 03.00 UTC).

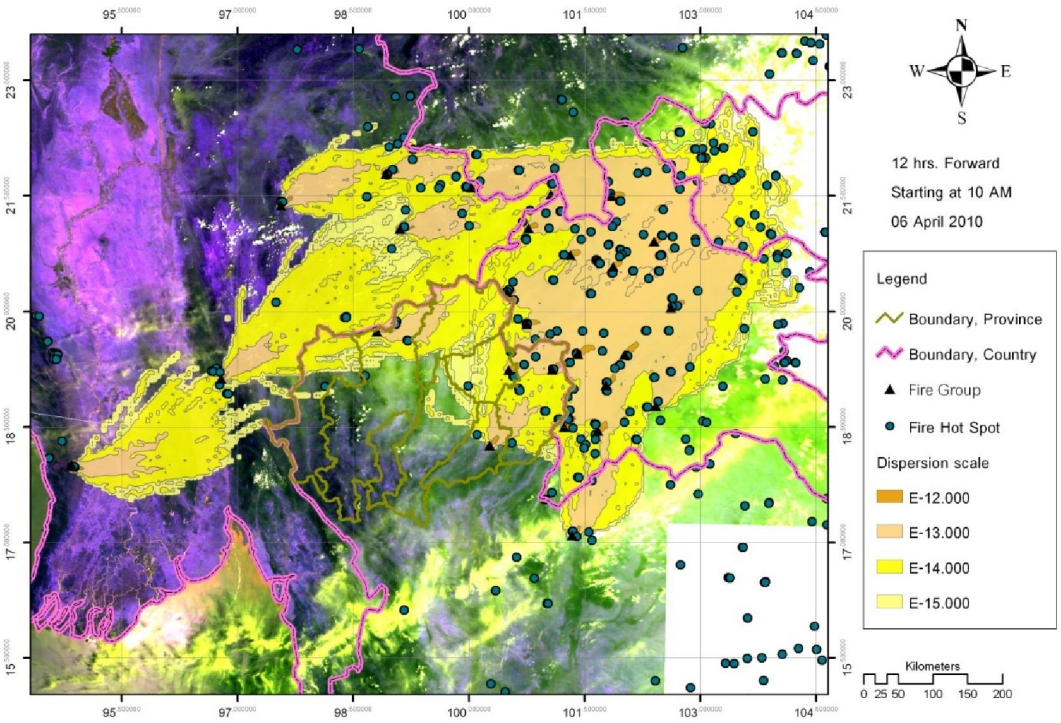

Figure 5.5b Distributing pattern of smoke plumes originated on 6th April 2010 from the pre-assigned fire clusters (12-hour forward starting at 10 AM).

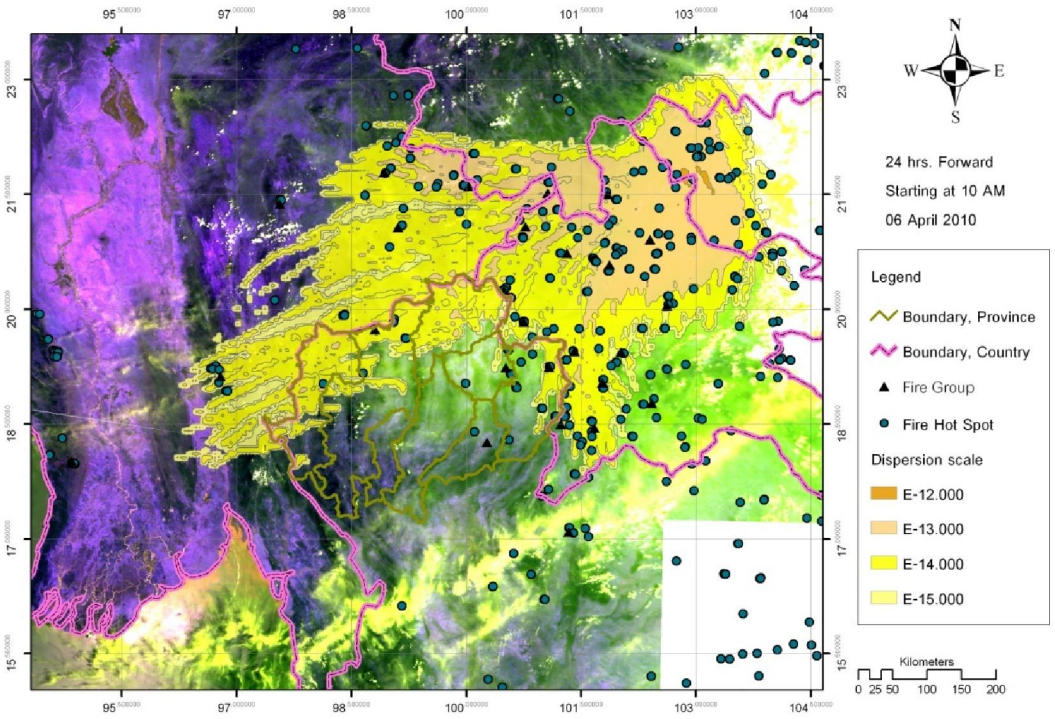

Figure 5.5c Distributing pattern of smoke plumes originated on 6th April 2010 from the pre-assigned fire clusters (24-hour forward starting at 10 AM).

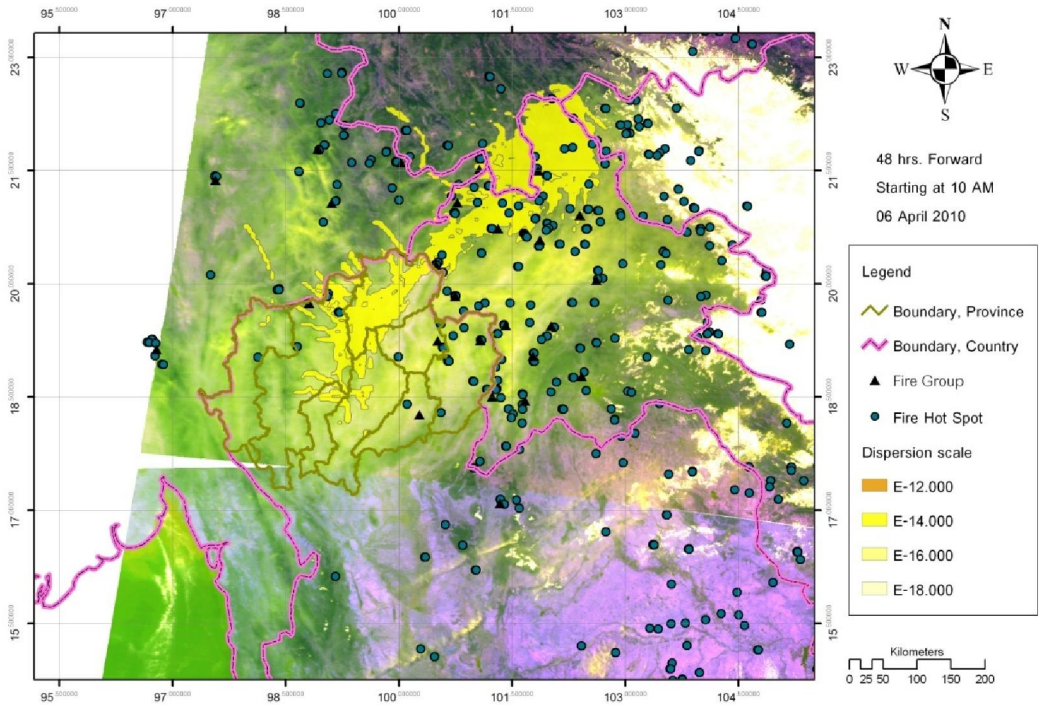

Figure 5.5d Distributing pattern of smoke plumes originated on 6th April 2010 from the pre-assigned fire clusters (48-hour forward starting at 10 AM).

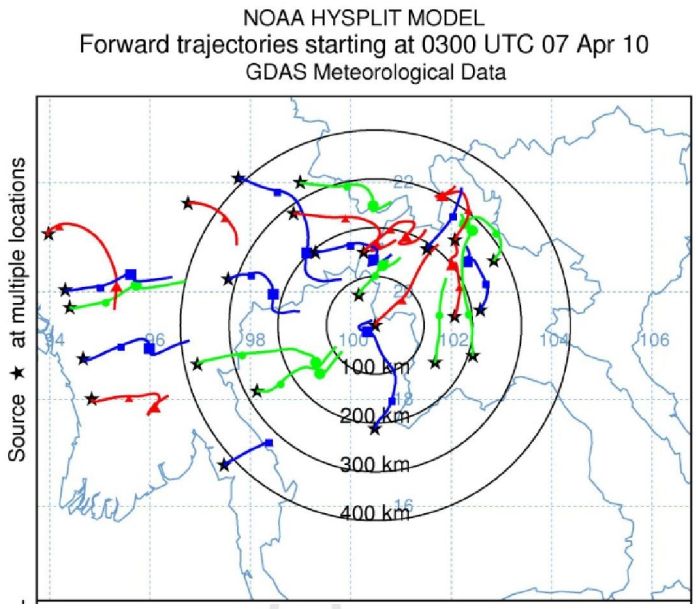

Figure 5.6a Forward trajectories of smoke plumes originated on 7th April 2010 from the pre-assigned fire clusters (starting at 03.00 UTC).

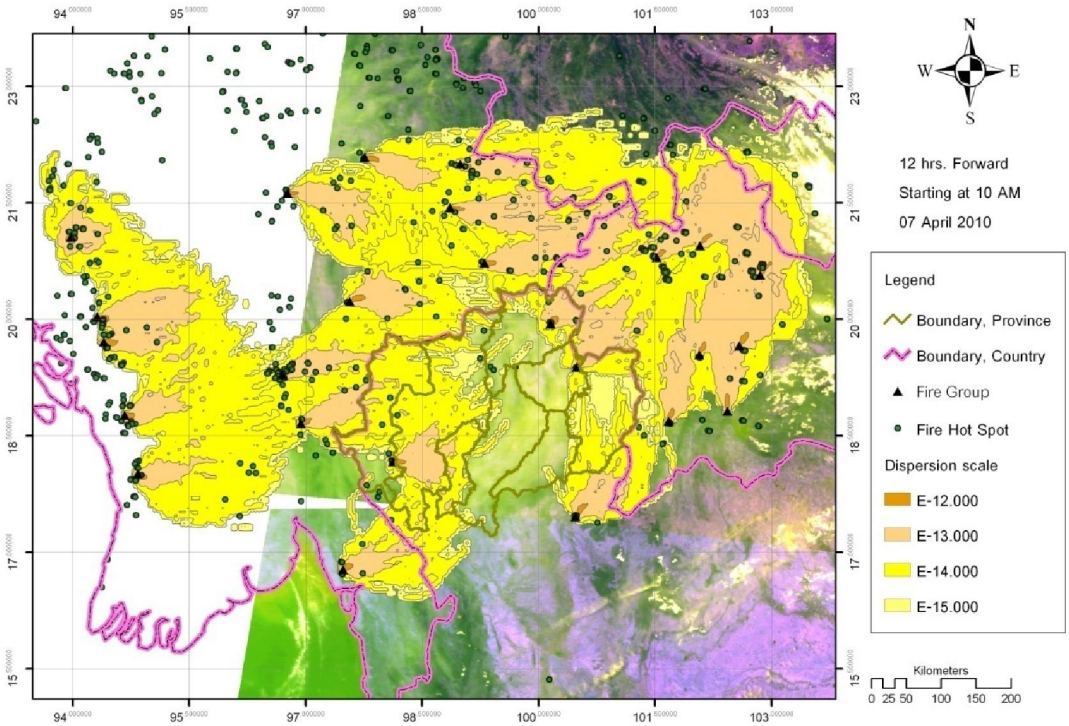

Figure 5.6b Distributing pattern of smoke plumes originated on 7th April 2010 from the pre-assigned fire clusters (12-hour forward starting at 10 AM).

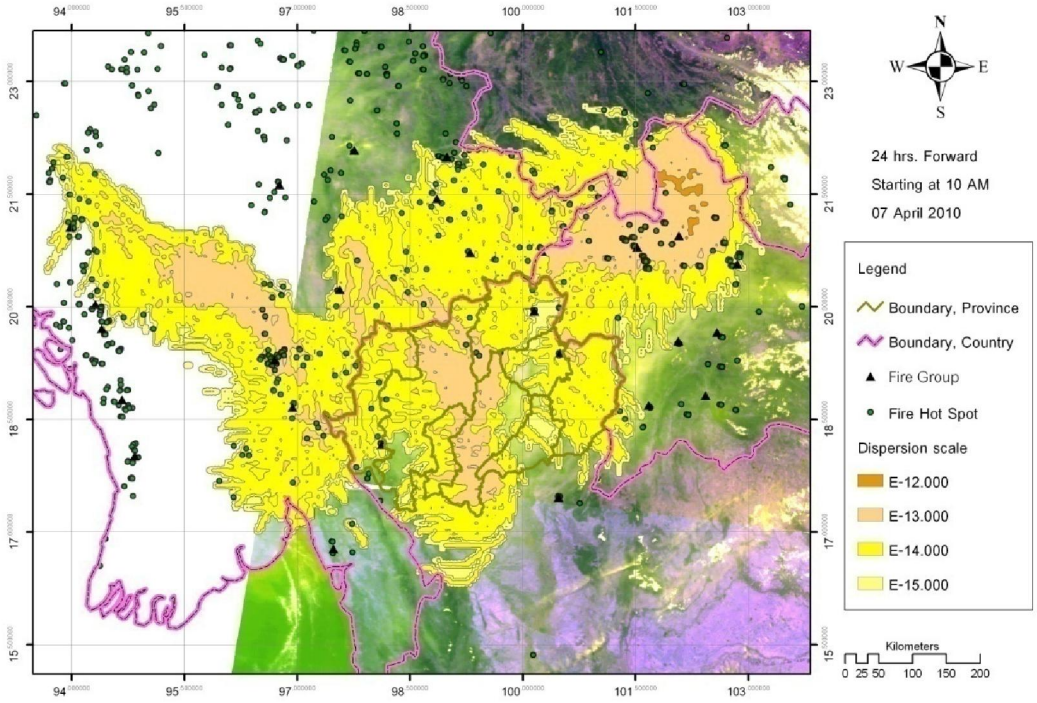

Figure 5.6c Distributing pattern of smoke plumes originated on 7th April 2010 from the pre-assigned fire clusters (24-hour forward starting at 10 AM).

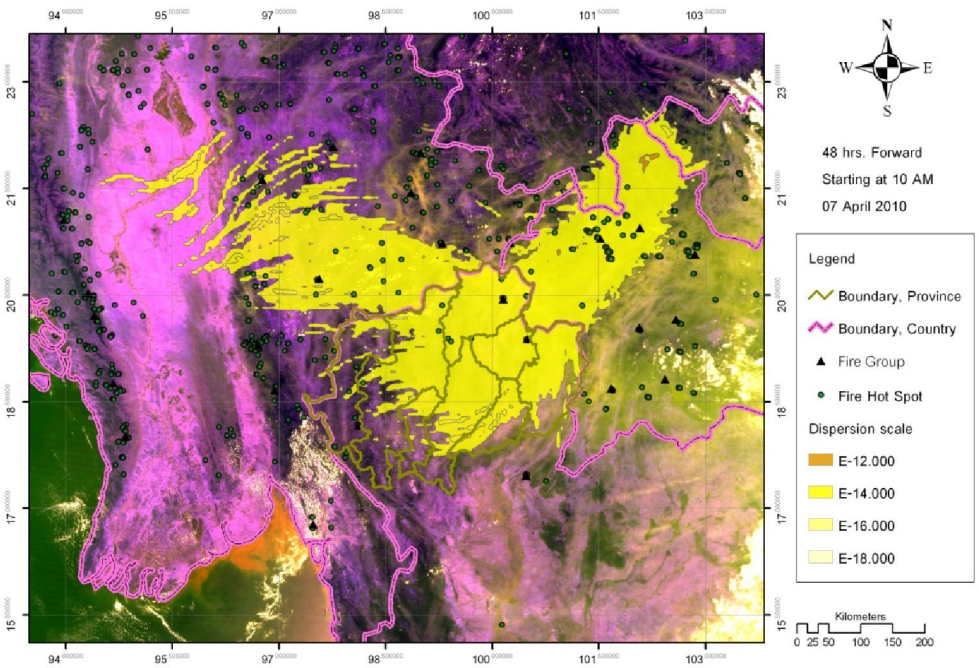

Figure 5.6d Distributing pattern of smoke plumes originated on 7th April 2010 from the pre-assigned fire clusters (48-hour forward starting at 10 AM).

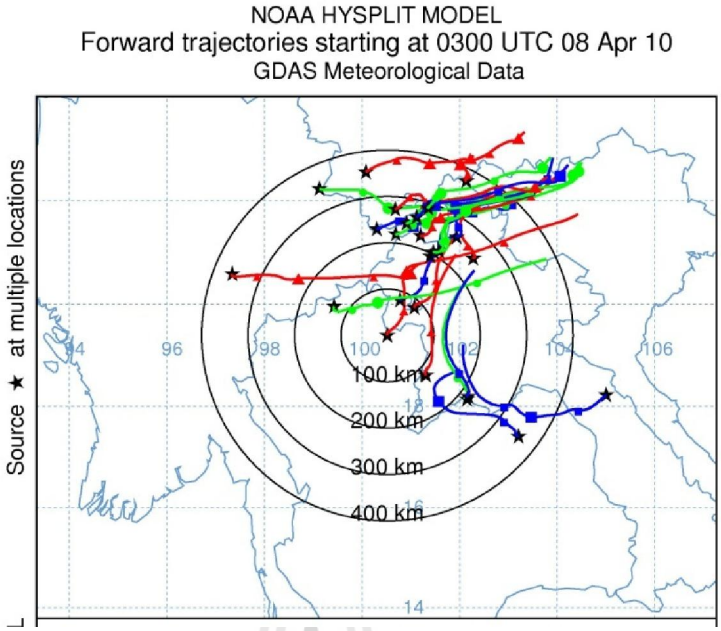

Figure 5.7a Forward trajectories of smoke plumes originated on 8th April 2010 from the pre-assigned fire clusters (starting at 03.00 UTC).

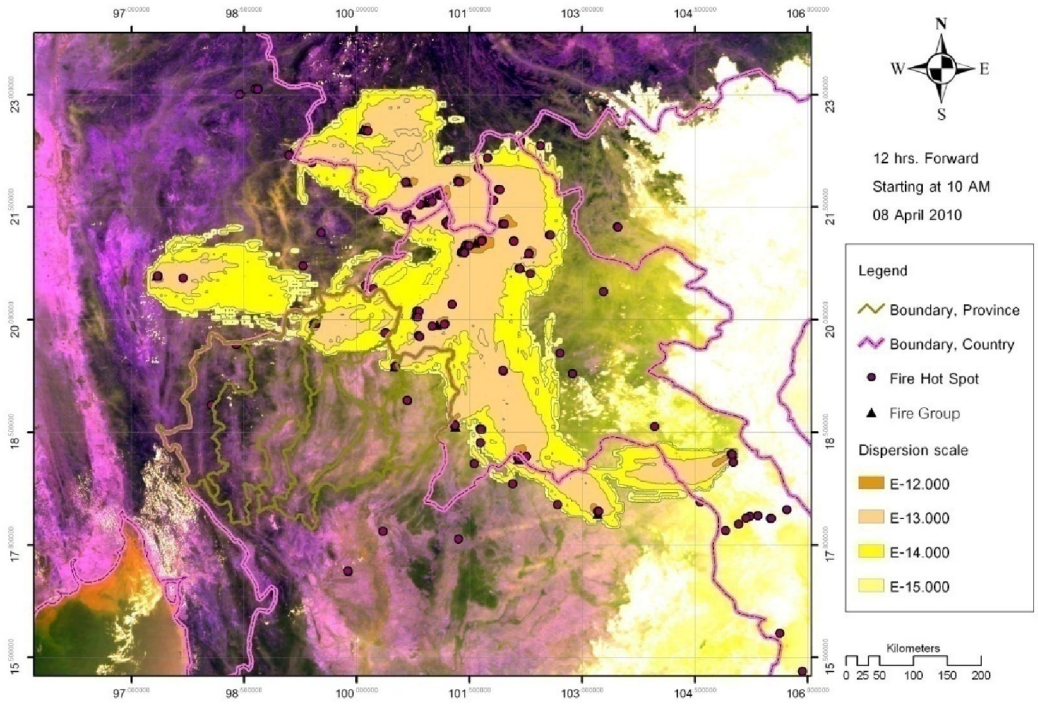

Figure 5.7b Distributing pattern of smoke plumes originated on 8th April 2010 from the pre-assigned fire clusters (12-hour forward starting at 10 AM).

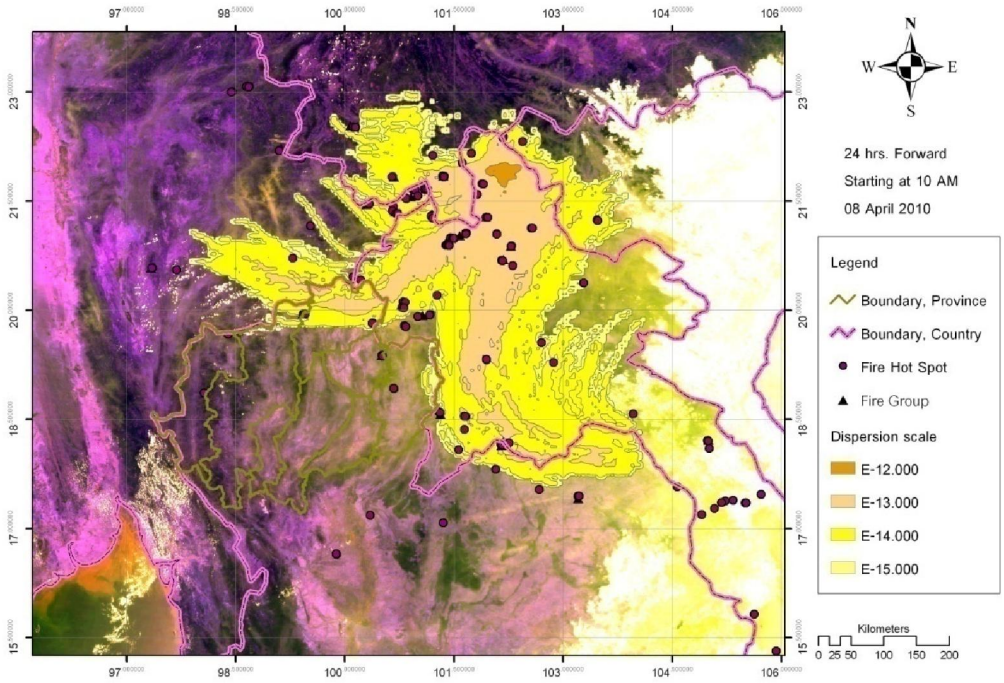

Figure 5.7c Distributing pattern of smoke plumes originated on 8th April 2010 from the pre-assigned fire clusters (24-hour forward starting at 10 AM).

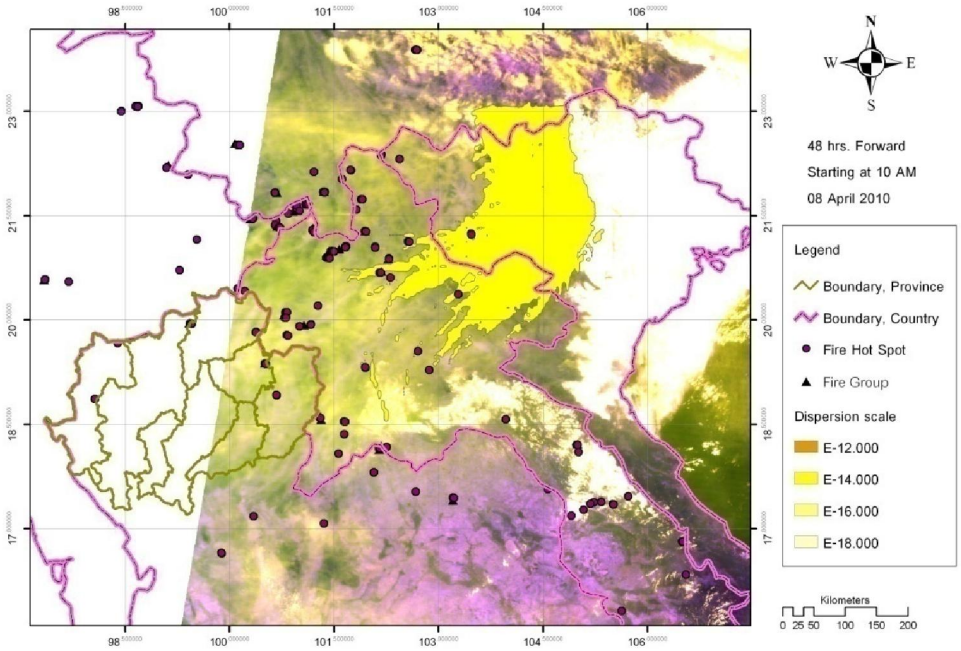

Figure 5.7d Distributing pattern of smoke plumes originated on 8th April 2010 from the pre-assigned fire clusters (48-hour forward starting at 10 AM).

It can be concluded from results reported in Figures 5.3-5.7 that the long-range dispersion of smok plumes originated from fire sources in Myanmar did have huge impact on the observal air pollution severity over upper northern Thailand, especiallly for provinces located along the Thai/Myanmar border like Mae Hong Son, Chiang Mai, or Chiang Rai. However, provinces located on the eastern side far opposite to the border (on the west) were also experience this effect like Nan or Payao Provinces. For eaxmples, after undergoing 24 hour dispersion, the smoke plumes originated on 4th April shall move northeasward pass the area and cluster densly over the western provinces like Nan, Payao and Chiang Rai and also in the upper part of Laos (Figure 5.3c). This stated characteristic was strongly supported by the AOD and PM10 maps derived for 5th April at about 10.30 AM as depicted in Figures 4.6b and 4.7b, and also as indicated by green tone in Figure 3.4.

Similarly, the smoke plumes started on 5th April shall move northeasward and concentrate mostly over provinces on the upper east like Chiang Rai, Payao and in the middle like Lampang and in upper Chiang Mai within 24 hours of their release (Figure 5.4c). This pattern was also reflected in the generated AOD and PM10 maps on 6th April shown in Figures 4.6c and 4.7c. However, it was found that patterns of the AOD and PM10 distribution on 7th April (in Figures 4.6d and 4.7d) did not correspond much to the pattern of existing smoke plumes generated 24 hours erlier on the previous day (Figure 5.5c). This is because on this date, the aerosol pollution was clearly dominant over most provinces on the upper east like Chiang Rai, Payao and also over the upper parts of Chiang Mai and Nan but none of these were obviously portrayed on the relevant smoke plume dispersion map.

This result indicates that the aerosol pollutants observed on this day over the area migt come from other sources that were not included in the HYSPLIT simulation or it might be a left-over part of the aerosol material from the previous day (on 6th April) that was got intensified somehow by the meteorological condition or some other factors to attain more strength in terms of AOD and PM10 concentration as seen over the areas stated earlier.

The 24-hr dispersion pattern of plumes originated on 7th April (Figure 5.6c) indicates the widespread polluted atmosphere over most parts of the area especially in the upper part of Ching Mai and in western Lampang. This prediction looks broadly similar to ones obtained in the AOD and PM10 maps of the area on 8th April (as given in Figure 4.6e and 4.7e). However, the simulated smoke plume distribution map still cannot explain the relatively high amount of the PM10 data visible in some provinces like Nan and Mae Hong Son on this date. Similar to the situation encountered on the previous date, the 24-hr dispersion pattern of plumes originated on 8th April (Figure 5.7c) indicates relatively low aerosol atmosphere for all parts of the study area except in the uppermost part of Chiang Rai which is generally true for western part of the study area if compared to the derived AOD and PM10 maps on 9th April (as shown in Figure 4.6f and 4.7f). However, rather high aerosol pollution can be identified on the eastern part, especially in Nan and Phare on the PM10 map. This aerosol appearance still cannot be accounted for by the corresponding dispersion map displayed in Figure 5.7c. Nevertheless, this dispersion map did predict high concentration of the aerosol polluatants over the upper part of Laos which is strongly supported by the aerosol map displayed in Figure 3.7.

In conclusion, the aerosol pollution observed over the study area during 4^{th}-9^{th} April 2010 is influenced by smoke plumes originated on the western and southwestern directions of the area the most, especially those located in Myanmar territory. After being released from their sourced, these plumes would gradually spread out along the way and often merge together to form a large body of smoke plume which is clearly visible on the simulated dispersion maps. This intensified smoke plume shall move continuously under influence of the prevailing regional winds over the area during that time. And, according to Jiemjai Kreasuwun, Chakrit Chodamornsuk, Pakpook Ratjiranukool, and Orawan Wirunvedchayan (2008), there are two types of prevalent wind systems found over the upper northern Thailand during fire season; the northeast monsoon wind (which is cold and dry) and the southwest monsoon wind (which is rather humid). The former category would mostly dominate in winter months (January and February in particular) and in early summer (March) while the latter is observable from March and April in particular.

Through, it is possible that results found in this study was contributed by the action of southwest monsoon the most as most identified fire-induced smoke plumes were exhibited the predominant eastward or northeastward movement during that time. In general, the plumes can travel for a distance of upto about 300-400 kilometers per day (estimated from data shown in Figures 5.8-5.15), therefore, it might take about 1-2 days for them to move across the study area from west to east (about 400 kilometers apart). After releasing from its original source the plume shall be moving downwind and gradually dispersed along the way. Eventually, they shall completely dissipated within 2-3 days as suggested from Figures 5.3-5.7.

5.2 Backward trajectory assessment

In this part, information of the backward trajectories of smoke plumes that arrive at the aerosol measuring station for each province were examined with two tasks achieved here. In the first task, back trajectories of all air masses arrived at each representative stations of the provinces during March 2010, when the worst aerosol pollution situation occurred, were mapped at the certain time interval of 3, 12, 24, and 48 hours backward. Gained results are reported in Figures 5.8-5.15, respectively. In the second task, mean back trajectories (over 48 hours) of all air masses arrived at the referred stations (for each province) during each month of the 2010 fire season, and during the entire season, were investigated. Results are reported in form of trajectory maps illustrating six major travelling directions and amount of the associated air mass (in percent) along each particular direction as described in Figures 5.16-5.17 and Tables 5.2-5.4, respectively.

5.2.1 Backward trajectory analysis for March 2010

It was found that in case of the 3-hour back trajectory mapping for the Chiang Mai-CM1 station, origins of the identified air mass still locate within the province and in the neighboring province of Lamphoon at radial distance of less than about 30 km (Figure 5.8-5.15). Howere, after 12 hours, source locations were extended further mostly along the west/southwest directions beyond Thai-Myanmar border at radial distance of about 200 km. And this trend was continued for the longer time steps; i.e. 24 or 48 hours, in which locations of the original sources steadily move deeper into Myanmar territory. For the 48-hour tracing back, origins of most air mass situate in southern Myanmar at distance as far as 500 km away.

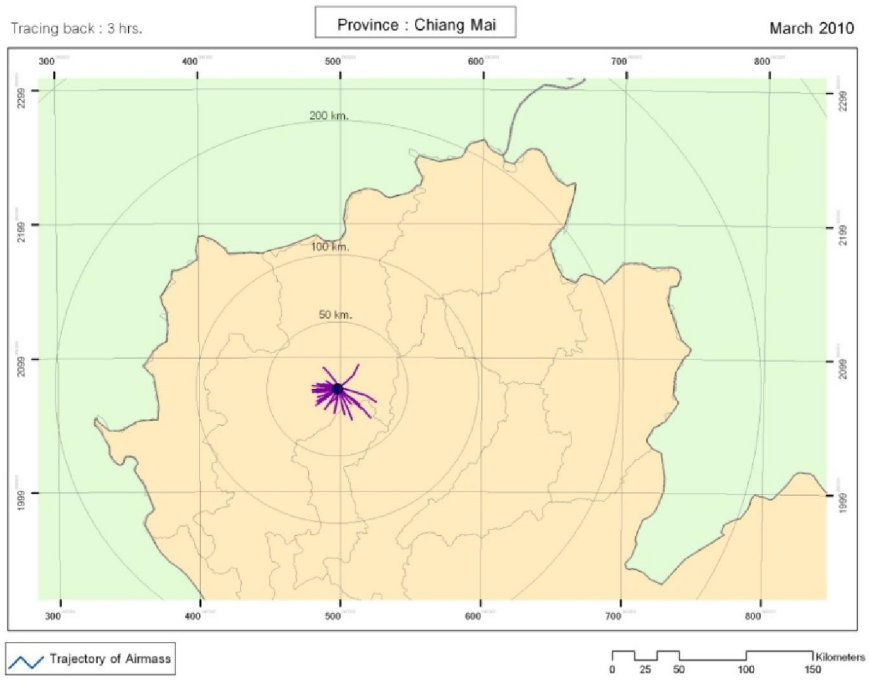

(a)

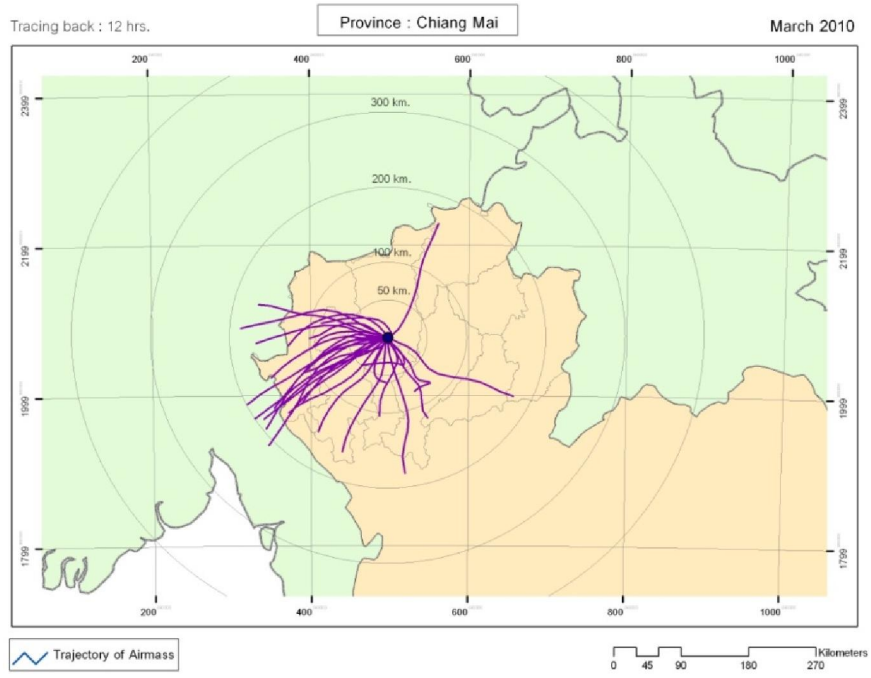

(b)

Figure 5.8 Back trajectory maps for the CM1 station in Chiang Mai Province (during March 2010) over the (a) 3, (b) 12, (c) 24, and (d) 48-hour periods.

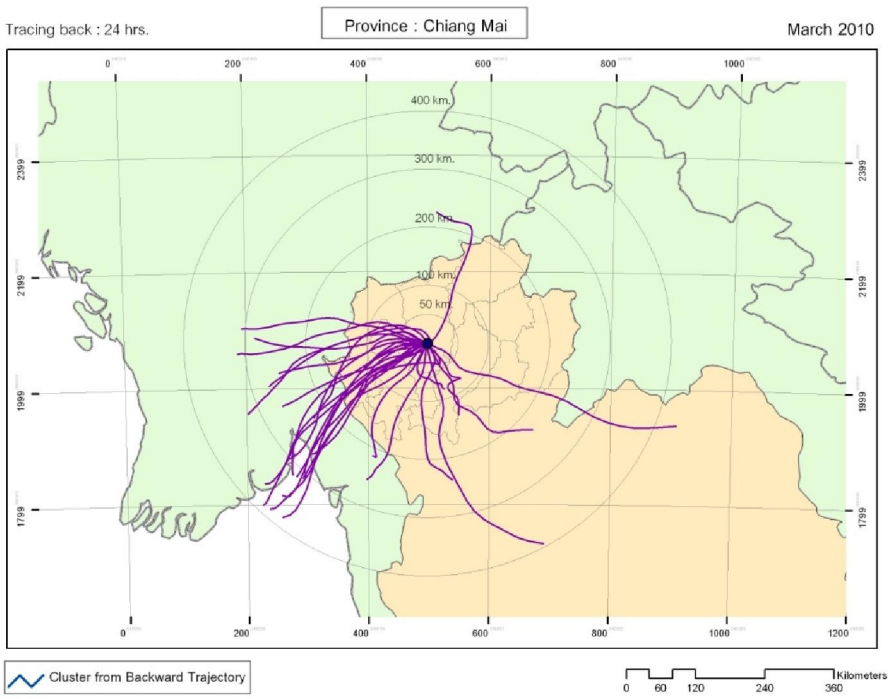

(c)

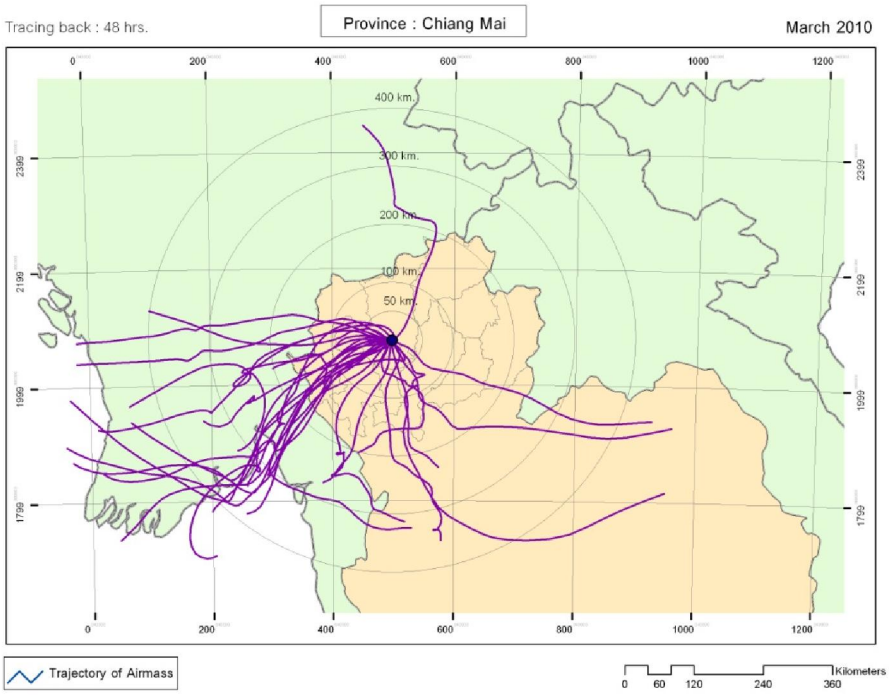

(d)

Figure 5.8 (Continued -For the CM1 station).

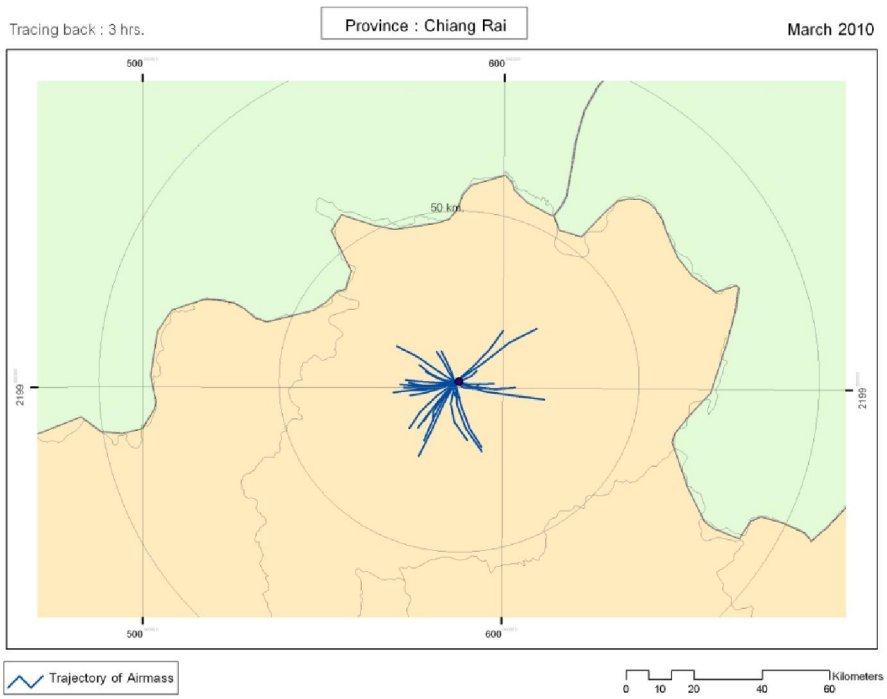

(a)

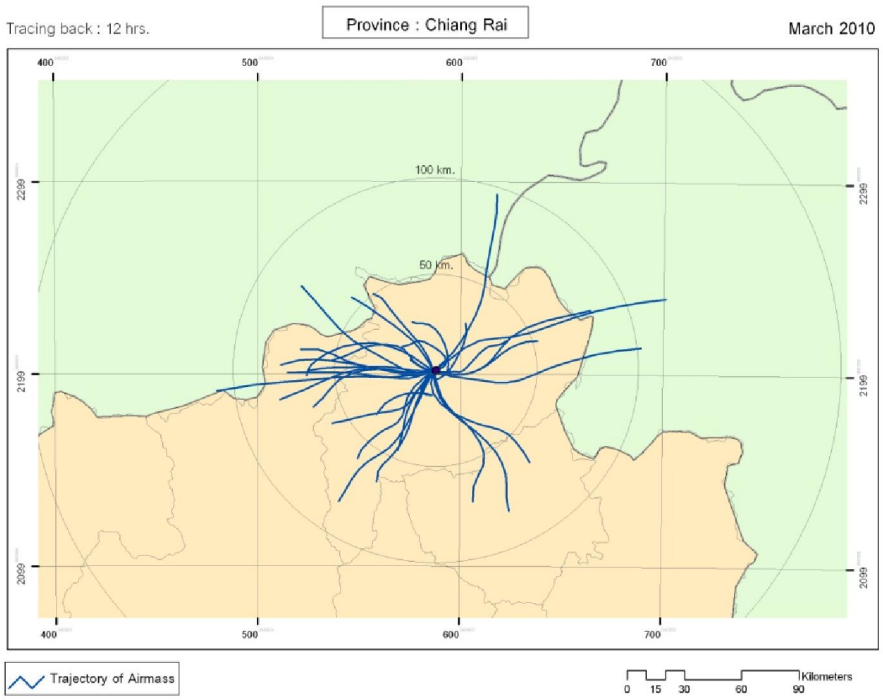

(b)

Figure 5.9 Back trajectory maps for the CR1 station in Chiang Rai Province (during March 2010) over the (a) 3, (b) 12, (c) 24, and (d) 48-hour periods.

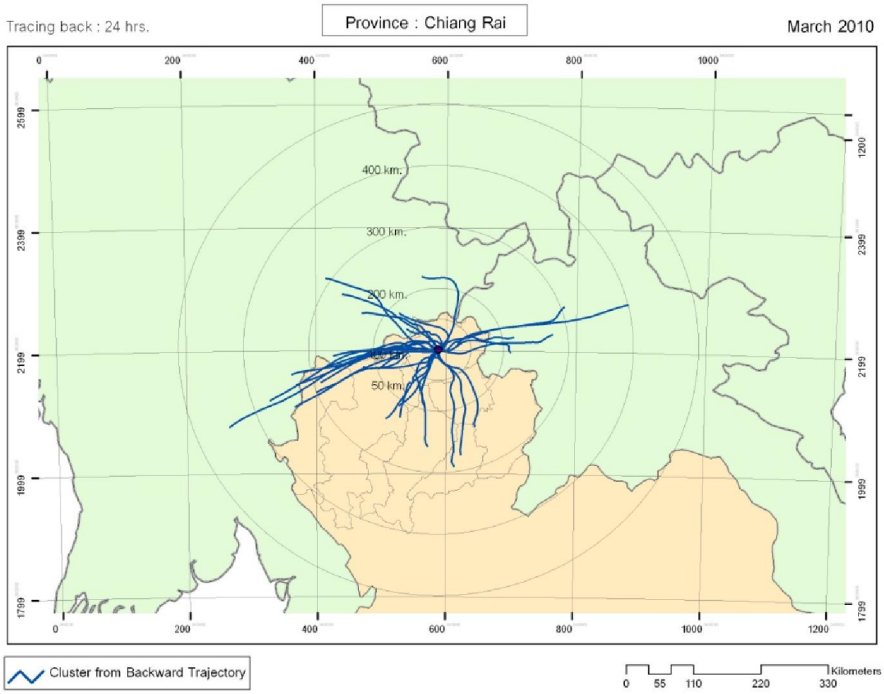

(c)

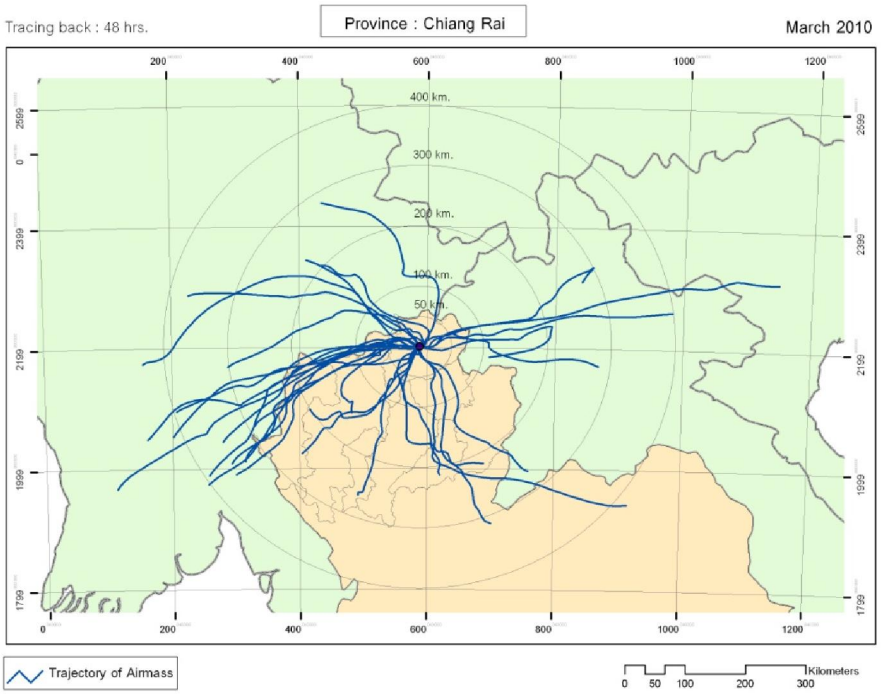

(d)

Figure 5.9 (Continued -For the CR1 station).

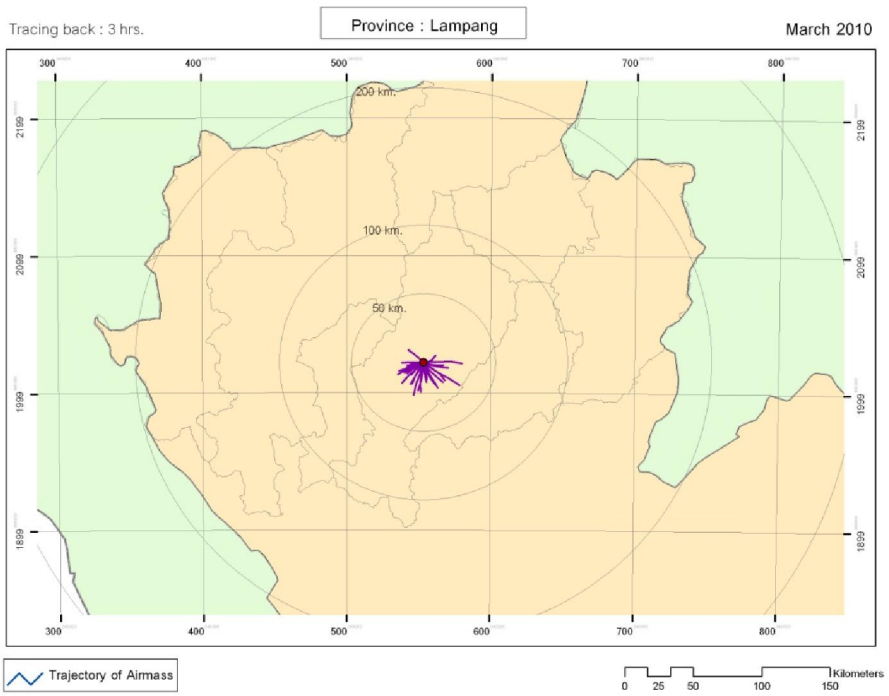

(a)

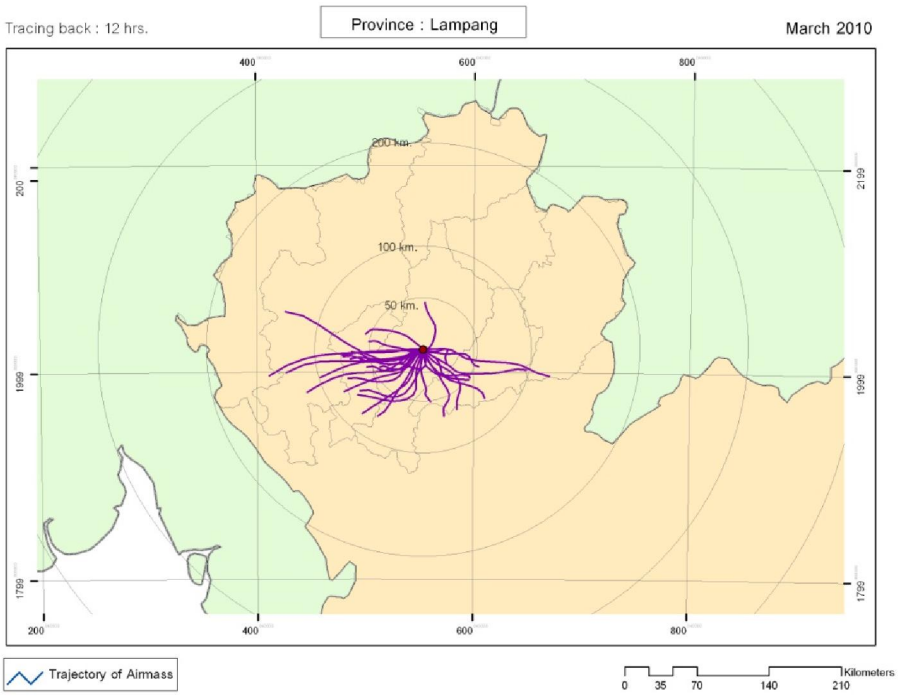

(b)

Figure 5.10 Back trajectory maps for the LPA1 station in Lampang Province (during March 2010) over the (a) 3, (b) 12, (c) 24, and (d) 48-hour periods.

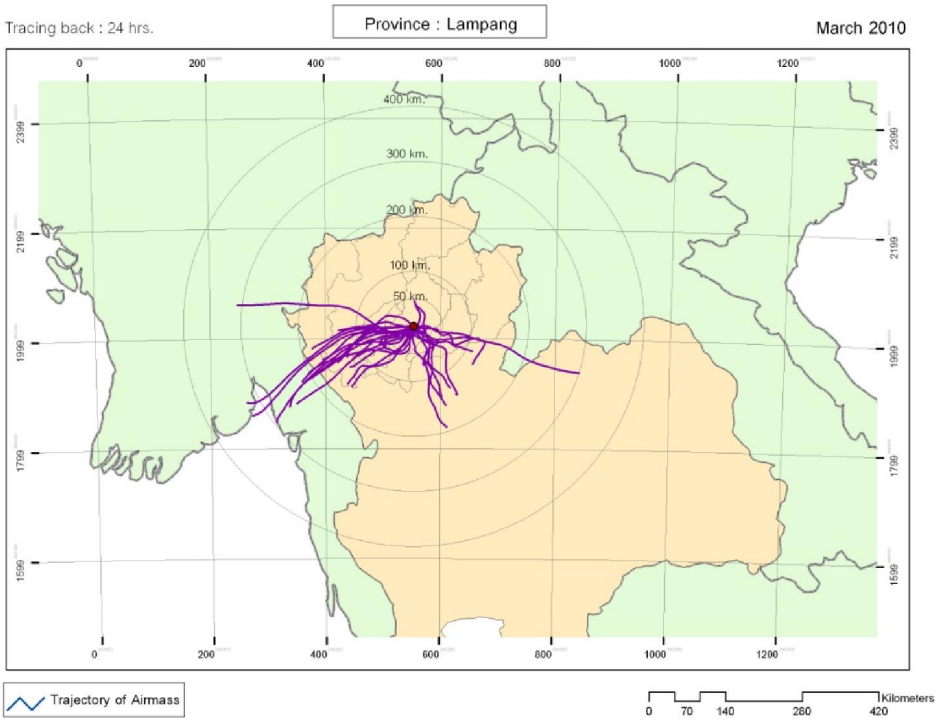

(c)

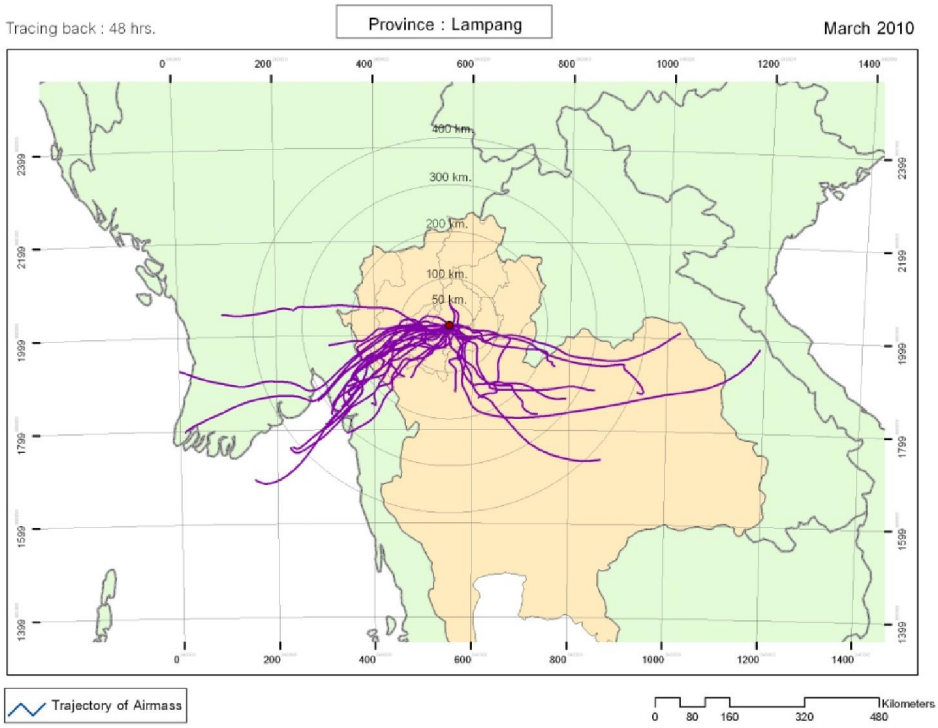

(d)

Figure 5.10 (Continued -For the LPA1 station).

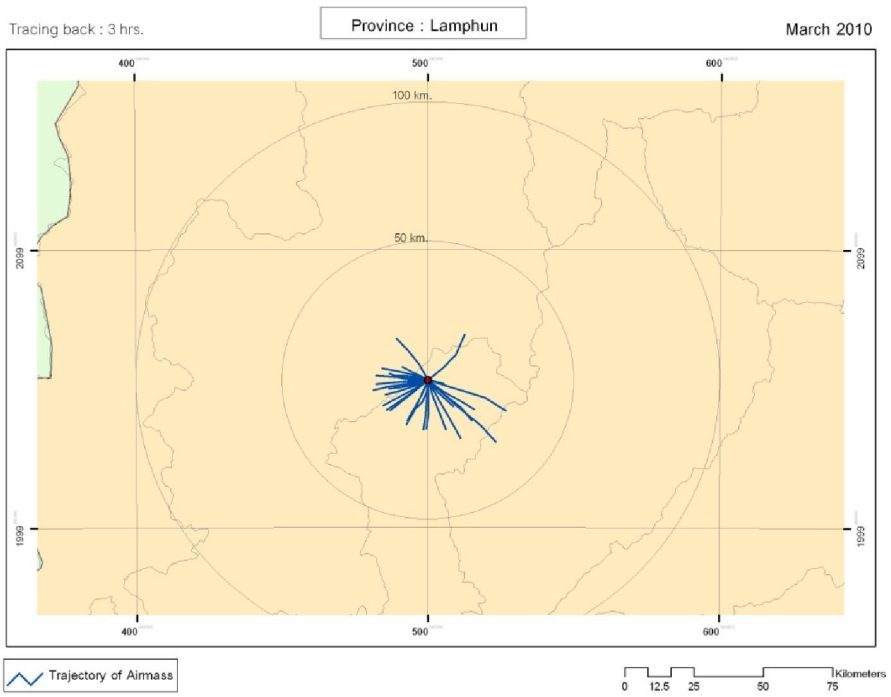

(a)

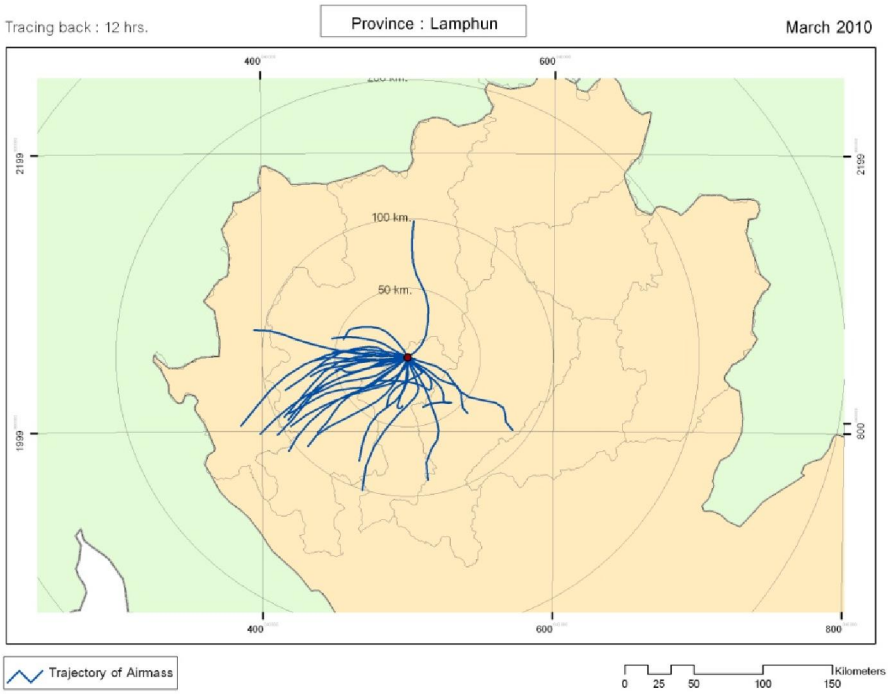

(b)

Figure 5.11 Back trajectory maps for the LPH1 station in Lamphun Province (during March 2010) over the (a) 3, (b) 12, (c) 24, and (d) 48-hour periods.

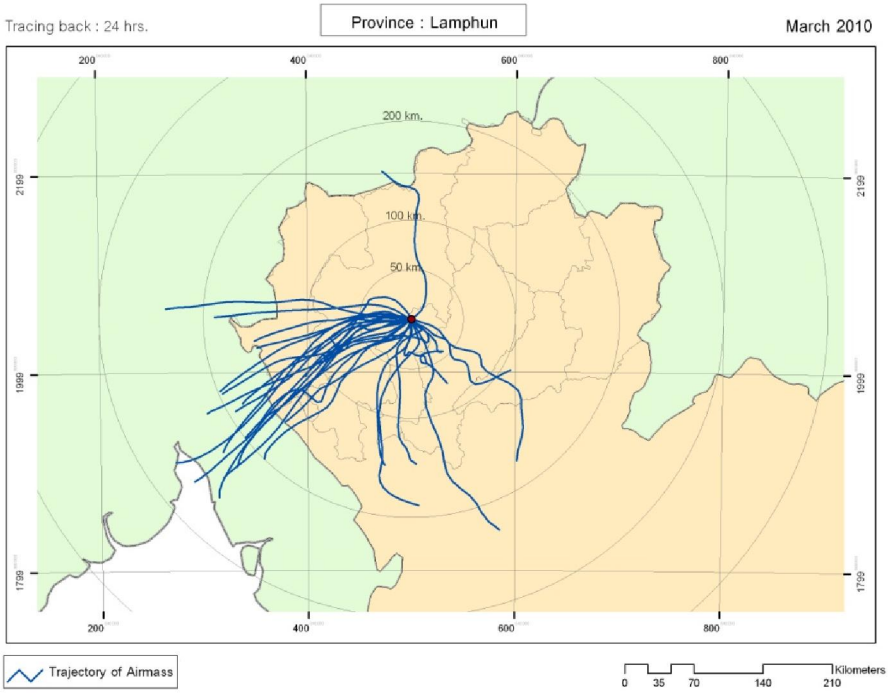

(c)

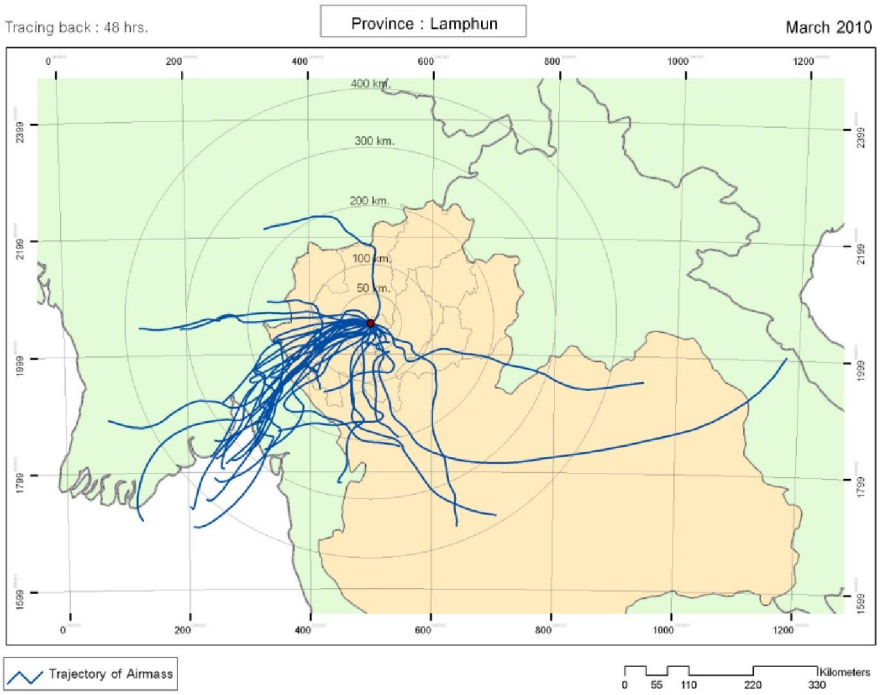

(d)

Figure 5.11 (Continued -For the LPH1 station).

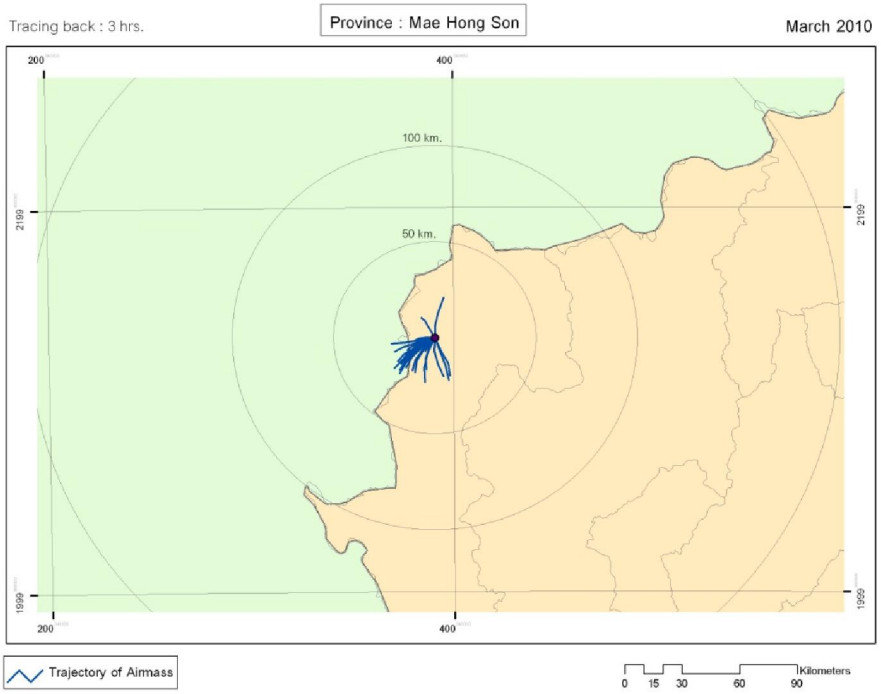

(a)

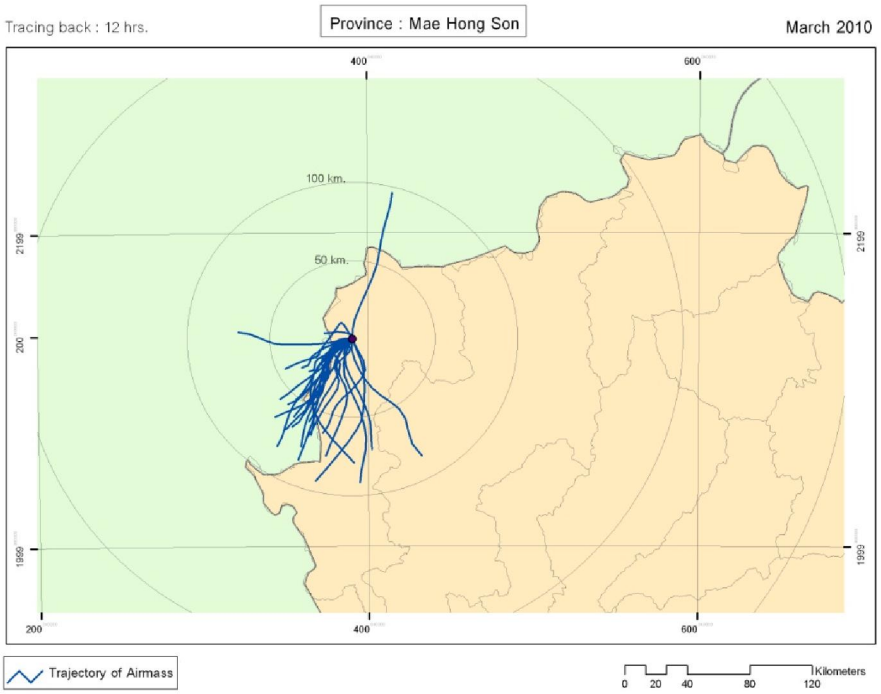

(b)

Figure 5.12 Back trajectory maps for the MHS1 station in Mae Hong Son Province (during March 2010) over the (a) 3, (b) 12, (c) 24, and (d) 48-hour periods.

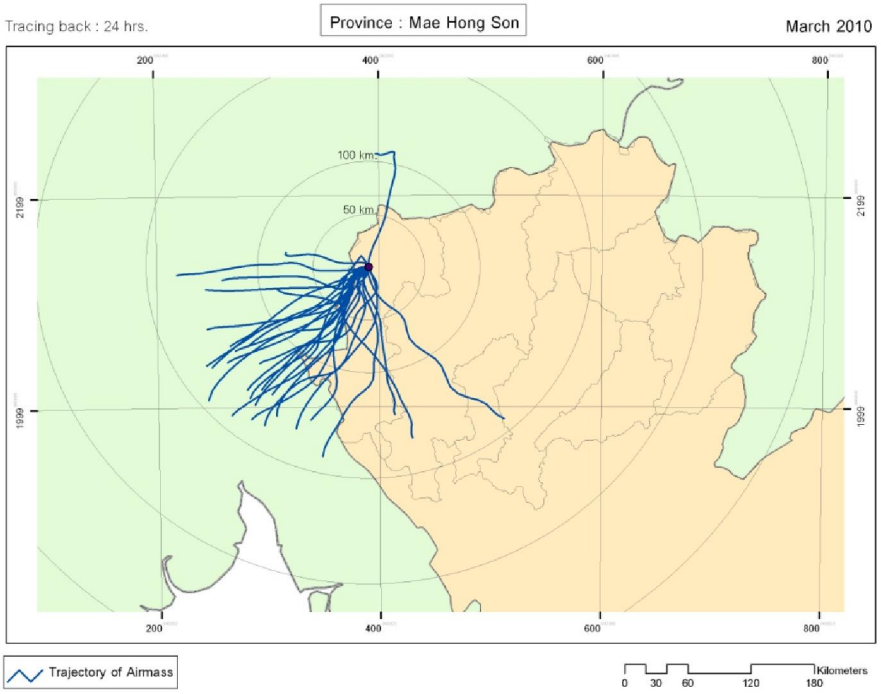

(c)

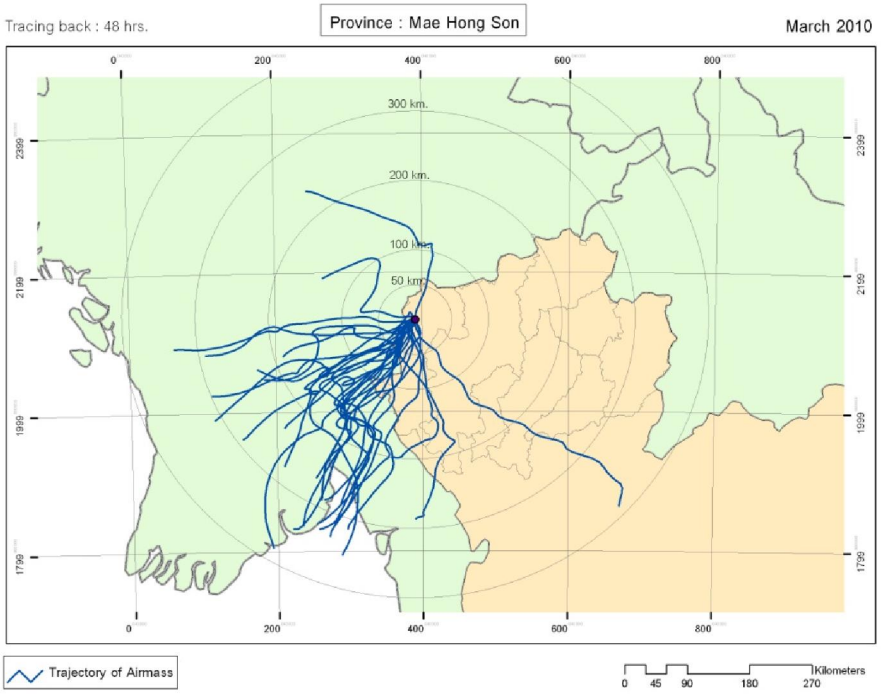

(d)

Figure 5.12 (Continued -For the MHS1 station).

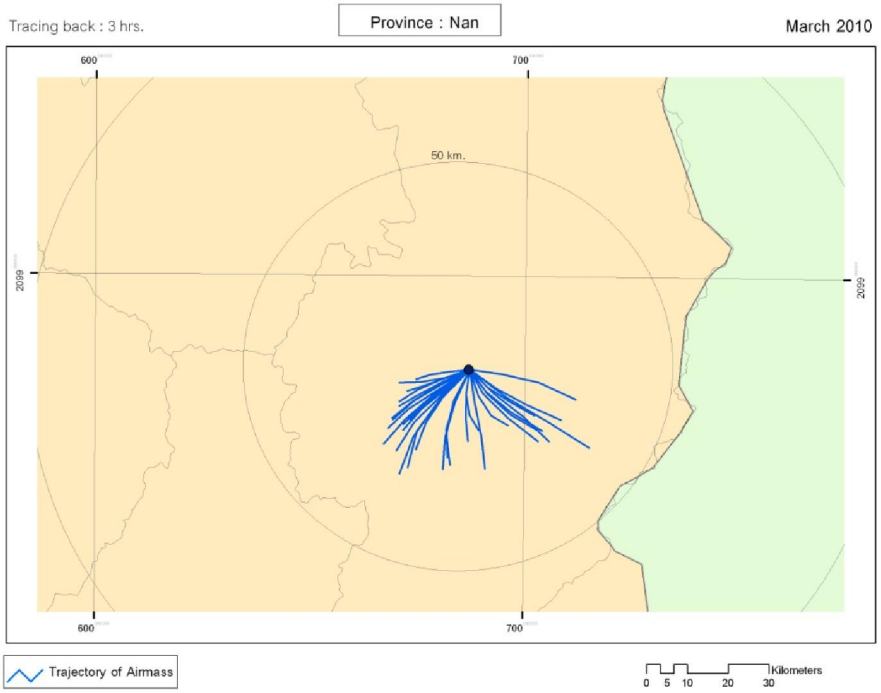

(a)

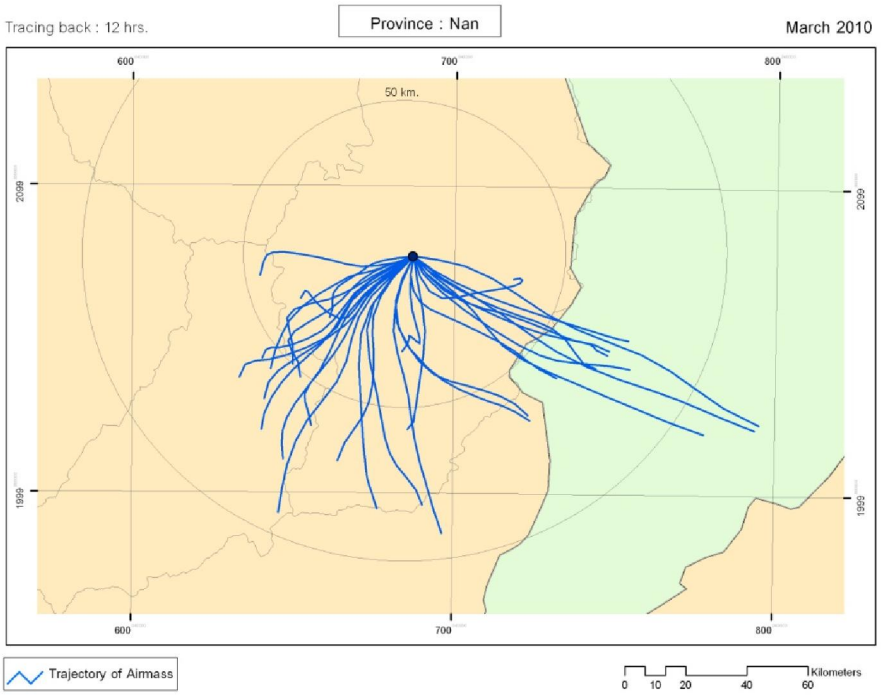

(b)

Figure 5.13 Back trajectory maps for NAN1 station in Nan Province (during March 2010) over the (a) 3, (b) 12, (c) 24, and (d) 48-hour periods.

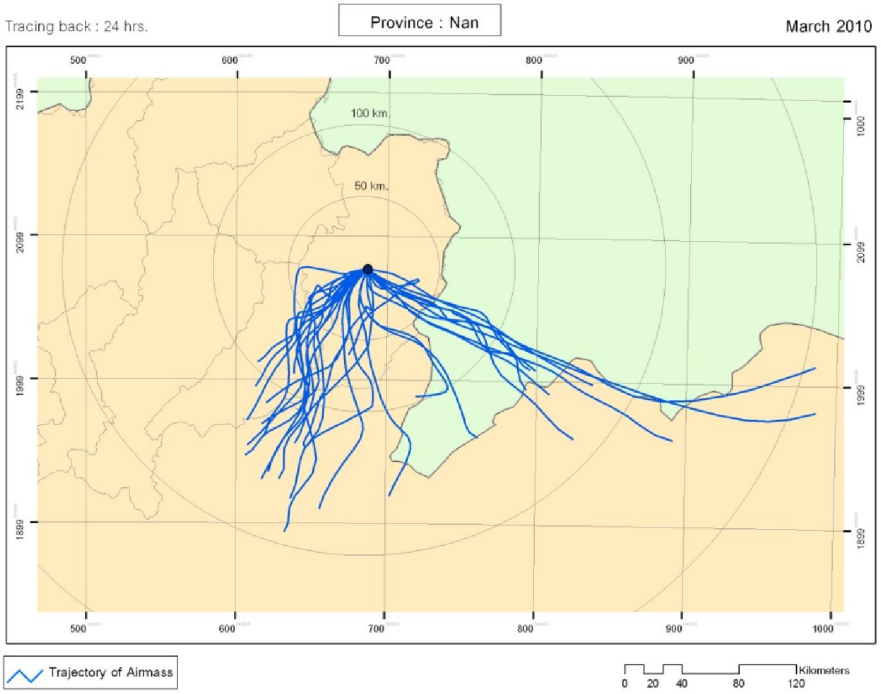

(c)

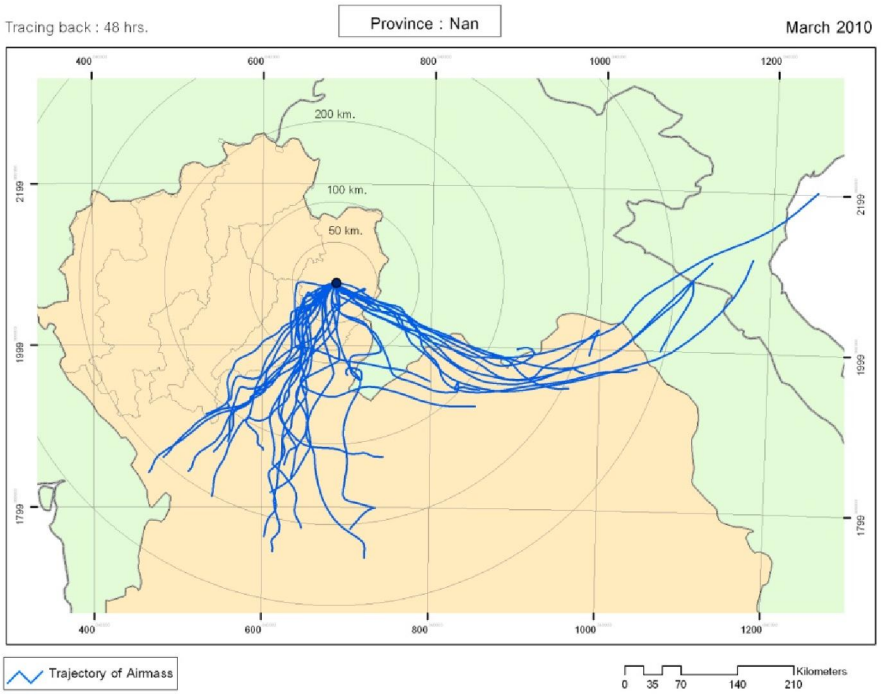

(d)

Figure 5.13 (Continued -For the NAN1 station).

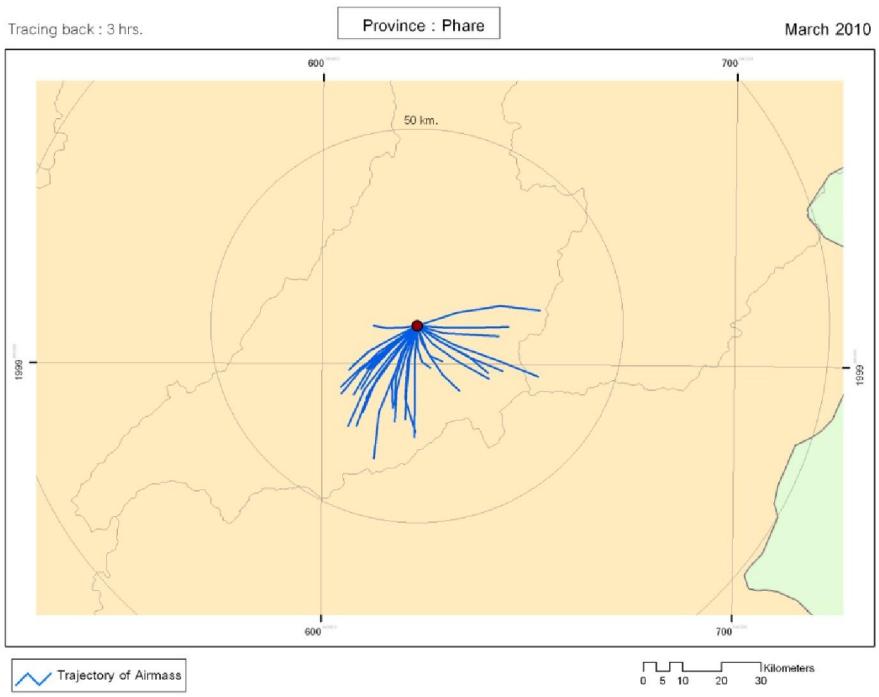

(a)

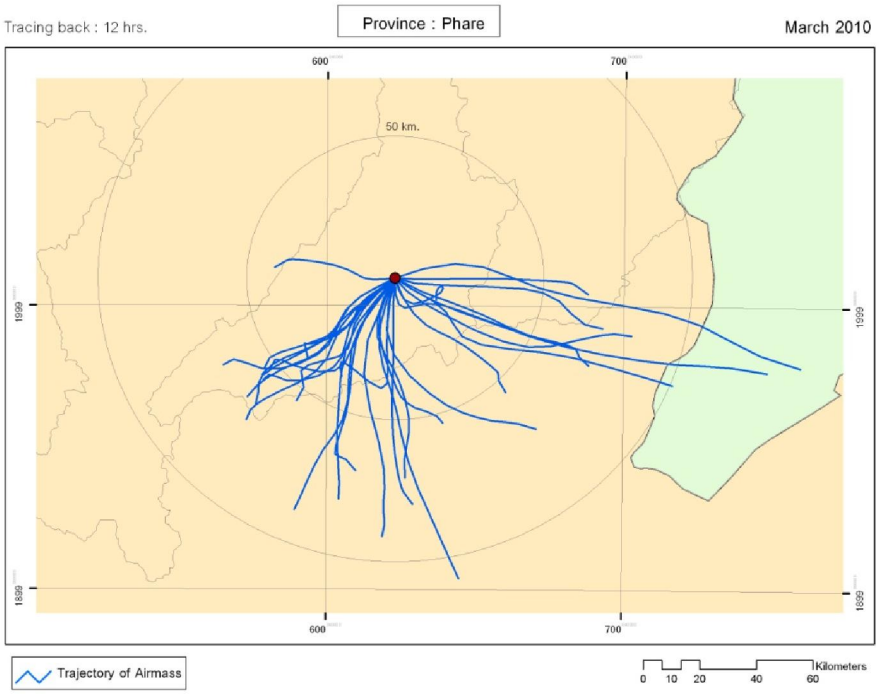

(b)

Figure 5.14 Back trajectory maps for PH1 station in Phrae province (during March 2010) over the (a) 3, (b) 12, (c) 24, and (d) 48-hour periods.

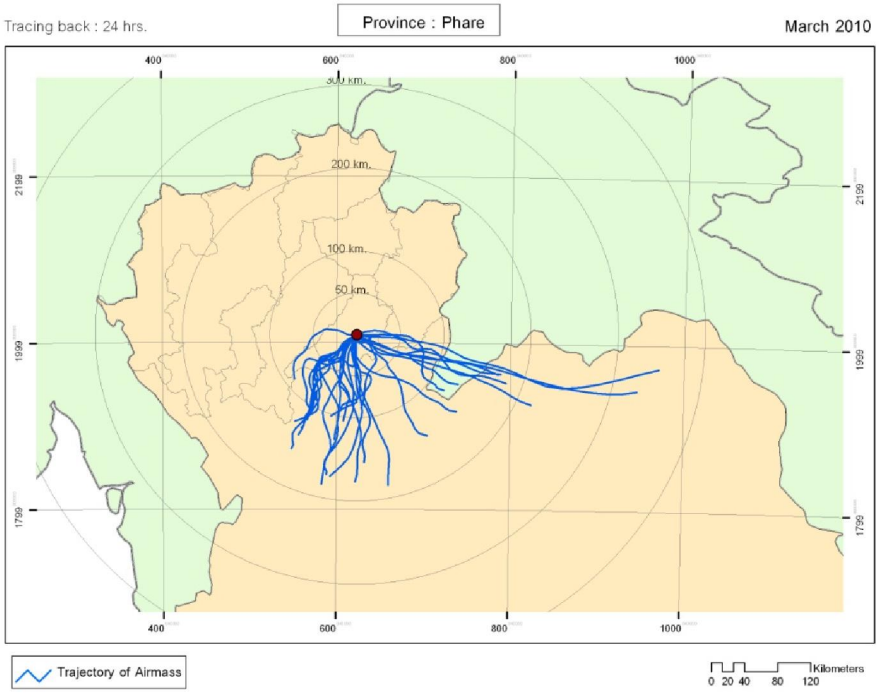

(c)

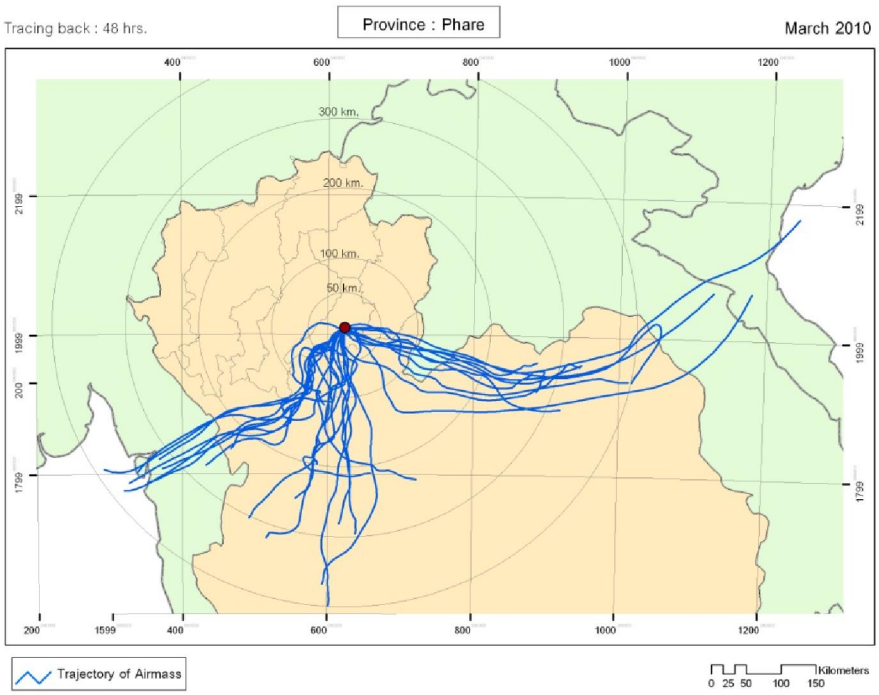

(d)

Figure 5.14 (Continued -For the PH1 station).

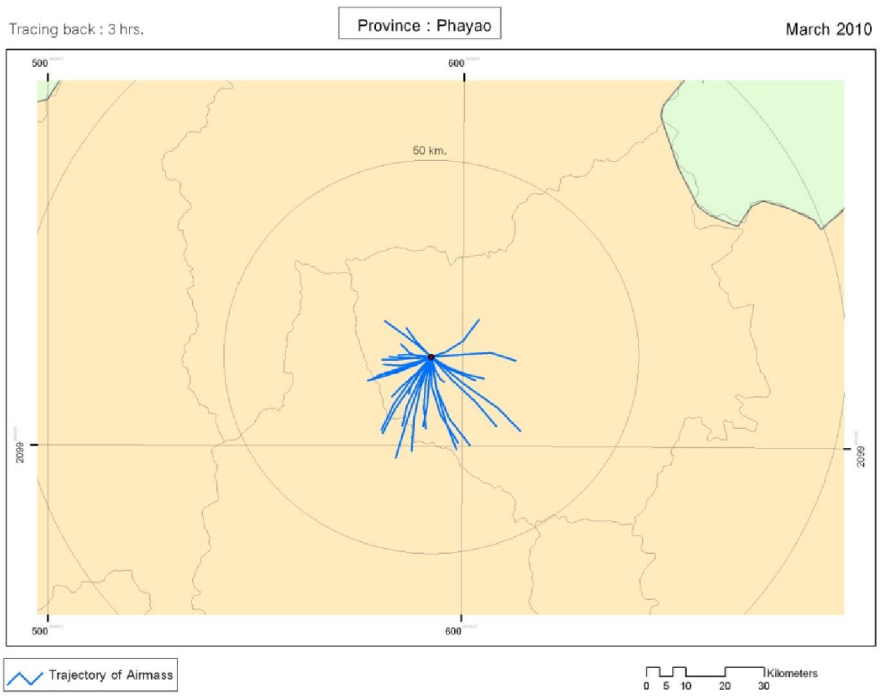

(a)

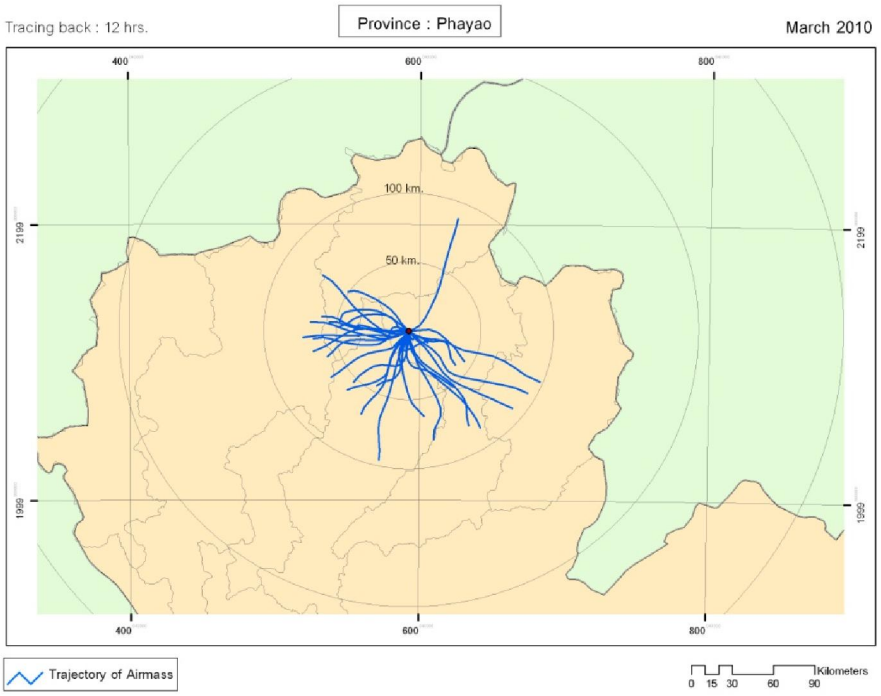

(b)

Figure 5.15 Back trajectory maps for PY1 station in Phayao Province (during March 2010) over the (a) 3, (b) 12, (c) 24, and (d) 48-hour periods.

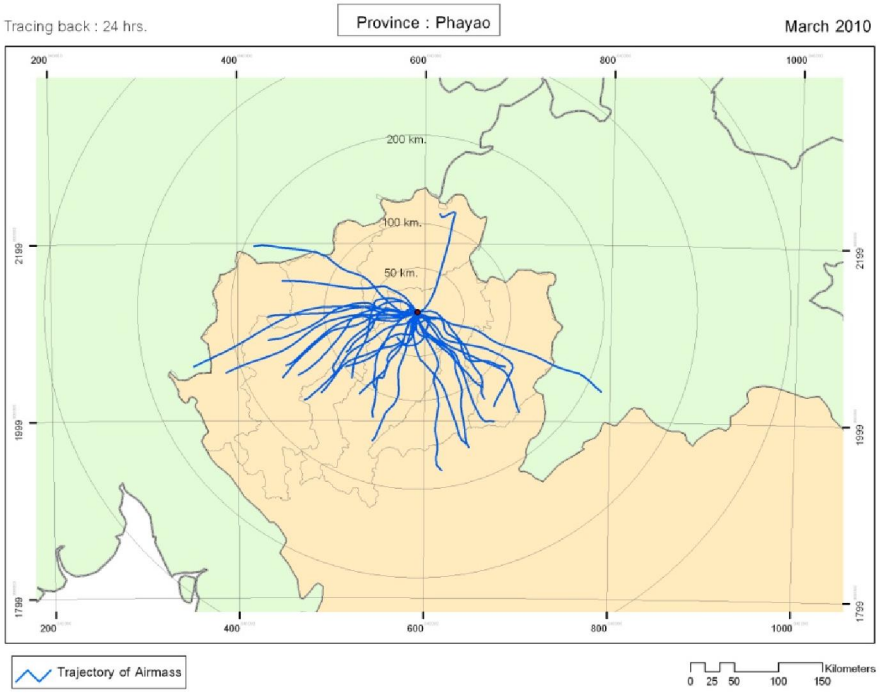

(c)

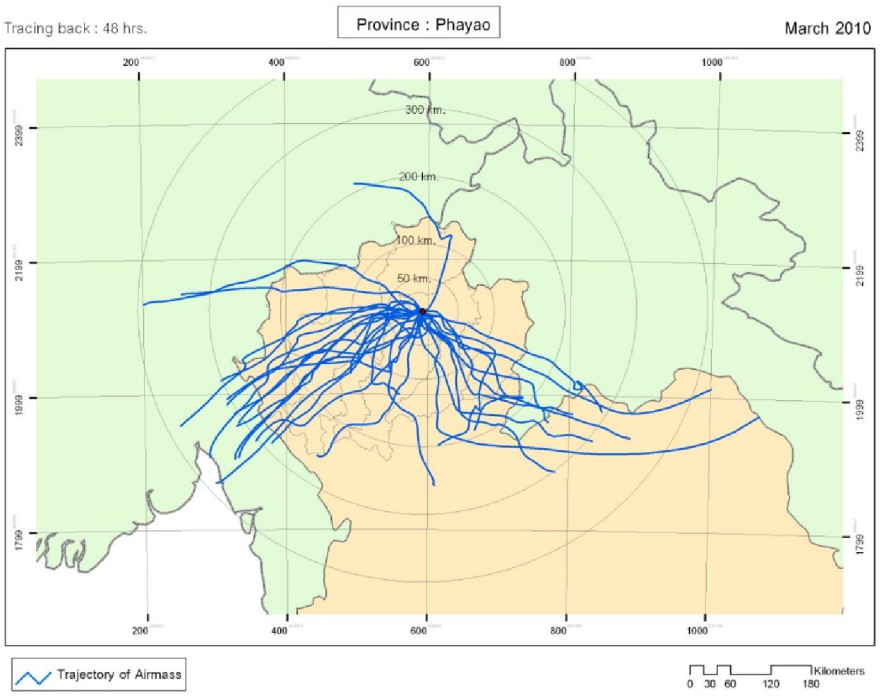

(d)

Figure 5.15 (Continued -for the PY1 station).

For the Chiang Rai Province, observed trajectories of the air mass arrived at the CR1 station had more diverse directions than that of the CM1 station. It was found that for the 12-hr tracing back, origins of most air masses still located within northen Thailand but for longer evaluated periods, i.e. 24 and 48 hours, these source origins were moved further deep inside both neighbouring countries, Myanmar and Laos, at a distance as far as about 400 kilometers away from the CR1 station (in the 48-hr case). Domestic sources located far down south at distance of up to 300 kilometers were also found prominent in this case.

For the Lampang Province, origins of most air masses arrived at the LPA1 station under the 24-hr tracing back were still located within Thailand territory at distance far as 200 kilometers away. The predominant moving paths are along the west and southwest directions toward Myanmar territory and along the south and southeast directions (mostly for domestic sources). This pattern was also shown for the LPH1 station in Lamphun Province in which the most prominent moving paths are aligned with west and southwest directions deeper inward the Myanmar territory and the second prominent one is the southward direction.

For the Mae Hong Son Province (at MHS1 station), within the first 12 hours of the tracing back process, many of the source origins were still found residing in the country at distance < 100 kilometers away. Hower, for the longer periods, locations of most sources shall move deepeer in Myanmar territory and they can reach distance of more than 300 kilometers away for the 48-hr tracing back. At this time period, very few domestic sources were still identified by the model. The predominant moving paths are along the west/southwest/south directions.

For the Nan (at NAN1 station) and Phrae (at PH1 station), they have similar patterns of the determined back trajectary maps for each time period ranging from 3 to 48 hours, in which, the predominant moving paths of the most air masses are along the southwest/south/southeast directions. Among these, the southeast portion of the trajectorie shall have longest distance in average (upto 500 kilometers for the 48-hr period compared to approximately < 300 km for the majority of other path directions). Major differece between these two provinces is that, for 48-hr period, Nan shall have much less impact from the sources in Myanmar (no source origin identified) than that of Phare due to its location which is more further away from Myanmar border on the far west than that of Phare.

For Phayao Province (at PY1 station), the predominant moving paths are not specifically clustered but distributing along the west/south/east directions as seen in Figure 5.15. For the first 24-hr period, the air mass trajectoris were found originated from the domestic sources within the country only, but influence of the foreign sources situsated in Myanmar was more apparent on the resulted map of the 48-hr back trajectory analysis (due to rather long distance of nearly 400 km of the identified trajectory paths moving toward Myanmar).

In conclusion, during March 2010, the most prominent moving paths of the exmined air masses in the area were along the west/sothwest/south direction toward the referred station which is likely due to influence of the strong southwest monsoon wind usually experianced during that month. Long-distance travelling of the polluted smoke plume originated from the original sources in southern and weatern Myanmar shall have impact to most provinces in the area eventually.

5.2.2 Backward trajectory analysis for 2010 fire season

In this part, mean back trajectories (over 48 hours) of air masses arrived at the referred stations for each province during 2010 fire season were investigated. Results are reported as trajectory maps illustrating six major travelling directions and amount of the associated air mass (in percent) along each particular direction as described in Figures 5.15-5.18 and Tables 5.2-5.4, respectively.

It was foud that, for the entire season, the most dominant directions are west and southwest (as shown in Figure 5.18). Among eight studied provinces, five of them are predominated by the southwestward trajectory, i.e. Chiang Mai (70.5%), Lampang (60.5%), Mae Hong Son (84%), Nan (46.9%), Phrae (46.3%). And the other three are mostly in favor of westward movements, i.e. Chiang Rai (46.2%), Lamphun (69.7%), Phayao (44.2%). From results of the monthly analysis detailed in Tables 5.2 and 5.3, they lead to the summarize of the predominant directions for each province (and each month) as described in Table 5.4.

In can be concluded from this study that high amount of aerosol pollutants observed during 2010 fire season over eight provinces of upper northern Thailand might be originated from both domestic sources located further away down south of the referred station (especially for provinces in the lower part of the area like Phayao or Phare) or the foreign fire sources located beyond the border deep into territory of the neighboring countries, i.e. Myanmar and Laos. The fire events in Mynmar should be of the most worried as they occur in substantial amount each year and the released smoke plume can be effectively carried into the area along the west or southwestern directions under the influence of prevailing southweast monsoon.

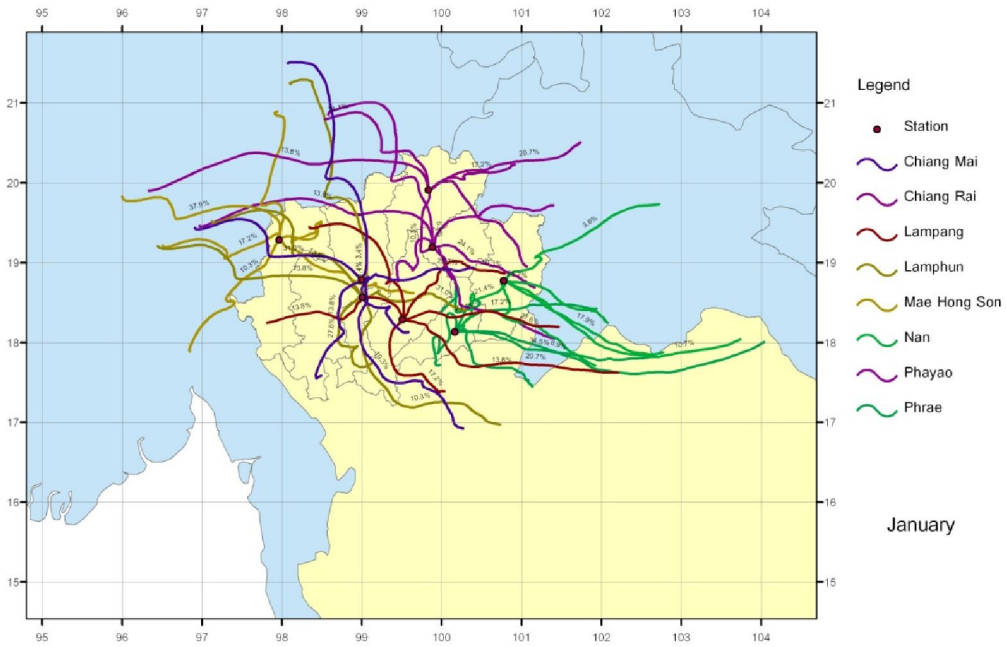

(a)

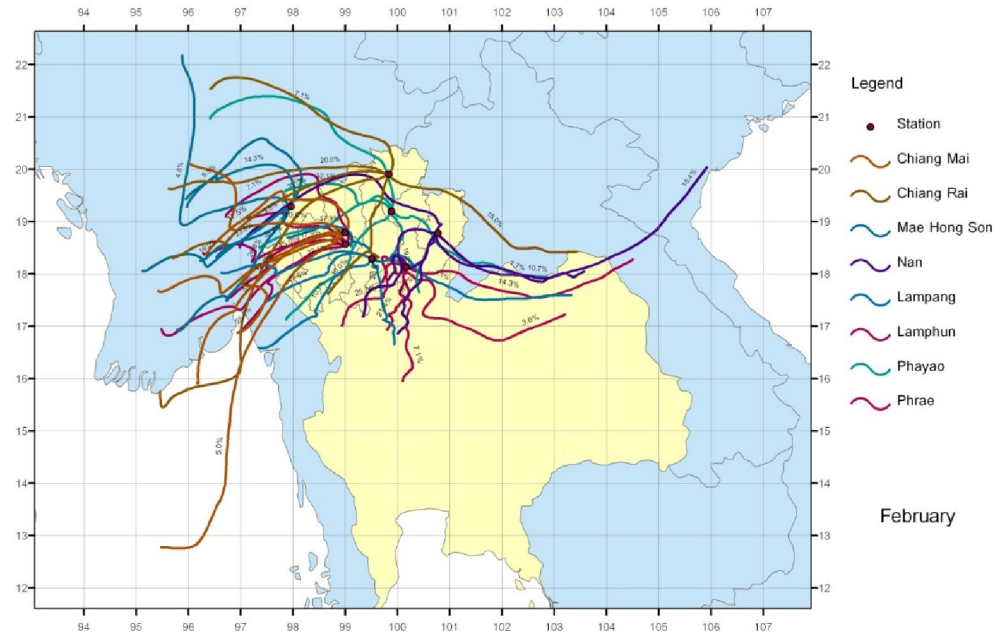

(b)

Figure 5.16 Mean back trajectory maps (48-hr. period) for (a) January, (b) February, (c) March, and (d) April 2010. The presented numbers (in percent) are proportion of data along each direction.

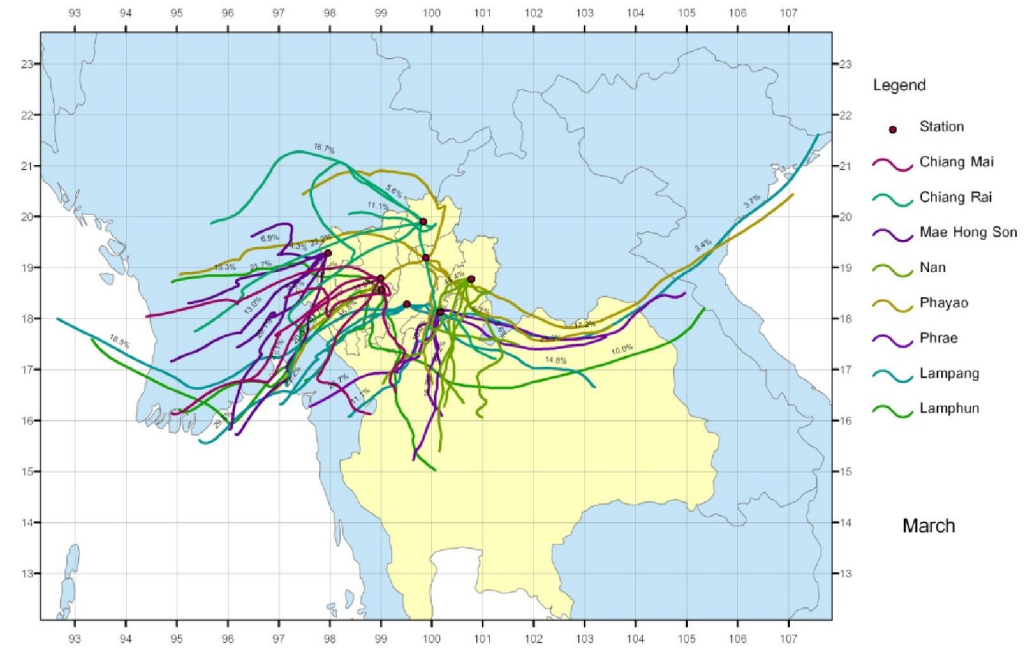

(c)

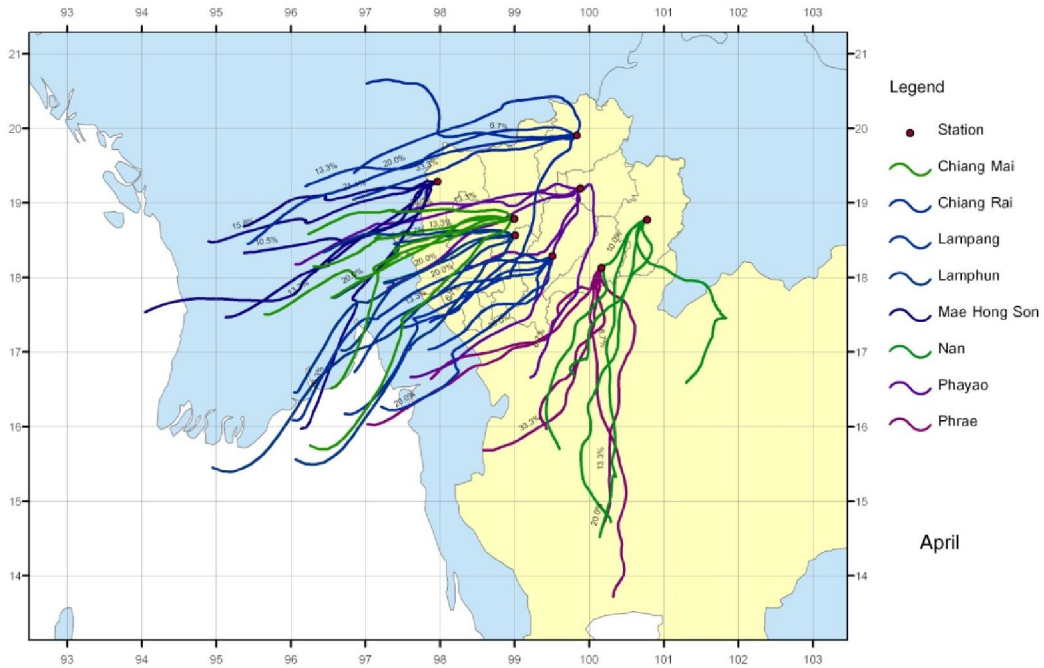

(d)

Figure 5.16 (Continued -For March and April).

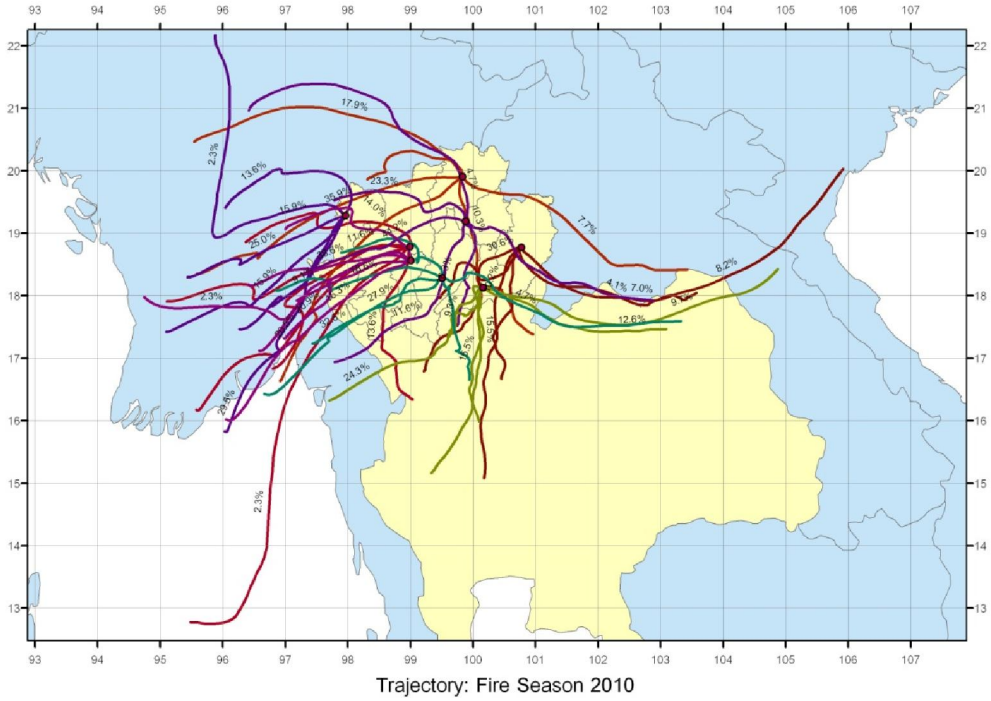

Figure 5.17 Mean back trajectory map (48-hour period) for the 2010 fire season. The presented numbers (in percent) are propotion of data along each direction.

มหาวิทยาลัยเทคโนโลยีสุรนารี

Table 5.2 Percentage of total data associated to each mean back trajectory (or cluster) for each month (from Figure 5.15). Note: DIR ≡ Direction.

Province	Cluster	January		February		March		April	
		DIR	%	DIR	%	DIR	%	DIR	%
Chiang Mai	1	N	3.4	SW	45.0	SW	21.1	SW	13.3
	2	S	20.7	W	17.5	SW	15.8	SW	13.3
	3	E	20.7	SW	5.0	W	21.1	W	26.7
	4	S	10.3	SW	10.0	SW	21.1	SW	20.0
	5	NW	31.0	W	10.0	S	15.8	SW	13.3
	6	SW	13.8	SW	12.5	W	5.3	W	13.3
Chiang Rai	Cluster	DIR	%	DIR	%	DIR	%	DIR	%
	1	NW	24.1	SW	35.0	SW	27.8	W	20.0
	2	SE	13.8	SE	15.0	NW	16.7	W	13.3
	3	E	20.7	NW	15.0	S	16.7	SW	13.3
	4	W	13.8	S	10.0	W	11.1	W	13.3
	5	S	10.3	SW	5.0	SW	22.2	W	6.7
	6	E	17.2	W	20.0	NW	5.6	W	33.3
Lampang	Cluster	DIR	%	DIR	%	DIR	%	DIR	%
	1	N	13.8	W	32.1	W	29.6	SW	20.0
	2	S	17.2	S	7.1	SE	14.8	SW	13.3
	3	E	24.1	NW	17.9	W	18.5	SW	20.0
	4	SE	20.7	W	25.0	S	11.1	SW	13.3
	5	W	13.8	E	7.1	E	3.7	SW	13.3
	6	NE	10.3	SW	10.7	W	22.2	SW	20.0
Lamphun	Cluster	DIR	%	DIR	%	DIR	%	DIR	%
	1	N	3.4	NW	14.3	W	33.3	SW	26.7
	2	S	27.6	W	17.9	S	10.0	W	26.7
	3	E	31.0	NW	28.6	S	10.0	SW	6.7
	4	S	10.3	W	7.1	NW	13.3	SW	20.0
	5	NW	13.8	W	25.0	W	20.0	SW	6.7
	6	NW	13.8	N	7.1	SW	13.3	W	13.3

Table 5.2 (Continued).

Province	Cluster	January		February		March		April	
		DIR	%	DIR	%	DIR	%	DIR	%
Mae Hong Son	1	N	10.3	SW	28.6	SW	13.0	SW	10.5
	2	N	37.9	NE	9.5	SW	26.1	SW	26.3
	3	W	17.2	SW	23.8	SW	21.7	W	21.1
	4	SE	13.8	W	4.8	W	4.3	SW	10.5
	5	E	10.3	SW	19.0	SW	21.7	SW	15.8
	6	SW	10.3	NE	14.3	SW	13.0	SW	15.8
Nan	Cluster	DIR	%	DIR	%	DIR	%	DIR	%
	1	E	35.7	SW	26.9	S	22.2	S	20.0
	2	SW	21.4	SE	7.7	SW	44.4	S	20.0
	3	SE	10.7	W	19.2	S	5.6	S	20.0
	4	S	10.7	SE	15.4	S	16.7	S	10.0
	5	SE	17.9	NW	3.8	S	5.6	S	20.0
	6	NE	3.6	SW	26.9	SW	5.6	S	10.0
Phrae	Cluster	DIR	%	DIR	%	DIR	%	DIR	%
	1	N	10.3	SW	28.6	S	16.7	S	13.3
	2	NE	17.2	E	14.3	E	6.7	S	13.3
	3	E	34.5	S	21.4	SW	26.7	S	13.3
	4	SE	13.8	SW	25	SE	23.3	S	6.7
	5	E	6.9	SE	3.6	S	16.7	S	20.0
	6	S	17.2	S	7.1	S	10.0	S	33.3
Phayao	Cluster	DIR	%	DIR	%	DIR	%	DIR	%
	1	N	6.9	NW	32.1	SW	51.7	SW	20.0
	2	SE	24.1	S	7.1	SE	17.2	S	20.0
	3	NW	13.8	W	35.7	S	17.2	W	13.3
	4	NE	18.8	N	7.1	NW	6.9	S	20.0
	5	NW	13.8	SE	10.7	NE	3.4	W	20.0
	6	SE	27.6	SW	7.1	SE	3.4	S	6.7

Table 5.3 Predominant directions for each province during 2010 fire season.

Month	Order	Provinces							
		CM	CR	LPA	LPH	MHS	NAN	PH	PY
January	1	S/NW	NW	E	S	N	E	E	SE
	2	E	E	SE	E	W	SE	NE/S	NW
February	1	SW	SW	W	W	SW	SW	SW	W
	2	W	W	NW	NW	NE	W	S	NW
March	1	SW	SW	W	W	SW	S	S	SW
	2	W	NW	SE	S	W	SW	SW	SE
April	1	SW	W	SW	SW	SW	S	S	S
	2	W	SW	-	W	W	-	-	W

Table 5.4 Percentage of total data associated to each mean back trajectory (or cluster) for the 2010 fire season (from Figure 5.16). Note: DIR ≡ Direction.

Cluster	Chiang Mai		Chiang Rai		Lampang		Lamphun	
	DIR	%	DIR	%	DIR	%	DIR	%
1	SW	20.5	SW	17.9	SW	27.9	SW	16.3
2	S	13.6	S	10.3	S	4.7	NW	14
3	W	15.9	NW	17.9	SW	32.6	W	20.9
4	SW	38.6	W	35.9	W	18.6	W	25.6
5	SW	2.3	W	10.3	NW	11.6	W	20.9
6	SW	9.1	SE	7.7	E	4.7	W	2.3
Cluster	Mae Hong Son		Nan		Phrae		Phayao	
	DIR	%	DIR	%	DIR	%	DIR	%
1	SW	13.6	S	30.6	S	15.5	W	44.2
2	SW	29.5	SE	4.1	E	9.7	S	9.3
3	NW	13.6	SW	30.6	SW	24.3	NW	23.3
4	SW	25.0	SW	16.3	SW	22.3	SE	7
5	SW	15.9	S	10.2	E	12.6	N	4.7
6	W	2.3	SE	8.2	S	15.5	SW	11.6

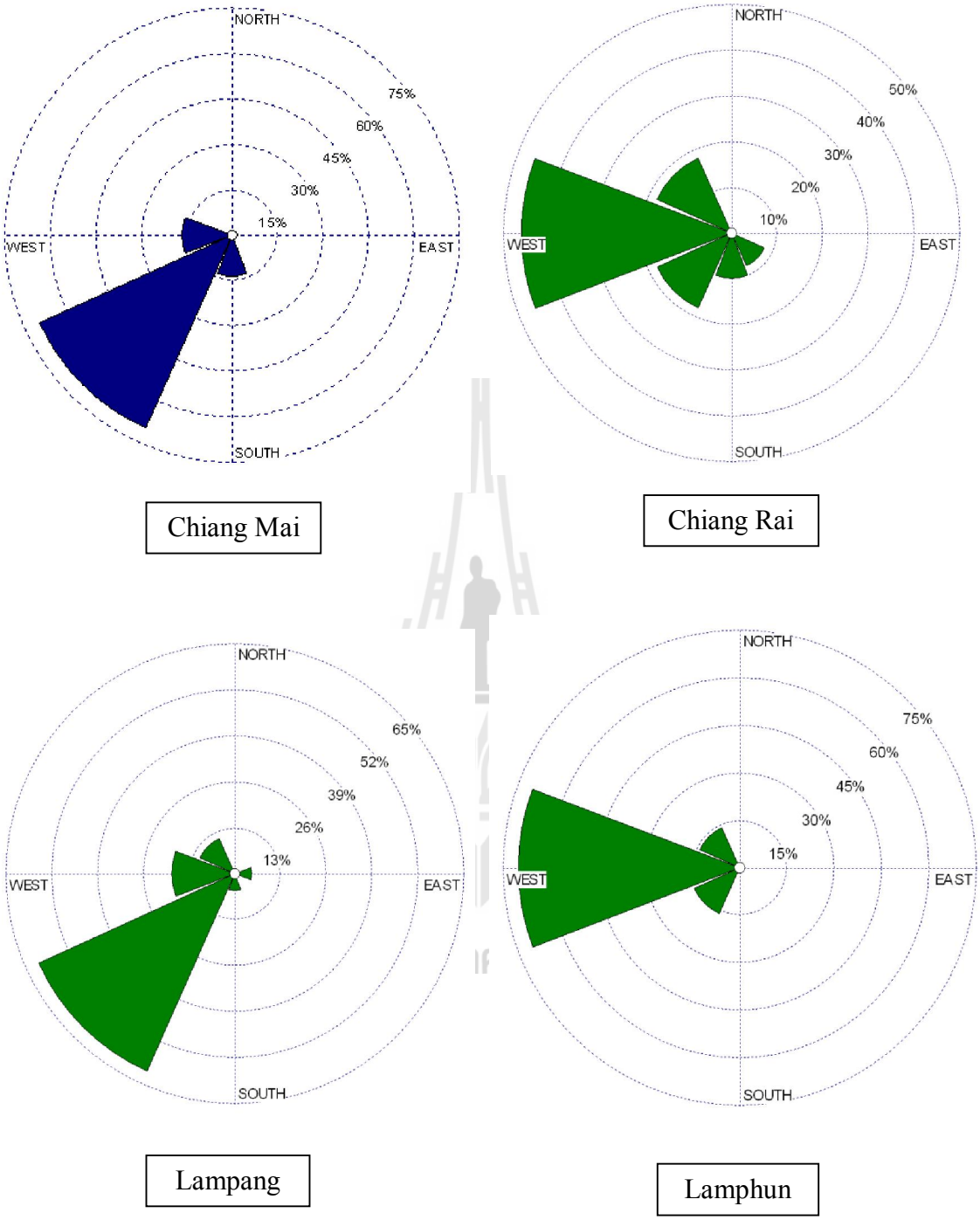

Figure 5.18 Mean back trajectory diagram (48-hour period) for 2010 fire season for all provinces in the study area.

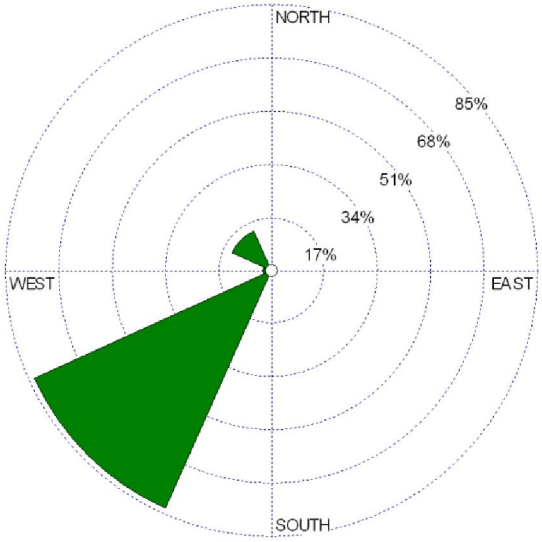

Mae Hong Son

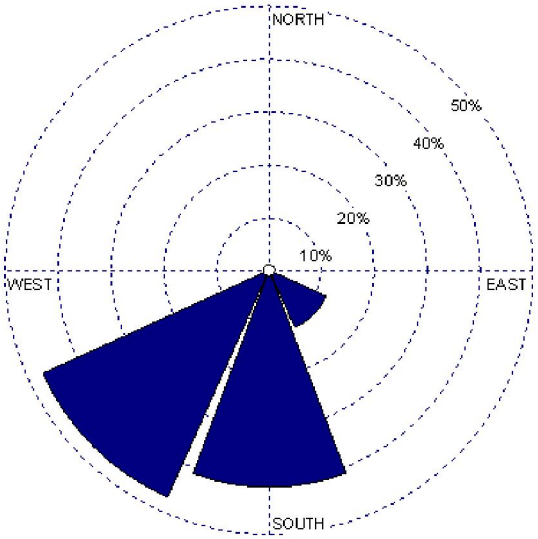

Nan

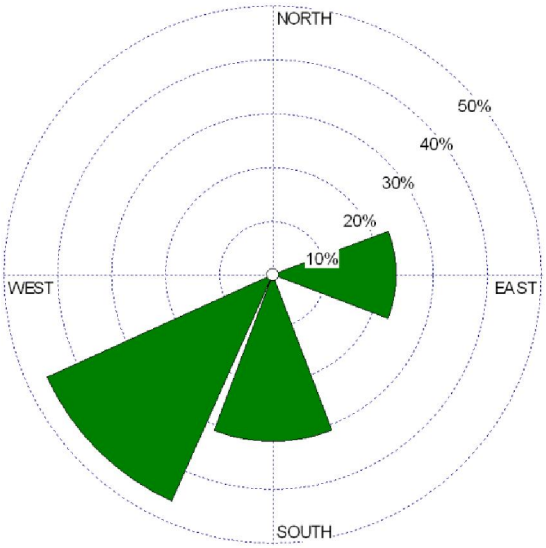

Phrae

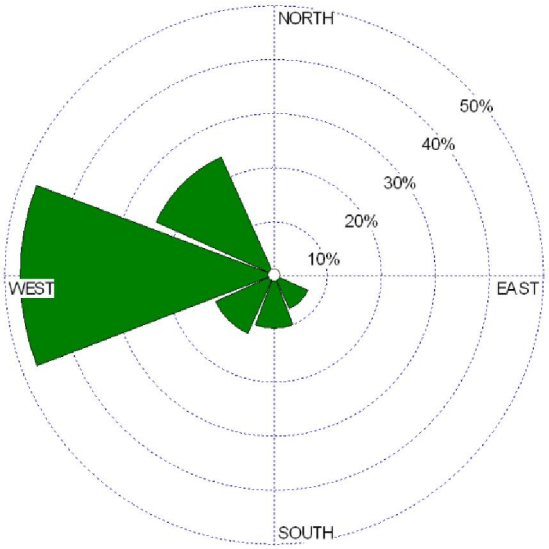

Phayao

Figure 5.18 (Continued).

CHAPTER VI

CONCLUSIONS AND RECCOMENDATIONS

This chapter summarizes the achievements of all the works carried out in this thesis in accordance with the three objectives stated in Chapter I, which are, (1) evaluation of the apparent relationships of the MODIS-based parameters (and AERONET-AOD) and reference PM10 data, (2) derivation and application of the daily NDAI, AOD, PM10 and AQI maps over the study area and (3) application of the HYSPLIT model to the analysis of the fire-induced smoke plume trajectory and dispersion pattern for the 2010 fire season (both forward and backward analysis). Details are as follows.

6.1 Relationships of MODIS-based parameters and PM10 data

The study found a rather strong relation (in terms of R^2) between the MODIS spectral reflectance radiance in the blue band and reference PM10 data in the near-ground air layer ($R^2 = 0.71$). The longer wavelength data, i.e. green and red bands, demonstrate lower significant levels (with $R^2 = 0.616$ and 0.563, respectively) and the MIR band exhibit the least relation (with $R^2 = 0.029$). The linear relationship functions found also support traditional believe that the shorter wavelength should be the most sensitive to changes of the aerosol mixture in the lower atmosphere.

Other chosen parameters also yield satisfactory relationships to the reference PM10 data in use; i.e. the ΔR (Blue) ($R^2 = 0.667$), NDAI ($R^2 = 0.661$), MODIS-AOD

(R^2 =0.72), BAER-AOD (R^2 = 0.784) and the AERONET-AOD (R^2 = 0.86). Among these, the BAER-AOD was considered as being the optimal parameter, due mainly to its high relation level to the reference PM10 data and its high potentiality to formulate the AOD and associated near-ground PM10 maps at a fine spatial resolution of 500 m, which is preferred in the subsequent works (including AQI mapping).

Apart from the aforementioned quality, BAER-AOD data were also found to have a strong relation to the concurrent AERONET-AOD data (R^2 = 0.828) with nearly a 1:1 fit to each other based on the following relation:

$$\text{AERONET} = 1.05(\text{BAER}) - 0.061. \tag{6.1}$$

The R^2 of 0.828 achieved here is fairly comparable to those attained in other reports In addition, MODIS-AOD was also found to have a strong correlation to AERONET-AOD (R^2 = 0.832), but it was not in favored here due to its coarse resolution of 10 km.

6.2 Derivation and application of NDAI, AOD, PM10 and AQI maps

In this part, the NDAI maps were produced and applied first to the study area. NDAI is a new air quality index introduced in this thesis for being a primary indicator of the aerosol pollution severity level found over a particular area. Its definition is:

$$\text{NDAI} = \frac{\text{Blue} - 0.25\text{MIR}}{\text{Blue} + 0.25\text{MIR}}. \tag{6.2}$$

The strong points of NDAI are that it is easy to calculate (from MODIS radiance data) and its relation to the reference PM10 data:

$$\text{PM10} = 300.6\text{NDAI} + 4.527, \tag{6.3}$$

is rather strong (R^2 = 0.661) with low bias at low NDAI values. Its normalized values of -1 to 1 with potential ranging from 0 to 1 for the aerosol-polluted atmosphere make it easy to interpret (like the NDVI parameter that is used for quantifying the amount of vegetation cover over a particular area). In addition, frequent update of the MODIS radiance data (up to four times per day) is also an appealing outlook of the parameter. Relation of the NDAI-derived PM10 data to the actual PM10 data examined during 4^{th}-9^{th} April 2010 attained an R^2 of 0.648 and mean absolute error (MAE) of 10.78% which are considered acceptable.

Then, the AOD maps during 4^{th}-9^{th} April 2010 were formulated for the entire study area using the BAER method with spatial resolution of 500 m, which has rarely been achieved before from the previous studies after an extensive literature review. In this study, standard MODIS-AOD maps at resolution of 10 km were also prepared and then compared with the derived BAER-AOD maps of the same date. It was found that, in general, AOD maps generated from both sources are rather similar in terms of distributing pattern, despite the substantial difference in their spatial scales. However, the BAER-AOD maps were found much superior in terms of the fine details of AOD information, due to their much better resolution (about 20 times better).

The PM10 maps for the entire study area were then produced from the derived BAER-AOD maps using the found relation:

$$PM10 = 227.8(BAER\text{-}AOD) + 1.167. \quad (6.4)$$

These maps were found having impressive agreement to the actual observed data over the same period with R^2 of 0.744 and MAE of 2.2%. It was found from these derived PM10 data that during the 4^{th}-9^{th} of April 2010, most areas of upper northern Thailand

were experienced severe aerosol pollution, especially for provinces located on eastern region of the area, i.e. Nan, Phayao and Chiang Rai. Upper parts of Chiang Mai, Mae Hong Son, Lampang and Phrae were also encountered continuous aerosol pollution. More than 90% of the PM10 data are in range of 100-300 $\mu g/m^3$ with peak values at 175-200 $\mu g/m^3$. Urban area was found more polluted than other LULC types.

This kind of the satellite-based PM10 density map with the spatial resolution of < 1 km has never been reported in the reviewed literature before and this should hugely benefit routine monitoring of the aerosol pollution situation from local to global scales on a daily basis (due to frequent update of the MODIS image mentioned earlier). However, robust use of the BAER-AOD and its associated PM10 mapping method described here still needs to be verified in further works over different locations or different episodes of fire-induced aerosol pollutions of interest.

Derivation and application of AQI data maps

The daily AQI maps for the entire area were produced from the derived PM10 maps (from the BAER-AOD data) based on four chosen methods: PCD standard (for Thailand), US-EPA standard, UK standard and the newly-proposed system. The latter was designed to highlight the PM10 regulating targets introduced by the WHO and to serve as a compromise between the EPA-standard (with rather broad AQI category) and UK standard (with rather narrow AQI category). This system comprises of twelve AQI bands to accommodate observed PM10 data from 0 up to 400 $\mu g/m^3$, principally, with bandwidth of 20 to 50 $\mu g/m^3$. The focus was on the indexing of the PM10 data ranging between 100-300 $\mu g/m^3$, which were found the most during the study period. The new system provides five AQI bands to quantify them (Bands 5-9) while the PCD

gave just approximately one, as did the UK standard, while the US-EPA system gave approximately three bands.

It was found that, the newly-proposed system worked substantially better than other listed systems, especially the PCD and UK systems, as it could provide better details on the general outlook of derived AQI maps for the area. This information is very limited by the use of the PCD or UK standards for PM10 data of 100-300 $\mu g/m^3$ as only small variations can be detected using the PCD system (only a single AQI band mostly identified) and none can be detected using the UK standards (always only one class identified). The use of US-EPA standard gave more dynamic results on the variation of AQI conditions over the area (with three AQI bands available), but still not as good as the newly-proposed system. The most dominant AQI situations discovered from the study are Band 7 (for PM10 = 151-200 $\mu g/m^3$) and 8 (for PM10 = 201-200 $\mu g/m^3$); both bands are classified into the "High" category of this newly-established system. In terms of associated health impact, these situations might be harmful for sensitive group (like children or people with respiratory or lung diseases) similar to the "Unhealthy (for sensitive group)" category being used in the US-EPA standard.

The proposed system is considerably useful for the monitoring of air quality level over large region from local to global scale on daily basis (due to wide covering area and frequent update of the MODIS imagery) to gain comprehensive overview of the aerosol pollution situation at fine scale of 500 m, which is still not commonly fulfilled by other methods known so far. The gained aerosol density map that is classified into 12 levels (or AQI bands) of PM10 concentration under the procedure described in this thesis can be related directly to the pre-evaluated potential health

effects that might be experienced by the people over a particular area. This information can draw the public's attention to the actual situation of the aerosol pollution problem and to raise awareness on its possible impact as well.

6.3 Applications of HYSPLIT model

According to the MODIS active fire maps covering the entire area during the 4^{th}-8^{th} of April, 2010, more than 2500 active fire locations were identifed both within and outside the study area. About 90% of these observed fires located beyond the Thai border where about 40% were situated within Myanmar territory and about 30% in Laos. The forward analysis by the HYSPLIT model indicates that the long-range dispersion of the smoke plumes that originated from fire sources in Myanmar did have a huge impact on the air pollution severity seen over upper northern Thailand, especiallly for provinces located along the Thai/Myanmar border like Mae Hong Son, Chiang Mai, or Chiang Rai. However, provinces located on the eastern side far opposite to the border like Nan or Payao (on the west), also experienced this effect.

In conclusion, the aerosol pollution observed over the study area during the 4^{th}-9^{th} of April, 2010 was influenced by smoke plumes that originated to the west and southwest of the area the most, especially those located in Myanmar territory. After being released from their original sources, these plumes would gradually spread out along the way and often merge to form a large body of aerosol layer that moved continuously under the influence of the prevailing regional winds over the area during that time, which are the northeast monsoon and the southwest monsoon winds. This study indicated that movements of most plumes were under strong influence of the southwest monsoon, which resulted in the predominant eastward or northeastward

traveling pattern reported during that time. In general, the plumes can travel for long distances of up to 300-400 kilometers per day and be move along the controlling wind system before thet completely dissipate within 2-3 days.

According to the back trajectory analysis, the most predominant directions of air mass movement for the 2010 fire season were from the west and southwest. Among the eight studied provinces, southwestward movement was found most superior in five of them, i.e. Chiang Mai (70.5%), Lampang (60.5%), Mae Hong Son (84%), Nan (46.9%), Phrae (46.3%). The other three mostly experianced the westward movements, i.e. Chiang Rai (46.2%), Lamphun (69.7%) and Phayao (44.2%). Dominancy of the SW movement was most recognised in March and April for most provinces. In general, for the 3-hr tracing back, most identified sources situate within radial distance of about 30-40 km distance from the referred station. This distance was then extended to be about 70-100 km and 150-200 km for the 12-hr and 24-hr periods, respectively. For two-day tracing back (48-hr period), locations of the source origins were found at the radial distances of about 300-500 km from the considerred station moving deeper within the territory of the neighboring countries, mostly Myanmar.

It can be concluded that, the high amount of aerosol pollutants observed during 2010 fire season over eight provinces of upper northern Thailand might have originated from both domestic sources of fire activities located south of the preferred station (especially for provinces in the lower part of the area like Phayao or Phrae) or from the foreign fire sources located beyond the Thai border deep into territory of the neighboring countries, i.e. Myanmar and Laos (mostly Myanmar). The fire activities in Mynmar should be of the most worrisome as they occur in substantial amounts

each year during fire season and the released smoke plume can be effectively brought into the area from the western or southwestern directions under the influence of prevailing southweast monsoon, especially in March and April. As a consequence, more detailed investigation on this issue should be carried out in the near future. The result of the foregoing is useful in assessing the probability of obtaining effect from pollution sources of the receptor at different times and its easier to manage the surveillance area.

6.4 Recommendations

The work achieved in this thesis provides initial results on the applications of several standard and newly-proposed methods to the study in field of aerosol pollution monitoring and mapping at a spatial scale of < 1 km, and also on the AQI mapping and implementation for the benefit of public health as a whole. These results indicate very promising usefulness of all the proposed methods or systems in their respective fields and the recommendations for possible further work are as follows.

(1) Applications of the daily BAER-based PM10, AQI maps and population data to estimate the number of people at risk from the aerosol pollution during the fire season and also to predict aerosol-related hotspots, in terms of health concerns, over the region of interest for further prevention and mitigation planning.

(2) Integration of the BAER-based AOD and PM10 maps with data from other sources, like ground-based lidar or CALIPSO satellite, to accumulate more in depth knowledge of aerosol pollution structure and evolution over the area.

(3) Application of the HYSPLIT model to simulate consequences on air quality degradation from the releasing of large smoke plumes from some assumed incidences, e.g. an expansive forest fire in Myanmar over some particular area.

(4) Integration of a BAER-based AOD/PM10 mapping method and the HYSPLIT model to examine potential sources and evolution of the high aerosol pollution found at some cities in Thailand, like Bangkok or Chiang Mai.

REFERENCES

มหาวิทยาลัยเทคโนโลยีสุรนารี

REFERENCES

Ackerman, S., Strabala, K., Menzel, P., Frey, R., Moeller, C., Gumley, L., Baum, B., Seemann, S. W., and Zhang, H. (2006). **Discriminating clear-sky from cloud with MODIS algorithm theoretical basis document (MOD35)** [On-line]. Available: http://modis-atmos.gsfc.nasa.gov/docs/atbd_mod06.pdf.

Alföldy, B., Osán, J., Tóth, Z., Török, S., Harbusch, A., Jahn, C., Emeis, S., and Schäfer, K. (2007). Aerosol optical depth, aerosol composition and air pollution during summer and winter conditions in Budapest. **Science of the Total Environment.** 383(1-3): 141-163.

Andreae, M. O., and Rosenfeld, D. (2008). Aerosol-cloud-precipitation interactions. Part 1. The nature and sources of cloud-active aerosols. **Earth-Science Reviews.** 89(1-2): 13-41.

Ångström, A. (1964). The parameters of atmospheric turbidity. **Tellus.** 16(1): 64-75.

Air Resources Laboratory. (2013). **HYSPLIT4 user's guide-NOAA's air resources laboratory** [On-line]. Available: http://www.arl.noaa.gov/documents/report/hysplit_user_ guide.pdf.

Azri, C., Mabrouk, C., and Medhioub, K. (2009). Diurnal evolutions of nitrogen oxides (NOx), ozone (O3), and PM10 particles at a busy traffic cross-road in the city of Tunis. **Environmental Progress & Sustainable Energy.** 28(1): 143-154.

Beeson, W. L., Abbey, D. E., and Knutsen, S. F. (1998). Long-term concentrations of ambient air pollutants and incident lung cancer in California adults: results from the AHSMOG study. Adventist Health Study on Smog. **Environ Health Perspect.** 106(12): 813-823.

Bellasio, R., Scarpato, S., Bianconi, R., and Zeppa, P. (2012). APOLLO2, a new long range Lagrangian particle dispersion model and its evaluation against the first ETEX tracer release. **Atmospheric Environment.** 57: 244-256.

Berico, M., Luciani, A., and Formignani, M. (1997). Atmospheric aerosol in an urban area-measurements of TSP and PM10 standards and pulmonary deposition assessments. **Atmospheric Environment.** 31(21): 3659-3665.

Bohren C. F., and Huffman, D. (1983). Absorption and scattering of light by small particles. New York: Wiley&Sons.

Brasseur, G. P., Prinn, R. G., and Alexander Pszenny, A. P. (2003). Atmospheric chemistry in a changing world. Berlin: Springer-Verlag.

Brunekreef, B., and Holgate, S. T. (2002). Air pollution and health. **The Lancet.** 360(19): 10.

Bucholtz, A. (1995). Rayleigh-scattering calculations for the terrestrial atmosphere. **Applied Optics.** 34(15): 2765-2773.

Caltrans. (1989). **CALINE4-A dispersion model for predicting air pollutant concentrations near roadways**: California, Department of Transportation. (Final report. November 1984. Revised June 1989).

Charlson, R. J., Schwartz, S. E., Hales, J. M., Cess, R. D., Coakley, J. A., Hansen, J. E., and Hofmann, D. J. (1992). Climate forcing by anthropogenic aerosols. **Science.** 255(5043): 423-430.

Cheng, S., Wang, F., Li, J., Chen, D., Li, M., Zhou, Y., and Ren, Z. (2013). Application of trajectory clustering and source apportionment methods for investigating trans-boundary atmospheric PM10 pollution. **Aerosol and Air Quality Research**. 13(1): 333-342.

Chew, B. N., Chang, C. W., Salinas, S. V., and Liew, S. C. (2007). Remote sensing measurements of aerosol optical thickness and correlation with in-situ air quality parameters during a haze episode in THAILAND. **Proc. 28th Asian Conference on Remote Sensing (ACRS2007)**. (TS27.2). Kuala Lumpur: Curran Associates.

Chin, M., Kahn, R., and Schwartz, S. (2009). **Atmospheric aerosol properties and climate impacts** [On-line]. Available: http://www.climatescience.gov/ Library/sap/sap2-3/default.php.

Chu, D. A., Kaufman, Y. J., Ichoku, C., Remer, L. A., Tanré, D., and Holben, B. N (2002). Validation of MODIS aerosol optical depth retrieval over land. **Geophysical Research Letter.** 29(12): 8007.

Chu, D. A., Kaufman, Y. J., Zibordi, G., Chern, J. D., Mao, J., Li, C., and Holben, B. N. (2003). Global monitoring of air pollution over land from the earth observing system-terra moderate resolution imaging spectroradiometer (MODIS). **Geophysical Research.** 108(4661): ACH 4.1 -7.

Chudnovsky, A. A., Lee, H. J., Kostinski, A., Kotlov, T., and Koutrakis, P. (2012). Prediction of daily fine particulate matter concentrations using aerosol optical depth retrievals from the geostationary operational environmental satellite (GOES). **Journal of the Air & Waste Management Association.** 62(9): 1022-1031.

Curtis, L., Rea, W., Smith-Willis, P., Fenyves, E., and Pan, Y. (2006). Adverse health effects of outdoor air pollutants. **Environment International.** 32(6): 815-830.

Daly, A., and Zannetti, P. (2007). Air pollution modeling - An overview [On-line]. Available: http://www.arabschool.org.sy.

Davis, R. E., Normile, C. P., Sitka, L., Hondula, D. M., Knight, D. B., Gawtry, S. P., Stenger, P. J. (2010). A comparison of trajectory and air mass approaches to examine ozone variability. **Atmospheric Environment.** 44(1): 64-74.

Department for Environment Food and Rural Affairs. (2012). **Daily Air Quality Index** [On-line]. Available: http://uk-air.defra.gov.uk/air-pollution/daqi.

Deuzé, J. L., Bréon, F. M., Devaux, C., Goloub, P., Herman, M., Lafrance, B., Maignan, F., Marchand, A., Nadal, F., Perry, G., and Tanré, D. (2001). Remote sensing of aerosols over land surfaces from POLDER-ADEOS-1 polarized measurements. **Journal of Geophysical Research.** 106(D5): 4913-4926.

Diner, D. J., Braswell, B. H., Davies, R., Gobron, N., Hu, J., Jin, Y., Kahn, R. A., Knyazikhin, Y., Loeb, N., Muller, J.-P., Nolin, A. W., Pinty, B., Schaaf, C. B., Seiz, G., and Stroeve, J. (2005). The value of multiangle measurements for retrieving structurally and radiatively consistent properties of clouds, aerosols, and surfaces. **Remote Sensing of Environment.** 97(4): 495-518.

Dinoi, A., Perrone, M. R., and Burlizzi, P. (2010). Application of MODIS products for air quality studies over southeastern Italy. **Remote Sensing.** 2(7): 1767-1796.

Draxler, R. R. (2004). **HYSPLIT training seminar** [On-line]. Available: http://www.arl.noaa.gov/HYSPLIT_workshop.php.

Draxler, R. R. (2011). **An overview of the HYSPLIT modeling system for trajectory and dispersion applications** [On-line]. Available: http://www.epa.gov/scram001/9thmodconf/draxler.pdf.

Dubovik, O., Smirnov, A., Holben, B. N., King, M. D., Kaufman, Y. J., Eck, T. F., and Slutsker, I. (2000). **Accuracy assessments of aerosol optical properties retrieved from Aerosol Robotic Network (AERONET) Sun and sky radiance measurements** (Vol. 105). Washington, DC: American Geophysical Union.

Eck, T. F., Holben, B. N., Reid, J. S., Dubovik, O., Smirnov, A., O'Neill, N. T., Slutsker, I., and Kinne, S. (1999). Wavelength dependence of the optical depth of biomass burning, urban, and desert dust aerosols. **Journal of Geophysical Research: Atmospheres.** 104(D24): 31333-31349.

Elshout, S. v. d., and Léger, K. (2006). **Comparing urban air quality across borders : A review of existing air quality indices and the proposal of a common alternative.** Rijnmond: Environmental Protection Agency.

Engel-Cox, J. A., Hoff, R. M., and Haymet, A. D. J. (2004). Recommendations on the use of satellite remote-sensing data for urban air quality. **Journal of the Air & Waste Management Association.** 54(11): 1360-1371.

Englert, N. (2004). Fine particles and human health--a review of epidemiological studies. **Toxicology Letters.** 149(1-3): 235-242.

European Union. (2012). **CAQI air quality index-comparing urban air quality across borders** [On-line]. Available: http://www.airqualitynow.eu/ download/CITEAIR-Comparing_Urban_Air_Quality_across_ Borders.pdf.

Fenger, J. (2009). Air pollution in the last 50 years - from local to global. **Atmospheric Environment.** 43(1): 13-22.

Feng, Q., Wu, S., Du, Y., Li, X., Ling, F., Xue, H., and Cai, S. (2010). Variations of PM10 concentrations in Wuhan, China. **Environment Monitoring Assessment.** 2011(176):259–271.

Garivait, S. (2009). **Current aerosol observation network in Thailand** [Slide]. Bankok: The Joint Graduate School of Energy and Environment.

Giglio, L., Descloitres, J., Justice, C. O., and Kaufman, Y. J. (2003). An enhanced contextual fire detection algorithm for MODIS. **Remote Sensing of Environment.** 87: 273-282.

Glantz, P., Kokhanovsky, A., von Hoyningen-Huene, W., and Johansson, C. (2009). Estimating PM2.5 over southern Sweden using space-borne optical measurements. **Atmospheric Environment.** 43(36): 5838-5846.

Goddard Space Flight Center. (2010). **Aerosol Robotic Network** [On-line]. Available: http://aeronet.gsfc.nasa.gov/.

Greenpeace. (2012). **Dangerous breathing, PM2.5: measuring the human health and economic impacts on China's largest cities** [On-line]. Available: http://www.greenpeace.org/eastasia/publications/reports/climate_energy/2012/air-pollution-health-economic/.

Grey, W. M. F., North, P. R. J., Los, S. O., and Mitchell, R. M. (2006). Aerosol optical depth and land surface reflectance from multiangle AATSR measurements: global validation and intersensor comparisons. **Geoscience and Remote Sensing.** 44(8): 2184-2197.

Grosso, N., Ferreira, F., Mesquita, S., Carlos, B., and Eberhard, R. (2007). Chapter 3.1 Improvement in particles (PM10) urban air quality mapping interpolation using remote sensing data. **In C. Borrego and E. Renner (eds.). Developments in Environmental Science.** (pp. 265-274). New York: Elsevier.

Gupta, P., Christopher, S. A., Wang, J., Gehrig, R., Lee, Yc, and Kumar, N. (2006). Satellite remote sensing of particulate matter and air quality assessment over global cities. **Atmospheric Environment.** 40(30): 5880-5892.

Gupta, P., and Christopher, S. A. (2008). Seven year particulate matter air quality assessment from surface and satellite measurements. **Atmospheric Chemistry and Physics.** 8(1): 327-365.

Gupta, P., Khan, M. N., Silva, A. d., and Patadia, F. (2013). MODIS aerosol optical depth observations over urban areas in Pakistan: quantity and quality of the data for air quality monitoring. **Atmospheric Pollution Research.** 4(1): 43-52.

Hansen, J. E., and Travis, L. D. (1974). Light scattering in planetary atmospheres. **Space Science Reviews.** 16(4): 527-610.

Harrison, R. M., and Yin, J. (2000). Particulate matter in the atmosphere: which particle properties are important for its effects on health. **Science of the Total Environment.** 249(2): 85-101.

Hoff, R. M., and Christopher, S. A. (2009). Remote sensing of particulate pollution from space: have we reached the promised land. **Journal of the Air & Waste Management Association.** 59(6): 645-675.

Holben, B. N., Eck, T. F., Slutsker, I., Tanr'e, D., Buis, J. P., Setzer, A., Vermote, E., Reagan, J. A., Kaufman, Y. J., Nakajima, T., Lavenu, F., Jankowiak, I., and Smirnov, A. (1998). AERONET-A federated instrument network and data archive for aerosol characterization. **Remote Sensing of Environment.** 66(1): 1-16.

Holmes, N. S., and Morawska, L. (2006). A review of dispersion modelling and its application to the dispersion of particles: An overview of different dispersion models available. **Atmospheric Environment.** 40(30): 5902-5928.

Hutchison, K. D. (2003). Applications of MODIS satellite data and products for monitoring air quality in the state of Texas. **Atmospheric Environment.** 37(17): 2403-2412.

Hutchison, K. D., Faruqui, S. J., and Smith, S. (2004). The use of MODIS data and aerosol products for air quality prediction. **Atmospheric Environment.** 38(30): 5057-5070.

Hutchison, K. D., Faruqui, S. J., and Smith, S. (2008). Improving correlations between MODIS aerosol optical thickness and ground-based PM2.5 observations through 3D spatial analyses. **Atmospheric Environment.** 42(3): 530-543.

Institute for Atmospheric and Climate Science-ETH. (2012). **Aerosol particles. Institute for Atmospheric and Climate Science, ETH, Switzerland** [On-line]. Available: http://www.iac.ethz.ch/edu/courses/bachelor/vertiefung/atmospheric_physics/Script-2012/Script-aerosols.pdf.

Ichoku, C., Kaufman, Y. J., Remer, L. A., and Levy, R. (2004). Global aerosol remote sensing from MODIS. **Advances in Space Research**. 34(4): 820-827.

Intergovernmental Panel on Climate Change. (2007). **Indirect effects of aerosols on clouds and precipitation** [On-line]. Available: http://www.ipcc.ch/publications_and_data/ar4/wg1/en/ch7s7 -5-2.html.

Jacob, D. J. (1999). **Introduction to atmospheric chemistry.** New Jersey: Princeton University Press.

Jiang, X., Liu, Y., Yu, B., and Jiang, M. (2007). Comparison of MISR aerosol optical thickness with AERONET measurements in Beijing metropolitan area. **Remote Sensing of Environment.** 107(1-2): 45-53.

Jim'enez, E., Linares, C., Rodriguez, L. F., Bleda, M. J., and Diaz, J. (2009). Short-term impact of particulate matter (PM2.5) on daily mortality among the over-75 age group in Madrid (Spain). **Science of the Total Environment.** 407(21): 5486-5492.

Jiemjai Kreasuwun, Chakrit Chodamornsuk, Pakpook Ratjiranukool, and Orawan Wirunvedchayan (2008). **Weather analysis and air pollution warning (in Thai)** [On-line]. Available: http://elibrary.trf.or.th/ project_content.asp? PJID = RDG5130002.

Justice, C. O., Giglio, L., Korontzi, S., Owens, J., Morisette, J. T., Roy, D., Descloitres, J., Alleaume, S., Petitcolin, F., and Kaufman, Y. (2002). The MODIS fire products. **Remote Sensing of Environment.** 83: 244-262.

Kacenelenbogen, M., Le'on, J. F., Chiapello, I. and Tanŕe, D. (2006). Characterization of aerosol pollution events in France using ground-based and POLDER-2 satellite data. **Atmospheric Chemistry and Physics.** 6(12): 4843-4849.

Kacenelenbogen, M., Vaughan, M. A., Redemann, J., Hoff, R. M., Rogers, R. R., Ferrare, R. A., Russell, P. B., Hostetler, C. A., Hair, J. W., and Holben, B. N. (2011). An accuracy assessment of the CALIOP/ CALIPSO version 2/version 3 daytime aerosol extinction product based on a detailed multi-sensor, multi-platform case study. **Atmospheric Chemistry and Physics.** 11(8): 3981-4000.

Kalivitis, N., Gerasopoulos, E., Vrekoussis, M., Kouvarakis, G., Kubilay, N., Hatzianastassiou, N., Vardavas, I., and Mihalopoulos, N. (2007). Dust transport over the eastern Mediterranean derived from Total Ozone Mapping Spectrometer, Aerosol Robotic Network, and surface measurements. **Journal of Geophysical Research: Atmospheres.** 112(D3): D03202.

Kampa, M., and Castanas, E. (2008). Human health effects of air pollution. **Environmental Pollution.** 151(2): 362-367.

Kan, H., and Chen, B. (2004). Particulate air pollution in urban areas of Shanghai, China: health-based economic assessment. **Science of the Total Environment.** 322(1-3): 71-79.

Kant, Y., Ghosh, A. B., Sharma, M. C., Gupta, P. K., Prasad, V. K., Badarinath, K. V. S., and Mitra, A. P. (2000). Studies on aerosol optical depth in biomass burning areas using satellite and ground-based observations. **Infrared Physics & Technology.** 41(1): 21-28.

Kaskaoutis, D. G., and Kambezidis, H. D. (2006). Investigation into the wavelength dependence of the aerosol optical depth in the Athens area. **Quarterly Journal of the Royal Meteorological Society.** 132(620): 2217-2234.

Karnieli, A., Kaufman, Y. J., Remer, A., and Andrew, A. (2001). AFRI - aerosol free vegetation index. **Remote Sensing of Environment.** 77(1): 10-21.

Kaskaoutis, D. G., Kosmopoulos, P. G., Kambezidis, H. D., and Nastos, P. T. (2010). Identification of the aerosol types over Athens, Greece: The Influence of Air-Mass Transport. **Advances in Meteorology.** 2010: 1-15.

Kaufman, Y. J., Andrew E. W., Remer, L. A., Bo-Cai Gao, Rong-Rong Li, and Luke Flynn. (1997). The MODIS 2.1- μm channel-correlation with visible reflectance for use in remote sensing of aerosol. **Geoscience and Remote Sensing**. 35(5): 1286-1298.

Kaufman, Y. J., Tanŕe, D., Remer, L. A., Vermote, E. F., Chu, D. A., and Holben, B. N. (1997). Operational remote sensing of tropospheric aerosol over land from EOS moderate resolution imaging spectroradiometer. **Geophysical Research.** 102(D14): 17,051-17,067.

Kaufman, T. J., Gobron, N., Pinty, B., Widlowski, J. L., and Verstraete, M. M. (2002). Relationship between surface reflectance in the visible and mid-IR used in MODIS aerosol algorithm. **Geophysical Research Litter.** 29(23): 311- 315.

Kaufman, Y. J., Tanŕe, D., and Boucher, O. (2002). A satellite view of aerosols in the climate system. **The Nature.** 419(6903): 215-223.

Kawata, Y., Fukui, H., Takemata, K., and Takeuchi, N. (2005). Surface reflectance ratios between visible and infrared bands of satellite images over land areas in Japan for retrieval of aerosol optical thickness. **Advances in Space Research.** 36(5): 773-777.

Kim Oanh, N. T., Upadhyay, N., Zhuang, Y. H., Hao, Z. P., and Murthy, D. V. S. (2006). Particulate air pollution in six Asian cities: Spatial and temporal distributions, and associated sources. **Atmospheric Environment.** 40(18): 3367-3380.

Kishi, H., Takeuchi, W., and Sawada, H. (2008). Exhaust emissions assessment over asian megacities with satellite remote sensing and city traffic modeling. 29th Asian conference on remote sensing (ACRS), Colombo, Sri Lanka.

Koelemeijer, R. B. A., Homan, C. D., and Matthijsen, J. (2006). Comparison of spatial and temporal variations of aerosol optical thickness and particulate matter over Europe. **Atmospheric Environment.** 40: 5304–5315.

Kokhanovsky, A. A., and Leeuw, G. H. (2009). **Satellite aerosol remote sensing over land.** Berlin: Springer.

Kokhanovsky, A. A., Breon, F. M., Cacciari, A., Carboni, E., and Diner, D. (2007). Aerosol remote sensing over land: A comparison of satellite retrievals using different algorithms and instruments. **Atmospheric Research.** 85(3-4): 372-394.

Krecl, P., Strom, J., and Johansson, C. (2008). Diurnal variation of atmospheric aerosol during the wood combustion season in Northern. **Atmospheric Environment.** 42: 4113-4125.

Kumar, N., Chu, A., and Foster, A. (2007). An empirical relationship between PM2.5 and aerosol optical depth in Delhi Metropolitan. **Atmospheric Environment.** 41(21): 4492-4503.

Kusmierczyk-Michulec, J. (2011). Optical Measurements of Atmospheric Aerosols in Air Quality Monitoring. In D. Popovic (ed.), **Air Quality - Models and Applications** (pp. 153-172). Rijeka, Croatia: In Tech.

Land Development Department. (2007). **Digital Land Use Maps** [CD]. Bangkok: Office of Soil Survey and Land Use Planning.

Langkulsen, U., Jinsart, W., Karita, K., and Yano, E. (2006). Health effects of respirable particulate matter in Bangkok schoolchildren. **International Congress Series.** 1294: 197-200.

Lee, H., Park, S. S., Kim, K. W., and Kim, Y. J. (2008). Source identification of PM2.5 particles measured in Gwangju, Korea. **Atmospheric Research.** 88(3-4): 199-211.

Lee, K. H., Kim, J. E., Kim, Y. J., Kim, J., and von Hoyningen-Huene, W. (2005). Impact of the smoke aerosol from Russian forest fires on the atmospheric environment over Korea during May 2003. **Atmospheric Environment.** 39(1): 85-99.

Lee, K. H., Kim, Y. J., and Kim, M. J. (2006). Characteristics of aerosol observed during two severe haze events over Korea in June and October 2004. **Atmospheric Environment.** 40(27): 5146-5155.

Lee, K. H., Kim, Y. J., von Hoyningen-Huene, W., and Burrow, J. P. (2007). Spatio-temporal variability of satellite-derived aerosol optical thickness over Northeast Asia in 2004. **Atmospheric Environment.** 41(19): 3959-3973.

Lee, K. H., Lee, D. H., Kim, Y. J., and Kim, J. (2008). MODIS 500 × 500-m2 Resolution Aerosol Optical Thickness Retrieval and Its Application for Air Quality Monitoring. In Y. J. Kim & U. Platt (eds.). **Advanced Environmental Monitoring** (pp. 217-230). London: Springer-Verlag.

Lee, K. H., Park, S. S., Kim, K. W., and Kim, Y. J. (2008). Source identification of $PM_{2.5}$ particles measured in Gwangju, Korea. **Atmospheric Research.** 88(3-4): 199-211.

Lee, K. H., Kim, Y. J., Li, Z., and Kokhanovsky, A. (2009). Atmospheric Aerosol Monitoring from Satellite Observations: A History of Three Decades. In Y. J. Kim, U. Platt, M. B. Gu and H. Iwahashi (eds.). **Atmospheric and Biological Environmental Monitoring** (pp. 13-38). New York: Springer.

Levin, Z., and Cotton, W. R. (eds.). (2009). **Aerosol pollution impact on precipitation: A scientific review**. London: Springer-Verlag.

Li, C., Lau, A. K. H., Mao, J., and Chu, D. A. (2005). Retrieval, validation, and application of the 1-km aerosol optical depth from MODIS measurements over Hong Kong. **Geoscience and Remote Sensing.** 43(11): 2650-2658

Lim, S. S., Vos, T., Flaxman, A. D., Danaei, G., Shibuya, K., Adair-Rohani, H., AlMazroa, M. A., Amann, M., Anderson, H. R., Andrews, K. G., Aryee, M., Atkinson, C., Bacchus, L. J., Bahalim, A. N., Balakrishnan, K., Balmes, J., Barker-Collo, S., Baxter, A., Bell, M. L., Blore, J. D., Blyth, F., Bonner, C., Borges, G., Bourne, R., Boussinesq, M., Brauer, M., Brooks, P., Bruce,

N. G., Brunekreef, B., Bryan-Hancock, C., Bucello, C., Buchbinder, R., Bull, F., Burnett, R. T., Byers, T. E., Calabria, B., Carapetis, J., Carnahan, E., Chafe, Z., Charlson, F., Chen, H., Chen, J. S., Cheng, A. T., Child, J. C., Cohen, A., Colson, K. E., Cowie, B. C., Darby, S., Darling, S., Davis, A., Degenhardt, L., Dentener, F., Des Jarlais, D. C., Devries, K., Dherani, M., Ding, E. L., Dorsey, E. R., Driscoll, T., Edmond, K., Ali, S. E., Engell, R. E., Erwin, P. J., Fahimi, S., Falder, G., Farzadfar, F., Ferrari, A., Finucane, M. M., Flaxman, S., Fowkes, F. G. R., Freedman, G., Freeman, M. K., Gakidou, E., Ghosh, S., Giovannucci, E., Gmel, G., Graham, K., Grainger, R., Grant, B., Gunnell, D., Gutierrez, H. R., Hall, W., Hoek, H. W., Hogan, A., Hosgood, H. D., Hoy, D., Hu, H., Hubbell, B. J., Hutchings, S. J., Ibeanusi, S. E., Jacklyn, G. L., Jasrasaria, R., Jonas, J. B., Kan, H., Kanis, J. A., Kassebaum, N., Kawakami, N., Khang, Y. H., Khatibzadeh, S., Khoo, J., Kok, C., Laden, F., Lalloo, R., Lan, Q., Lathlean, T., Leasher, J. L., Leigh, J., Li, Y., Lin, J. K., Lipshultz, S. E., London, S., Lozano, R., Lu, Y., Mak, J., Malekzadeh, R., Mallinger, L., Marcenes, W., March, L., Marks, R., Martin, R., McGale, P., McGrath, J., Mehta, S., Memish, Z. A., Mensah, G. A., Merriman, T. R., Micha, R., Michaud, C., Mishra, V., Hanafiah, K. M., Mokdad, A. A., Morawska, L., Mozaffarian, D., Murphy, T., Naghavi, M., Neal, B., Nelson, P. K., Nolla, J. M., Norman, R., Olives, C., Omer, S. B., Orchard, J., Osborne, R., Ostro, B., Page, A., Pandey, K. D., Parry, C. D. H., Passmore, E., Patra, J., Pearce, N., Pelizzari, P. M., Petzold, M., Phillips, M. R., Pope, D., Pope, C. A., Powles, J., Rao, M., Razavi, H., Rehfuess, E. A., Rehm, J. T., Ritz, B., Rivara, F. P., Roberts, T., Robinson,

C., Rodriguez-Portales, J. A., Romieu, I., Room, R., Rosenfeld, L. C., Roy, A., Rushton, L., Salomon, J. A., Sampson, U., Sanchez-Riera, L., Sanman, E., Sapkota, A., Seedat, S., Shi, P., Shield, K., Shivakoti, R., Singh, G. M., Sleet, D. A., Smith, E., Smith, Kirk R., Stapelberg, N. J. C., Steenland, K., Stöckl, H., Stovner, L. J., Straif, K., Straney, L., Thurston, G. D., Tran, Jimmy H., Van Dingenen, R., van Donkelaar, A., Veerman, J. L., Vijayakumar, L., Weintraub, R., Weissman, M. M., White, R. A., Whiteford, H., Wiersma, S. T., Wilkinson, J. D., Williams, H. C., Williams, W., Wilson, N., Woolf, A. D., Yip, P., Zielinski, J. M., Lopez, A. D., Murray, C. J. L., and Ezzati, M. (2012). A comparative risk assessment of burden of disease and injury attributable to 67 risk factors and risk factor clusters in 21 regions, 1990?2010: a systematic analysis for the Global Burden of Disease Study 2010. **The Lancet.** 380(9859): 2224-2260.

Liu, Y., Kahn, R. A., Chaloulakou, A., and Koutrakis, P. (2009). Analysis of the impact of the forest fires in August 2007 on air quality of Athens using multi-sensor aerosol remote sensing data, meteorology and surface observations. **Atmospheric Environment.** 43(21): 3310-3318.

Ma, C. J., and Choi, K. C. (2007). A Combination of bulk and single particle analyses for asian dust. **Water, Air & Soil Pollution.** 183(1): 3-13.

Martonchik, J. V., Kahn, R. A., and Diner, D. J. (2009). Retrieval of aerosol properties over land using MISR observations. In A. A. Kokhanovsky and G. d. Leeuw (eds.), **Satellite Aerosol Remote Sensing over Land** (pp. 267-293). Berlin: Sprinker.

McClellan, R. O. (2002). Setting ambient air quality standards for particulate matter. **Toxicology.** 181-182: 329-347.

Mei, L., Xue, Y., Kokhanovsky, A. A., von Hoyningen-Huene, W., de Leeuw, G., and Burrows, J. P. (2013). Retrieval of aerosol optical depth over land surfaces from AVHRR data. **Atmospheric Measurement Techniques.** 6(1): 2227-2251.

Ministry of Natural Resources and Environment. Pollution Control Department (2007). **Report of smoke pollution in northern region-Minister of Natural Resources and Environment** [On-line]. Available: http://www.rty9.com/s/cabt/112566.

Minnesota Pollution Control Agency. (2012). **Health effect of wood smoke** [On-line]. Available: http://www.pca.state.mn.us/index.php/air/air-quality-and-pollutants/general-air-quality/wood-smoke/health-effects-of-wood-smoke.html?nav=0.

Munchak, L. A., Levy, R. C., Mattoo, S., Remer, L. A., Holben, B. N., Schafer, J. S., Hostetler, C. A., and Ferrare, R. A. (2013). MODIS 3 km aerosol product: applications over land in an urban/suburban region. **Atmospheric Measurment Techniques.** 6(1): 1683-1716.

National Aeronautics and Space Administration. (2010). **MODIS Web** [On-line]. Available: http://modis.gsfc.nasa.gcv/.

Noor, N. M. (2013). **Air pollutant concentration models** [On-line]. Available: http://www.academia.edu/1744651/Air_Pollutant_Concentration_Model_and_genral_Idea_for_Air_Pollution_Control.

O'Connor, G. T., Neas, L., Vaughn, B., Kattan, M., Mitchell, H., Crain, E. F., Gruchalla, R., Evans Iii, R., Morgan, W., Stout, J., Adams, G. K., and Lippmann, M. (2008). Acute respiratory health effects of air pollution on children with asthma in US inner cities. **Journal of Allergy and Clinical Immunology.** 121(5): 1133-1139.

Pasquill, F. (1974). **Atmospheric Diffusion** (2nd ed.). New York: John Wiley& Sons.

Pollution Control Department. (2013). **AQI information-pollution control department (in Thai)** [On-line]. Available: http://aqmthai.servehttp.com/aqi_info.php.

Pollution Control Department. (2012). **Air quality and noise (in Thai)-pollution control department** [On-line]. Available: http://www.pcd.go.th/info_serv/en_air.html.

Pearce, D., and Crowards, T. (1996). Particulate matter and human health in the United Kingdom. **Energy Policy.** 24(7): 609-619.

Péré, J. C., Pont, V., Mallet, M., and Bessagnet, B. (2009). Mapping of PM10 surface concentrations derived from satellite observations of aerosol optical thickness over South-Eastern France. **Atmospheric Research.** 91(1): 1-8.

Pongkiatkul, P., and Kim Oanh, N. T. (2007). Assessment of potential long-range transport of particulate air pollution using trajectory modeling and monitoring data. **Atmospheric Research.** 85(1): 3-17.

Popovic, D. (2011). **Air quality - models and applications.** Rijeka: In Tech.

Qi, Y., Ge, J., and Huang, J. (2013). Spatial and temporal distribution of MODIS and MISR aerosol optical depth over northern China and comparison with AERONET. **Chinese Science Bulletin**: 1-10.

Ranjan, R. R, Ganguly, N. D., Joshi, HP., and Iyer, K. N. (2007). Study of aerosol optical depth and precipitable water vapour content at Rajkot, a tropical semi-arid station. **Indian Journal of radio and Space Physics.** 36(1): 27-32.

Remer, L. A., Kaufman, Y. J., Tanr, D., Mattoo, S., Chu, D. A., Martins, J. V., Li, R. R., Ichoku, C., Levy, R. C., Kleidman, R. G., Eck, T. F., Vermote, E., and Holben, B. N. (2005). The MODIS aerosol algorithm, products, and validation. **Journal of the Atmospheric Sciences.** 62(4): 947-973.

Remer, L. A., Kleidman, R. G., Levy, R. C., Kaufman, Y. J., Tanr'e, D., Mattoo, S. Martins, J. V., Ichoku, C., Koren, I., Yu, H., and Holben, B. N. (2008). Global aerosol climatology from the MODIS satellite sensors. **Journal of Geophysical Research.** 113: DS14S07.

Retalis, A., and Sifakis, N. (2010). Urban aerosol mapping over Athens using the differential textural analysis (DTA) algorithm on MERIS-ENVISAT data. **ISPRS Journal of Photogrammetry and Remote Sensing.** 65(1): 17-25.

Rohen, G. J., von Hoyningen-Huene, W., Kokhanovsky, A., Dinter, T., Vountas, M.., and Burrows, J. P. (2011). Retrieval of aerosol mass load (PM10) from MERIS/ Envisat top of atmosphere spectral reflectance measurements over Germany. **Atmospheric Measurment Techniques.** 4(3): 523-534.

Rückerl, R., Schneider, A., Breitner, S., Cyrys, J., and Peters, A. (2011). Health effects of particulate air pollution: A review of epidemiological evidence. **Inhalation Toxicology.** 23(10): 555-592.

Saliba, N. A., Jam, F. E., Tayar, G. E., Obeid, W., and Roumie, M. (2010). Origin and variability of particulate matter (PM10 and PM2.5) mass concentrations over an Eastern Mediterranean city. **Atmospheric Research.** 97: 106-114.

Sanjay, M., Kumar, P. P., Gupta, P., Devara, P. C. S., and Aher, G. R. (2013). Comparison of aerosol products retrieved from AERONET, MICROTOPS and MODIS over a tropical urban city, Pune, India. **Aerosoal and Air Quality Research.** 13(1): 107-121.

Scire, J. S., Strimaitis, D. G., and Yamartino, R. J. (2000). **A User's guide for the CALPUFF dispersion model (Version 5).** Concord, Massachusetts: Earth Tech.

Schaap, M., Apituley, A., Timmermans, R. M. A., Koelemeijer, R. B. A., and de Leeuw, G. (2009). Exploring the relation between aerosol optical depth and PM2.5 at Cabauw, the Netherlands. **Atmospheric Chemistry and Physics.** 9(3): 909-925.

SCRAM . U.S. Environmental Protection Agency. (2012). **Preferred/ recommended models** [On-line]. Available: http://www.epa.gov/ttn/scram/dispersion_prefrec.htm.

Seinfeld, J. H., and Pandis, S. N. (2006). **Atmospheric chemistry and physics: from air pollution to climate change.** New Jersey: John Wiley & Sons.

Shan, W., Yin, Y., Lu, H., and Liang, S. (2009). A meteorological analysis of ozone episodes using HYSPLIT model and surface data. **Atmospheric Research.** 93(4): 767-776.

Shooter, D., and Brimblecombe P. (2009). Air quality indexing. **International Journal of Environment and Pollution.** 36(1): 305-323.

Sifakis, N., and Deschamps, P. Y. (1992). Mapping of air pollution using SPOT satellite data. **Photogrammetric Engineer&Remote Sensing.** 58(10): 1433-1437.

Song, C. H., Park, M. E., Lee, K. H., Ahn, H. J., Lee, Y., Kim, J. Y., Han, K. M., Kim, J., Ghim, Y. S., and Kim, Y. J. (2008). An investigation into seasonal and regional aerosol characteristics in East Asia using model-predicted and remotely-sensed aerosol properties. **Atmospheric Chemistry and Physics.** 8(22): 6627-6654.

Srivastava, A., and Rao, B. P. S. (2011). Urban air pollution modeling. In D. Popovic (ed.). **Air quality - models and applications** (pp. 15-34). Rijeka, Croatia: In Tech.

Tao, W.-K., Chen, J.-P., Li, Z., Wang, C., and Zhang, C. (2012). Impact of aerosols on convective clouds and precipitation. **Reviews of Geophysics.** 50(2): RG2001.

Tian, J., and Chen, D. C. (2010). Spectral, spatial, and temporal sensitivity of correlating MODIS aerosol optical depth with ground-based fine particulate matter (PM2.5) across southern Ontario. **Journal of Remote Sensing.** 36(2): 119–128.

Thai Meteorological Department (2007). **Thailand weather and climate** [On-line]. Available: http://www.tmd.go.th/info/info.php.

Tsai, T. C., Jeng, Y. J., Chu, D. A., Chen, J. P., and Chang, S. C. (2011). Analysis of the relationship between MODIS aerosol optical depth and particulate matter from 2006 to 2008. **Atmospheric Environment.** 45(27): 4777-4788.

Trompetter, W. J., Davy, P. K., and Markwitz, A. (2010). Influence of environmental conditions on carbonaceous particle concentrations within New Zealand. **Journal of Aerosol Science.** 41(1): 134-142.

U.S. Climate Change Science Program. (2009). **Atmospheric aerosol properties and climate impacts**: NASA. (Synthesis and assessment product 2.3).

U.S. Environmental Protection Agency (2004). **User's guide for the AMS /EPA regulatory model - AERMOD** [On-line]. Available: http://www.epa.gov/scram001/7thconf/aermod/aermodugb.pdf.

U.S. Environmental Protection Agency. (2006). **Terms of environment :glossary, abbreviations and acronyms** [On-line]. Available:http://infohouse.p2ric.org/ref/01/00402/aterms.html.

U.S. Environmental Protection Agency. (2009). **AQI-A guide to air quality and your health** [On-line]. Available: http://www.epa.gov/airnow/aqi_brochure_08-09.pdf.

U.S. Environmental Protection Agency (2009). **Technical assistance document for the reporting of daily air quality-the air quality index (AQI)** [On-line]. Available: http://www.epa.gov/airnow/aqi_tech_assistance. pdf.

U.S. Environmental Protection Agency. (2010). **Particulate matter** [On-line]. Available: http://www.epa.gov/air/particlepollution/standards.html.

U.S. Environmental Protection Agency. (2012). **Six common air pollutants** [On-line]. Available: http://www.epa.gov/air/urbanair/.

U.S. Environmental Protection Agency. (2013). **Particulate matter (PM)-basic information** [On-line]. Available: http://www.epa.gov/pm/basic.html.

Vallero, D. A. (2008). **Fundamentals of air pollution.** Amsterdam; Boston: Academic Press.

van Donkelaar, A., Martin, R. V., Levy, R. C., da Silva, A. M., Krzyzanowski, M., Chubarova, N. E., Semutnikova, E., and Cohen, A. J. (2011). Satellite-based estimates of ground-level fine particulate matter during extreme events: A case study of the Moscow fires in 2010. **Atmospheric Environment.** 45(34): 6225-6232.

Vidot, J., Santer, R., and Aznay, O. (2008). Evaluation of the MERIS aerosol product over land with AERONET. **Atmospheric Chemistry and Physics.** 8(24): 7603-7617.

Vinitketkumnuen, U., Kalayanamitra, K., Chewonarin, T., and Kamens, R. (2002). Particulate matter, PM 10 & PM 2.5 levels, and airborne mutagenicity in Chiang Mai, Thailand. **Mutation Research/Genetic Toxicology and Environmental Mutagenesis.** 519(1-2): 121-131.

Voiland, A. (2010). **Aerosols: tiny particles, big impact** [On-line]. Available: http://earthobservatory.nasa.gov/Features/Aerosols/page1.php.

von Hoyningen-Huene, W., Freitag, M., and Burrows, J. P. (2002). Retrieval of spectral aerosol optical thickness from multi-wavelength space-borne sensors. **Advances in Space Research.** 29(11): 1765-1770.

von Hoyningen-Huene, W., Freitag, M., and Burrows, J. B. (2003). Retrieval of aerosol optical thickness over land surfaces from top-of-atmosphere radiance. **Journal of Geophysical Research.** 108 (D9, 4260): AAC 2 1-20.

von Hoyningen-Huene, W., Kokhanovsky, A. A., Burrows, J. P., Bruniquel-Pinel, V., Regner, P., and Baret, F. (2006). Simultaneous determination of aerosol- and surface characteristics from top-of-atmosphere reflectance using MERIS on board of ENVISAT. **Advances in Space Research.** 37(12): 2172-2177.

von Hoyningen-Huene, W., Yoon, J., Vountas, M., Istomina, L. G., Rohen, G., Dinter, T., Kokhanovsky, A. A., and Burrows, J. P. (2011). Retrieval of spectral aerosol optical thickness over land using ocean color sensors MERIS and SeaWiFS. **Atmos. Meas. Tech.** 4(2): 151-171.

Wagner, F., and Silva, A. M. (2008). Some considerations about Ångström exponent distributions. **Atmospheric Chemistry and Discussions.** 8: 481-489.

Wai, W. T. (2012). **A Study of the air pollution index reporting system.** School of Public Health and Primary Care: The Chinese University of Hong Kong.

Walthall, C. L., Norman, J. M., Welles, J. M., Campbell, G., and Bla, B. L. (1985). Simple equation to approximate the bidirectional reflectance from vegetative canopies and bare soil surfaces. **Optical Society of America.** 24(3): 383-387.

Wang, J., and Christopher, S. A. (2003). Intercomparison between satellite-derived aerosol optical thickness and PM2.5 mass: Implications for air quality studies. **Geophysical Research Letters.** 30(21): 2095-2098.

Wong, M. S., Nichol, J., Kwon Ho, L., and Zhanqing, L. (2008). Retrieval of aerosol optical thickness using MODIS 500 × 500m2, a study in Hong Kong and Pearl River delta region. In **2008 Earth Observation and Remote Sensing Applications** (pp. 1-6). Beijing, China: Institute of Electrical and Electronics Engineers.

WHO (2006a). **Healt risks of particulate matter from long-range transboundary air pollution** [On-line]. Available: http://www.euro.who.int/document/e88189.pdf.

WHO (2006b). **WHO_Air quality guidelines for particulate matter, ozone, nitrogen dioxide and sulfer dioxide** [On-line]. Available: http://www.who.int/phe/health_topics/outdoorair/outdoorair_aqg/en/index.html.

Wijeratne, I. K., and Bijker, W. (2006). Mapping dispersion of air pollution with remote sensing. In **ISPRS Technical Commission II Symposium** (pp. 125-130). Hannover, Germany: International Society for Photogrammetry and Remote Sensing.

Zha, Y., Gao, J. A. Y., Jiang, J., Lu, H., and Huang, J. (2010). Monitoring of urban air pollution from MODIS aerosol data: effect of meteorological parameters. **Tellus.** 62(2): 109-116.

APPENDICES

APPENDIX A

AEROSOL SIZE DISTRIBUTION AND RELATED OPTICAL PARAMETERS

Basic knowledge in the aerosol size distribution and related optical parameters is given in Kuśmierczyk-Michulec (2011) and its main content is presented here for being reference to the satellite-based PM observations described in Chapter II.

The aerosol size distribution can be addressed in terms of three distribution functions: the number size distribution *N(r)*, the volume size distribution *V(r)*, and the mass size distribution *m(r)*. In each case the lognormal function is typically used and details are presented, e.g., by Seinfeld and Pandis (2006). Among these, the aerosol number size distribution for a given aerosol type can be written as follows:

$$\frac{dN(r)}{d\ln r} = \frac{N_n}{\sigma\sqrt{2\pi}} \exp\left\{-\frac{(\ln r - \ln r_n)^2}{2\sigma^2}\right\} \qquad \text{(A.1)}$$

where r is the particle radius, r_n is the median radius, σ is the standard deviation and N_n is total particle concentration and $dN(r)$ is fraction of total particles with radius in the range r and r+dr. From the number size distribution (Eq. C.1), an effective radius R_{eff} (in μm) can be derived directly using the relation:

$$R_{eff} = \frac{\int r^3 \frac{dNr}{d\ln r} d\ln r}{\int r^2 \frac{dNr}{d\ln r} d\ln r} \quad . \qquad \text{(A.2)}$$

By definition effective radius is an area-weighted mean radius of the aerosol particles. This paremeter is a very useful in characterization of the aerosol mixtures.

To characterize the size of atmospheric particles, aerosols are usually divided into three modes: Aitken mode (diameter < 0.5 μm), accumulation mode (0.5 to 2.5 μm), and coarse mode (> 2.5 μm) (Figures C.1). The Aitken and accumulation modes are collectively referred to as fine particles. Human produced emissions (e.g biomass burning) are examples of small mode aerosols. Example of the coarse mode particles are the desert dust particles (IACETH, 2012).

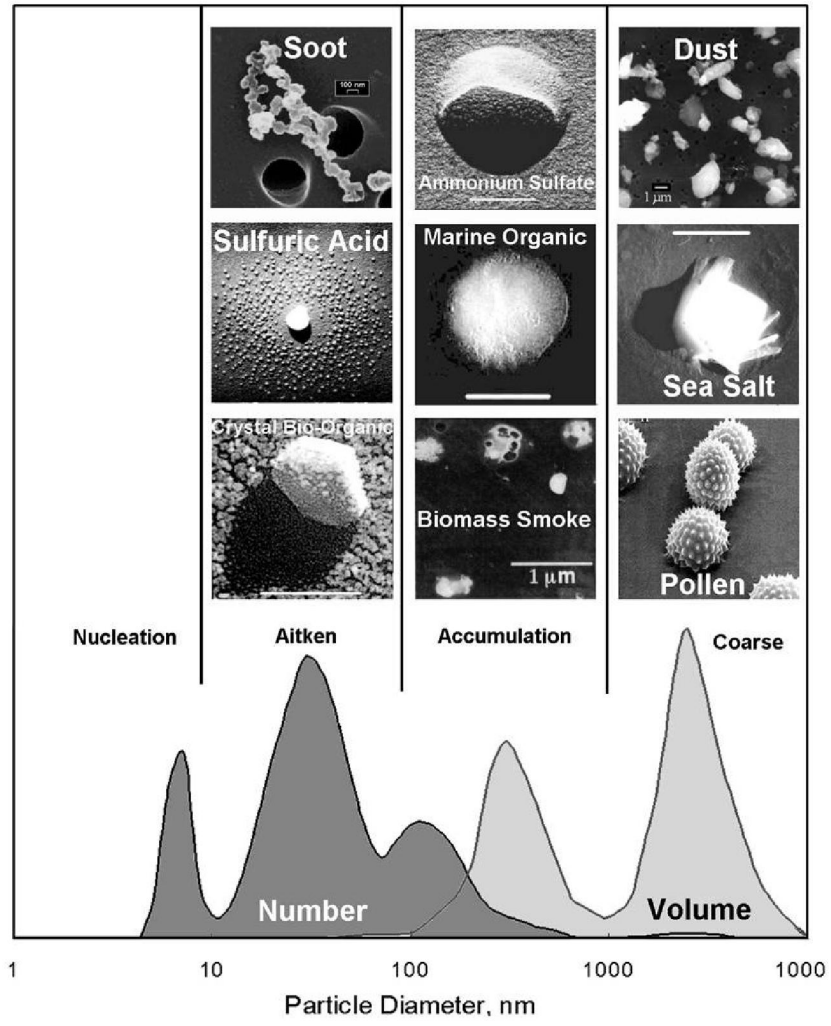

Figure A.1 Three typical aerosol modes regarding to their size (Brasseur, Prinn, and Pszenny, 2003).

Assuming that particles are spherical the following relation can be used to calculate the mass concentration PM at the surface in ($\mu g/m^3$):

$$PM = \frac{4}{3}\pi\rho\int_{r_{\min}}^{r_{\max}} r^3 \frac{dN(r)}{d\ln r} d\ln r \qquad (A.3)$$

where ρ is the aerosol mass density in ($\mu g/cm^3$). And the aerosol extinction coefficient $\sigma(\lambda)$ (in km^{-1}) can be calculated from the number size distribution:

$$\sigma(\lambda) = \pi\int_{r_{\min}}^{r_{\max}} r^2 Q_{ext} \frac{dN(r)}{d\ln r} d\ln r \qquad (A.4)$$

where λ is wavelength and Q_{ext} is the extinction efficiency factor, being a function of the complex index of refraction. The coefficient Q_{ext} can be calculated according to algorithm given by Bohren and Huffman (1983). The size-distribution integrated extinction efficiency $<Q_{ext}>$ is defined as (Hansen andTravis, 1974):

$$< Q_{ext} >= \frac{\int_{r_{\min}}^{r_{\max}} r^2 Q_{ext} \frac{dN(r)}{d\ln r} d\ln r}{\int_{r_{\min}}^{r_{\max}} r^2 \frac{dN(r)}{d\ln r} d\ln r} \qquad (A.5)$$

The extinction coefficient integrated over the whole column of atmosphere is a dimensionless parameter and it is called the aerosol optical thickness (AOT):

$$\mathrm{AOT}(\lambda) = \int_{z_{\min}}^{z_{\max}} \sigma(\lambda, z) dz \qquad (A.6a)$$

or

$$\mathrm{AOT}(\lambda) \approx \int_{z_{\min}}^{z_{\max}} \sigma(\lambda) f(z) dz \qquad (A.6b)$$

where $\sigma(\lambda)$ is the aerosol extinction coefficient for wavelength λ, z is altitude, f(z) is vertical distributing function of the considered aerosol, and z_{min}, z_{max} are the lower and upper altitude of air thickness to be included in the integration (where a given aerosol type can be found), respectively. Variation of the extinction coefficient with the wavelength can be presented in the form of a power law function:

$$\sigma(\lambda) = \beta_{ext}\lambda^{-\alpha} \tag{A.7}$$

where $\sigma(\lambda)$ is the extinction coefficient at wavelength λ and β_{ext} is a proper constant. The constant α is a well-known parameter called the Ångström exponent (also known as Ångström coefficient or Ångström parameter). For molecules, it is about 4 and varies between about 0 and 2 for particles (Wagner and Silva, 2007).

The same type of relation is also valid for the aerosol optical thickness:

$$AOT(\lambda) = \beta_{AOT}\lambda^{-\alpha} \tag{A.8}$$

where $AOT(\lambda)$ is the AOT at wavelength λ and β_{AOT} is called the Ångström turbidity coefficient which equals to the AOT at 1 μm and also corresponds to the particle load. Usually, this parameter is determined in the spectral range from 440 nm to 870 nm.

From the set of Eqs. A.2-A.6, the following relation between PM and AOT can be derived:

$$\mathrm{PM} = \xi \cdot \mathrm{AOT}(\lambda) \tag{A.8a}$$

where coefficient ξ is defined as:

$$\xi = \frac{4\rho R_{\mathrm{eff}}}{3\langle Q_{\mathrm{ext}}\rangle H} \tag{A.8b}$$

and the vertical distribution H is given by:

$$H = \int_{z_{\min}}^{z_{\max}} \mathrm{f(z)dz}. \tag{A.8c}$$

APPENDIX B

ADDITIONAL MODIS-BASED DAILY DATA

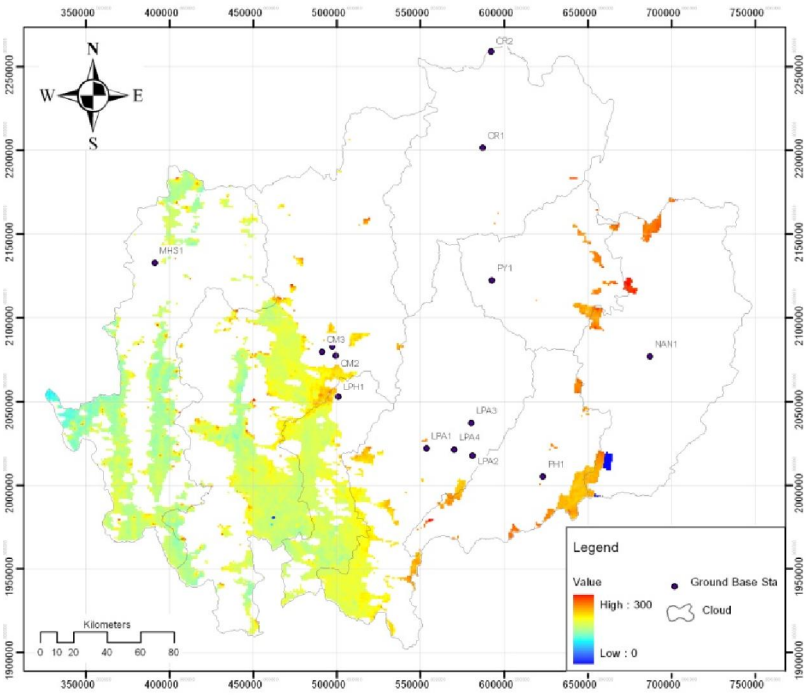

11th March 2010

Figure B Derived BAER-AOD map on 11th-30th March 2010.

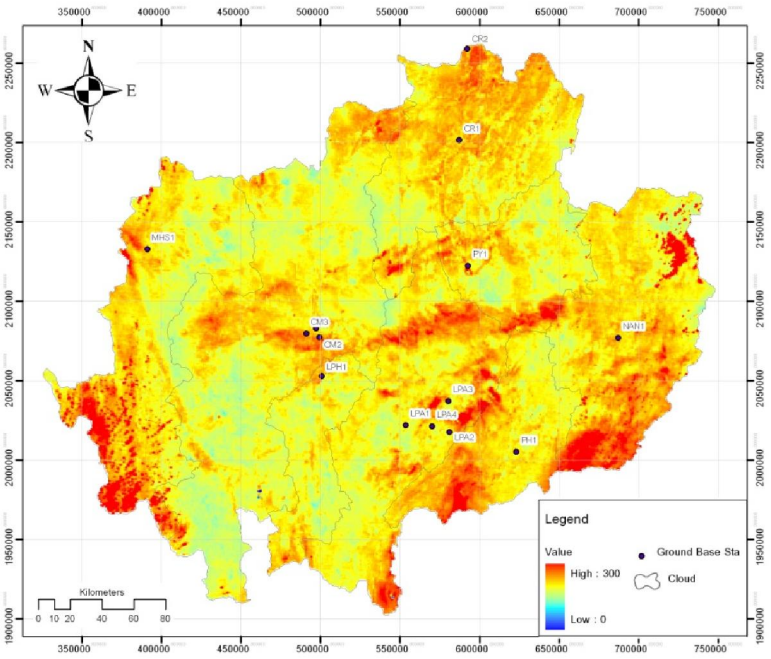

12th March 2010

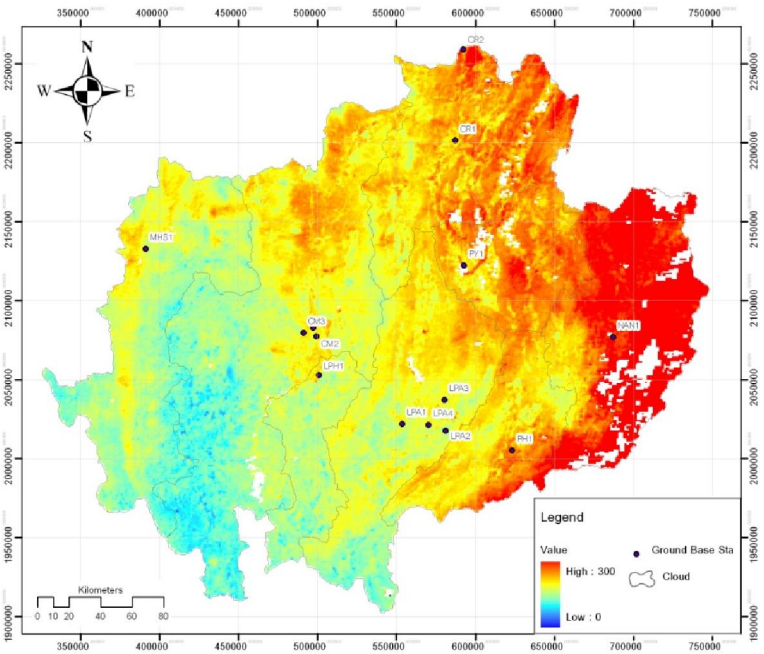

13th March 2010

Figure B (Continued).

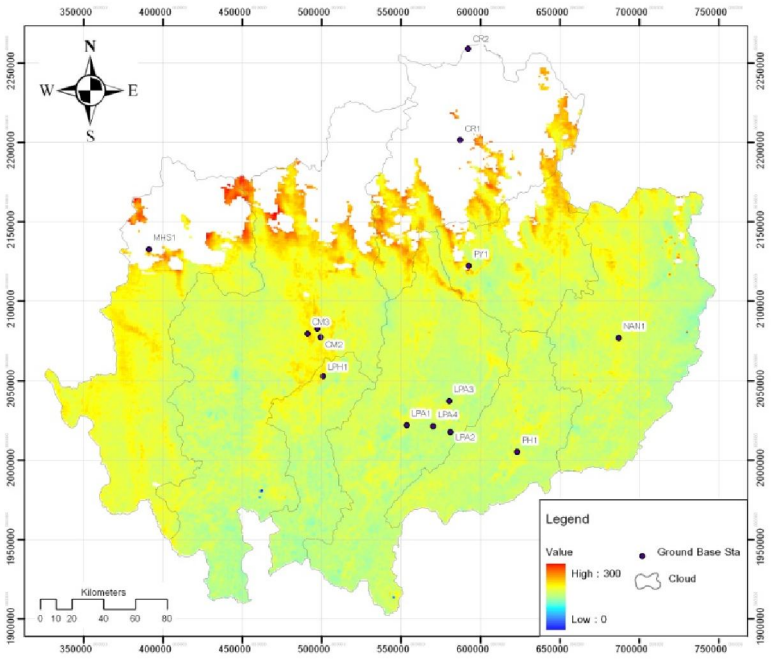

14th March 2010

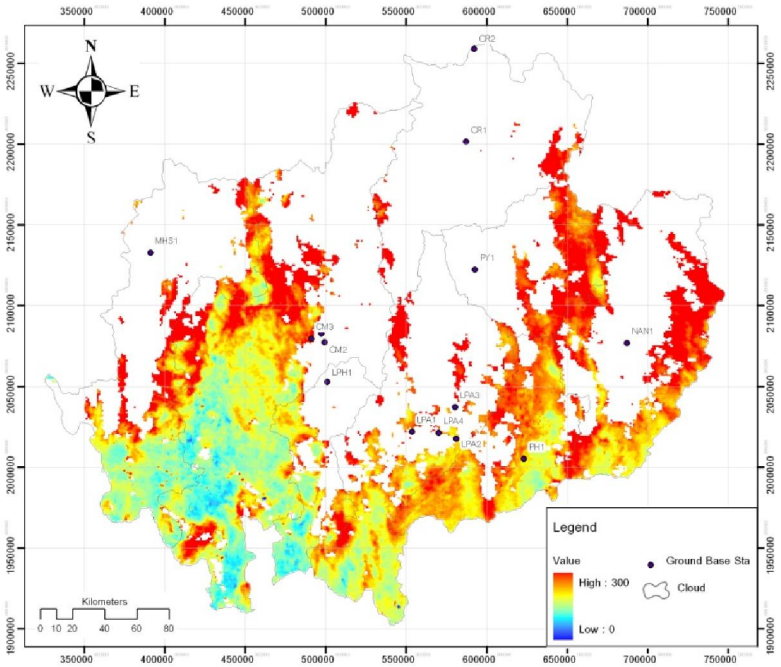

15th March 2010

Figure B (Continued).

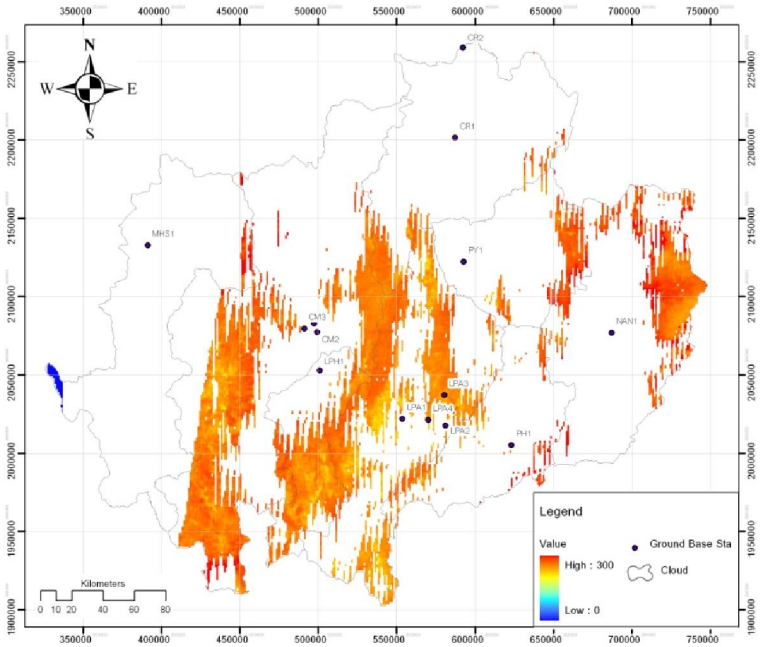

16th March 2010

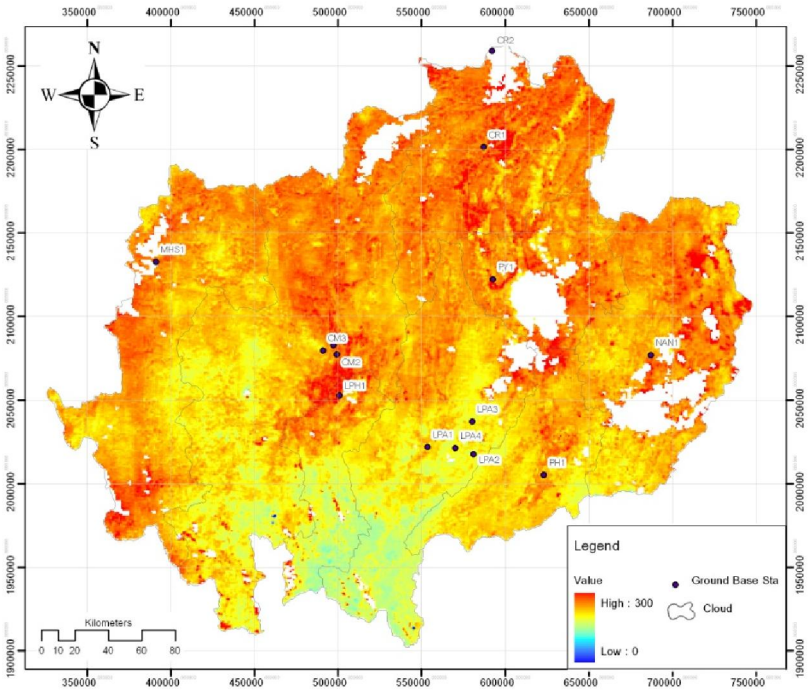

17th March 2010

Figure B (Continued).

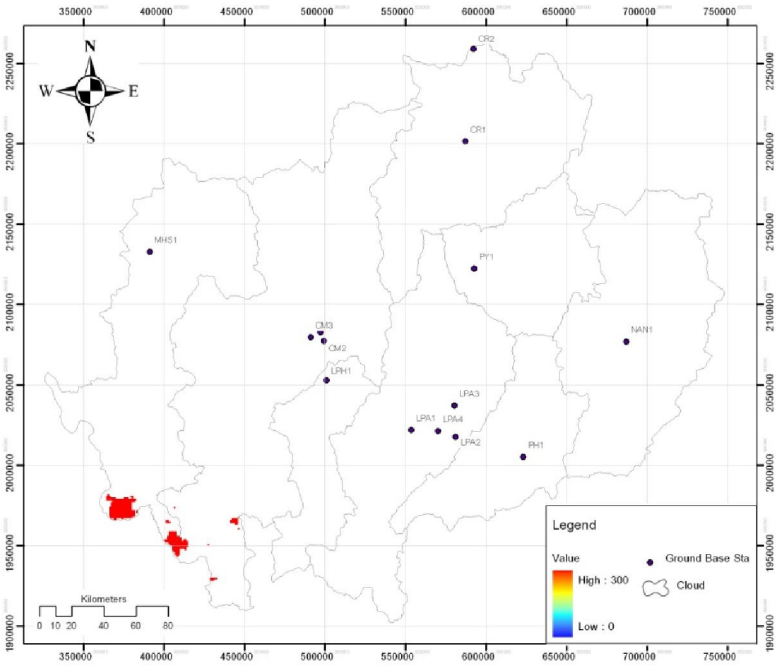

18th March 2010

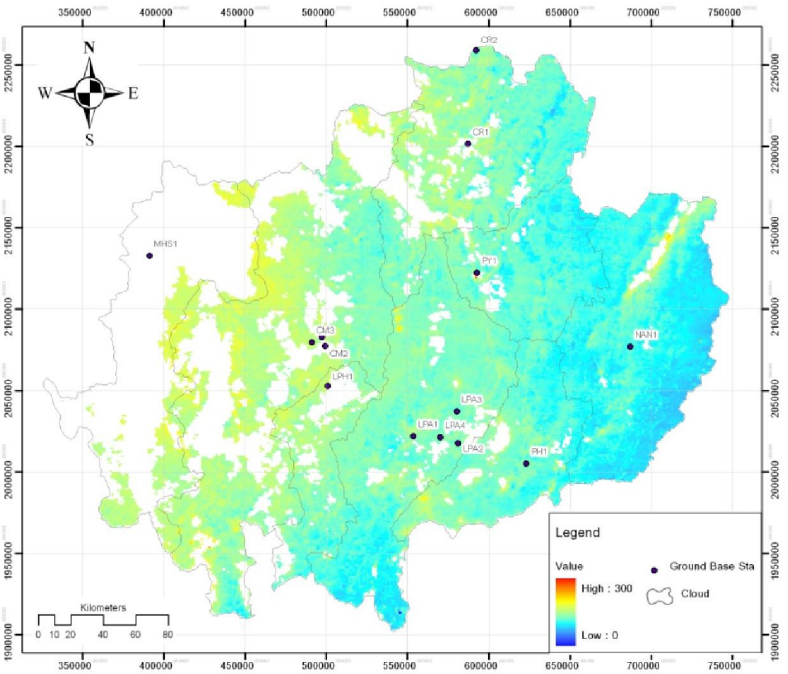

19th March 2010

Figure B (Continued).

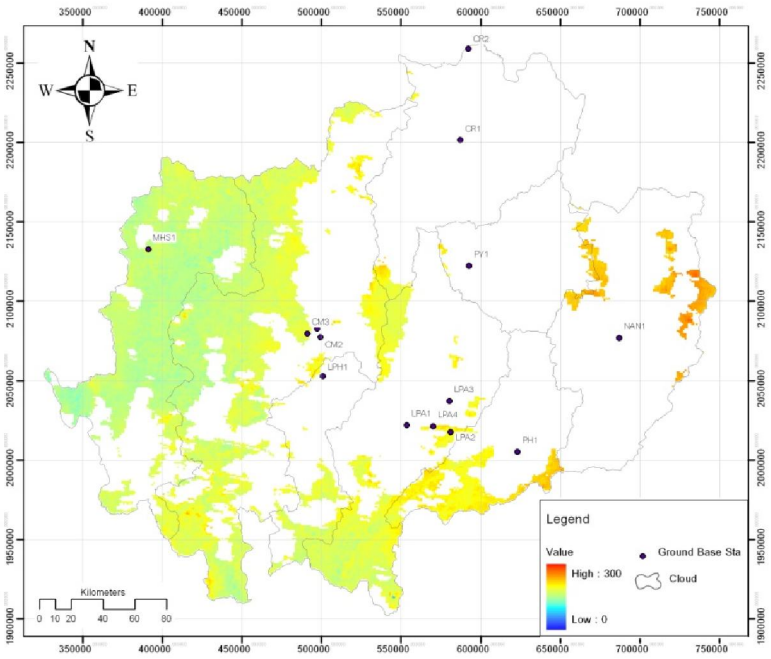

20th March 2010

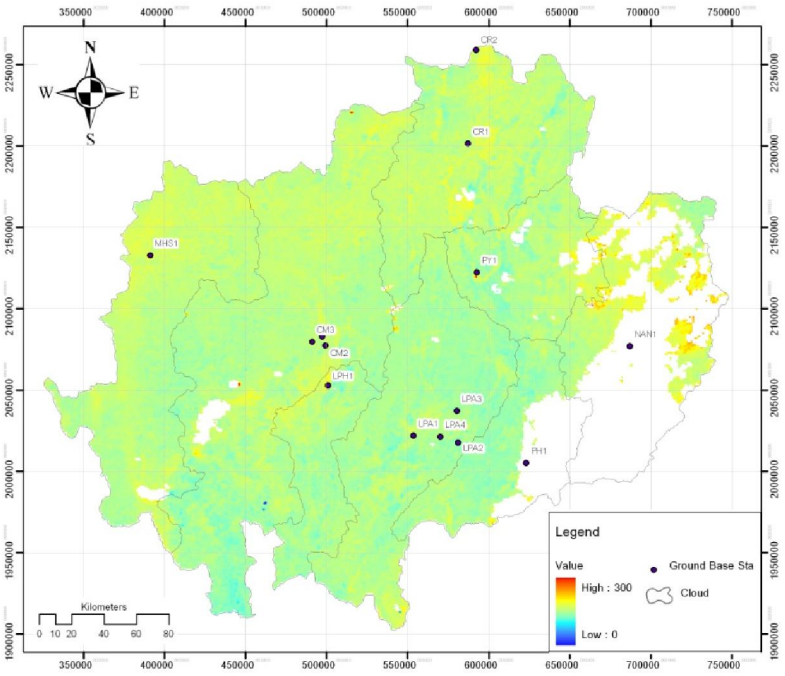

21th March 2010

Figure B (Continued).

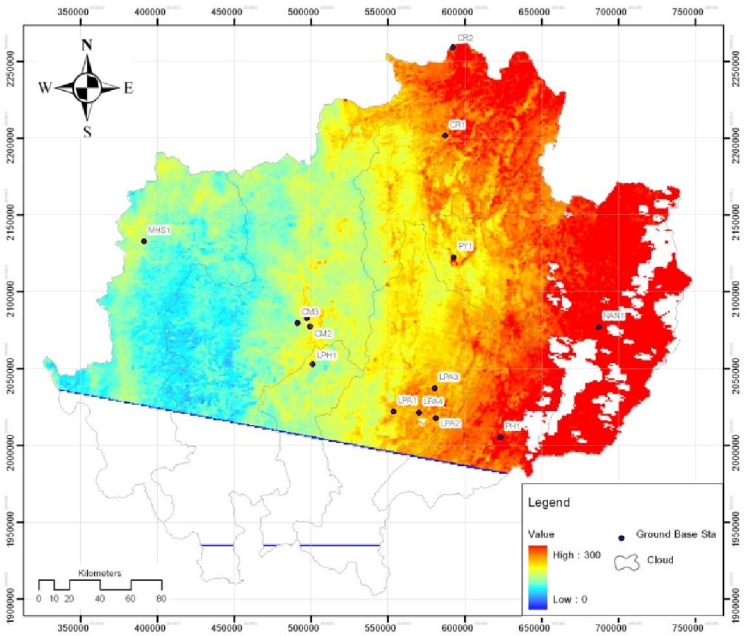

22th March 2010

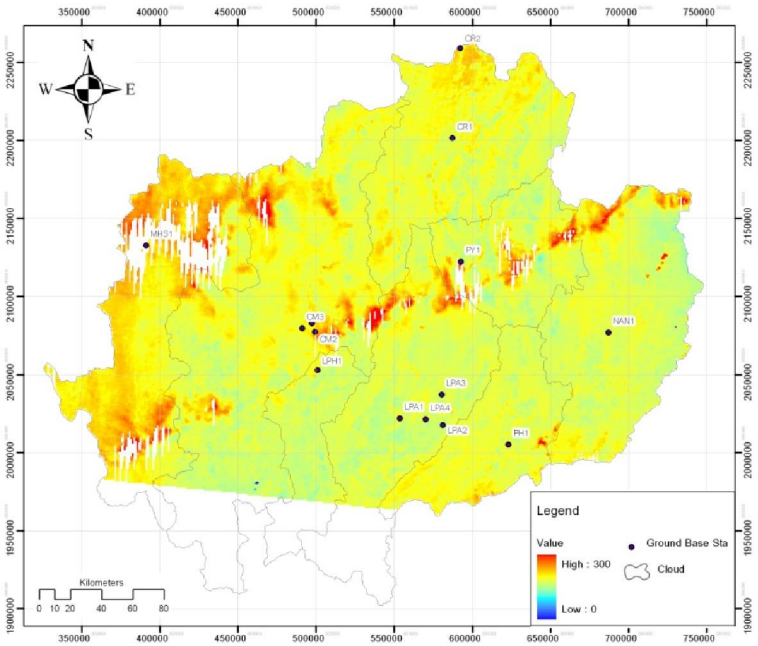

23th March 2010

Figure B (Continued).

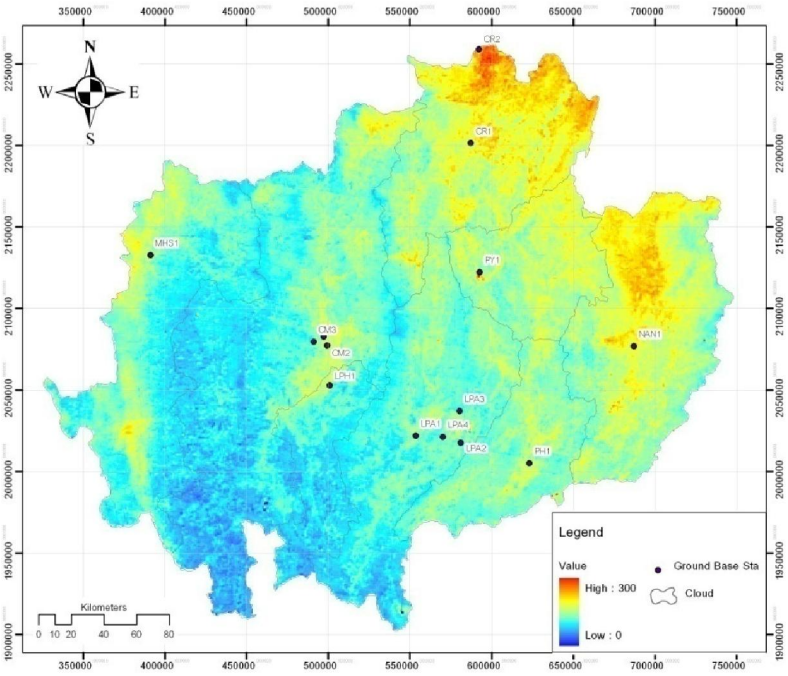

24th March 2010

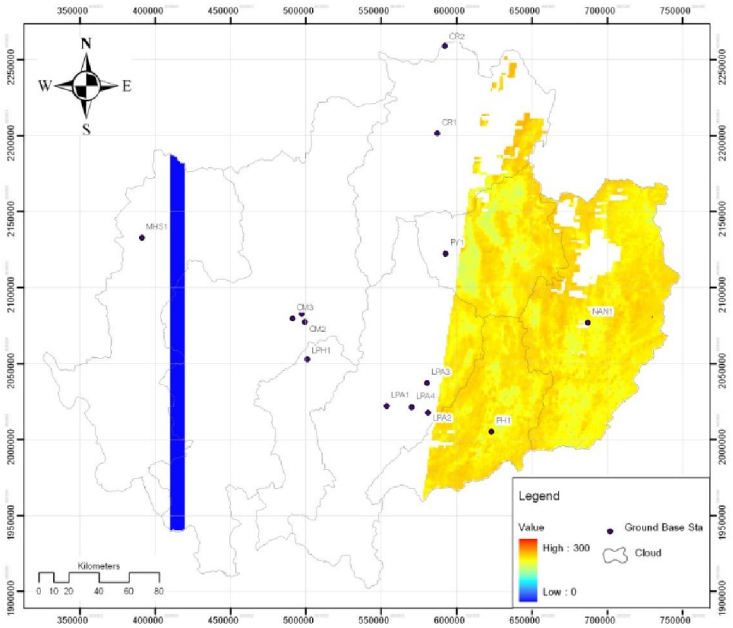

25th March 2010

Figure B (Continued).

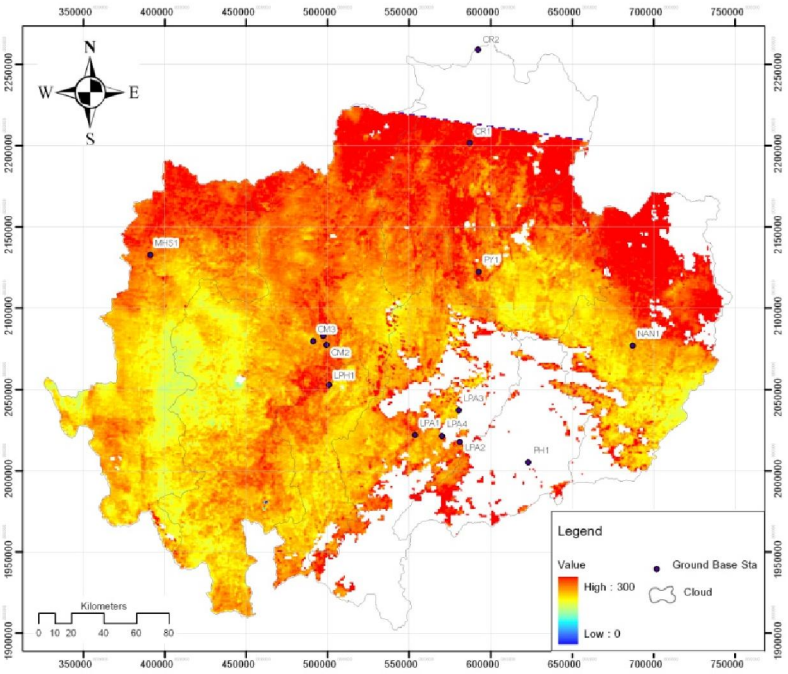

26th March 2010

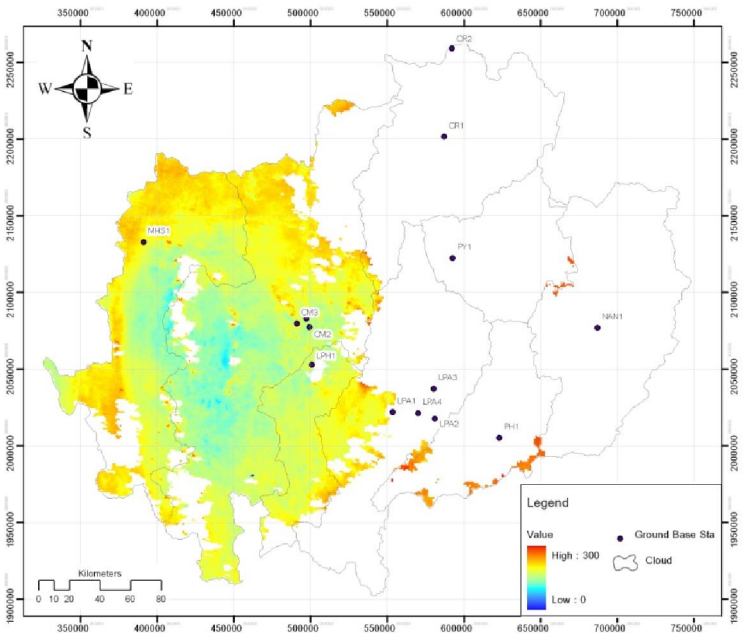

27th March 2010

Figure B (Continued).

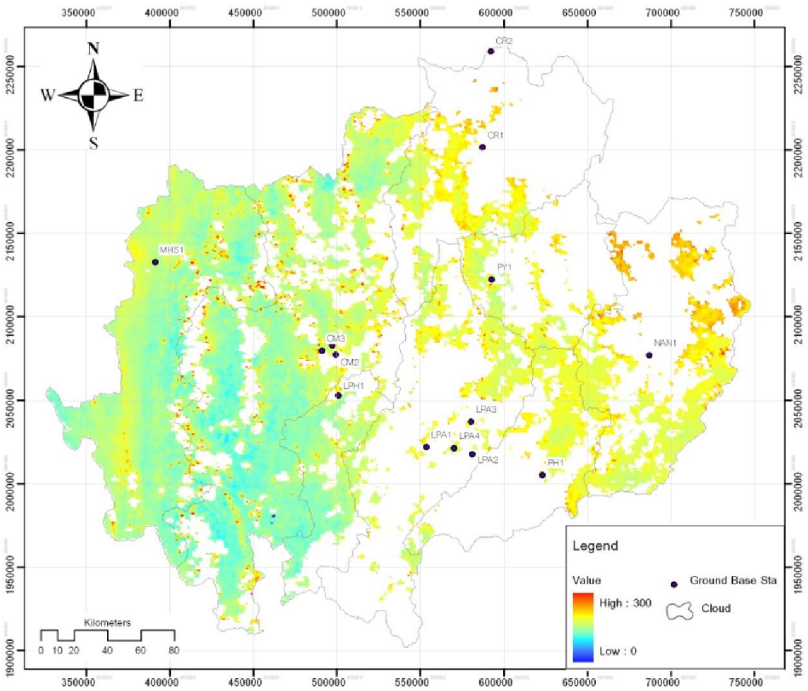

28th March 2010

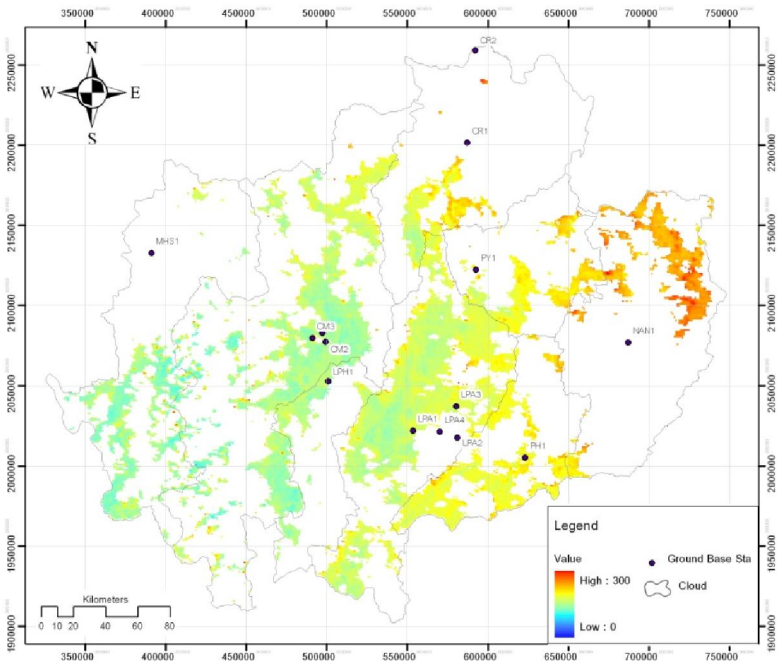

29th March 2010

Figure B (Continued).

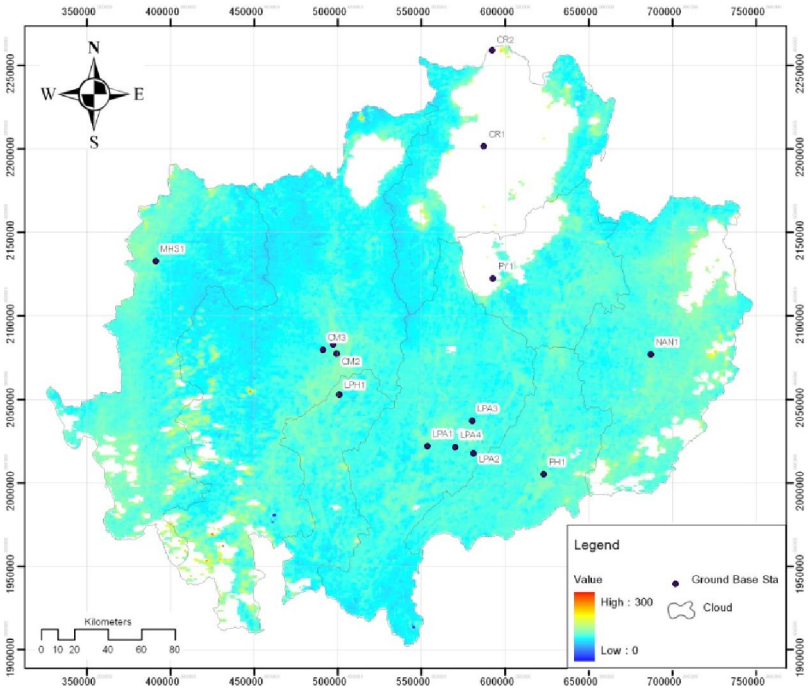

30th March 2010

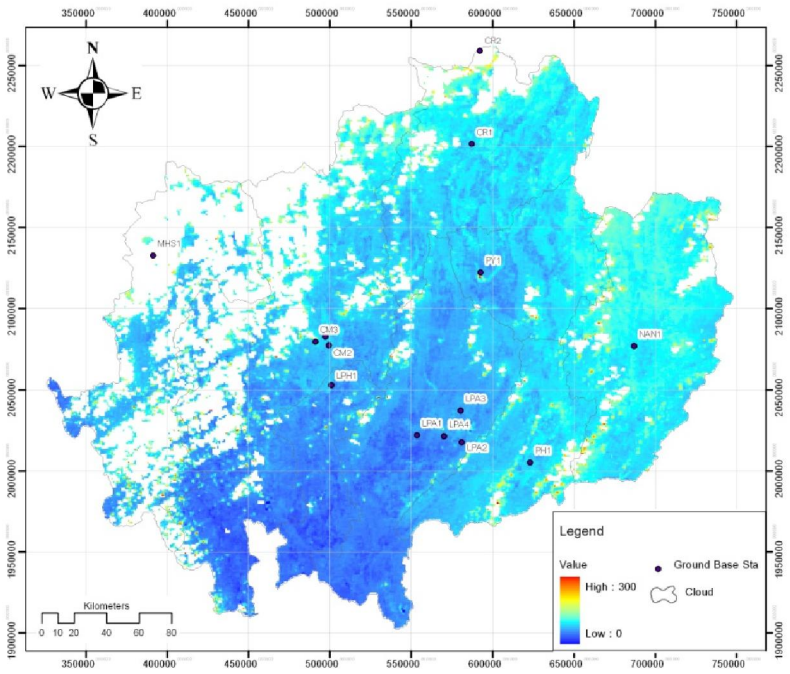

31th March 2010

Figure B (Continued).

APPENDIX C

VALIDATION OF DERIVED PM10 MAPS

Table C.1 Error estimation for the NDAI-based PM10 maps.

Province	Actual and derived PM10 data pairs at each province (unit: μg/m^3)								Average DIF
	PM10	1	2	3	4	5	6	7	
CM	Actual	190	137	183	202	221	184	186	6.59
	Derived	160	114	178	208	224	180	194	
	DIF (%)	15.79	16.79	2.73	2.97	1.36	2.17	4.30	
CR	Actual	165	150	179	203	242	275	229	12.3
	Derived	122	118	176	211	219	215	225	
	DIF (%)	26.06	21.33	1.68	3.94	9.50	21.82	1.75	
LPA	Actual	100	88	140	104	114	105	118	22.63
	Derived	86	100	135	150	90	146	91	
	DIF (%)	14.00	13.64	3.57	44.23	21.05	39.05	22.88	
LPH	Actual	188	133	175	204	230	178	162	4.19
	Derived	185	111	177	204	228	177	148	
	DIF (%)	1.60	16.54	1.14	0.00	0.87	0.56	8.64	

Note: DIF ≡ Difference. $\mathrm{DIF}(\%) = \dfrac{\left|\mathrm{PM10}_{\mathrm{Derived}} - \mathrm{PM10}_{\mathrm{Actual}}\right|}{\mathrm{PM10}_{\mathrm{Actual}}} \mathrm{x}100\%$

Table C.1 (Continued).

Province	Actual and derived PM10 data pairs at each province (unit: μg/m^3)								Average DIF
	PM10	1	2	3	4	5	6	7	
MHS	Actual	167	107	183	210	230	136	337	9.67
	Derived	124	92	171	209	233	140	281	
	DIF (%)	25.75	14.02	6.56	0.48	1.30	2.94	16.62	
NAN	Actual	188	139	178	199	216	187	171	7.07
	Derived	142	117	173	197	214	192	168	
	DIF (%)	24.47	15.83	2.81	1.01	0.93	2.67	1.75	
PH	Actual	-	-	-	-	-	-	-	-
	Derived	-	-	-	-	-	-	-	
	DIF (%)	-	-	-	-	-	-	-	
PY	Actual	150	135	168	179	210	150	217	13.37
	Derived	110	103	168	190	214	110	153	
	DIF (%)	26.67	23.70	0.00	6.15	1.90	26.67	29.49	
Mean absolute error (MAE) = 17.59 (from Eq. 4.3)									

มหาวิทยาลัยเทคโนโลยีสุรนารี

Table C.2 Error estimation for the BAER AOD-based PM10 maps.

Province	Actual and derived PM10 data pairs at each province (unit: μg/m^3)								Average DIF
	PM10	1	2	3	4	5	6	7	
CM	Actual	129	113	135	172	163	220	199	4.19
	Derived	127	114	141	177	182	223	195	
	DIF (%)	1.55	0.88	4.44	2.91	11.66	5.91	2.01	
CR	Actual	173	203	201	150	182	236	280	5.58
	Derived	165	204	201	148	200	222	233	
	DIF (%)	4.62	0.49	0.00	1.33	9.89	5.93	16.79	
LPA	Actual	89	192	148	140	189	143	104	9.33
	Derived	83	206	158	142	210	164	122	
	DIF (%)	6.74	7.29	6.76	1.43	11.11	14.69	17.31	
LPH	Actual	121	130	132	176	141	208	179	6.90
	Derived	114	141	156	186	135	218	177	
	DIF (%)	5.79	8.46	18.18	5.68	4.26	4.81	1.12	

Note: DIF ≡ Difference. $\mathrm{DIF}(\%) = \frac{\left|\mathrm{PM10}_{\mathrm{Derived}} - \mathrm{PM10}_{\mathrm{Actual}}\right|}{\mathrm{PM10}_{\mathrm{Actual}}} \mathrm{x}100\%$

มหาวิทยาลัยเทคโนโลยีสุรนารี

Table C.2 (Continued).

Province	Actual and derived PM10 data pairs at each province (unit: μg/m^3)								Average DIF
	PM10	1	2	3	4	5	6	7	
MHS	Actual	133	145	210	184	114	223	171	6.65
	Derived	121	132	195	179	127	225	160	
	DIF (%)	9.02	8.97	7.14	2.72	11.4	0.9	6.43	
NAN	Actual	114	219	174	109	230	120	117	6.87
	Derived	100	241	171	113	250	134	117	
	DIF (%)	12.28	10.05	1.72	3.67	8.70	11.67	0.00	
PH	Actual	80	246	144	-	-	-	-	8.36
	Derived	73	252	164	-	-	-	-	
	DIF (%)	8.75	2.44	13.89	-	-	-	-	
PY	Actual	220	195	258	142	138	170	222	6.05
	Derived	194	190	242	140	140	193	210	
	DIF (%)	11.82	2.56	6.2	1.41	1.45	13.53	5.41	
Mean absolute error (MAE) = 6.62 % (from Eq. 4.3)									

มหาวิทยาลัยเทคโนโลยีสุรนารี

CURRICULUM VITAE

Name Mr. Chat Phayungwiwatthanakoon

Date of Birth November 10, 1968

Place of Birth Burirum Province, Thailand.

Education

- Bachelor of Engineering (Agricultural): Faculty of Engineering, Khon Kaen University, Thailand.
- Bachelor of Public Administration (General Management): December, 2003. School of Management Science, Sukhothai Thammathirat Open University, Thailand.
- Master of Science (Geographic Information System): August, 2006. Faculty of Science and Technology, Nakhon Ratchasima Ratjabat University, Thailand.

Grants and Fellowships

Scholarship, Rajamangala University of Technology Isan.

มหาวิทยาลัยเทคโนโลยีสุรนารี